METAL COMPLEXES OF FERROCENYLPHOSPHINES: CATALYTIC PROPERTIES OF SOME RHODIUM COMPLEXES

by

TAE-JEONG KIM

M.Sc., Korea University, 1978

A THESIS SUBMITTED IN PARTIAL FULFILMENT OF

THE REQUIREMENTS FOR THE DEGREE OF

DOCTOR OF PHILOSOPHY

in

THE FACULTY OF GRADUATE STUDIES

Department of Chemistry

We accept this thesis as conforming

to the required standard

The University of British Columbia

March, 1984

In presenting this thesis in partial fulfilment of the requirements for an advanced degree at the University of British Columbia, I agree that the Library shall make it freely available for reference and study. I further agree that permission for extensive copying of this thesis for scholarly purposes may be granted by the head of my department or by his or her representatives. It is understood that copying or publication of this thesis for financial gain shall not be allowed without my written permission.

Department of CHEMISTRY

The University of British Columbia
2075 Wesbrook Place
Vancouver, Canada
V6T 1W5

Date MAY 10, 1984

ABSTRACT

A series of achiral and chiral ferrocenylphosphines have been prepared with special emphasis on those containing bulky tert-butyl groups on phosphorus (I and V were previously known):

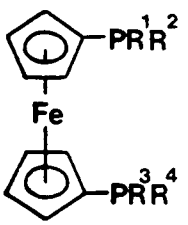

	R^1	R^2	R^3	R^4
I	Ph	Ph	Ph	Ph
II	Ph	CMe_3	Ph	CMe_3
III	Ph	Ph	CMe_3	CMe_3
IV	CMe_3	CMe_3	CMe_3	CMe_3

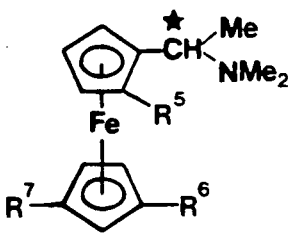

	R^5	R^6	R^7
V	$P(CMe_3)_2$	H	H
VI	$P(CMe_3)_2$	$P(CMe_3)_2$	H
VII	$P(CMe_3)_2$	$P(CMe_3)_2$	$P(CMe_3)_2$

They form a number of transition metal complexes such as $[Rh(L\text{-}L)(NBD)]ClO_4$ (L-L = I-VII; NBD = norbornadiene), $M(L\text{-}L)X_2$ (M = Pd, Ni; L-L = I-IV; X = Cl, Br), $M(L\text{-}L)(CO)_4$ (M = Cr, Mo; L-L = I), and $Fe_x(L\text{-}L)(CO)_y$ (x = 1, y = 3, x = 2, y = 8, L-L = I). All these ligands and their metal complexes have been fully characterized by analytical and spectroscopic techniques. In a number of cases these results are confirmed by X-ray analyses. The configuration of VII proved to be, for example, (S,S) with regard to central and planar chirality rather than the expected (S,R) found for V and VI.

The achiral Rh(I) complexes $[Rh(L\text{-}L)(NBD)]ClO_4$ (L-L = I-IV) are efficient catalyst precursors for the hydrogenation of a range of olefins (1 atm H_2, 30°C). The presence of bulky tert-butyl groups enhances reaction rates except when bulky olefins are the substrates. The chiral trisphosphine Rh(I) complex $[Rh(L\text{-}L)(NBD)]ClO_4$ (L-L = VII) is a very efficient catalyst precursor for the asymmetric hydrogenation of acylaminocinnamic, acylaminoacrylic, and (E)-α-methylcinnamic acids, giving 91, 95, and 61% e.e., respectively. The chiral Rh(I) complex, where L-L = VI, is a relatively poor catalyst for asymmetric hydrogenation as compared with the other two complexes (L-L = V , VII). Here again the presence of tert-butyl groups increases the reaction rates, and the rates become greater as the number of tert-butyl groups increases. These results and other comparative hydrogenation studies are discussed and rationalized in terms of the steric (including ligand conformation) and electronic effects of the substituents on the phosphorus atom(s).

The reaction of H_2 with the hydrogenation catalyst precursor $[Rh(L\text{-}L)(NBD)]ClO_4$ (L-L = II) in MeOH results in crystals which have the structure $[(L\text{-}L)(H)Rh(\mu\text{-}H)_3Rh(H)(L\text{-}L)]ClO_4$. When L-L = IV, the same reaction results in a similar rhodium hydride although the positions of the hydrogen atoms are not well established. A number of other hydrides, some fluxional, are also obtained in various solvents from the catalyst precursors $[Rh(L\text{-}L)(NBD)]ClO_4$ (L-L = I-VII). Where possible these have been characterized on the basis of their NMR spectra. The implication of these results with respect to the mechanisms of catalytic hydrogenation is discussed.

TABLE OF CONTENTS

LIST OF TABLES

LIST OF FIGURES

ACKNOWLEDGEMENTS

This thesis could not have been written without the advice and help from a number of people, especially those mentioned here, who have acted as both friends and advisors to me.

First of all, I wish to express my sincere gratitude to Professor W.R. Cullen, my research advisor, for his expert guidance and assistance during the course of this work. My association with him has been pleasant and rewarding.

Special thanks are due to Dr. T.G. Appleton for the assistance of many NMR experiments and invaluable suggestions.

I am very much indebted to Professors F. Aubke, A.V. Bree, B.R. James for their suggestions and comments on my work and for proof-reading the manuscript of this thesis.

My thanks are extended to Professor F.W.B. Einstein, Professor J. Trotter, Dr. T. Jones, Dr. S. Rettig and Mr. S. Evans for the crystal structure determinations and the help they have given to me.

My thanks go also to my lab colleagues Dr. I.R. Butler, Dr. C. Nurse, Mr. N.F. Han, Mr. J.J. Ni for the assistance of some experiments, for many helpful discussions, and for the friendly atmosphere created by them.

I am very grateful to the technical staff of this department, in particular Dr. Chan and his staff members for the assistance of a number of NMR experiments, and Mr. P. Borda for his expert microanalyses.

I also want to thank Mrs. T. Schreinders for typing the manuscript.

To my wife, I express my greatest thanks for her encouragement and unflagging faith in me and my work.

To my parents and my wife

PART I

INTRODUCTION

CHAPTER 1

HOMOGENEOUS CATALYTIC HYDROGENATION

1.1 HISTORICAL REVIEW

Homogeneous catalytic hydrogenation of organic substrates by soluble transition-metal complexes is probably the most widely studied class of organometallic reactions. Olefins have been the most thoroughly examined substrates (equation 1.1), but many other functional groups such as acetylenes, aldehydes, ketones, nitro groups, and arenes have also been studied.

$$>C=C< + H_2 \xrightarrow{\text{catalyst}} -\overset{H}{\underset{|}{C}}-\overset{H}{\underset{|}{C}}- \qquad (1.1)$$

The first hydrogenation of an organic molecule using a soluble transition-metal complex was reported in 1938 by Calvin, who discovered that quinone was reduced to quinoline by a cuprous acetate-guinoline mixture at atmospheric hydrogen pressure and 100°C [1].

Iguchi in 1942 discovered that hydrogen was absorbed by aqueous solutions of cobalt(II) chloride containing potassium cyanide [2]; at room temperature the absorption corresponded to one hydrogen atom per cobalt atom. Such solutions were used for the hydrogenation of various organic compounds. This finding led to the most widely studied homogeneous hydrogenation catalyst, $[Co(CN)_5]^{3-}$. Such systems have been reviewed by Kwiatek and Seyler [3].

In the early 1950, investigators found that hydrogenation of the olefin was a side reaction of the oxo process of hydroformylation of olefins by $HCo(CO)_4$ [4-5] and that the product aldehyde itself could be reduced to alcohol in the same catalyst pot.

In 1954, Flynn and Hulbert discovered that at low temperatures ($\leqq$ 0°C) the complex $[Pt(C_2H_4)Cl_2]_2$ catalyzes homogeneously the hydrogenation of ethylene [6]. Reports of the more active hydrogenation catalysts in 1960-1963 did involve ruthenium [7-9] and platinum [10] complexes and considerable progress in the understanding of hydrogenation was also made during this period by Halpern's group and by others [7-11]. Yet very significant advances have been made by Wilkinson's group in the isolation and detailed study of the extremely active hydrogenation catalysts, $RhCl(PPh_3)_3$ [12] and $HRuCl(PPh_3)_3$ [13] both originally reported in 1965.

The last decade has seen a virtually exponential growth in the number of papers on the subject of homogeneous hydrogenation catalyzed by transition metal complexes, with a large number of reviews and specialized texts [14-27]. In particular, a comprehensive account of the whole field of transition-metal catalyzed homogeneous hydrogenation has also been available [16, 24].

1.2 SCOPE OF DISCUSSION

The reason for this unprecedented interest in homogeneous hydrogenation may lie in three primary research motives. First, both academic and industrial chemists have been searching for new selective and stereospecific catalyst systems. Secondly, interest in hydrogenation has been part of a general investigation of organometallic patterns of reactions. Finally, chemists have hoped that the relatively easily studied homogeneous systems would provide insights into the mode of activation of heterogeneous catalysts (but this appears to have a rational basis only in the little explored metal cluster complexes and in the supported homogeneous catalysts). Both industrial and academic reseachers have noted distinct advantages of homogeneous catalyst over heterogeneous counterparts: (1) milder reaction conditions; (2) ease of catalyst regeneration; (3) high efficiency, selectivity, and stereospecificity; (4) convenience for kinetic study.

As a result of this interest there are now numerous transition metal complexes which can function as homogeneous hydrogenation catalysts and virtually all transition metals have been studied in combination with various ligands in an effort to discover more efficient catalytic systems [16, 20, 24]. Complexes of the Group VIII elements, among others, have been found to be the most efficient catalysts. Especially effective combinations with π-acceptor ligands or strong ligand fields resulted in d^8 low-spin configurations. Such complexes have a number of properties

which influence their catalytic activity and selectivity. For example, bond stability, ligand substitution, number of electrons, and coordination sites available are among those properties.

Here, it must be recognized that the terms "catalyst" and "catalyst precursor" can apply to distinct species. The latter is the transition-metal complex that is synthesized and handled but when subjected to the catalytic reaction may undergo considerable modification (ligand dissociation and substitution, as well as metal valence change) before being converted into the active catalyst(s) directly involved in the catalytic cycle. Ideally the structure of the active species, as well as that of all other intermediates directly involved in the catalytic cycle should be established in order to study the various factors influencing catalytic behaviour. Unfortunately, such intermediates, by their very nature, are often too unstable to isolate, and indirect evidence of their constitution must be relied on. As a consequence few systems have been so thoroughly investigated that the mechanism proposed for them have been generally accepted. Nevertheless, it is useful to discuss basic processes occurring in a reaction such as hydrogenation, and classify the catalysts according to their characteristic features (mechanism, selectivity, etc.).

Discussion in this chapter is limited to hydrogenations catalyzed by the class of complexes known as the "Rhodium-Phosphine" type. These complexes have some unique advantages over other transition metal complexes. For example, most reactions require easily prepared and handled catalyst precursors. Mechanisms for some of these systems have been studied in

considerable detail and their catalytic behaviours have also been characterized very well. Most importantly, it has been this class of catalyst which has been employed, in the main, for asymmetric hydrogenation.

1.3 HYDROGENATION CATALYTIC CYCLES

Although mechanisms of homogeneous hydrogenations may differ from system to system, some common features are present in all hydrogenation cycles. They are:

(1) activation of hydrogen by formation of M-H bonds,

(2) activation of substrate by its coordination to metal,

(3) hydride transfer from the central metal to the coordinated substrate followed by formation of the reduced product. These are now discussed in this section.

1.3.1. Hydrogen Activation

The essential feature in catalytic hydrogenation is the activation of hydrogen. Yet, the precise manner in which molecular hydrogen reacts with the active catalyst species is not known. One possibility (for square planar d^8 complexes) is that an anti-bonding orbital of the hydrogen molecule accepts an electron from a filled metal orbital; another is that the bonding electrons of hydrogen attack a vacant metal orbital. In any event, a complex containing a hydride ligand is formed. The accumulated evidence concerning the mechanism of both homogeneous and heterogeneous catalytic hydrogenations indicates that hydrogen atoms of metal hydrides are trans-

ferred to the substrate in discrete steps by "insertion" and "reductive elimination" reactions. Thus the formation of metal hydrides from molecular hydrogen is an obligatory step in the catalytic cycle.

Two types of hydrogen activation have been distinguished:

(A) homolytic splitting by "oxidative addition" of hydrogen in which three different patterns can be recognized,

(a) monometallic H_2 oxidative addition to coordinatively unsaturated complexes with an over-all, two electron change (equation 1.2),

(b) monometallic H_2 oxidative addition to coordinatively saturated complexes accompanied by the loss of a ligand with a two-electron change (equation 1.3),

(c) bimetallic (mononuclear or dinuclear) H_2 oxidative addition in which the metal undergoes a one-electron change (equation 1.4).

(B) heterolytic splitting which does not require formal oxidation of the metal (equation 1.5),

$$M^n + H_2 \rightleftharpoons H_2M^{n+2} \qquad (1.2)$$

$$M^nCO + H_2 \rightleftharpoons H_2M^{n+2} + CO \qquad (1.3)$$

$$2M \text{ (or } M^n\text{-}M^n) + H_2 \rightleftharpoons 2HM^{n+1} \qquad (1.4)$$

$$M^n + H_2 \rightleftharpoons [HM^n]^- + H^+ \qquad (1.5)$$

The reverse reaction of equation (1.2), (1.3) or (1.4) is referred to as monometallic or bimetallic reductive elimination and the reverse reaction of equation (1.5) is well known as the protonolysis of a metal hydride.

The most thoroughly studied example of category (a) includes addition of H_2 to the families of Vaska's complex, $(R_3P)_2Ir(CO)Cl$ (equation 1.6) and Wilkinson's catalyst; $(R_3P)_3RhCl$, which will be discussed in the next section in more detail.

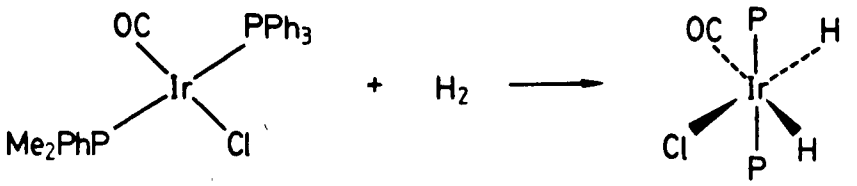

(1.6)

Such a concerted hydrogen addition would be expected to afford a cis-adduct and, for example, has shown to be so for reaction (1.6) [28, 29]. A reaction yielding a trans-adduct has also been reported, but these results seem best explained by isomerization of an initially formed cis-adduct [30].

Several coordinatively saturated complexes adding H_2 with the loss of a neutral ligand such as CO, R_3P, or N_2 (category b) are shown in equations (1.7) to (1.9).

$$Ir^+(CO)_3L_2 + H_2 \rightleftharpoons CO + H_2Ir^+(CO)_2L_2 \qquad (1.7)$$

$$Ir^+(CO)(PPh_2Me)_4 + H_2 \longrightarrow PPh_2Me + H_2Ir^+(CO)(P)_3 \qquad (1.8)$$

$$H_2Ru(N_2)(PPh_3)_3 + H_2 \longrightarrow N_2 + H_4Ru(PPh_3)_3 \qquad (1.9)$$

It may be considered that in these cases the ligand is lost prior to H_2 addition to avoid the formation of a high-energy, 20-electron intermediate.

It is probable that bimetallic oxidative addition of H_2 (category c) occurs at some stage of the catalytic cycle for "monohydride" catalysts (cf. section 1.4).

There is another mode of metal-hydride formation which does not require formal oxidation of the metal, the "heterolytic" cleavage of hydrogen (equation 1.5). This type of reaction is difficult to distinguish from oxidative addition of H_2 forming an intermediate dihydride adduct, followed by deprotonation of a hydride with a base (equation 1.10).

$$M{-}Y + H_2 \rightleftharpoons H{-}\underset{\displaystyle H}{\overset{\displaystyle |}{M}}{-}Y \xrightarrow{:B} HM + H^+BY^- \qquad (1.10)$$

Heterolytic H_2 activation is more likely with metal complexes in higher oxidation states where oxidative addition is less feasible. Equation (1.11) is an example of the over-all reaction without regard to the detailed pathway of heterolytic splitting of hydrogen [31].

$$RuX_2(PPh_3)_3 + H_2 \xrightarrow[C_6H_6]{Et_3N} HRuX(PPh_3)_3 + H^+NEt_3X^- \qquad (1.11)$$

It can now be recognized that both homolytic and heterolytic H_2 cleavage require the presence of a vacant coordination site on the metal. Among the four modes of H_2 activation it appears that monometallic H_2 oxidative addition (equation 1.2) is the most commonly encountered.

Coordinately unsaturated complexes are invariably more reactive than analogous saturated complexes toward the oxidative addition reaction due to the very nature of the reaction. Other factors controlling the reactivities of metal complexes can be the steric and electronic effects of ligands, and the nature of the metal [25].

The remaining aspect of H_2 activation is that this step must be reversible. Not only must the hydride complex be of sufficient stability that it is readily formed, it must be also labile enough that subsequent transfer of the hydride ligand to a substrate can occur. Nevertheless, many hydride complexes which are catalytically active are stable enough to be characterized and/or isolated (cf. sections 1.4, 3.3, and 6.3).

1.3.2 Substrate Activation

It is generally accepted that coordination of a substrate at a vacant site on the metal is necessary for hydrogenation to proceed. The formation of a π-olefin complex serves both to lessen the double bond character of the substrate (activation) and to place it in a favorable position (<u>cis</u>) for interaction with a hydride ligand (equation 1.12).

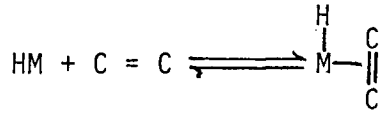

(1.12)

The hydride ligand may be present in the active catalyst species, or may be introduced by hydrogen activation. Although there has been little direct evidence for the formation of π-olefin hydride complexes in the course of

hydrogenation reactions, accumulated evidences indicate that transfer of the hydride ligand, leading to the formation of an alkylmetal intermediate, involves the oxidative addition-migratory insertion sequence (cf. section 1.4). Thus it may be assumed that the rate of transfer of the hydride is so fast that this intermediate cannot be detected. Osborn et al [32] studied in detail the activation of alkenes and alkynes as substrate during hydrogenation.

1.3.3 Hydride Transfer

The "intramolecular migratory insertion" of hydride into a coordinated substrate (equation 1.13) is another obligatory step in the hydrogenation cycle although this path has rarely been directly observed.

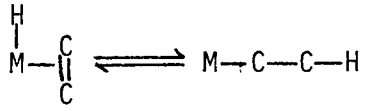

(1.13)

The migration of a hydride to an olefin is quite facile. The reverse process is known as "β-hydride elimination" which is one of the most important paths for metal-alkyl decomposition and olefin isomerization (cf. section 1.4). Consequently, complexes which contain both olefin and hydride groups are rare although there exists a known example [33].

It is believed that the hydride-olefin migratory-insertion step is highly stereospecific. For this reaction to occur, the hydride, the metal and the olefin π-bond must all become coplanar as shown in equation (1.14).

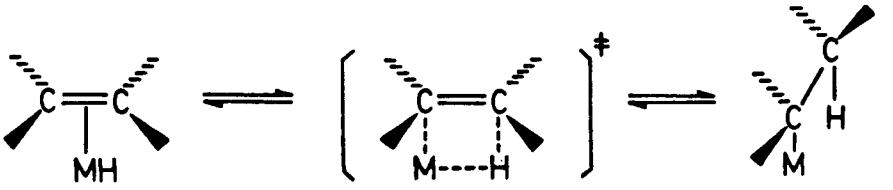

(1.14)

This stereochemical requirement has important consequences. For example, catalytic hydrogenations of olefins must be rigorously cis.

1.3.4 Product Formation

Four types of hydrogen transfer to alkyl groups (R) leading to the formation of hydrogenated product (RH) and regeneration of the active catalyst have been distinguished (equations 1.15 - 1.18):

$$HM^nR \longrightarrow M^{n-2} + RH \qquad (1.15)$$

$$HM^n + M^nR \longrightarrow 2M^{n-1} + RH \qquad (1.16)$$

$$HM^n + \cdot R \longrightarrow M^{n-1} + RH \qquad (1.17)$$

$$HX + M^nR \longrightarrow M^nX + RH \qquad (1.18)$$

Equations (1.15) - (1.17) involve homolytic cleavage and are known as intramolecular and intermolecular reductive elimination, respectively. In homolytic transfers, the formal oxidation state of the metal atom is decreased but in heterolytic transfers (equation 1.18) no change is involved. Reactions described by equation (1.18) have thus far been limited to those systems which activate hydrogen heterolytically. Electro-

philic displacement by proton of the metal-bonded alkyl group (with retention of configuration) has been suggested [7, 34, 35].

Transfers shown in equations (1.16) and (1.17) have been proposed mostly for monohydride catalysts (cf. section 1.4.1). On the other hand, intramolecular reductive elimination of an alkane from a cis-hydridoalkylmetal complex (equation 1.15) has frequently been postulated for dihydride catalysts (cf. section 1.4.2) in the belief that cis-hydridoalkylmetal complexes are usually kinetically and thermodynamically less stable than their dihydrido and dialkyl analogues. However, the evidence has so far been mainly indirect as failure of the proposed hydridoalkyl intermediate to accumulate in detectable concentration has generally precluded direct observation of this step.

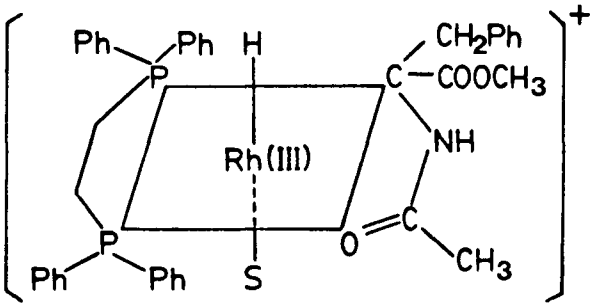

Fig. 1.1: The first known example of hydrido alkyl intermediate; S = solvent [46c].

The intermediate shown in Fig. 1.1 is the first hydrido alkyl complex to be directly observed in a catalytic hydrogenation. Halpern

and coworkers [46c] were able to intercept and characterize this intermediate using low-temperature NMR spectroscopy (^{1}H, ^{31}P, ^{13}C, ^{15}N for S = $MeCN^{15}$). The intermediate accumulated when the hydrogenation of methyl-(Z)-α-acetamidocinnamate in methanol solution, catalyzed by $[Rh(DIPHOS)(CH_3OH)_2]^+$ (DIPHOS = 1,2-bis(diphenylphosphino)ethane), was conducted at low temperature (<-40°C). A more recent report [36] describes the formation of analogous relatively stable hydridoalkyliridium complexes by insertion of activated olefins into one of the Ir-H bonds of cis-dihydridoiridium complexes and concludes that such hydrido alkyl complexes are intermediates in catalytic hydrogenation reactions. The subject of the formation of C-H bonds by reductive elimination has been reviewed recently by Halpern [37].

1.3.5 Summary

So far four basic steps involved in homogeneous hydrogenation catalytic cycles have been discussed without regard to the sequence of each step. These basic steps may combine in various ways in completing a catalytic cycle and the main combinations which have been distinguished for most Group VIII metal complex catalysts are summarized in Fig. 1.2. The operation of such hydrogenation cycles in "rhodium-phosphine" systems is discussed in the following section.

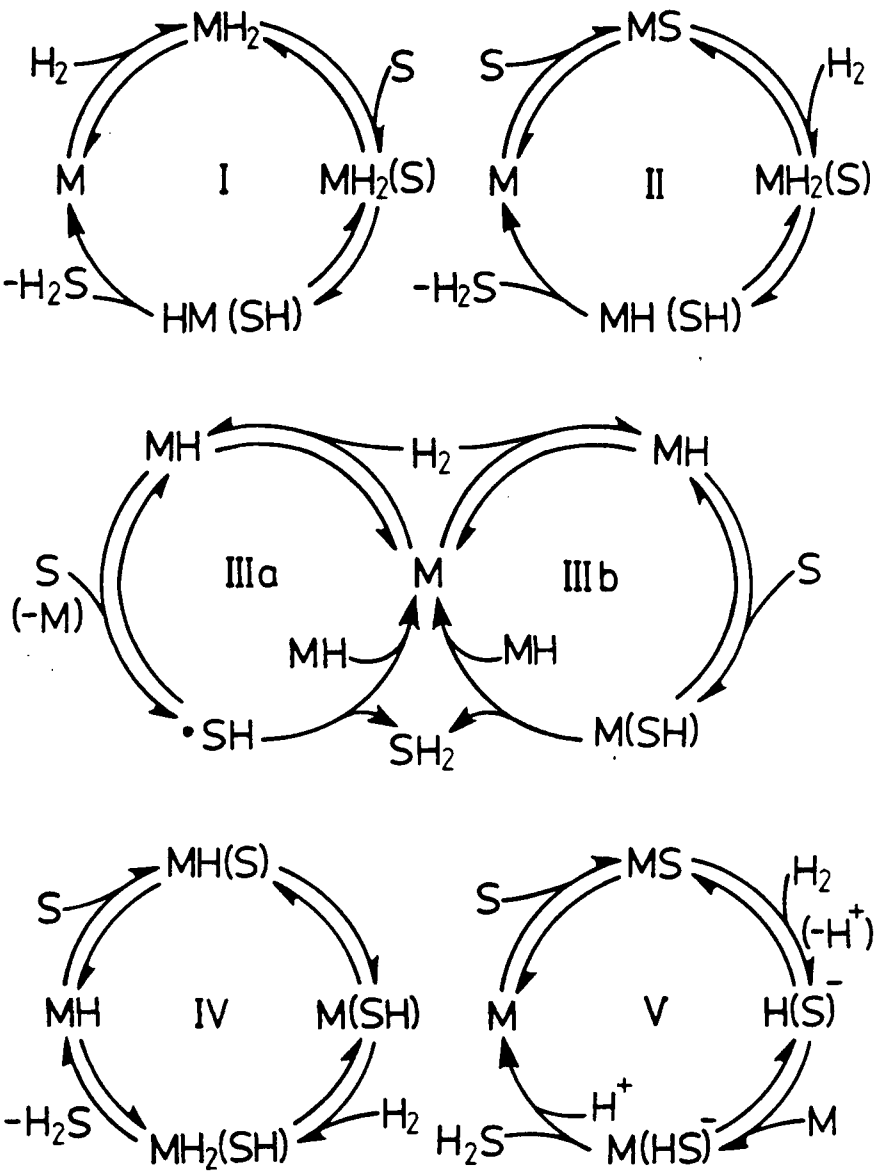

Fig. 1.2: Classification of homogeneous hydrogenation catalytic cycles. Cycles I - IV involve the homolytic cleavage of H_2; cycle V involves heterolytic cleavage. M or MH = active catalyst; S = substrate; SH = alkyl.

1.4 RHODIUM-PHOSPHINE CATALYSTS

The mononuclear, homogeneous rhodium-phosphine type catalysts can be roughly divided into the following two classes:

(1) monohydride catalysts having a single M-H group present at some characterized stage of the catalytic cycle,

(2) dihydride catalysts having two adjacent hydrides (cis-MH_2) present in one stage of the catalytic cycle; this class of catalysts can be subdivided into three groups:

(A) neutral rhodium-monophosphine systems,

(B) cationic rhodium-monophosphine systems,

(C) cationic rhodium-di(tertiary phosphine) systems.

Some characteristic features of each of these catalysts are discussed in the following subsections.

1.4.1 Monohydride Catalysts

This class of catalysts is well examplified by the complex $HRh(CO)(PPh_3)_3$. A proposed generalized catalytic cycle for hydrogenation and isomerization by monohydride catalysts is illustrated in Fig. 1.3.

The mechanisms of monohydride catalysts have been much less studied than those of the dihydride catalysts; so certain gross features of the mechanism of the former have not been well-established. A major uncertainty concerns the hydrogenolysis of the metal alkyl intermediate to form the products. This may involve simple oxidative addition of hydrogen, followed by reductive elimination of alkyl-hydride (outer circle

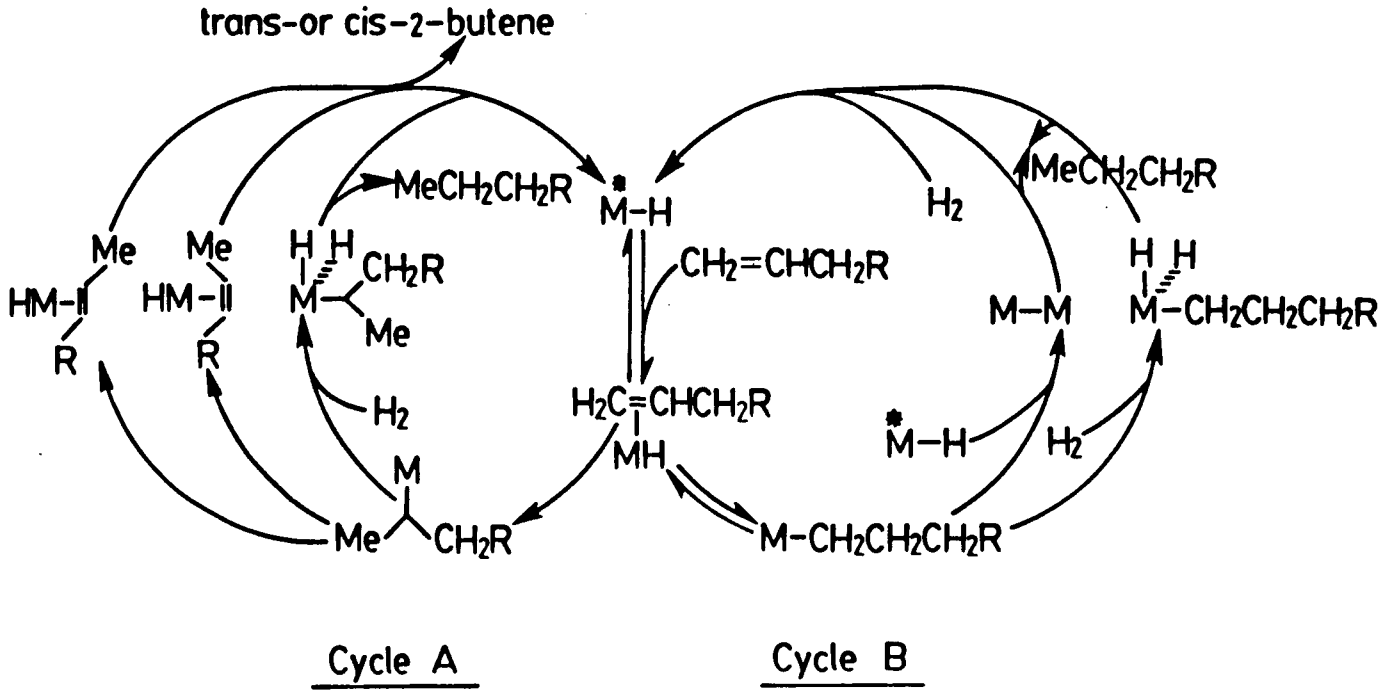

Fig. 1.3: The probable catalytic cycles for hydrogenation (cycle B) and isomerization (cycle A) of a terminal olefin. An asterisk indicates a site of unsaturation on metal. Ligands on metal atoms are omitted for clarity.

of the hydrogenation cycle B in Fig. 1.3), or intermolecular reductive elimination of the product affording a metal-metal bond, followed by oxidative addition of hydrogen to the metal atoms (inner circle of the cycle B in Fig. 1.3). Either path is plausible but so far neither has been well-established in any individual case. In both cases, however, the first step requires complexation of an olefin (simple, nonconjugated) to a coordinatively unsaturated metal hydride (M^*-H). The reversibility of the first two steps in the cycle B provides for the isomerization of simple olefins and the isotope exchange between the initial hydride (M^*-H) and hydrogens on the olefin, reactions which are characteristic of the monohydride catalysts. One such example of isotope exchange is given in equation (1.19).

$$CH_2\overset{MD}{=}CHR \rightleftharpoons M-CH_2\overset{D}{C}HR \rightleftharpoons CH_2\overset{MH}{=}CDR \qquad (1.19)$$

The metal-alkyl intermediate in the isomerization cycle A may undergo, in principle, two pathways to complete the catalytic cycle. The first pathway involves the isomerization of a terminal olefin to an internal olefin via "β-hydride elimination" forming a <u>cis</u>- or <u>trans</u>-π-olefin complex, followed by dissociation of the olefin as a product and regeneration of the monohydride catalyst. The second pathway involves simple oxidative addition of H_2 to the metal-alkyl complex followed by reductive elimination of H-R to yield the same hydrogenated product as is obtained from cycle B.

Both steric and electronic effects play important roles determining which catalytic cycle will operate preferentially. Steric bulk around the metal inhibits both formation of $M(CH(Me)CH_2R)$ and of M-M (Fig. 1.3), thus giving rise to hydrogenated products predominantly via oxidative addition of H_2 and reductive elimination sequences (outer circle of cycle B). On the other hand, catalysts with strongly acidic ligand(s) preferentially undergo the isomerization cycle to yield isomerized products, cis- and/or trans-olefin, since oxidative addition of H_2 and M-H to $M-CH_2CH_2CH_2R$ is retarded.

Equation (1.20) shows hydrogenation of terminal olefins catalyzed by a monohydride catalyst $HRh(CO)(PPh_3)_3$ under mild conditions[38].

$$RCH = CH_2 + H_2 \xrightarrow[25°C,\ <1\ atm,\ H_2]{HRh(CO)(PPh_3)_3} RCH_2CH_3 \qquad (1.20)$$

The pronounced substrate selectivity exhibited by this catalyst is illustrated by its failure to promote the reduction of cyclohexene due to the bulk of the phosphines [39]. Internal olefins are isomerized, but are not competitively reduced. It is also observed [40, 41] that in the absence of H_2, 1-pentene is isomerized to cis-2-pentene, but this isomer is quickly converted to the trans form. Internal olefins are isomerized more slowly than terminal ones.

1.4.2 Dihydride Catalysts

Quite a number of hydrogenation catalysts which function by a dihydride pathway have been discovered. The mechanism is thought to involve two possible routes, both of which may be simultaneously operative; both routes require vacant coordination sites for addition of H_2 and complexation of substrate after generating active catalyst(s) from the catalyst precursor.

As illustrated in Fig. 1.4, the "hydride route" involves oxidative addition of H_2 followed by coordination of substrate to form a dihydride intermediate with complexed substrate. The "unsaturate route" consists of coordination of substrate before oxidative-addition of H_2 to form the same dihydride-substrate intermediate. In addition to this important difference between the two routes some other features arise in the hydride route depending upon the types of catalyst precursors (vide infra). As mentioned in the preceeding section three groups of catalysts fall in this class of dihydride catalysts. Each of these will be discussed with reference to reaction mechanisms and other general features.

(A) Neutral Rhodium-Monophosphine Systems.

This group of catalysts can be best examplified by the complex $RhCl(PPh_3)_3$ known as Wilkinson's catalyst [12, 42]. The over-all catalytic cycle and side reactions for this catalyst are outlined in Fig. 1.5

This mechanism is a synthesis of Wilkinson's earlier studies [42] and Halpern's recent stepwide kinetic analysis [43]. Within this catalytic system, five rhodium intermediates have been directly observed and characterized, either by solution ^{31}P NMR studies or as isolated solids: $ClRhL_3$,

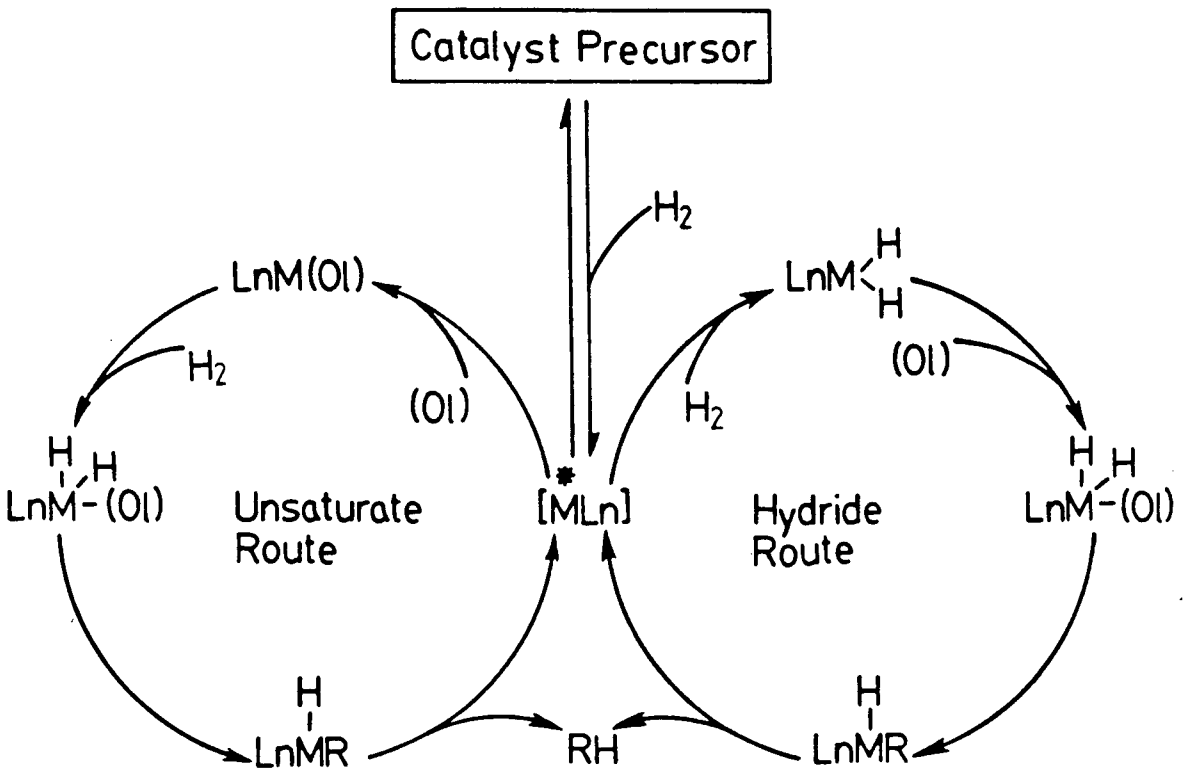

Fig. 1.4: Two possible catalytic hydrogenation cycles for dihydride catalysts. An asterisk on metal indicates a site of unsaturation. Ol ≡ olefin; R ≡ alkyl; RH ≡ reduced product.

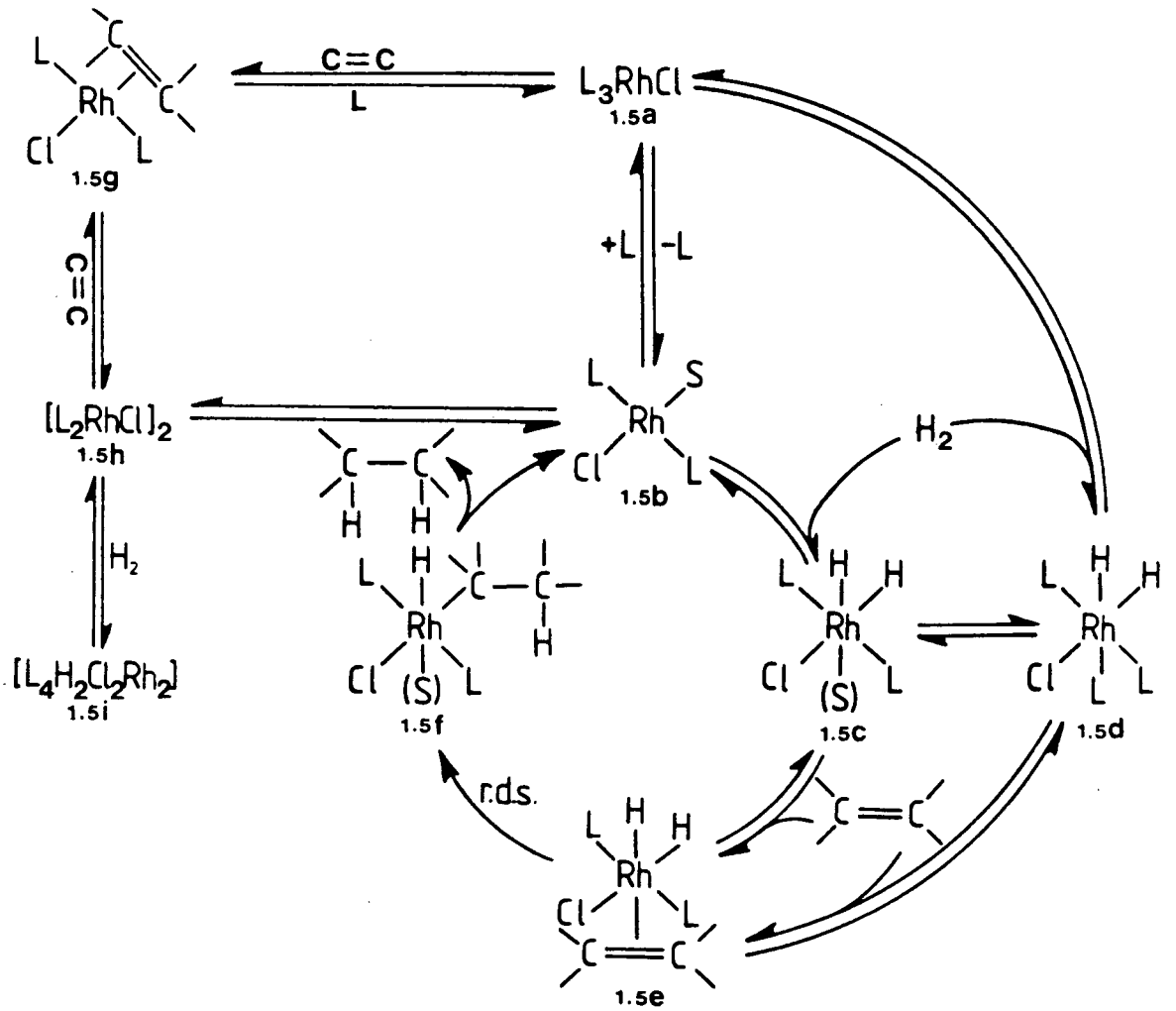

Fig. 1.5: Halpern's mechanism for hydrogenation of cyclohexene by Wilkinson's catalyst. S ≡ solvent; L = PPh_3 [25].

$ClRhL_2(C{=}C)$, $Rh_2Cl_2L_4$, $Rh(H)_2ClL_3$, and $Rh_2(H)_2Cl_2L_4$. However Halpern's studies reveal that none of these is directly involved in the kinetically significant catalytic cycle which is contained in the circle (Fig. 1.5). In fact, the accumulation of any of these five species should retard the over-all reaction rate. The over-all reaction can be divided into two parts:

(a) hydrogenation of catalyst precursor, $ClRhL_3$; and

(b) reaction of H_2RhClL_3 with substrate, i.e. cyclohexene.

The combination of these two parts corresponds to a "hydride route".

Halpern has shown that dissociation of a ligand from 1.5a affords the 14-electron intermediate 1.5b which then undergoes very fast hydrogenation to form the unsaturated dihydride 1.5c which is in equilibrium with free PPh_3, giving 1.5d. This route (1.5a $\rightleftharpoons$ 1.5b $\rightleftharpoons$ 1.5c $\rightleftharpoons$ 1.5d) is much faster than the direct hydrogenation of 1.5a, which was independently measured in the presence of excess PPh_3. Wilkinson originally proposed such a path for hydrogenating 1.5a but his proposal was based on the erroneous presumption that the dissociative equilibrium (1.5 a $\rightleftharpoons$ 1.5b) lies far toward the 14-electron complex, 1.5b. More recent measurements have shown this equilibrium to lie to the left. This discrepancy derives from the great air sensitivity of 1.5a, which reacts with O_2, giving dissociated $Ph_3P = O$ and values of low apparent molecular weight. Actually the intermediate 1.5b has a pronounced tendency to dimerize [44] and the dimer, 1.5h, adds H_2 on one rhodium atom forming 1.5i. However, in the presence of H_2 these side reactions are insignificant, since H_2 effectively

intercepts the complex 1.5b before it can dimerize. The complex 1.5g observed in the absence of H_2 is also insignificant in the catalytic hydrogenation of cyclohexene and similar substrates. A separate kinetic study of the reaction between the dihydride 1.5d and cyclohexene under pseudo-first-order conditions has revealed that the "migratory insertion" step (1.5e → 1.5f) is the slowest step in the over-all catalytic cycle. The subsequent reductive elimination step is apparently so fast that the reverse reaction, 1.5f → 1.5e, is kinetically insignificant, too. It may be noted that four complexes (1.5b, 1.5c, 1.5e and 1.5f) are invisible in the sense that these have not been directly observed, but their existence and stoichiometry were deduced from kinetic and equilibrium measurements. The stereochemistry suggested for the postulated alkyl hydride intermediate 1.5f is based on the trans effect. Tolman [45] used NMR to show that the phosphine trans to hydride in 1.5d is substitution-labile and to assign the stereochemistry of 1.5d.

The general characteristics of the Wilkinson catalyst can be summarized as follows.

Unconjugated olefins and acetylenes are readily reduced under mild reaction conditions but such substrates as arenes, ketones, carboxylic esters (and acids), amides, and nitro compounds are not reduced. Relative substrate reactivities for unconjugated olefins tend to parallel their tendencies to coordinate to Rh, thus reflecting the steric crowding exerted by the bulky phosphine ligands (vide infra).

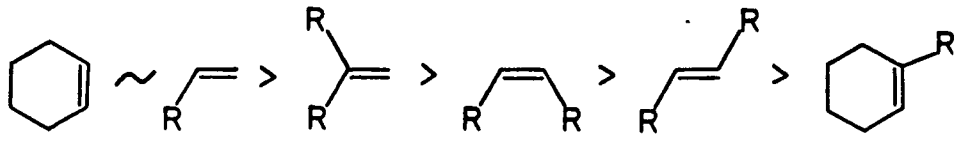

However certain good olefinic ligands appear to inactivate the catalyst and to inhibit the reduction. These include ethylene and 1.3-butadiene which are reduced at higher temperature or by using $RhI(PPh_3)_3$ instead of $RhCl(PPh_3)_3$. Examination of the reaction mechanism (Fig. 1.5) provides an explanation for this effect of the more strongly bonding olefins in terms of an alteration in mechanism (1.5a → 1.5g → 1.5h → 1.5i).

A remarkable feature of this catalyst is the lack of isomerization and isotopic exchange between D_2 and protons on the solvent or of scrambling between H_2 and D_2. These results can be explained in terms of the fact that the rate-determining step is migratory insertion of substrate into the Rh-H bonding followed by the rapid product-forming step (Fig. 1.5). The addition of H_2 is stereospecific (cis), which was proven by Wilkinson [42] in the deuteration of maleic and fumaric acids to give the meso- and dℓ-dideuterosuccinic acids, respectively. Both regio- and stereospecificity of such hydrogenations result in a number of features. Ergosterol acetate, for example, is reduced at the least hindered olefinic site from the less-crowded face of the steroid (equation 1.21) [20].

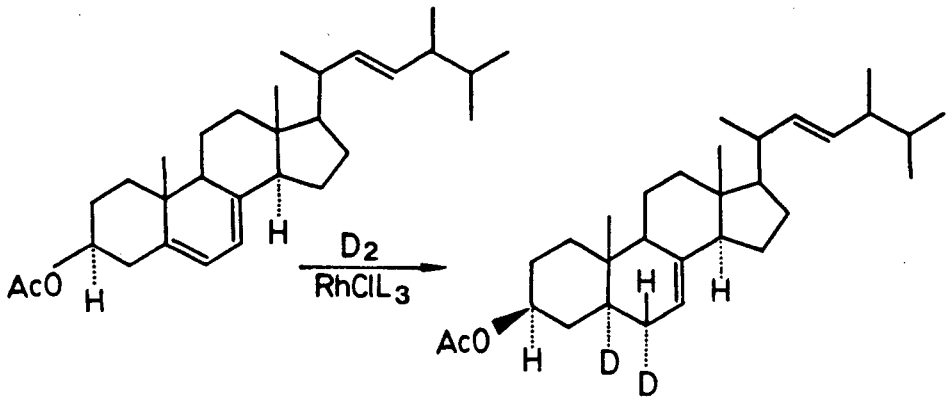

(1.21)

(B) Cationic Rhodium-Monophosphine Systems.

The complex of the type $[Rh(L)_2(Diene)]^+A^-$ (L = neutralphosphine or phosphite; Diene = 1,5-cyclooctadiene (COD), 2,5-norbornadiene (NBD); A^- = noncoordinating anion, ClO_4, BF_4, PF_6) fall into this group. This new system has been studied in considerable detail by Osborn's group [32].

Their work establishes that the cationic dihydride is generated by treatment of the catalyst precursor, $[Rh(NBD)(PPh_3)_2]BF_4$, for example, in an appropriate solvent S (S = acetone, THF, EtOH, etc.) and in the absence of substrate. In this pre-hydrogenation stage, the NBD ligand is reduced to give norbornane and the structure of the dihydride catalyst is proposed as a <u>cis</u>-dihydride with <u>trans</u>-phosphine as shown in equation (1.22).

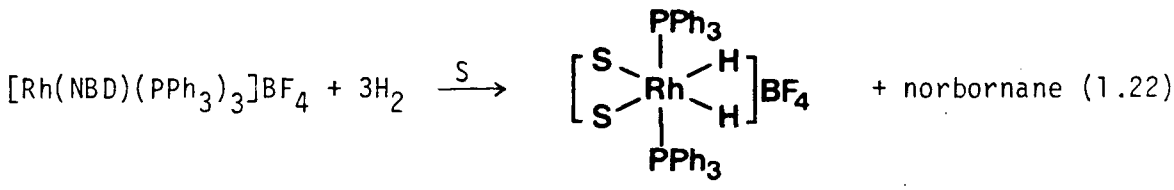

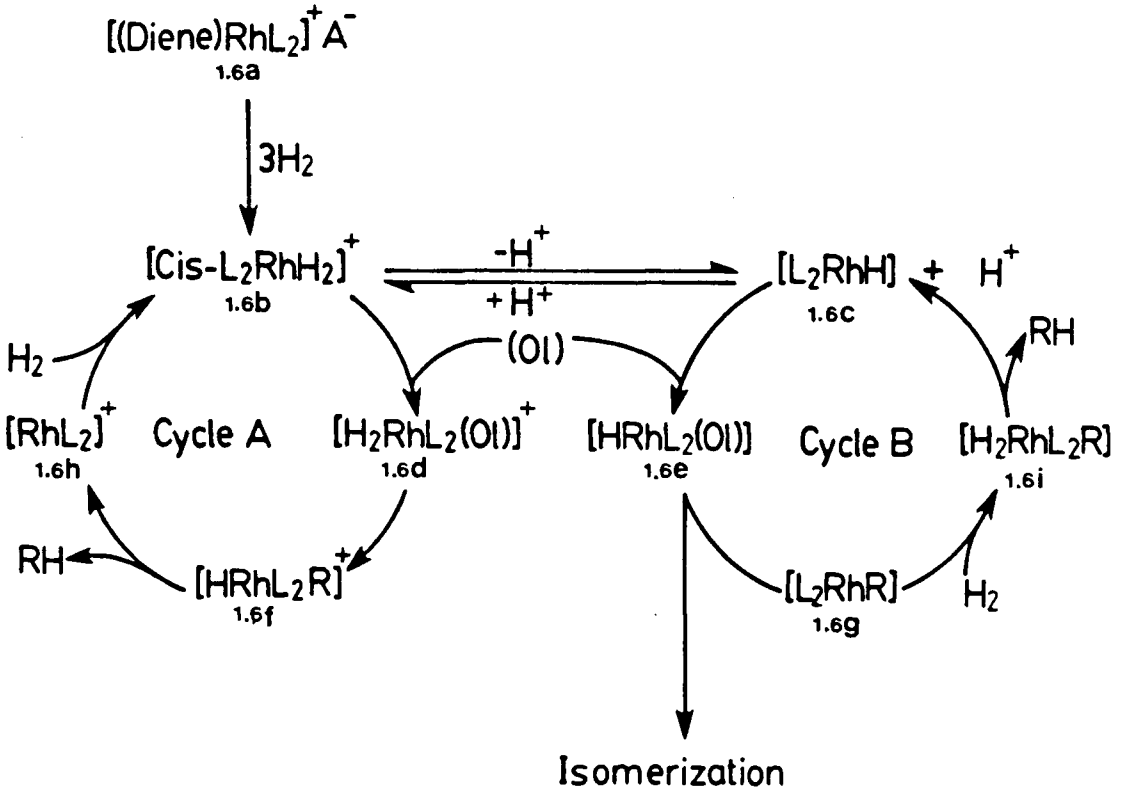

Fig. 1.6: Two possible catalytic hydrogenation cycles for cationic rhodium-monophosphine systems. Ol ≡ olefin; coordinated solvent is omitted.

As shown in Fig. 1.6, an important difference between these catalytic systems and the related Wilkinson-type systems is the presence of the Rh(I) monohydride catalyst governed by equilibrium; this is sensitive to the nature of L and S and can be shifted by addition of acid or base. Thus, for example, in the presence of excess acid the equilibrium is tilted toward the formation of the dihydride 1.6b which is a moderately active hydrogenation catalyst via a hydride route (cycle A). On the other hand, a base, i.e. NEt_3, shifts the equilibrium to the right to generate the monohydride 1.6c which is a powerful hydrogenation catalyst for simple olefins, as well as an isomerization catalyst (cf. section 1.4.1). One possible hydrogenation mechanism via 1.6c is shown in cycle B which is one of two hydrogenation pathways for monohydride catalysts illustrated in Fig. 1.3. It can be readily seen that if the rate of oxidative addition of H_2 to generate 1.6i is rate determining, then the isomerization in the figure is realized.

(C) Cationic Rhodium-Di(tertiary phosphine) Systems.

The complexes of the type $[Rh(L\text{-}L)(Diene)]^+A^-$ (L-L = chelating di(tertiary phosphine) ligands; Diene = NBD, COD; A^- = ClO_4, BF_4, PF_6, etc.) represent this group of catalysts. In general these complexes can be readily prepared by replacing two equivalents of monophosphines with one equivalent of di(tertiary phosphine).

The complex having two monodentate phosphines absorbs three equivalents of H_2, affording the dihydride catalyst (equation 1.22), whereas

those containing a conventional chelating, bidentate ligand such as "DIPHOS" (= $Ph_2PCH_2CH_2PPh_2$) absorb two equivalents of H_2, yielding the highly unsaturated complex (equation 1.23).

$$[Rh(DIPHOS)(NBD)]^+ + 2H_2 \xrightarrow{S} [(DIPHOS)Rh(S)_2]^+ + \text{norbornane} \qquad (1.23)$$

The difference between these two reactions has been rationalized on the basis that phosphines avoid becoming <u>trans</u> to hydrides whenever possible.

Halpern et al [46] and Brown et al [47] independently elucidated, in considerable detail, the mechanism of hydrogenation of some olefins involving di(tertiary phosphine) ligands. Their work establishes that the dominant mechanism for these systems involves an unsaturate route rather than a hydride route, as shown in Fig. 1.7. Here the ligand (L-L) is "DIPHOS".

An olefin complex 1.7c is in equilibrium with the catalyst 1.7b which is generated from the reaction of the catalyst precursor 1.7a with two equivalents of hydrogen. Halpern has measured equilibrium constants Keq for a series of olefin substrates. At ambient temperatures the rate-determining step, k_1, involves oxidative addition of H_2 to the unsaturated Rh(I) complex, 1.7c, giving a Rh(III) dihydride 1.7d which rapidly forms 1.7e by migratory insertion and subsequently product by reductive elimination. Three complexes in the catalytic cycle (1.7b, 1.7c and 1.7e) were

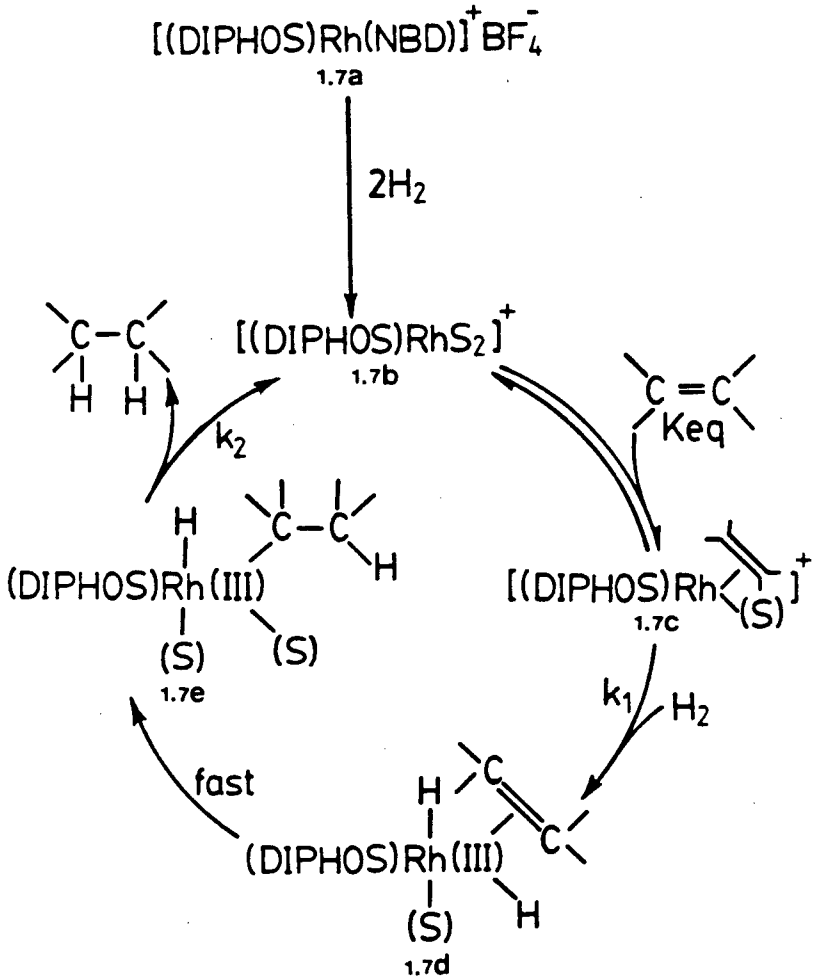

Fig. 1.7: Hydrogenation cycle for $[Rh(DIPHOS)(S)_2]^+$:

S ≡ solvent; olefin ≡ 1-hexene, etc.

characterized by NMR measurements, and by X-ray diffractions (1.7b and 1.7c). The complex 1.7b is a disolvated monomer, but is isolated as a binuclear $[Rh_2(DIPHOS)_2][BF_4]_2$ salt, in which each Rh atom is bonded to two P atoms and, through symmetrical π-arene coordination, to a phenyl ring of the diphosphine ligand of the other Rh atom (Fig. 1.8).

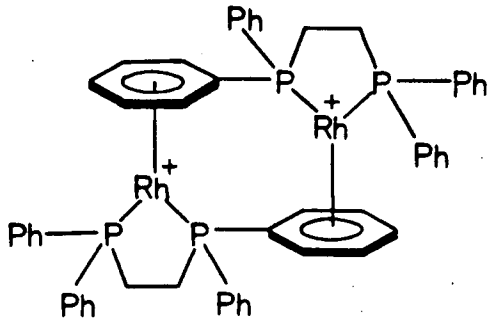

Fig. 1.8: Crystal structure of $[Rh_2(DIPHOS)_2]^{2+}$; 1.7b was isolated as the dimeric BF_4^- salt.

At low temperatures (<-40°C), k_2, a dissociative reaction, becomes slower than k_1, so that under these conditions, 1.7e accumulate and can be characterized by NMR (^1H, ^{31}P, ^{13}C, ^{15}N for S = MeCN[15]). As mentioned earlier, 1.7e is the first hydride alkyl complex to be directly observed in a catalytic hydrogenation. Failure to intercept the proposed 1.7d reflects

the very rapid transformation of 1.7d to 1.7e. The affinity of 1.7b for olefins strongly depends on the structure of the olefin. The amido-cinnamic acid forms a very strong complex with this Rh(I) center. As will be seen in Chapter 2, an X-ray structure of this complex accounts for its large association constant. The NMR studies of 1.7e (where S = MeCN) reveal the stereochemistry shown in Fig. 1.7. In passing from 1.7d to 1.7e, the hydride migrating to the olefin is <u>trans</u> to a phosphine.

Similar results with a range of chelating phosphines have also been reported by Baird et al [48] and Brown et al [47], demonstrating that hydrides are quite disfavored in these cases and broadly supporting the unsaturate route for a range of systems. However it must be emphasized that this generalization is not always followed. For example, the complex generated from pre-hydrogenation of $[Rh(AMPP)_2(NBD)]^+A^-$ (AMPP = O-anisyl-methylphenylphosphine) has the two monodentate phosphines <u>cis</u> according to ^{31}P NMR spectra (vide infra) [47a, b].

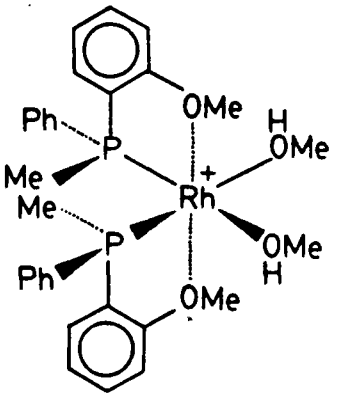

The O-methoxy groups are thought to be weakly coordinated, thus stabilizing this unexpected coordination geometry.

Furthermore the present investigation has found that some complexes having chelating phosphines produce metal hydride intermediates from the initial hydrogenation of catalyst precursors $[Rh(L\text{-}L)(NBD)]ClO_4$ (L-L = chiral and achiral ferrocenylphosphines), suggesting that some chelating di(tertiary phosphine) catalysts can undergo either a hydride route or a quite different mechanism which has not been distinguished so far. These observations will be discussed in Chapter 6.

CHAPTER 2

ASYMMETRIC CATALYTIC HYDROGENATION

2.1 GENERAL ASPECTS

Ever since Pasteur, in 1848, succeeded in separating two types of optically active crystals from sodium ammonium tartrate by hand with the aid of a microscope, there has been a great deal of interest in the production of optically active compounds. The importance of these compounds from a practical viewpoint can be readily recognized considering the fact that many substances are needed as the pure enantiomers. The pharmaceutical industry, for instance, is particularly interested in this area since an increasing number of drugs, food additives, and flavoring agents are being prepared as pure enantiomers. For example, in the late 1960's, it was found that L-3,4-dioxyphenylalanine (L-DOPA) could be used to treat Parkinson's disease and, in 1968, Knowles et al [82] succeeded in synthesizing L-DOPA with almost 100% optical yield using an asymmetric Wilkinson type catalyst. Their discovery provided the impetus for the large amount of work published since then in the field of asymmetric catalysis.

The field of asymmetric synthesis has been reviewed by a number of authors during the last decade [49-53]. The most comprehensive account of the whole field, covering all literature data up to 1975, is given in the books by Morrison and Mosher [54], and by Izumi and Tai [55]. There have also been published other reviews [56-64] on asymmetric catalysis with

special emphasis on asymmetric catalytic hydrogenation which is the topic of this chapter.

2.2 TERMINOLOGY

There are several terms that have been used routinely but somewhat confusingly in the field of asymmetric synthesis. It is, therefore, useful to review these terms before launching into the subject of asymmetric catalytic hydrogenation. The terminology here and in the subsequent discussion is based on the work of many pioneers in this field [65-68].

2.2.1 Types of Chirality

It is well known that the only requirement for optical activity is that a molecule should not be superposable on its mirror image. Therefore, in order to avoid confusion, the term "chiral" should be used for the necessary and sufficient condition for the existence of enantiomers. Overall chirality can be further factorized into three elements, which are treated in the order of chiral centers, chiral axes, and chiral planes whenever necessary.

(A) Central Chirality

There are four different types of molecules which possess this class of chirality. The most familiar and by far the most extensive group is that of asymmetry (point Group C_1), as in C^*_{abcd}, the asymmetric carbon atom.

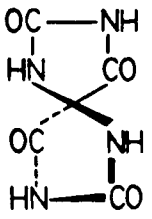

2.1a

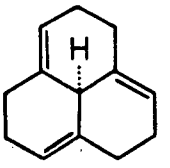

2.1b

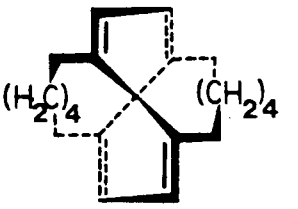

2.1c

Fig. 2.1: Molecules with central chirality.

The next higher symmetry point group contains one C_2 axis (point Group C_2) (2.1a in Fig. 2.1). The third of the point groups, as examplified by 2.1b, contains one C_3 axis as its only symmetry (point Group C_3). Finally, the fourth group has three C_2 axes (point group D_2). This case can be derived from tetrahedral C_{aaaa} by connecting the a's cyclicly as in 2.1c with four bridges of two kinds introduced alternately, each bridge having a plane of symmetry. As will be seen in section 2.4, most of the chiral rhodium-phosphine catalysts adopt chiral center(s) as the sole source of chirality.

(B) Axial Chirality

Here, the axis of chirality is derived by desymmetrization from a S_4 axis: this is its fundamental property. This form of chirality is examplified by allenes (2.2a), alkylidene-cycloalkanes (2.2b), spiranes (2.2c),

biaryls (2.2d), and admantoids (2.2e), as shown in Fig. 2.2.

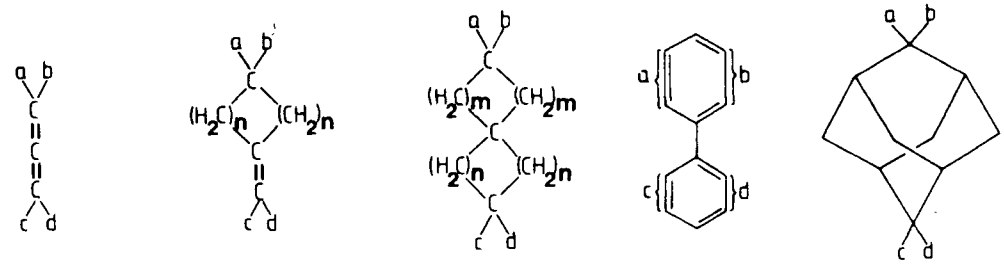

2.2a 2.2b 2.2c 2.2d 2.2e

Fig. 2.2: Molecules with axial chirality.

It can be noted that, if there is no distinction between the four groups, a, b, c, d, each compound has an S_4 axis. However, the four groups need not all be different: if a and b are different, and c and d are different, these molecules will be chiral.

(C) Planar Chirality

A plane of chirality is derived by desymmetrization of a plane of symmetry in such a way that chirality depends on a distinction between one side of the plane and the other. Thus metallocenes with two different substituents in one ring and other compounds shown in Fig. 2.3 are known to possess chiral plane(s).

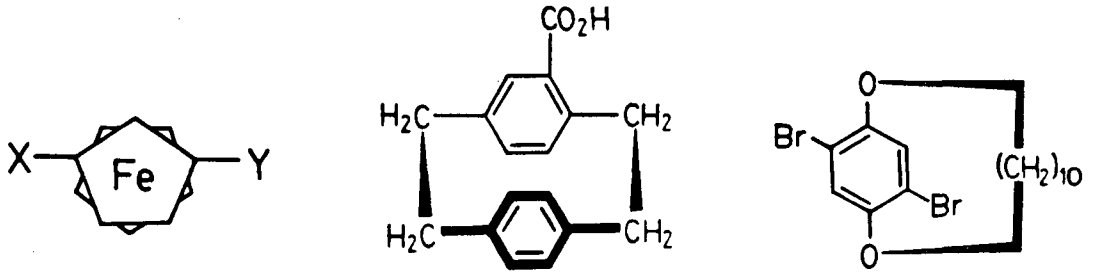

Fig. 2.3: Molecules with planar chirality.

2.2.2 Stereoisomeric Relationships [67b, 69]

In defining the spatial relationships of portions (atoms, groups, or faces) of molecules, one must distinguish between internal and external comparisons. In the former, the comparison takes place between portions of the same molecule, whereas in the latter it takes place between corresponding portions which are parts of different molecules.

(A) Internal Comparison

Groups (or faces of an olefin) are defined as "equivalent" if they can be internally interchanged by a C_n axis ($\infty > n > 1$). Fig. 2.4 illustrates some olefins with equivalent groups and/or faces.

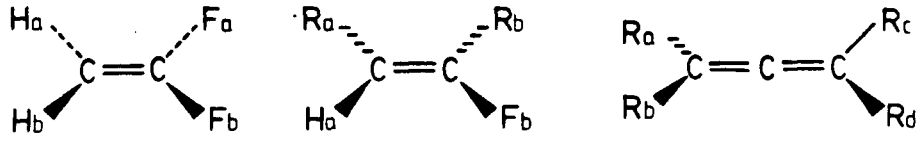

Fig. 2.4: Olefins with equivalent groups and/or faces by internal comparisons.

If groups (or faces) are internally interchanged only by an improper axis of rotation $S_n(n \geq 1)$, they are defined as "enantiotopic". The pairs of hydrogen atoms H_1/H_4 and H_2/H_3 in 2.5a are equivalent, whereas the pairs of hydrogen atoms H_1/H_2, H_3/H_4, H_1/H_3, and H_2/H_4 are enantiotopic. Although two R groups (or two H's) in 2.5b are equivalent, two faces of the molecule are enantiotopic.

2.5a 2.5b

Fig. 2.5: Molecules with enantiotopic groups or faces by internal comparisons.

If groups (or faces) cannot be internally interchanged by any symmetry operation, they are defined as "diastereotopic" (Fig. 2.6).

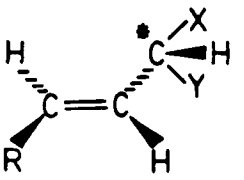

2.6a

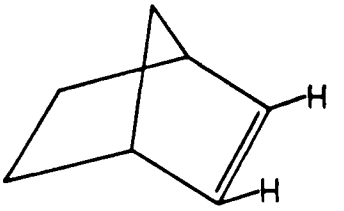

2.6b

Fig. 2.6: Molecules with diastereotopic groups or faces by internal comparisons.

The compound 2.6a is chiral while 2.6b is achiral. The molecule 2.6b possesses an enantiotopic pair of olefinic protons.

(B) External Comparisons

The internal symmetry criteria are equally applied to external comparison. The comparison can be achieved either by comparing two resulting molecules, or in a simple way, by applying the symmetry operation (C_n or S_n) to a molecule then comparing it with the resulting molecule. For example, two metal-olefin complexes shown in Fig. 2.7 are equivalent by external comparison since the two complexes are interchangeable by a C_2 operation.

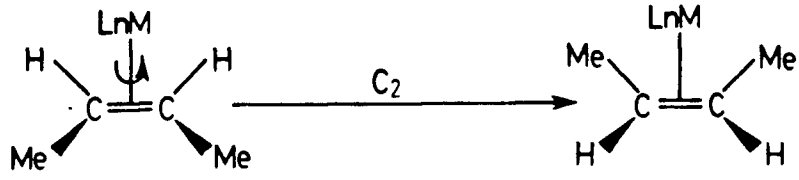

(R,S) - 2.7a (S,R) - 2.7a

Fig. 2.7: Equivalent metal-olefin complexes by external comparison.

If the resulting metal-olefin complexes are equivalent by external comparison then the faces of the free olefin are equivalent by internal comparison, but the converse is not always true. The absolute configurations of olefinic carbon atoms of 2.7a and 2.7b are determined on the basis of a hypothetical, three-membered metalocyclic compound in which the carbon atoms adopt a pseudo-tetrahedral geometry.

In the same vein, if the complexes are enantiomeric (i.e., complexes are non-superposable mirror images), then the faces of the free olefin are enantiotopic by internal comparison (Fig. 2.8).

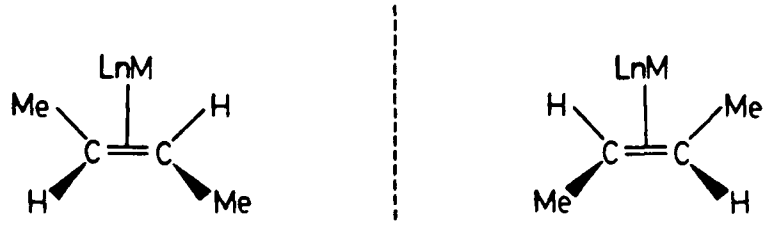

(S,S) - 2.8a (R,R) - 2.8b

Fig. 2.8: Enantionmeric metal-olefin complexes.

It can be noted in Fig. 2.8 that an achiral olefin with enantiotopic faces becomes chiral upon coordination to a metal. A molecule with enantiotopic groups or faces is said to be "prochiral".

When two metal olefin complexes are diastereomeric by external comparison (i.e., non-enantiomeric stereoisomers), then the free olefin has diastereotopic faces by internal comparison. There are two cases where diastereomeric complexes can be formed. They are:

(a) a complex in which a prochiral olefin is coordinated to a metal with chiral ligand(s) (Fig. 2.9),

(R, 2R, 3S) (R, 2S, 3R)

Fig. 2.9: Chiral diastereomeric metal-olefin complexes, not related by any symmetry operation.

(b) complexes in which an olefin with diastereotopic faces (chiral or achiral) is coordinated to a metal with chiral or achiral ligands (i.e., MLn or (R)-MLn) (Fig. 2.10),

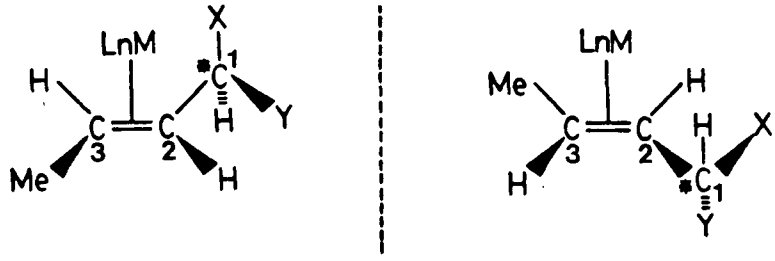

(1R, 2S, 3R) (1R, 2R, 3S)

Fig. 2.10: Diastereomeric complexes formed by coordination of a chiral olefin to an achiral metal complex. The MLn moiety can be either chiral or achiral.

It is the interaction shown in Fig. 2.9 that is the basis for most of asymmetric hydrogenation of olefins catalyzed by chiral Rh-phosphine complexes.

2.2.3 Stereo-Differentiating Reactions

The term "asymmetric reaction" was first used in 1894 by Fisher [70] and defined in 1904 by Marckwald [71] as "a reaction which produces optically active substances from symmetrically constituted compounds with the intermediate use of optically active materials but with the exclusion of all analytical processes". Later Morrison and Mosher [54] redefined an asymmetric reaction as "a reaction in which an achiral unit in an ensemble of substrate molecules is converted by a reactant into a chiral unit in such a manner that the stereoisomeric products are produced in unequal amounts".

Izumi and Tai [55] introduced the term "differentiation" and classified asymmetric reactions into two classes of stereo-differentiation reactions, each of which can be further divided into three types as follows:

(A) When the chirality participating in the differentiation occurs in a reagent, the catalyst, or the reaction medium, the reaction is classified as an enantio-differentiating reaction. Typically it yields enantiomers as products.

(B) When the chirality related to the differentiation is present in the substrate, the reaction is classified as a diastereo-differentiating reaction. It yields diastereomers as products.

(C) When the differentiation occurs at a prochiral face, prochiral center, or chiral center, the reaction is considered to be face-differentiating, topos-differentiating, or isomer-differentiating, respectively. These new definitions and classification for asymmetric reactions include not only those defined by Morrison and Mosher, but kinetic resolution of enantiomer and diastereomers with the exclusion of "asymmetric transformation" [54]. Although the terms asymmetric reaction and stereo-differentiating reaction are used interchangeably, the latter, whenever necessary, will be used throughout this thesis.

In conclusion, a stereo-differentiating reaction is achieved when a molecule containing enantiotopic or diastereotopic groups (or faces) is converted to a chiral molecule in such a way that one enantiomer (or diastereomer) is formed in excess. The efficiency of enantio-differentiation is expressed either as "enantiomeric excess (e.e.)" (equation 2.1) or as

"optical purity". The latter is equal to the rotation of the product of a reaction, [α] reaction, divided by the rotation of the optically pure compound, [α] pure (equation 2.2).

$$\% \text{ e.e.} = \frac{|R|-|S|}{|R|+|S|} \times 100 \qquad (2.1)$$

$$\% \text{ optical purity} = \frac{[\alpha]\text{reaction}}{[\alpha]\text{pure}} \times 100 \qquad (2.2)$$

The optical yield is defined as the optical purity or enantiomeric excess of the reaction product divided by the optical purity of the chiral reagent used. When the reagent is optically pure the three terms are equal.

2.3 ASYMMETRIC CATALYTIC HYDROGENATION

2.3.1 General

Of various types of stereo-differentiating reactions, catalytic enantio-differentiating reactions are in principle the most effective way of obtaining optically active compounds. In this regard the most spectacular achievements, obtaining high optical yields approaching 100% e.e., have been observed in the hydrogenation of prochiral olefinic substrates. The catalysts are chiral rhodium-phosphine complexes (Fig. 2.11).

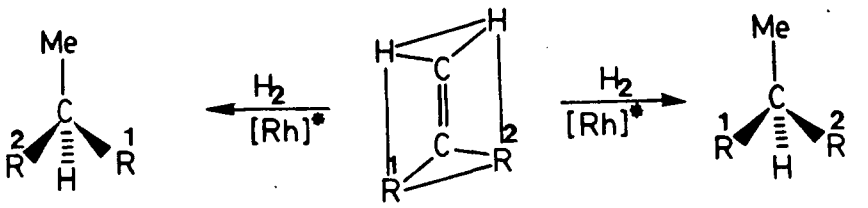

Fig. 2.11: An example of enantioface-differentiating reaction of a prochiral olefin by a chiral rhodium catalyst.

The mechanism of enantioface-differentiation (commonly called asymmetric induction) in the reactions represented in Fig. 2.11 is of particular importance, and has been the subject of intensive studies. This is because general guidelines can hardly be given as to how to design asymmetric reactions to obtain maximum optical yields without a precise knowledge of the mechanism.

The last decade has seen the burgeoning of both experimental and theoretical studies in this area. The former has been mainly concerned with the empirical modification of catalysts and substrates to increase optical yields and thus to gain an insight into the origin of stereo-differentiation. This leads, inevitably, to less emphasis on detailed reaction mechanism. The clarification of mechanism in terms of both kinetic data and stereochemical models is vital to the understanding of the origin of stereo-differentiation. The purpose of the next section is to review the research devoted to these studies.

2.3.2 Over-all Reaction Mechanism

Although chiral rhodium-phosphine complexes have been employed almost universally for studies of asymmetric catalytic hydrogenation, it is only with a relatively limited combination of catalysts and substrates that very high optical yields (>95% e.e.) have been obtained. The best substrates are amino acid precursors as shown in equation (2.3) and the hydrogenation is catalyzed by cationic rhodium-phosphine systems in polar solvents such as acetone or alcohols. The catalytic complexes typically involve chiral rhodium-di(tertiary arylphosphine) systems (Fig. 2.12), although reasonably high optical yields also have been obtained with rhodium-monophosphine systems.

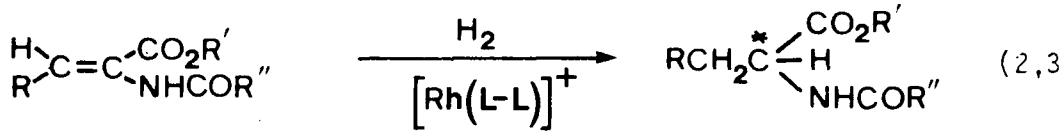

(2.3)

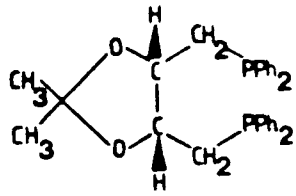

(R,R)-DIOP

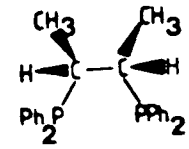

(S,S)-CHIRAPHOS

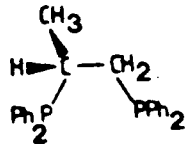

(R)-PROPHOS

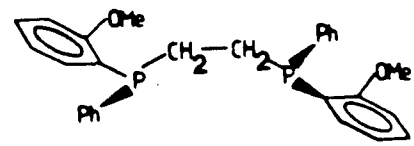

(R,R)-DIPAMP

Fig. 2.12: Some representative chelating di(tertiaryarylphosphine) ligands.

The mechanism of asymmetric hydrogenations represented by equation (2.3) has been studied in considerable detail by several research groups [46, 47, 64, 72-74]. Their work establishes that the kinetic and mechanistic features of the achiral $[Rh(DIPHOS)(solvent)_2]^+$ system depicted in Fig. 1.7 [46] are virtually identical with those of its chiral counterparts $[Rh(L\text{-}L)^*(solvent)_2]^+$ ($L\text{-}L^*$ = DIOP, DIPAMP, CHIRAPHOS, and PROPHOS) (Fig. 2.12) with the exception of the features discussed below that are specifically related to the formation of diastereomeric intermediates (Fig. 2.13). It should be noted, however, that almost all studies to date employ di(tertiary arylphosphine) ligands in which four aryl groups are bound to phosphorus.

Fig. 2.13 outlines the mechanism of asymmetric hydrogenation depicted by equation (2.3). As stated previously, when the chiral catalytic systems are employed, the mechanistic scheme of Fig. 1.7 must be modified, in accordance with the fundamental principle discussed in section 2.2.2 (B), so as to accommodate the formation of diastereomeric forms of the adduct corresponding to 1.7c and of the further reaction intermediates. The structure of the $[Rh(L\text{-}L)(substrate)]^+$ adduct has been established by NMR (^{31}P, ^{13}C, and ^{1}H) and by x-ray analysis (when L-L = DIPHOS, R^1 = Ph, R^2, R^3 = Me; when L-L = (S,S)-CHIRAPHOS, R^1 = Ph, R^2 = Et, R^3 = Me), revealing chelation of the substrates to the Rh atom through the carbonyl oxygen of the amide group as well as through normal η^2-coordination of the C = C bond [46, 72]. The stereochemistry of the product can thus be correlated with that of the adduct diastereomer from which it is derived

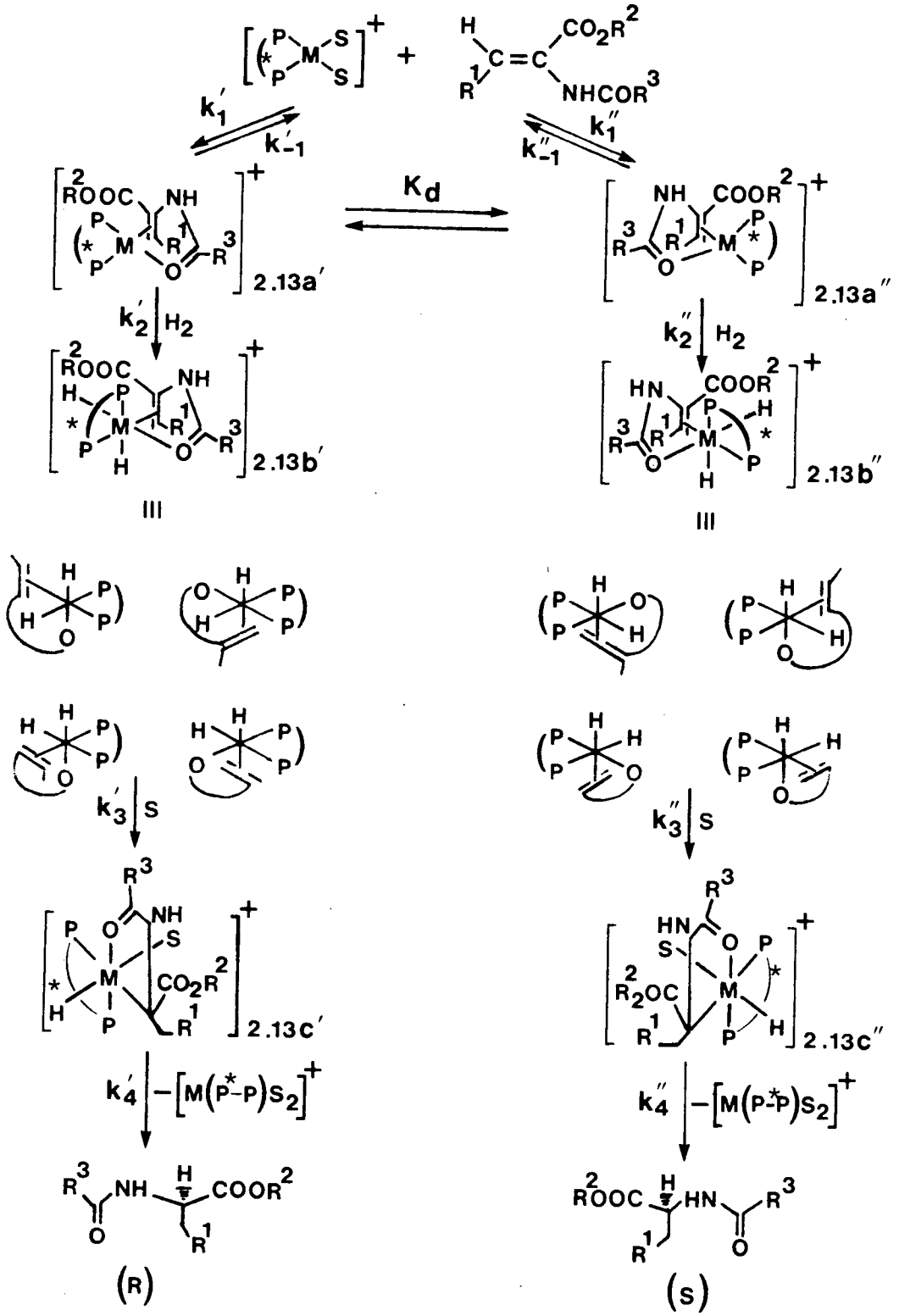

Fig. 2.13: The mechanism of asymmetric hydrogenation of amino acids with $[M(P^{*}\text{-}P)S_2]^{+}$ ($P^{*}\text{-}P$ = CHIRAPHOS, DIPAMP; M = Rh; S = MeOH)[64,76d].

in accordance with Fig. 2.13, since it is known that, for the catalytic systems employing di(tertiary phosphine) ligands, (i) the oxidative addition of H_2 and subsequent steps are irreversible, and (ii) the migratory insertion of H_2 to the coordinated substrate is stereospecific giving a cis-endo product. Thus the (R)-product is produced from 2.13a′ and the (S)-product from 2.13a′′

2.3.3 Mechanisms of Enantioface-Differentiation

Asymmetric hydrogenation (an enantioface-differentiating reaction) as shown in Fig. 2.13 is a multistep process, and there is more than one stage in which a pair of diastereomeric transition states (or intermediates) are formed competitively, giving rise to stereoisomers in different portions.

$$\begin{array}{ccccccc} A & \xrightarrow{k'_1} & I'_1 & \longrightarrow & \cdots\cdots & \xrightarrow{k'_n} & P' \\ \Big\Vert\!\uparrow K_d & & & & & & \\ B & \xrightarrow{k''_1} & I''_1 & \longrightarrow & \cdots\cdots & \xrightarrow{k''_n} & P'' \end{array} \qquad (2.4)$$

$$[P']/[P''] = k'_1[A]/k''_1[B] = k'_1K_d/k''_1 = e^{\Delta\Delta G^{\ddagger}/RT} \qquad (2.5)$$

Equations (2.4) and (2.5) show that the ratio of stereoisomers produced (either as products or as intermediates), or the ratio of the reaction rates in competitive reactions, depend on the difference between the activation energies of the transition states $\Delta\Delta G^{\ddagger}$ (Curtin-Hammett principle) [75]. The origin of stereo-differentiation can thus be ascribed to this energy

difference which is often referred to as diastereotopic discrimination. Equation (2.5) represents a special case in which only a single stage process is involved to produce stereoisomeric products from two diastereomers A and B, but some other circumstances should be taken into consideration in a multistep process such as asymmetric hydrogenation in order to predict the degree and origin of stereo-differentiation.

In this regard two mechanisms of enantioface-differentiation can be recognized as follows.

(A) The use of stereochemical models

If the corresponding rate constants in the two columns in Fig. 2.13 are the same, that is, $k'_2 = k''_2$, $k'_3 = k''_3$, and $k'_4 = k''_4$, then the enantiomeric excess can be determined by the value of K_d, independently of the reaction process. Therefore the predominant enantiomer of the product will arise from the predominant diastereomer of the catalyst-substrate adduct. The Curtin-Hammett principle then reduces to equation (2.6), where $\Delta\Delta G^{\ddagger}$ is the free energy difference between two diastereomeric transition states leading to the corresponding catalyst-substrate adducts.

$$[R]/[S] = K_d = e^{\Delta\Delta G^{\ddagger}/RT} \qquad (2.6)$$

The other way in which K_d can affect the enantiomeric excess is that the attainment of K_d is slow, namely, the first step (k'_1/k''_1) is the rate determining step. In any event, it is the preferred mode of initial binding of the prochiral substrate to the catalyst that dictates the

mechanism of enantioface-differentiation of these catalyst systems. Thus if the catalyst-substrate adduct 2.13a (Fig. 2.13) exists as a single static chiral conformer 100% e.e. would be expected in hydrogenation.

This type of argument has been used by Bosnich et al [76] who have suggested that steric rigidity of the metal complex containing chiral di(tertiary arylphosphine) ligands is a necessary condition to maximize the K_d value (Fig. 2.13). Namely, among many possible chiral conformations of five membered or higher membered chelate rings formed by this class of bidentate ligands, the most stable chiral conformation predominates due to the result of steric requirement that non-hydrogen substituent(s) of the chiral ring atom(s) be disposed equatorially. In Fig. 2.14(A) are shown the preferred conformations of (S,S)-CHIRAPHOS, (R)-PROPHOS, (S,S)-SKEWPHOS, and (S)-CHAIRPHOS. Except for (S)-CHAIRPHOS, they dispose the four phenyl groups as well as the substituents on the carbon back-bone in a preferred chiral array. As a result a prochiral olefin approaching a metal atom incorporating this chiral ring is now induced to adopt a preferred (energetically more stable) diastereomeric configuration by this chiral array of the aryl groups. If the chiral conformation of these catalyst systems were non rigid at least two diastereomeric conformers would result through the ring interconversion process (Fig. 2.14B). The effect would be to "wash-out" any discrimination in such non rigid systems. The same authors [76] have tested this hypothesis and successfully predicted optical yields and product configurations using the chiral ligands shown in Fig. 2.14. For example, (S,S)-CHIRAPHOS and (R)-PROPHOS stabilize enan-

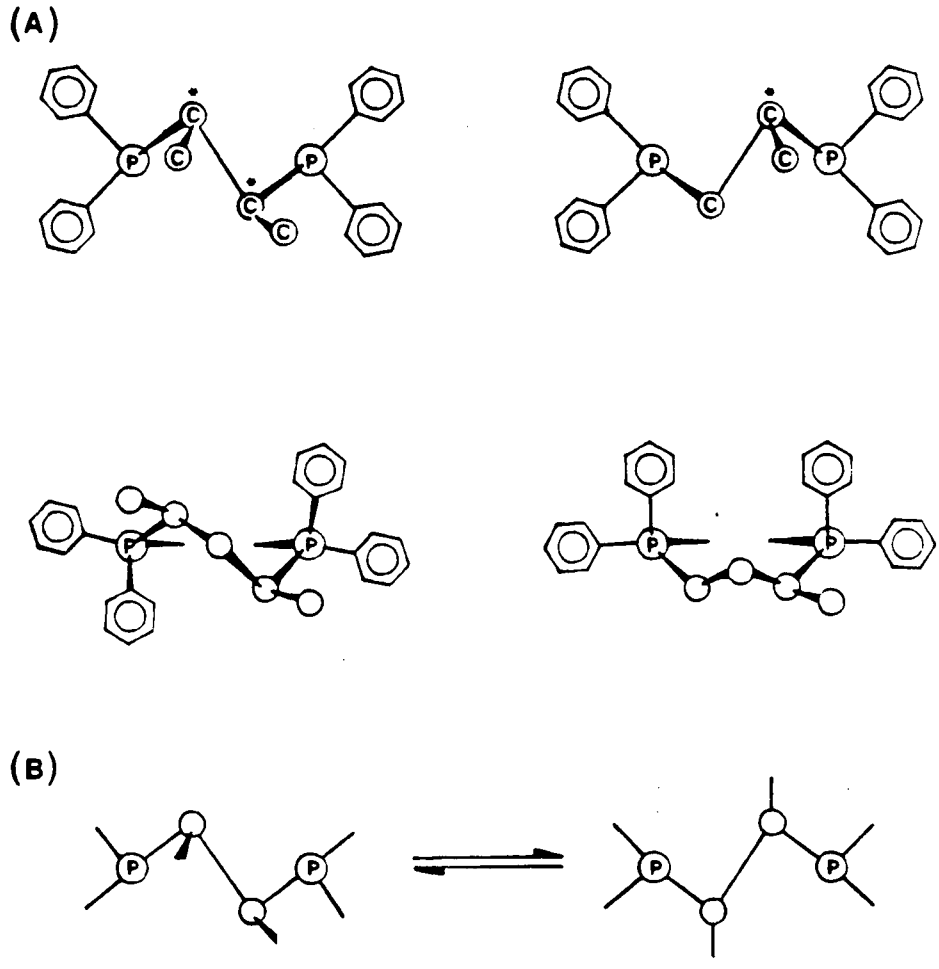

Fig. 2.14: (A) The preferred conformation of (S,S)-CHIRAPHOS, (R)-PROPHOS, (S,S)-SKEWPHOS, and (S)-CHAIRPHOS.

(B) The ring interconversion process between two diastereomeric conformers [76]. The Rh atom to which the two P atoms are bound is omitted for clarity.

tiomeric (more precisely diastereomeric) ring conformations and thereby generate opposite product configurations.

Knowles' group [77] had earlier produced evidences for these ideas on the basis of stereochemical models of complexes of the type $[Rh(L\text{-}L)^*(Diene)]A$ ($L\text{-}L^*$ = chelating di(tertiary arylphosphine)). They suggested, without definitive mechanistic proof, that the absolute configurations of products are solely determined by the orientation of the four aryl groups in these catalyst precursors where they are arranged around the metal in an alternating edge-face manner as if the whole molecule had a C_2 axis of symmetry. In the case of (R,R)-DIPAMP, for instance, substituents in a prochiral olefin lying in the quadrants 2 and 4 experience less steric repulsion than those lying in 1 and 3 (Fig. 2.15). Therefore, a (S)-amino acid is produced predominantly from (Z)-α-acetamidocinnamic acid but, in the case of (E)-olefin, as in the third and fourth boxes, both re- and si-faces force a large group to be in a hindered quadrant, thus resulting slower reaction rates and inefficient low optical yields [78] although the preferred isomer is still the same (S)-configuration.

(B) Kinetic approach

If, however, the rate constants in a given pair in Fig. 2.13 are different in all steps, then the final enantiomeric excess will be determined by the difference in the relative energies of two diastereomeric

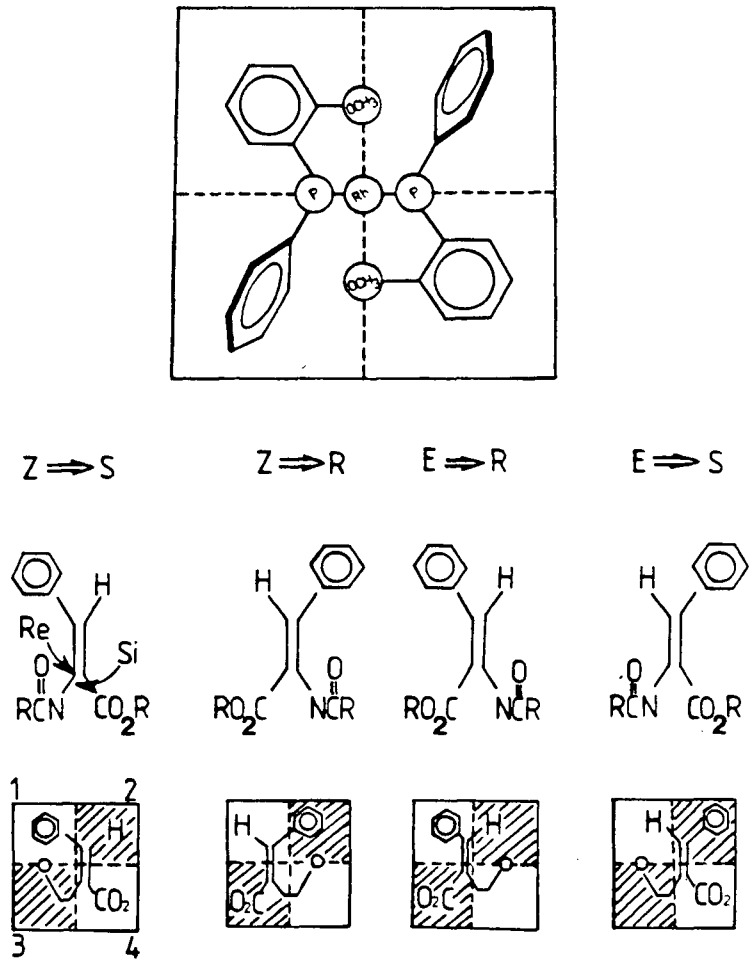

Fig. 2.15: Quadrant theory suggested by Knowles [77].

transition states lying in the rate-determining step (k'_n/k''_n). The Curtin-Hammett principle then requires (cf. equation 2.4)

$$[R]/[S] = k'_n[I'_n]/k''_n[I''_n] = e^{\Delta\Delta G^{\ddagger}/RT} \qquad (2.7)$$

Thus in one extreme the K_d value can be unity and yet significant enantio-differentiation will be achieved, and in another extreme the predominant enantiomer of the product arises from the minor diastereomer of the catalyst-substrate adduct due to the much higher reactivity of the minor diastereomer. In this connection Halpern et al [73], for the first time, demonstrated that, for the reaction depicted by Fig. 2.13, it is not the preferred mode of initial binding of the prochiral olefinic substrate to the catalyst but rather differences in the rates of oxidative-addition of H_2 that dictates the enantiomeric excess. The most striking features of their findings are: (i) the predominant diastereomer of the catalyst-substrate adduct $[Rh((S,S)\text{-CHIRAPHOS})(\text{substrate})]^+$ is the one in which the C_α-re face of the olefin is coordinated contrary to the Knowle's quadrant theory (cf. Fig. 2.14), (ii) the configuration of the

product is derived from the minor diastereomer not the major one. Evidence for the same conclusion has also been obtained in the $[Rh(R,R\text{-DIPAMP})]^+$-catalyzed hydrogenation of related substrates. Brown et al [47a, c] initially reported that, with this catalyst at room temperature, the ratio of diastereomeric catalyst-substrate adducts (although the absolute configurations could not be assigned) was approximately equal to that of two enantiomeric products. The prevailing chirality of the product was that derived from the major diastereomer. However, at low temperature ($\sim$ -40°C), where the interconversion of the diastereomers is frozen out, it was found that only the minor diastereomer reacts directly with H_2 to yield, for example, the (S)-amino acid in the case of (Z)-α-cinnamic acids. The major diastereomer reacts slowly at a rate independent of the H_2 concentration [64, 74]. Judging from these observations, the minor diastereomer should be the one in which the C_α-re face is coordinated (Fig. 2.13) again contrary to the Knowles' prediction.

Thus, according to these results, it is expected that the enantiomeric excess should decrease, with the possibility of eventual reversal of predominant product chirality, with increasing H_2 pressure, since the product chirality is again governed by the relationship expressed in equation (2.7) with the initial binding step (k''_1/k''_1) becoming rate deter-

mining. Another consequence is that, provided the major diastereomer exhibits some reactivity toward H_2 (as it must if the enantiomeric excess is less than 100%), the optical yield may decrease with decreasing temperature due to the fact that the diastereomeric interconversion process becomes "frozen out" at sufficiently low temperature. There are reports supporting this argument [79]. The striking difference between reactivities of the diastereomeric adducts toward H_2 is difficult to explain although it is not unexpected that the less stable of a pair of diastereomers exhibits the higher reactivity due to its higher initial free energy. One possible explanation suggested by Bosnich [76c] and by Halpern [64] is that, if the H_2 oxidative addition step is endothermic and rate determining, then the more stable the cis-dihydride intermediate, the lower will be the corresponding transition state energy (Hammond hypothesis). The relative stabilities of the diastereomeric products now become opposite to that of the parent catalyst-substrate adducts as shown in Fig. 2.16. Thus the rate of hydrogenation becomes fastest via the most stable of four dihydrido intermediates derived from the minor diastereomeric adduct (cf. Fig. 2.13). The authors reported that the space-filling models were inconclusive in deciding which of the four intermediates is the most stable. However, it is also possible that the H_2 addition step is an exothermic process, and thus the relative rates for the formation of the dihydrido intermediates depends both on the relative reactivities of two diastereomers (k'_2/k''_2) and on the equilibrium concentration (k_d) of the two. Furthermore, any other step, for example,

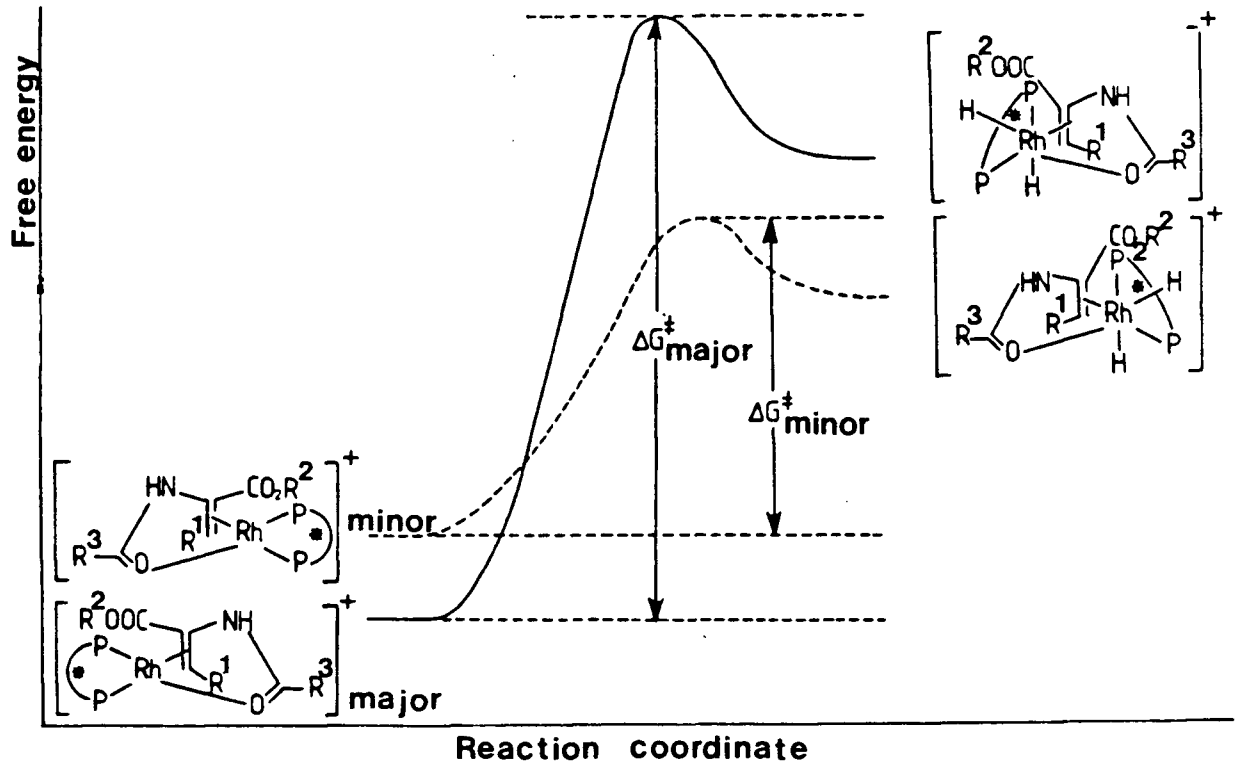

Fig. 2.16: Schematic reaction coordinate profiles for the enantioface-differentiating reactions of the diastereomeric $[Rh(P\text{-}P)^{*}(substrate)]^{+}$ with H_2 [64, 76c, d].

the migratory insertion step (k'_3/k''_3) may be rate determining. In the event the same assumptions and the Curtin-Hammett principle can be applied to describe the mechanisms of stereo-differentiation. It should be pointed out that at low temperature k_3 is rate determining for the Rh-DIPHOS catalyzed hydrogenation (cf. section 1.4.2(C)). Finally, in connection with this mechanism, it should also be pointed out that, if (although unlikely) rate constants are different in all stages except in the rate determining step, then again the enantiomeric excess will be determined by the pre-equilibrium constant K_d.

The overall mechanism shown in Fig. 2.13 can be used to explain the results of a number of studies. However, there are instances where the effects of solvent, temperature, and H_2 pressure are not as expected (cf. section 2.4). Furthermore, little has been said about the possibility of electronic effect on stereo-differentiation and the effects of substituent ligands other than aryl groups.

2.4 CHIRAL RHODIUM-PHOSPHINE CATALYSTS

Most of the chiral catalysts which have been studied so far for asymmetric homogeneous hydrogenations involve rhodium complexes of chiral phosphine ligands. In a majority of these cases, it can be assumed that, as shown in the previous section, kinetic and mechanistic features for these chiral systems are virtually identical with those of their achiral counterparts discussed in the previous chapter. With this in mind, the rhodium-phosphine systems can be conveniently classified into the following

three classes of chiral catalysts according to the source(s) of chirality in the ligands. They are:

(1) Ligands with central chirality,

(2) Ligands with axial chirality,

(3) Ligands with both central and planar chirality.

The purpose of this section is to review briefly some representative examples of the above ligands which have been successfully employed in asymmetric hydrogenation reactions.

2.4.1 Ligands with Central Chirality

Here three types can be recognized.

(A) Chirality at phosphorus, $R_1R_2R_3P^*$

The discovery of Wilkinson's catalyst [12] and the nearly simultaneous development of chiral phosphine technology by Mislow et al [80] and by Horner et al [81] prompted initially intense research on this type of ligand. This choice was based on the "proximity rule" that the chiral centers should be as near as possible to the central rhodium atom to obtain a high degree of asymmetric induction. This restriction is no longer regarded as valid.

The first examples of asymmetric hydrogenation based on this principle were reported in 1968 by Knowles et al [82]. Rhodium complexes of the type RhL_3Cl_3 were used in the hydrogenation of α-phenylacrylic acid and itaconic acid under the conditions indicated in Fig. 2.17.

$$CH_2=C(Ph)COOH \xrightarrow[60°C,C_6H_6\text{-}EtOH\text{-}Et_3N]{RhL_3Cl_3/H_2(20\ atm)} CH_3{}^*CH(Ph)COOH \quad 15\%\ e.e.\ (S)$$

$$CH_2=C(COOH)CH_2COOH \longrightarrow CH_3{}^*CH(COOH)CH_2COOH \quad 3\%\ e.e.$$

Fig. 2.17: Early examples of asymmetric hydrogenation with RhL_3Cl_3 [82].

When L was (R)-(-)-methylphenyl-n-propylphosphine (MPPP), 15% optically pure (S)-(+)-α-phenylpropionic acid and 3% optically pure methylsuccinic acid (configuration unreported) were obtained. The Monsanto group suggested that Wilkinson type Rh(I) complexes might be involved as an active catalyst.

At the same time, Horner's group [83] reported the reduction of α-substituted styrenes using an *in situ* catalyst prepared from (S)-MPPP (Fig. 2.18), again assuming a mechanism paralleling the one for Wilkinson's catalyst.

$$CH_2=C(R)Ph \xrightarrow[((S)\text{-}MPPP)_3RhCl/\textit{in situ}]{H_2(1\ atm),C_6H_6,25°C} CH_3{}^*CH(R)Ph$$

R = Et, 7-8% e.e. (S)

R = OMe, 3-4% e.e. (R)

Fig. 2.18: Early examples of asymmetric hydrogenation with a Wilkinson type catalyst. The *in situ* catalyst was prepared from $[Rh(1.5\text{-hexadiene})]_2$ and (S)-MPPP [83].

Subsequent to these experiments, both the Horner and Monsanto groups extended their studies to other substrates and other chiral monophosphines. The most significant success was achieved by Knowles et al [84] in the hydrogenation of amino acid precursors using cationic rhodium-monophosphine catalysts of the type $[Rh(COD)(ACMP)_2]A$ (COD = 1,5-cyclooctadiene; A = BF_4^-, PF_6^-, BPh_4^-; ACMP = o-anisylcyclohexylmethylphosphine). Catalysts prepared from (R)-(+)-ACMP gave (S)-amino acids and those containing the (-)-phosphine gave R-enantiomers. In many instances, the enantiomeric excess reached 85-90% [84]. Further studies on ACMP by Knowles et al led to the synthesis of a new catalyst precursor of the type $[(COD)Rh(L\text{-}L)^*]BF_4$ ($L\text{-}L^*$ = R,R-DIPAMP) which adopts a five-membered chelate ring as shown in Fig. 2.12. Excellent enantiomeric excesses (95-96%) have been achieved in the reduction of (Z)-α-acetamidocinnamic acids by the catalyst precursor (Table 2.1).

Table 2.1: Asymmetric hydrogenation of (Z)-α-acetamidocinnamic acids by Rh(I)-DIPAMP [85].

R^1	R^2	% e.e.	Configuration
H	Me	94	S
Me	Me	96	S
H	Ph	93	S

This system was used successfully not only to reduce other α-acetamido-acrylic acids with high optical yields but also to product L-DOPA on an industrial scale [86].

(B) Chirality at carbon

This type of ligands has several practical advantages over the ligands discussed previously: inexpensive, naturally occurring optically active compounds can be used as starting materials. These include menthol, camphor, lactic acid, tartaric acid, L-hydroxyproline, and various saccharides. The preparation of ligands with chiral phosphorus atoms of necessity requires classical resolution steps.

The first rhodium catalyst containing a chiral carbon atom, diphenylneomethylphosphine (NMDPP) was synthesized from menthol [87]. Hydrogenation of (E)-β-methylcinnamic acid in the presence of $Rh(NMDPP)_3CL$ (prepared in situ) and triethylamine (0.17 mol/mol. of substrate) gave (S)-(+)-3-phenylbutannic acid in 61% e.e.

At about the same time as the successful use of NMDPP, a new, chiral di(tertiary phosphine) ligand, (-)-2,3-isopropylidene-2,3-dihydroxy-1,4-bis(diphenylphosphino) butane (DIOP) (Fig. 2.12), was prepared by Kagan et al [88], and soon became one of the best known chiral ligands. Optical yields in the range of 70-80% have been reported in the reduction of various olefinic acids using RhCl(R,R-DIOP)(S) (prepared in situ) (Table 2.2). Folowing the discovery of DIOP, a great number of analogues were prepared either to attempt to clarify the reaction mechanism or to

obtain even better optical yields. The fundamental structure of DIOP was varied by changing either the aromatic substituents, the acetal substituents, or the acetonide ring by a carbocycle [89].

Table 2.2: Asymmetric hydrogenation of some olefinic acids with RhCl(-)-DIOP]S (S = C_6H_6) [88].

R	substrate/Rh	% e.e.	product: yield (%)
H	150	73	R ; 96
Ph	540	72	R ; 95
HOC_6H_4	100	80	R ; 92

Achiwa in Japan [90] prepared a series of efficient chiral di(tertiary phosphine) ligands (vide infra) from natural L-hydroxyproline.

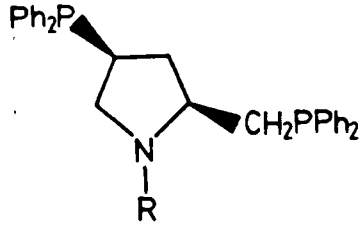

R=CO_2Bu^t; BPPM
=CO-Bu^t; PPPM
=H ; PPM
=$CO_2C_{27}H_{45}$; CPPM

The *in situ* Rh-BPPM catalyst with added Et_3N gave optical yields up to 91% for reduction of substituted cinnamic acids to various alanines (usually the D-form) at 50 atm hydrogen pressure in ethanol. It was also reported that optical yields were strongly dependent on both solvents and the N-substituents of PPM [90c, d].

Morrison et al, from commercially available (+)-camphoric acid, prepared a chiral di(tertiary-phosphine) ligand, (+)-(1R,3S)-1,2,2-trimethyl-1,3-bis(diphenylphosphinomethyl)cyclopentane (CAMPHOS).

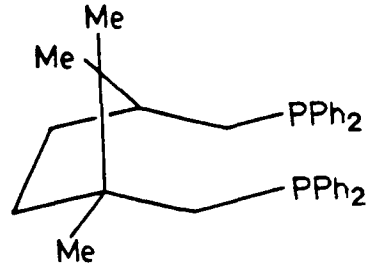

CAMPHOS

Reduction of α,β-unsaturated carboxylic acids in the presence of a rhodium catalyst prepared from $[Rh(COD)Cl]_2$ and (+)-CAMPHOS in a 1:1 mixture of ethanol and benzene, at 60°C and 21 atm (H_2) gave low optical yields [56].

One of the most remarkable successes has been achieved by Fryzuk and Bosnich [76a, b] using the complex $[Rh(S,S\text{-CHIRAPHOS})(COD)]^+$, where the chiral ligand is synthesized from (2R, 3R)-butanediol. The (Z)-α-N-acylaminoacrylic acid substrates were hydrogenated at ambient conditions to (R)-products with very high enantiomeric excess; indeed, leucine and phenylalanine derivatives were obtained in complete purity (Table 2.3).

Table 2.3: Asymmetric hydrogenation of amino acid precursors with $[Rh(S,S\text{-CHIRAPHOS})(COD)]^+$ [76a].

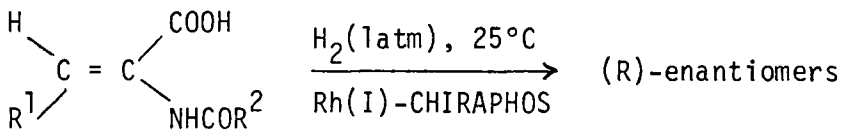

R^1	R^2	product	% e.e. in THF	% e.e. in ETOH
H	Me	alanine	88	91
Ph	Ph	phenylalanine	99	95
Oh	Me	"	74	89
i-C_3H_7	Me	leucine	100	93
i-C_3H_7	Ph	"	87	72
4-HOC_6H_3	Ph	tyrosine	80	88
3-MeO-4-AcD-C_6H_3	Me	DOPA	80	83

A crystal structure of the cationic moiety adopts the preferred (S,S)-conformation, the methyl groups being equatorially disposed to give the single static five-membered δ-chelate ring which, as discussed earlier, the authors believed to be responsible for the high optical yields. The same authors extended the rationalization for the design of (S,S)-CHIRAPHOS to the synthesis of (R)-PROPHOS which, when coordinated to the Rh atom, gives rise to the virtual enantiomeric chiral conformation (λ-chelate ring). Indeed products with (S)-configuration were obtained with equally high optical yields [76b].

D-glucose was utilized as starting material for the preparation of methyl 2,3-bis(O-diphenylphosphino)-4,6-O-benzylidene-α-D-glucopyranoside, designated as PO-OP [91].

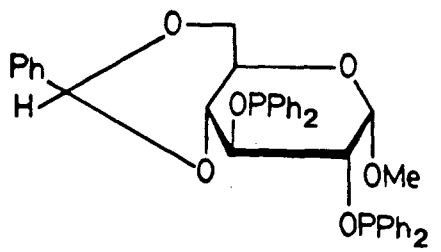

PO-OP

Hydrogenation of α-acetamidoacrylic acids and their esters was carried out in the presence of $[Rh(PO\text{-}OP)(NBD)]PF_6$ in ethanol at -20°C to 30°C and 1 atm of H_2. High optical yields up to 80% was achieved while substrates without the acetamido substituents were not hydrogenated. Interestingly, higher optical yields were obtained at lower temperatures than at higher temperatures.

(C) Chirality at both phosphorus and carbon

The first ligands of this type were the l-menthylmethylphenylphosphines (MMPP) possessing opposite configurations at phosphorus as shown below.

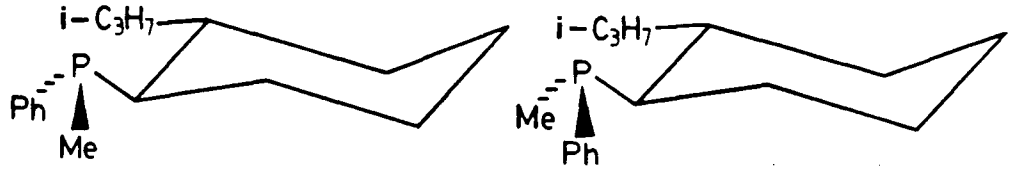

MMPP

Several olefinic acids were reduced by the catalyst prepared from (S)- or (R)-MMPP (configuration at P) and $[Rh(COD)Cl]_2$, in benzene/ethanol (1:1) in the presence of triethylamine. The enantiomeric excess ranged between 13-70% [92].

2.4.2 Ligands with Axial Chirality

A new class of phosphines containing only an axial element of chirality has been prepared [93]. An <u>in situ</u> 1:1 $[Rh(1,5\text{-hexadiene})Cl]_2$/(S)-(-)-NAPHOS (NAPHOS = 2.2´-bis(diphenylphosphinomethyl)-1,1-binaphthyl) system (vid infra) hydrogenated α-acetamidocinnamic acid to a 54% e.e. (S) using 50 atm H_2 (the solvent not reported). The corresponding diphenylphosphite system (X = oxygen) in toluene-acetone was particularly effective (76% e.e.) for hydrogenation (95 atm) of α-acetamidocinnamic acid and α-acetamidoacrylic esters.

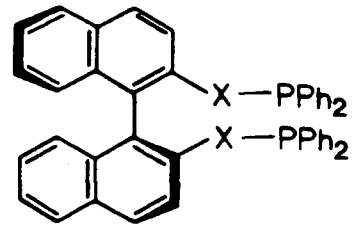

2.4.3 Ligands with Both Central and Planar Chirality

This third class of chiral ligands is represented by a series of ferrocenylphosphines [101, 102]. Two ligands shown in Fig. 2.19 are, among others, the first examples that have been used in asymmetric hydrogenation studies.

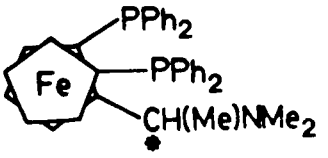

(S,R)-/(R,S)-BPPFA

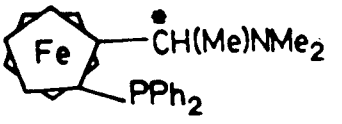

(S,R)-/(R,S)-PPFA

Fig. 2.19: Early examples of chiral ferrocenylphosphines.

In the presence of $[Rh(1,5\text{-hexadiene})Cl]_2$ and (S,R)-BPPFA in a 1:2.4 ratio, hydrogenation of α-acetamidoacrylic acids was completed in 20 hr at 50 atm (H_2) and room temperature, giving high optical yields (86-94% e.e.) [94]. At about the same time, both enantiomers of PPFA were prepared by Cullen et al [102a] who reported optical yields in the range of 73-84% in the reduction of α-acetamidocinnamic acids using the catalyst precursor $[Rh(PPFA)(Diene)]^+A^-$ (Diene = COD, NBD; $A^- = ClO_4$, BF_4, PF_6).

It is this class of ligands (achiral and chiral) with which this thesis is chiefly concerned, and the results will be discussed in more detail in subsequent chapters.

CHAPTER 3

FERROCENYLPHOSPHINES IN HOMOGENEOUS CATALYSIS

3.1 GENERAL ASPECTS

Since the discovery of ferrocene in 1951 [95] this molecule has opened a new era of organometallic chemistry and played a major role in this field. As a result, there have been a vast number of papers and reviews devoted to studies of its fascinating chemistry [96]. Upon examination of the literature, it is apparent that much interest has been focused on two aspects of the chemistry of this sandwich compound. They are as follows.

3.1.1 Aromatic Electrophilic Substitution

Ferrocene has been shown to undergo aromatic eletrophilic substitution readily, resulting in a wide variety of derivatives through acylation, alkylation, metalation, etc. Of particular interest in organometallic chemistry is the metalation reaction of ferrocene, since a number of potential bidentate ligands for metal complexes may be prepared utilizing this reaction. For example, symmetrically 1,1'-disubstituted ferrocenes I were prepared by way of dilithiation of ferrocene followed by treatment with halophosphines and haloarsines [97].

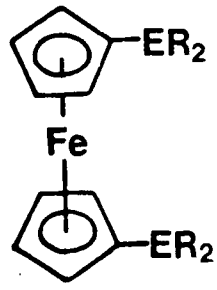

I	$ER_2 = PPh_2$ (BPPF)
Ia	$= PMe_2$ (BMPF)
b	$= AsPh_2$ (BPAF)
c	$= AsMe_2$ (BMAF)

There are now numerous examples of metal complexes containing these compounds as chelating bidentate ligands [96c].

3.1.2 Stereochemistry of Ferrocenes

There has also been a great deal of interest in the area of stereochemistry of ferrocene derivatives. This interest lies in the fact that, due to the particular molecular geometry, special problems of isomerism are encountered. In fact, suitably substituted ferrocenes can exhibit optical isomerism. These chiral ferrocene derivatives can be classified into three groups:

(A) Ferrocenes with central chirality

(B) Ferrocenes with planar chirality

(C) Ferrocenes with both central and planar chirality.

Many representatives of the first group have been prepared, in which the ferrocenyl moiety is attached either to the center of chirality or separated from it by one or more atoms [98]. This group includes, among others, N,N-dimethylamino-ethylferrocene (FA) as shown below.

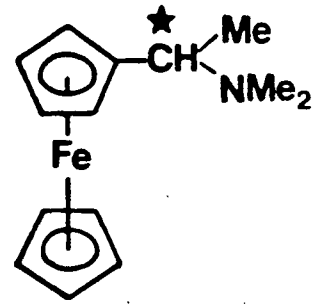

FA

The resolution of this compound can be achieved by a conventional recrystallization of diastereomeric tartrate. The second group of chiral ferrocenes can be obtained when one ring is substituted with at least two different groups as shown in Fig. 3.1.

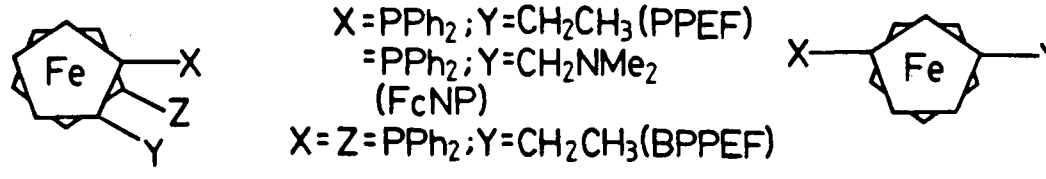

Fig. 3.1: Ferrocene derivatives with planar chirality.

The substituents X, Y, and Z have no center of chirality. They are known to be stable to racemization and epimerization. The third group of chiral ferrocenes can be generated if either X or Y carries central chirality. The ligands PPFA and BPPFA shown in Fig. 3.2 are representative examples. As shown in the figure, these and other related chiral ferrocenes can be prepared by way of the stereoselective lithiation of (R)- or (S)-FA which

affords the stabilized derivative (R,R)- or (S,S)-3.2a, respectively, in high optical yield (96%) due to the attractive interaction between Li and the nitrogen lone pair electrons.

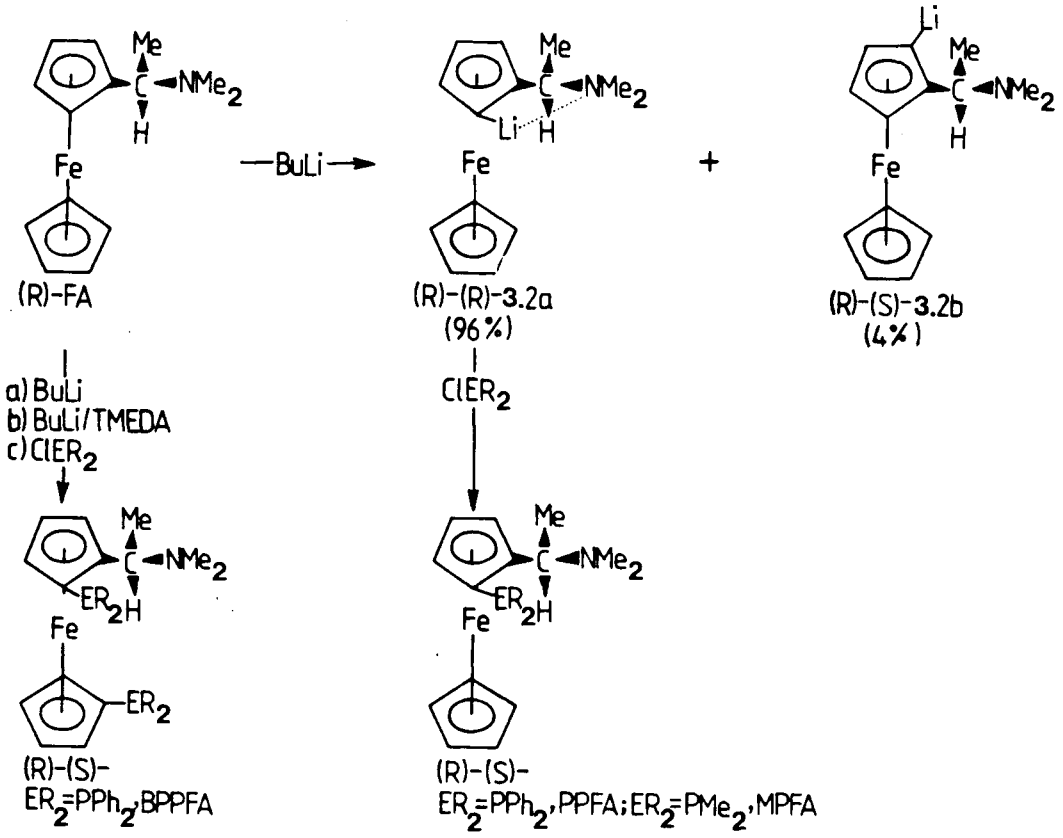

Fig. 3.2: Preparative routes to ferrocenylphosphines with central and planar chirality [101, 102a, b].

Schlögel et al [99] and Ugi et al [100] suggested the following rules for defining chirality in this type of chiral ferrocenes. First, the planar chirality is determined as follows. The observer looks along the C_5 axis of the parent rings with the more highly substituted ring directed towards him. The planar chirality is "R" if the ligands X and Y (Fig. 3.1) descend in priority in the shortest clockwise arc ("priority" here has the same meaning as used for the usual RS nomenclature). Likewise, if the priority ascends in a clockwise direction, the planar chirality becomes "S". If more than three groups are present, only the three with highest priority are considered. Secondly, if there are different types of chirality in one compound, then the (R,S) symbols will refer to those various elements of chirality in the order: central > axial > planar. Finally, in connection with the central chirality, if the bonds proceeding from the Fe atom are arbitrarily regarded as single bonds, then asymmetric substitution of a ring causes all the ring C atoms to become chiral centers and the symbol (R) or (S) can be assigned to each of them, i.e. (1S), (2R), etc. This third assignment, however, will not be made in this thesis for simplicity. Therefore, in the case of (R,S)-PPFA, the first "R" refers to the configuration at the carbon atoms of the $-CH(Me)NMe_2$ group and the second "S" to the planar chirality (This molecule, like all other chiral ferrocene derivatives described in this thesis, lacks axial chirality).

3.2 METAL COMPLEXES OF FERROCENYLPHOSPHINES

Relatively little attention has been focused on the preparation and the use of ferrocenylphosphines (chiral and achiral) in homogeneous catalysis. As a result, there have been only a few studies in this area, most of which have been carried out by Kumada et al [101] and by Cullen et al [102]. Their work establishes that ferrocenylphosphines are very useful ligands for metal complexes in the following three types of catalytic reactions.

3.2.1 Asymmetric Hydrogenation

The chiral ligands BPPFA and PPFA have been found to be very effective for Rh-catalyzed asymmetric hydrogenation of α-acetamido-cinnamic and acrylic acids (cf. section 2.4.3). The crystal structure of $[Rh(NBD)(PPFA)]ClO_4$ has recently been determined, which shows that both N and P are bound to rhodium [102b]. On the other hand, it seems that BPPFA uses both P atoms to bind to rhodium [103]. It is worth noting that BPPFA and PPFA give products of the opposite absolute configuration. Thus, (S,R)-BPPFA leads to (S)-acylamino acids while (S,R)-PPFA leads to (R)-isomers. Kumada et al [104a] reported that optical yields are lower when these substrates are hydrogenated under similar conditions using catalysts derived from modified BPPFA and PPFA (i.e. by replacement of the $-CH_3$ group on the chiral center with phenyl or isopropyl groups). A cationic complex [Rh(R,S-BPPOH)(COD)]-ClO_4 (BPPOH is produced when the $-NMe_2$ group is replaced by OH) has been used for the reduction of some chiral carbonyl compounds at 50 atm of H_2

and 0°- 30°C. Moderate to high optical yields (43 - 95%) were obtained [105]. The OH group is crucial for high optical yields, since much lower optical yields are obtained with other ligands lacking the OH group, i.e. BPPFA, BPPEF.

Further studies on PPFA by Cullen et al led to the synthesis of a new chiral ligand 1-N,N-dimethylaminoethyl-2-di-tert-butylphosphinoferrocene abbreviated as B^tPFA [102c] (vide infra).

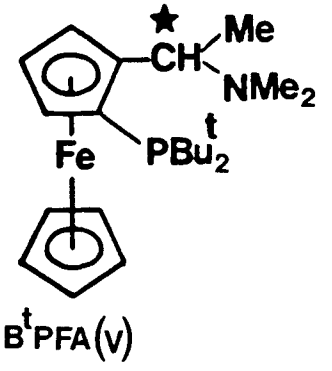

$B^tPFA(V)$

It was shown that the hydrogenation of a series of olefins can be completed in a shorter time with this ligand than with PPFA. Furthermore, in some cases, even higher optical yields with reversal of product configuration were obtained. There are few reports of asymmetric hydrogenation by metal complexes of aliphatic phosphines and the results cast doubt on the current "dogma" regarding the mechanism of asymmetric hydrogenation (cf. section 2.3.2), since high optical yields were obtained in spite of the absence of the supposedly necessary chiral array of phenyl groups. Furthermore, this is one of few aminophosphines which have been successfully used in homogeneous

catalysis, particularly with rhodium [106]. Therefore, for these reasons, further research into mixed PN donor systems is desirable. There is also a growing interest in ligand system containing both "soft" and "hard" donor atoms [107].

3.2.2 Other Catalytic Reactions; Hydrosilation and Grignard Cross Coupling

The palladium complex $Pd[(R,S)\text{-}PPFA]Cl_2$ is a catalyst precursor for the hydrosilation of olefins [108]. This is a useful procedure since the products can be converted into optically active alcohols or bromides [109]. Another useful synthetic application of ferrocenylphosphines can be found in the palladium and nickel catalyzed Grignard cross-coupling reactions (equation 3.1).

$$RMgX + R'X' \longrightarrow R\text{-}R' + MgXX' \qquad (3.1)$$

Kumada et al [110] discovered that complexes of the type $Pd(L\text{-}L)X_2$ and $Ni(L\text{-}L)X_2$ catalyze a large number of cross-coupling reactions of secondary alkyl Grignard reagents with organic halides. Here L-L are BPPF, (S)-FcNP, (R)-PPEF, (S,R)-PPFA, and other PPFA derivatives (Figs. 3.1 and 3.2). In some cases, optical yields as high as 95% have been obtained. It is worth noting that here the planar chirality seems to play a more important role than the central chirality.

3.3 GOALS OF THE PRESENT INVESTIGATION

The unique features of ferrocenylphosphine systems and observations like those described in the previous two sections indicate that more studies on these systems would be desirable. Some of these attempts during the present investigation can be summarized as follows.

3.3.1 New Rhodium-Ferrocenylphosphine Complexes as Hydrogenation Catalysts

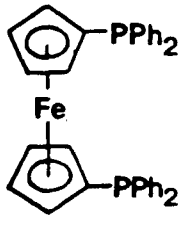

I

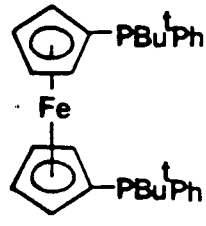

II

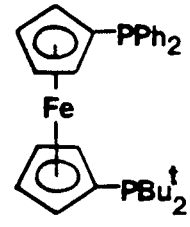

III

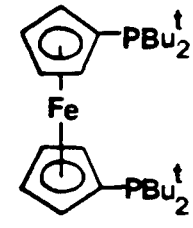

IV

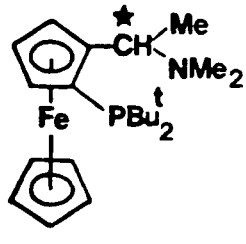

V

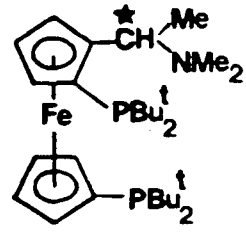

VI

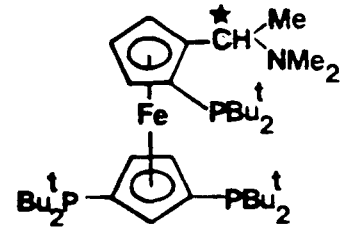

VII

Although the chemistry of easily prepared symmetrically 1,1´-disubstituted ferrocenes such as I (cf. section 3.2.1) has been explored quite extensively, little attention has been focused on the preparation and the use of related ligands II - IV in homogeneous catalysis. Of particular interest would be those ligands containing the bulky tert-butyl groups as well as phenyl rings (II - IV). In this connection, the chiral ligands V ∿ VII should provide further valuable information about the electronic and steric effects of those ligands containing the bulky tert-butyl groups on reaction rates and, more importantly, the mechanism of asymmetric hydrogenation. In this regard, these new chiral ligands deserve special attention since they not only possess the bulky alkylphosphines but also belong to the aminophosphine ligand. It seems also desirable to attempt to isolate any reaction intermediates such as metal hydrides formed in the course of the catalytic cycle. These issues will be addressed in Chapters 5 and 6.

3.3.2 Other Metal Complexes of Ferrocenylphosphines

It would be also desirable to synthesize a series of metal complexes to establish the steric effects of bulky phosphorus substituents in the hope that this would help explain rates and mechanism of catalytic reactions. As part of these studies, some of the ligands described above would be used to form group VI and other group VIII metal complexes such as (1) $M(P\text{-}P)X_2$ (M = Pd, Ni; P-P = I - IV; X = Cl, Br), (2) $M(P\text{-}P)(CO)_4$ (M = Cr, Mo; P-P = I, and (3) some iron carbonyl complexes.

These syntheses, crystal structures, and other studies will be presented in Chapter 5.

PART II

EXPERIMENTAL

CHAPTER 4

GENERAL EXPERIMENTAL SECTION

4.1 GENERAL

Unless otherwise specified air-sensitive reagents and products were manipulated in a nitrogen atmosphere using a double-manifold vacuum system and Schlenk techniques.

4.1.1 Materials

All commercial reagents were of reagent grade and were used as received unless otherwise stated.

Solvents were purified and dried by standard techniques. In particular, cyclohexane, diethyl ether, dichloromethane, hexane, and THF were refluxed over $LiAlH_4$ and freshly distilled under N_2 before use. Benzene and toluene were refluxed over sodium wire and stored under N_2 over molecular sieves, Ethanol and methanol were refluxed over magnesium and iodine and, freshly distilled under N_2 before use.

Hydrogen was obtained from the Matheson Gas Co. and was passed through a "deoxo" catalytic purifier before use.

4.1.2 Olefin Substrates

α-N-acetamidoacrylic, α-N-acetamidocinnamic, and α-methylcinnamic acids were purchased from Aldrich Chemical Co.; itaconic acid, from Eastman Kodak Co.; cyclohexene, 1-octene, and styrene from MCB Co.

All liquid olefins were passed through an Alumina (neutral, purchased from Fisher Scientific Co.) column prior to use in hydrogenation reactions.

4.1.3 Instrumentation

^{1}H NMR spectra were recorded on Bruker WP-80, Varian XL-100, or Bruker WH-400 spectrometers operating at 80 MHz, 100 MHz, or 400 MHz, respectively.

Proton decoupled ^{31}P NMR spectra were recorded on Bruker WP-80 or XL-100 spectrometers operating at 32.3 MHz or 40.5 MHz, respectively. All chemical shifts are positive to lower shielding. ^{1}H shifts are relative to external standard TMS (δ = 0 ppm) and ^{31}P shifts are relative to 85% H_3PO_4, with $P(OMe)_3$ (δ = +141.0 ppm) used as an external standard. The peak multiplicity, coupling constants, integrated peak areas, and proton (or phosphorus) assignments are reported in parentheses.

Infrared spectra were recorded on a Perkin-Elmer 598 spectrophotometer. Solid state spectra were obtained as Nujol mulls between NaCl, KBr, or CsI plates and solution spectra were recorded using KBr cells with path length 0.25 mm.

CD spectra were measured with a JASCO J-20 spectropolarimeter.

Mass spectra were obtained using a Kratos MS-50 instrument.

A Hewlett Packard 5880A gas chromatograph equipped with an OV-101 column was used for gas liquid chromatography.

Melting points were determined using a Gallenkamp Melting Point apparatus and are reported without correction.

Microanalyses were performed by Mr. P. Borda of this department.

4.2 HYDROGENATION EXPERIMENTS

4.2.1 Gas-Uptake Apparatus

A constant pressure gas-uptake apparatus shown in Fig. 4.1 was used for hydrogenation.

A Pyrex round-bottom 25 mL flask with a side arm was connected via a glass spiral with a tap F to the oil manometer S through the tap G. The oil manometer was made of thick wall capillary tubing filled with n-butyl phthalate, a liquid with negligible vapor pressure. S was connected to the mercury manometer T which consisted of a calibrated burette in the left side, and a mercury reservoir in the right. The right arm of the mercury manometer was in turn connected via a Teflon stopcock L to the gas handling part of the apparatus. This part consisted of the mercury manometer U, the gas inlet tap O, the connecting tap M, and tap N connecting the system to a pump.

The reaction flask was thermostatted in a glycerine bath W. The bath consisted of a cylindrical glass container surrounded by polystyrene insulation and enclosed in a wooden box on four supports. A magnetic stirrer P was placed under the box. A shaker Y was used to mix the reaction solution.

Both manometers S and T were immersed in a water bath X in a transparent plexiglass container. Both baths were independently regulated by thermoregulators with relay control circuits. The heat was provided by 25 W elongated electric light bulbs. These, with the aid of mechanical

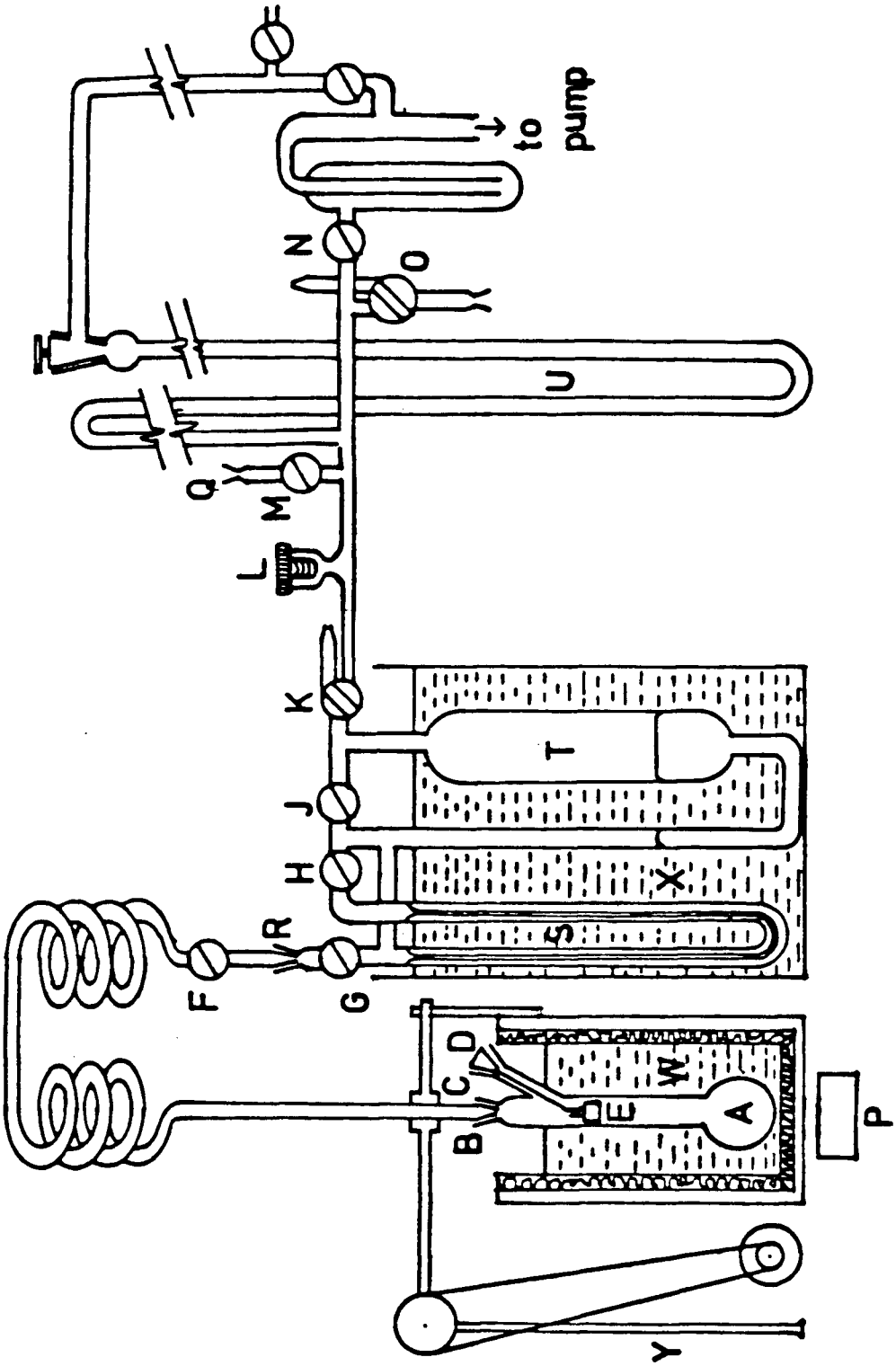

Fig. 4.1: Apparatus for constant gas-uptake measurements.

stirrers ensured temperature control within ±0.1°C. Time was recorded with a Labchron 1405 timer.

4.2.2 Gas-Uptake Experimental Procedure

In a typical gas-uptake experiment, the required amount of substrate and 10 mL of solvent were placed in flask A. Accurately weighed catalyst precursor in bucket E was suspended with a glass hook. The flask was connected through the glass spiral and tap F to tap Q.

The contents of the flask were degassed by the freeze and thaw method. During this operation the stopcock L was closed. The gaseous reactant was introduced, with tap N closed, through tap O at a pressure somewhat lower (∿710 mmHg) than that required for the experiment (760 mm-Hg) and then taps F and M were closed.

The spiral and the flask were disconnected from Q and reconnected to G with the flask being placed in the thermostated bath W. The flask was shaken with the electrical shaker Y and allowed to reach thermal equilibrium (∿5 min). In the meantime, the taps G, H, J, K, and N were opened to evacuate the whole apparatus except the spiral and the flask. It is recommended that H be opened before J during this operation.

The tap N was closed and the gaseous reactant was admitted through the tap O at roughly the same pressure (∿710 mmHg) as that in the reaction flask. Then tap F was opened and the pressure in the whole apparatus was adjusted to the desired level by opening the tap O very carefully. Taps O and L were closed and a reading of the mercury level in the left arm of

the manometer T was taken.

Bucket E was dropped into the solution by turning the hook D. At the same time the electric timer was started. Any gas-uptake resulted in a rising of the oil level in the left arm of the manometer S. At appropriate times tap L was carefully opened to equalize the oil levels in S. This resulted in a corresponding rise of the mercury level in the left arm of the manometer T. The change of height of the mercury was recorded as a function of time. Since the left arm of the manometer T was made of a calibrated pipette the volume of the gas which has reacted was known.

4.2.3 Work up of Hydrogenated Products

The hydrogenated products of the following olefins were identified from their ^1H NMR spectra or from gas chromatograms after they were separated as follows.

(A) α-N-acetamido-acrylic and cinnamic acids

After the solvent was pumped off the residue was dissolved in cold dichloromethane (∿5 mL) and the solution stirred for a few minutes until a yellowish white precipitate deposited. This was separated from the solution by filtration and washed with CH_2Cl_2 several times to give a pure white product. Since the product is slightly soluble in CH_2Cl_2, the filtrate was dried and the remaining solid treated as above to recover the product quantitatively.

(B) Itaconic and α-methylcinnamic acids

After the solvent was removed the residue was dissolved in 25 mL of 5% NaOH solution, stirred for a few minutes and filtered through Celite

to give a pale yellow filtrate. After acidifying with 10% HCl, the solution was extracted with diethyl ether (3 x 10 mL). The etheral extract was dried over $MgSO_4$, filtered, and evaporated to give the final product.

(C) Liquid Olefins

The hydrogenated solution from styrene was vacuum distilled, and those from cyclohexene, 1-octene, were distilled at one atmosphere using a microscale distillation apparatus.

4.2.4 Hydrogenation of the Catalyst Precursors

Hydrogenation of the catalyst precursors of the type $[Rh(L\text{-}L)(NBD)]ClO_4$ (L-L = I - VII) was also carried out in the absence of olefin substrate using the following three methods.

Method A: with measurement of H_2 up-take. The accurately weighed catalyst precursor (1.2×10^{-4} mol) and an appropriate solvent (3 mL) were placed in bucket E and flask A, respectively (Fig. 4.1). The typical gas-uptake experimental procedure for the hydrogenation of olefins was then followed (cf. section 4.2.2) to record the total amount of H_2 consumed.

Method B: with crystallization of the product. In order to isolate any product formed, the reaction described in Method A was duplicated as follows.

The same amount of catalyst precursor and solvent were placed in a Schlenk tube. This was connected to a double-manifold vacuum system which, in turn, was connected to both N_2 and H_2. The solution was degassed by the freeze-and-thaw method, and hydrogen was introduced to this solution with vigorous stirring at room temperature for $1 \sim 1.5$ h to ensure that the

reaction was complete. The final solution was either cooled at 0°C or allowed to stand at room temperature. The crystals thus obtained were isolated in a Schlenk filter, washed with diethyl ether, dried under vacuum, and redissolved in CD_2Cl_2 in order to obtain a variable temperature NMR spectrum. In some cases where crystallization was unsuccessful, the solvent was removed under vacuum, and the remaining solid was dissolved in the CD_2Cl_2.

Method C: with NMR monitoring of the in situ solutions. The catalyst precursor (5.0×10^{-5} mol) was dissolved in a deuterated solvent ($CDCl_3$, CD_3OD, or CD_3CN) in an NMR tube which was then connected to the vacuum system described above. The solution was degassed as above, and then hydrogen was introduced to the solution with occasional shaking. As the gas diffused through the solution and reacted with the complex, the color change progressed from the top meniscus to the bottom of the tube. No further color change was observed over a period of 1 h. The variable temperature NMR spectrum of the in situ solution was then recorded.

4.3 OPTICAL ROTATION MEASUREMENTS

All optical rotation values were recorded on a Perkin-Elmer 141 spectrometer at room temperature using a one decimeter path-length cell which could hold 1 mL of solution. The rotations were measured at the sodium-D line (589 nm).

The specific rotation of any chiral product was calculated using equation (4.1):

$$[\alpha]_D^T = \alpha/\ell \cdot c \qquad (4.1)$$

where $[\alpha]_D^T$ = specific rotation at temperature T measured at the sodium-D line.

α = observed rotation (+) or (-)

ℓ = path length of the cell in decimeters

c = concentration of solution in g/100 mL.

The enantiomeric excess (e.e.) of the reduced product was then determined using equation (2.1) and the specific rotation of the isolated products. They are listed in Table 4.1.

Table 4.1: Specific rotation of some chiral products [89, 111].

Substrate	Product	$[\alpha]_D^{RT}$
α-N-acetamidocinnamic acid	N-acetyl-phenylalanine	(R): -51.8(c1,EtOH)
α-N-acetamidoacrylic acid	N-acetylananine[a]	(R): +66.5(c2,H_2O)
(E)-α-methylcinnamic acid	β-phenyl-α-methylpropanoic acid	(R): -27.06(c3.7,C_6H_6) (S): +27.06(c3.7,C_6H_6)
Itaconic acid	2-methyl-succinic acid	(R): +17.09(c10.5,EtOH) (S): -17.09(c10.5,EtOH)

[a]The pure (S)-isomer was assumed to have the same degree of optical rotation with opposite direction.

4.4 SYNTHESES OF STARTING MATERIALS

All compounds described in this section were prepared according to literature methods with minor modifications, and were used for further reactions.

4.4.1 The Phosphines RR´PCl

(A) Chlorodi-tert-butylphosphine(Bu^t_2PCl) [112]

The Grignard reagent tert-butylmagnesium chloride was prepared as follows.

Magnesium turnings (24.3g, 1 mol) and freshly distilled diethyl ether (400 mL) were placed in a 2 L, round-bottom, three-necked flask equipped with a 500 mL, pressure-equalizing dropping funnel, a reflux condenser, a nitrogen inlet, and a magnetic stirrer. The magnesium turnings were etched with a trace of iodine. The reaction was then started by the addition of tert-butylchloride (92.5 g, 1 mol) dissolved in a total 1300 mL of ether. Subsequently, the etheral solution of Bu^tCl was added gradually so that the solvent kept at its boiling point (ca. 2h). To complete the reaction, the mixture was allowed to reflux for another hour.

N.B. The immediate use of the Grignard reagent thus obtained is important. Furthermore, if formation of large amounts of a white precipitate is observed at the end of the reaction, the reaction mixture should be discarded.

To this dark grey solution of Bu^tMgCl was added dropwise at room temperature phosphorus trichloride (34.4g, 0.25 mol) in ether (50 mL). A white precipitate was formed immediately. The reaction mixture was boiled and was allowed to reflux for 2 h. Then the ether solution containing the product was separated from the precipitate by careful decanting into a 1 L, round-bottom flask under N_2 through glass wool. Ether was removed from the decanted product by distillation at atmospheric pressure to leave a yellowish oil. This was transferred into a flask set up for vacuum distillation. The product thus obtained was an air-sensitive, colorless liquid (25 g, 55%). bp 62-65°C (4.6 mmHg) (lit. 69 - 70°C (10 mmHg)).

(B) Chloro(phenyl)-tert-butylphosphine [113]

Dichlorophenylphosphine (179 g, 1 mol) in ether (500 mL) was added slowly at room temperature to a stirred solution of Bu^tMgCl prepared from Bu^tCl (138.8 g, 1.5 mol) and Mg(36.5 g, 1.5 mol) in ether (1200 mL) as described above. After the exothermic reaction during the addition of $PhPCl_2$, the reaction mixture was allowed to reflux for 2 h after which the resulting suspension was filtered under N_2 and the filtrate distilled at atmospheric pressure to remove ether. The remaining oily residue was vacuum-distilled a few times until a colorless liquid with a constant boiling point was obtained (120 g, 60%), bp (60 - 63°C (0.45 mmHg)) (lit. 81 ∿ 88°C (0.8 mmHg)).

4.4.2 Ferrocene Derivatives

(A) 1,1´-dilithioferrocene·TMEDA [97]

Ferrocene (18.5 g, 0.1 mol) was placed in a 250 mL Schlenk tube. After the tube was evacuated and refilled with N_2, hexane (75 mL) was added. A solution of n-butyllithium in hexane (1.6 M, 75 mL) was added through a pressure equalizing dropping funnel. The suspension was rapidly stirred and freshly distilled N,N,N´,N´-tetramethylethylenediamine (TMEDA) (16.3 g, 0.14 mol) was added slowly. The reaction was exothermic and the ferrocene slurry reacted to give a deep cherry red solution. The reaction mixture was allowed to stir for 4 h during which time a fine orange precipitate deposited. This was filtered through a medium porosity Schlenk filter and washed with warm hexane (2 x 30 mL). Drying in vacuo yielded a fine orange pyrophoric powder (23.5 g, 75%). This compound can be stored for long periods under N_2 at room temperature.

(B) 1,1´-Ferrocenediylphenylphosphine [114]

1,1´-Dilithioferrocene·TMEDA (5.0 g, 15.9 mmol), isolated as described above, was suspended in freshly distilled ether (200 mL). To this well stirred suspension, maintained at -78°C, was added a solution of $PhPCl_2$ (2.85 g, 15.9 mmol) in diethyl ether (20 mL). The mixture was then allowed to warm to room temperature and was stirred for 1 h. Following hydrolysis with water (50 mL), the etheral layer was separated, dried over anhydrous $MgSO_4$, filtered, and the solution volume reduced to about 20 mL. This oily solution was then chromatographed on Florisil (100- 200 mesh). The resulting deep red solution (n-hexane eluate) was reduced in volume

at room temperature until crystallization just began. The solution was then stored at 0°C to afford deep red crystals (3.2 g, 70%).

(C) N,N-dimethylaminocyanomethylferrocene (Fe-CH(CN)NMe_2) [115]

Ferrocene carboxaldehyde (108 g, 0.5 mmol) dissolved in methanol (300 mL) was added at room temperature to a stirred solution of sodium bisulfite (52 g, 0.5 mol) in water (300 mL) in a 2 L, round-bottom flask. After stirring 10 min., a solution of dimethylamine (30 g, 0.7 mol) in 100 mL of 50% MeOH was added to the above mixture, followed by a solution of sodium cyanide (24.5 g, 0.5 mol) in water (100 mL). The color changed from dark to orange. Ether (500 mL) was added and the reaction mixture stirred overnight, then extracted with ether (5 x 500 mL). The combined etheral extract was dried over $MgSO_4$, and the solvent removed at a reduced pressure. The residual amber oil crystallized on adding petroleum ether to give the product as golden plates (113 g, 90%).

(D) N,N-dimethylaminoethylferrocene (FA) [115]

A solution of Fe-CH(CN)NMe_2 (80.4 g, 0.3 mol) in dry ether (500 mL) was added dropwise, through a pressure equalizing dropping funnel, to a solution of MeMgI prepared from methyl iodide (85.2 g, 0.6 mol) and Mg (14.6 g, 0.6 mol) in ether (450 mL) in a 2 L, round-bottom flask. The yellowish brown color of the aminonitrile changed to reddish orange. The reaction mixture was stirred overnight and slowly treated with aq. NH_4Cl. The etheral layer was separated and the aqueous layer extracted with ether (3 x 500 mL). The combined etheral extract was dried over K_2CO_3, and ether removed at a reduced pressure to give an amber oil;

^{1}H NMR (acetone-d_6) δ 1.25 (d, 3, Me), 1.98 (s, 6, NMe_2), 3.48 (qt, 1, CH), 4.08 (s, 9, Fc).

(E) (S)- and (R)- FA: Resolution of FA [100]

The racemic amine (51.4 g, 0.2 mol) and (R)-(+)-tartaric acid (30 g, 0.2 mol) were each dissolved in MeOH (70 mL) in 250 mL Erlenmeyer flasks. Both flasks were immersed in a water bath at 55°C for about 10 min to reach thermal equilibrium. The tartaric acid solution was then poured into the FA solution while stirring. The temperature of the bath was then allowed to fall at a rate of $2 \sim 5°/h$. When (-) seeding crystals were not available, the flask was occasionally scratched with a glass rod to aid solid formation. Stirring was continued overnight and the (S)(-)-amine tartarate was collected by suction filtration. The mother liquor was set aside for later use. The tartrate salt was added to aqueous NaOH solution in a separatory funnel and the amine extracted with ether (4 x 150 mL). The amine solution was dried over anhydrous K_2CO_3, and evaporated to give optically active amine. The amine (20 g) thus obtained and (R)-(+)-tartaric acid (17.53 g, 0.11 mol), each dissolved in 30 mL of MeOH were mixed at 55°C and a few (S)(-)-amine tartarate crystals were added. After slow cooling followed by the work-up procedure as described above, optically pure (S)-(-)-FA was obtained (15 g, 58.4%): $[\alpha]_D^{25}$ -14.3° (c 1.5, EtOH) (lit. $[\alpha]_D^{25}$ -14.1° (c 1.5, EtOH)). If the optical rotation of the amine was lower, one additional crystallization was required. The mother liquor from the first crystallization was concentrated to about one-fourth of its original volume. Diethyl ether was added slowly to the solution until precipitation

was complete. The mixture was left at 0°C overnight and the (R)-(+)-amine tartarate was collected. This was recrystallized by dissolving it in a minimum amount of hot water (70 - 80°C) and adding to this solution warm acetone in such a way that the ratio of water to acetone became 1 : 10. Optically pure (R)-(+)-FA was obtained from repeated recrystallization (2 ∿3 times) in this modified way: yield (17.2 g, 58.5%); $[\alpha]_D^{25}$ + 14.3° (C 1.5, EtOH) (lit. $[\alpha]_D^{25}$ + 14.1° (C 1.5, EtOH)).

4.4.3 Metal Complexes

(A) $[Rh(NBD)Cl]_2$ [116]

$RhCl_3 \cdot 3H_2O$ (0.7 g) was dissolved in 95% EtOH (10 mL) in a 100 mL Schlenk tube. The solution was degassed by the freeze-and-thaw method. To this solution was added norbornadiene (2 mL) with stirring. A yellow precipitate deposited about 1 h after the reaction had been started. The reaction mixture was further stirred for 24 h after which time the yellow precipitate was isolated by filtration, washed with cold ethanol (10 mL), and dried under vacuum to give a fine yellow powder. The product was not purified further.

(B) $Pd(PhCN)_2Cl_2$ [117]

A mixture of Na_2PdCl_4 (1 g) and benzonitrile (50 mL) were stirred at 100°C for 30 min. The resultant red solution was filtered and the filtrate poured into petroleum ether (200 mL) to deposit a yellowish orange precipitate. This was isolated and crystallized from benzene to afford an orange microcrystalline product (0.5 g, 50%).

(C) $Pd(NBD)Cl_2$ [117]

This complex was prepared by the direct reaction of $Pd(PhCN)_2Cl_2$ (0.2 g, 5.21×10^{-4} mol) and a slight molar excess of norbornadiene (3 mL) in $CHCl_3$ (50 mL). After stirring 1 h, a yellow precipitate was isolated from the solution, washed with $CHCl_3$, and dissolved in warm glacial acetic acid. The solution gave a yellow precipitate on cooling. This was washed with a mixture of methanol and acetone, and dried under vacuum: yield 43%.

4.5 SYNTHESES OF FERROCENYLPHOSPHINES

Analytical and spectroscopic data for these ligands are presented in Chapter 5.

4.5.1 Achiral Ligands

(A) 1,1´-Bis(diphenylphosphino)ferrocene (BPPF, I) [97]

1,1´-Dilithioferrocene TMEDA (10 g, 31.9 mmol), isolated as described previously was suspended in freshly distilled n-hexane (50 mL) in a 250 mL Schlenk tube. To this suspension, maintained at 0°C, was added Ph_2PCl (14.5 g, 65 mmol). The mixture was warmed to room temperature and was stirred for 5 h. Following careful hydrolysis with water (50 mL), the supernatant hexane layer was decanted from the brown solid, and the solid was washed successively with ethanol (2 x 30 mL) and hexane (3 x 30 mL), then finally dissolved in hot benzene (40 mL). Hot hexane was slowly added until the solution became turbid. The solution was then cooled to room tempera-

ture to give fine orange crystals (11.5 g, 65%).

(B) 1,1´-Bis(phenyl-tert-butylphosphino)ferrocene (BPB^{t}PF, II)

To a well stirred suspension of $(C_5H_4)_2FeLi_2 \cdot TMEDA$ (10 g, 31.9 mmol) in dry hexane (30 mL), maintained at -78°C, was added slowly $Bu^t(Ph)PCl$ (13 g, 65 mmol) in dry ether (15 mL). The reaction mixture was then warmed to room temperature and stirred overnight after which the mixture was hydrolyzed with water (20 mL). The organic layer was separated, dried over $MgSO_4$, and reduced in volume to about 10 mL. The oily solution was then chromatographed on Alumina (neutral, Grade I). Meso and racemic (d and ℓ) isomers were separated by rechromatographing the second orange band with a mixture of petroleum ether and diethyl ether (70/30). Both products were isolated as deep orange oils which solidified slowly on cooling (0°C): yield 55 - 60%.

(C) 1-Diphenylphosphino-1´-di-tert-butylphosphinoferrocene (PPB^{t}PF, III)

The title compound was prepared using the ring cleavage reaction of 1,1´-ferrocenediylphenylphosphine. To a stirred solution of 1,1´-ferrocenediylphenylphosphine (1.5 g, 5.14 mmol) in diethyl ether (30 mL) at -78°C was added dropwise phenyllithium (1.95 M, 4 mL) in benzene. The mixture was allowed to warm to room temperature slowly. The solution was then recooled to -78°C and excess Bu^t_2PCl (3 mL) in diethyl ether (5 mL) was added dropwise. The resultant mixture was slowly warmed to room temperature and was subsequently heated to a gentle reflux for 10 min. Precipitation of LiCl occurred. After stirring another 30 min at room

temperature the solution was hydrolyzed with water (20 mL), the etheral layer separated and dried over anhydrous $MgSO_4$. The solution volume was reduced to a few mL following filtration. The resultant oil was chromatographed on Alumina (neutral, Grade I) to give a single orange band (eluted with diethyl ether/petroleum ether, 10/90). Removal of solvent under vacuum from the resulting orange solution afforded a yellow crystalline solid (1.24 g, 47%).

(D) 1,1´-Bis(di-tert-butylphosphino)ferrocene (BB^tPF, IV)

$(C_5H_4)_2FeLi_2 \cdot TMEDA$ (7.5 g, 23.9 mmol), isolated as described previously, was suspended in freshly distilled n-hexane (40 mL) in a 250 mL Schlenk tube. To this suspension, maintained at -78°C, was added Bu^t_2PCl (8.7 g, 48.2 mmol). The mixture was allowed to warm to room temperature and stirred overnight. Following careful hydrolysis with water (20 mL), the hexane layer was separated, dried over anhydrous $MgSO_4$, filtered, and reduced in volume to about 10 mL. This oily solution was then chromatographed on Alumina (neutral, Grade I). Removal of solvent under vacuum from the resulting deep orange solution (the second band that eluted with a mixture of petroleum ether and diethyl ether, 70/30) afforded a dark oily product (4.5 g, 40%). The product was not purified further. N.B. Careful chromatography was required to separate the product from a mixture of ferrocene and a white phosphine by-product that eluted with petroleum ether.

4.5.2 Chiral Ligands

(A) (S,R)- and (R,S)-2-(di-tert-butylphosphino)-1-(N,N-dimethylaminoethyl)ferrocene(B^tPFA,V) [102c]

This ligand was prepared using the known method [102c] and isolated as a crystalline solid; acetone was used for crystallization.

(B) (S,R)- and (R,S)-1´,2-bis(di-tert-butylphosphino)-1-(N,N-dimethylaminoethyl)ferrocene(BB^tPFA,VI)

(S)-FA (3 g, 11.7 mmol) was dissolved in a mixture of diethyl ether (2.5 mL) and n-hexane (3.5 mL) in a Schlenk tube. To this solution was added slowly n-BuLi (1.6 M, 8 mL). The reaction was slightly exothermic and the color of the solution changed from yellowish brown to cherry red. The reaction mixture was stirred for 2 h, and a mixture of n-BuLi (1.6 M, 8 mL) in hexane and TMEDA (2 mL, 11.7 x 1.2 mmol) was added through a pressure equalizing dropping funnel. The reaction was slightly exothermic again, and the color of the solution deepened. The reaction mixture was further stirred for 6 h after which Bu^t_2PCl (4.1 g, 23 mmol) was added through a syringe. The reaction mixture was allowed to stir at room temperature for 2 days. Following hydrolysis with H_2O, the organic layer was separated, dried over $MgSO_4$, filtered, and reduced in volume to about 5 mL. The resulting red oil was chromatographed on neutral Alumina (Grade II) to give a single salmon-red band (eluted with diethyl ether/petroleum ether, 15/85). Removal of solvent under vacuum from the resulting orange solution afforded a dark orange oil (1.9 g, 30%). Attempted crystallization from acetone (or EtOH) was unsuccessful. (R,S)-BB^tPFA (VI) was obtained by treating (R)-FA in the same manner as above.

(C) (S,S)- and (R,R)-1´.2.3´-tris(di-tert-butylphosphino)-1-(N,N-

dimethylaminoethyl)ferrocene(TB^tPFA, VII)

(a) Method 1

(S)-FA (3 g, 11.7 mmol) was dissolved in diethylether (5 mL) in a Schlenk tube. To this solution was added n-BuLi (1.6 M, 9 mL) in hexane. After stirring 2 h, a mixture of n-BuLi (1.6 M, 10 mL) in hexane and TMEDA (1.5 g, 13 mmol) was added dropwise through a pressure equalizing dropping funnel. The reaction mixture was further stirred for 15 h at room temperature. This solution was added dropwise to a solution of Bu^t_2PCl (4.7 g, 26 mmol) in diethyl ether (30 mL) which was prepared in a 250 mL, round-bottom, three-necked flask equipped with a condenser, a N_2 inlet, and a pressure equalizing dropping funnel. After the initial exothermic reaction on addition of the $FALi_2$·TMEDA solution, the mixture was allowed to boil under reflux for 20 h. Following hydrolysis with water, the organic layer was separated, dried over $MgSO_4$, filtered, and reduced in volume to about 5 mL. The resulting oily solution was chromatographed on Alumina (neutral, Grade I). After removal of the white phosphine by-product by elution with petroleum ether, a second salmon-red band was eluted with a mixture of diethyl ether and petroleum ether (1/9, v/v). Removal of solvents from the resulting orange solution afforded a dark oil which crystallized on adding acetone (or ethanol) to give the product (S,S-TB^tPFA (0.32 g, 4%). (R,R)-TB^tPFA was obtained by treating (R)-FA in the same manner as above.

(b) Method 2

To the <u>in situ</u> solution of $FALi_2$·TMEDA prepared as described above was added Bu^t_2PCl (7.49, 41 mmol) at room temperature. The reaction mixture was stirred at room temperature for 3 h during which time the dark red solution turned to bright orange with precipitation of LiCl. The solution was

further stirred at room temperature for 4 days, and the product isolated as red crystals following the work-up described above: yield 3 ∿ 4%.

4.6 SYNTHESES OF Rh(I) COMPLEXES OF FERROCENYLPHOSPHINES

The complexes of the type $[Rh(L\text{-}L)(NBD)]ClO_4$ (L-L = I ∿ VII) were prepared essentially using the procedure of Schrock and Osborne [32e] with minor modifications, and were isolated as deep red crystals. Analytical, physical and NMR data for these compounds are presented in Chapter 5.

4.6.1 Achiral Complexes

(A) $[Rh(BPPF)(NBD)]ClO_4$ (VIII)

$[Rh(NBD)Cl]_2$ (300 g, 0.65 mmol) and BPPF (792 mg, 1.4 mmol) were dissolved in benzene (3 mL) in a Schlenk tube, and the solution was degassed. To this solution was added $NaClO_4$ (200 mg, 1.6 mmol) in THF (2 mL). The solution was stirred for 30 min during which time a fine orange precipitate deposited. This was isolated on a Schlenk filter, washed with diethyl ether (20 mL), dissolved in CH_2Cl_2 (5 mL), and filtered to remove any solid impurity. The filtrate was reduced in volume to aboue 2 mL to which was added cyclohexane (∿7 mL) without disturbing the dichloromethane layer. Large crystals were grown by allowing this solution to stand at room temperature: yield 75%.

(B) $[Rh(P\text{-}P)(NBD)]ClO_4$ (P-P = BPB^tPF, IX; P-P = PPB^tPF, X)

These complexes were prepared in the same manner as described above, replacing BPPF by BPB^tPF and PPB^tPF, respectively: yield 70 ∿ 75%.

(C) $[Rh(BB^tPF)(NBD)]ClO_4$ (XI)

The benzene solution (2 mL) of BB^tPF (1.1 g, 2.32 mmol) and $[Rh(NBD)Cl]_2$ (357 mg, 0.77 mmol) was degassed. To this solution was added $NaClO_4$

(189.47 mg, 1.55 mmol) in THF (2 mL). The mixture was allowed to stir for 2 days at room temperature after which time solvents were removed under vacuum to leave a reddish brown solid. This was washed with diethyl ether (20 mL), dissolved in CH_2Cl_2 (2 mL), and filtered through a Schlenk filter. To the filtrate was added a 3:2 mixture of diethyl ether and ethanol (5 mL), and the solution was cooled at 0°C to give deep red crystals. Large crystals were grown as described above for the preparation of VIII: yield 80%.

4.6.2 Chiral Complexes

(A) $[Rh((S,R)-/(R,S)-B^tPFA)(NBD)]ClO_4$ (XII; B^tPFA = V)

To a mixture of (S,R)-B^tPFA (0.24 g, 5.9×10^{-4} mol) and $[Rh(NBD)Cl]_2$ (0.124 g, 2.7×10^{-4} mol) in MeOH (5 mL) was added $NaClO_4$ (0.072 g, 5.9×10^{-4} mol) dissolved in MeOH (2 mL). The reaction mixture was allowed to stir for 12 h at room temperature after which time the solvents were removed under vacuum to leave an orange solid. This was washed with diethyl ether several times, dissolved in CH_2Cl_2, and filtered through a Schlenk filter. The filtrate was dried under vacuum, and the remaining orange solid was redissolved in a minimum amount of hot ethanol ($\sim$ 2 mL). Red crystals were obtained by cooling this solution to room temperature: yield (272, 34 mg, 55%). The (R,S)-complex was prepared by treatment of (R,S)-B^tPFA in the same manner.

(B) $[Rh(P\text{-}N)(NBD)]ClO_4$ (XIII ; P-N = (S,R)-/(R,S)-VI :XIV; P-N = (S,S)-/(R,R)-VII)

Both complexes were prepared using the same procedure as described above: yield 50%.

4.7 SYNTHESES OF OTHER METAL-FERROCENYLPHOSPHINE COMPLEXES

Analytical, physical and spectroscopic data for the complexes described

in this section are presented in Chapter 5.

4.7.1 Palladium Complexes

Palladium complexes of the type $[Pd(P\text{-}P)Cl_2]$ (P-P = I - IV) were prepared by the direct reaction of K_2PdCl_4, $Pd(NBD)Cl_2$, or $Pd(PhCN)_2Cl_2$ (10^{-3} molar scale) with a slight molar excess of the appropriate ligand in diethyl ether containing a few mL of dichloromethane. The product complexes were formed as red/orange precipitates in each case which were isolated by filtration and washed with diethyl ether. For crystallization the product ($\sim$ 300 mg) was dissolved in an appropriate solvent or a mixture of solvents. The crystals thus obtained were washed with n-hexane and dried in vacuum.

(A) $Pd(BPPF)Cl_2$ (XV)

The product was recrystallized from acetone to give red plates: yield 82%.

(B) $Pd(BPB^tP)Cl_2$ (XVI)

Large crystals were grown by dissolving the microcrystalline product in a mixture of CH_2Cl_2 and hexane, and allowing the solvents to vaporize in the air: yield 80%.

(C) $Pd(PPB^tP)Cl_2 \cdot CHCl_3$ (XVII)

For crystallization the product was dissolved in CH_2Cl_2 and a top layer of cyclohexane was allowed to diffuse slowly into the dichloromethane layer: yield 80%. The $CHCl_3$ crystallization was confirmed by its NMR.

(D) $Pd(BB^tPF)Cl_2$ (XVIII)

This complex was obtained as reddish brown needles by crystallization as described for XVI: yield 70%.

4.7.2 Nickel Complexes

Nickel complexes of the type $Ni(P\text{-}P)X_2$ (P-P = I , IV; X = Cl, Br) were prepared according to published procedures [118]:

A solution of the appropriate ligand (1.0×10^{-3} mol) in ethanol (20 $\sim$ 30 mL) was placed in a 250 mL round-bottom, two-necked flask equipped with a reflux condenser, a nitrogen inlet, and a magnetic stirrer. The solution was then brought to reflux and $Ni(H_2O)_6Cl_2$ (or $NiBr_2$) (8.5×10^{-4} mol) dissolved in hot ethanol (15 mL) was added. A fine green precipitate was formed immediately. This was separated by filtration while the solution was still warm, washed with cold ethanol several times, and dried under vacuum.

(A) $Ni(BPPF)Cl_2$ (XIX) and $Ni(BPPF)Br_2$ (XX)

Both complexes were isolated as dark green plates on crystallization from chloroform; yields 65 $\sim$ 70%.

(B) $Ni(BB^tPF)Cl_2$ (XXI)and $Ni(BB^tPF)Br_2$ (XXII)

These complexes were obtained as green microcrystalline solids on crystallization from a mixture of CH_2Cl_2 and cyclohexane: yields 60 - 65%.

4.7.3 Iron Complexes

Iron carbonyl complexes $Fe(BPPF)(CO)_3$ and $Fe_2(BPPF)(CO)_8$ were prepared using the general procedures described below. The reaction of BPPF with $Fe_3(CO)_{12}$ is also described here.

(A) $Fe(BPPF)(CO)_3$ (XXIII)

A THF solution (30 mL) of BPPF (1.0×10^{-3} mol) and $Fe_2(CO)_9$ (2.0 x

10^{-3} mol) (or $Fe(CO)_5$ (1.0 x 10^{-2} mol) in 20 mL of benzene) was placed in a Carius tube. The system was then evacuated by the freeze-and-thaw method, sealed, and irradiated with UV for 6 - 30 h. UV irradiation reactions were carried out with a 200 Watt mercury lamp (Hanovia S-654 A36) under a stream of air. Removal of solvent gave a solid residue which was dissolved in CH_2Cl_2 ($\sim$ 4 mL) and chromatographed on Florisil (80 - 100 mesh). The first orange band was eluted with a mixture of diethyl ether and hexane (5/95, v/v). Solvents were removed from the resulting orange solution and the remaining solid crystallized from n-hexane to afford the product as orange needles: yield 75%.
The reaction of BPPF with $Fe(CO)_5$ in benzene resulted in less than 5% yield of the above product.

(B) $Fe_2(BPPF)(CO)_8$ (XXIV)

This compound was obtained as the major product from the reaction of BPPF with $Fe(CO)_5$ in benzene as described above: yield 62%. The reaction of BPPF (0.55 g, 0.99 mmol) with $Fe_2(CO)_9$ (0.72 g, 1.98 mmol) in THF also yielded this product (82%) by stirring the reaction mixture at room temperature for 20 h, following the work-up procedures for the preparation of the compound XX.

(C) The reaction of BPFF with $Fe_3(CO)_{12}$

A mixture of BPPF (0.15 g, 0.27 mmol) and $Fe_3(CO)_{12}$ (0.27 g, 0.54 mmol) in THF (25 mL) in a Schlenk tube was stirred for 4 h at room temperature. During this time the initial dark green color turned to deep purple. Removal of solvent under vacuum afforded a dark purple residue which was

chromatographed on Florisil (100 - 200 mesh). The large purple band, following the green band of excess $Fe_3(CO)_{12}$, was eluted with a mixture of diethyl ether and petroleum ether (5/5, v/v), and solvents removed to give a dark purple oil. This compound readily decomposed in solution but appears to be reasonably stable in the solid state. It gives at least 7 ν(CO) bands including one at 1775 cm^{-1}.

4.7.4 Group VI Metal Complexes

The Group VI metal carbonyl complexes, $M(BPPF)(CO)_4$ (M = Cr, Mo), were prepared by the procedure of Davison [118] with minor modification.

(A) $Cr(BPPF)(CO)_4$ (XXV)

A benzene solution (20 mL) containing BPPF (2.52 g, 4.5 mmol) and $Cr(CO)_6$ (0.95 g, 4.5 mmol) was heated in an evacuated Carius tube at 150°C for 12 h. Removal of solvent in vacuum gave an orange solid which was dissolved in a minimum amount of CH_2Cl_2 ($\sim$ 3 mL) and chromatographed on Florisil (100 $\sim$ 200 mesh). The second orange band was eluted with a mixture of diethyl ether and petroleum ether (4/6, v/v), and solvents removed to give the orange microcrystalline product. Large crystals were grown by dissolving the product in a hot solution of benzene and heptane (1/4, v/v), and allowing the solution to cool slowly to room temperature: yield 2.59 g (87%).

(B) $Mo(BPPF)(CO)_4 \cdot C_6H_6$ (XXVI)

This was prepared similarly. The benzene of crystallization was confirmed by its crystal structure: yield 61%.

PART III

RESULTS, DISCUSSION, AND CONCLUSION

CHAPTER 5

SYNTHESIS AND CHARACTERIZATION OF FERROCENYLPHOSPHINES AND THEIR METAL COMPLEXES.

The compounds of most interest in the present studies are chiral and achiral ferrocenylphosphine ligands; in particular those containing bulky tert-butyl groups on phosphorus for the reasons given in section 3.3. With appropriate modifications of known procedures, a wide range of ferrocenylphosphines and their metal complexes can be prepared. This chapter is mainly concerned with the preparation and the characterization of these ligands (L-L) and their rhodium complexes of the type $[Rh(L\text{-}L)(NBD)]ClO_4$ which are hydrogenation catalyst precursors (cf. Chapter 6). Some other metal (Group VI and VIII) complexes of these ligands were prepared, and are also described. In the subsequent discussion the notation P-P and P-N is also used to denote the achiral ferrocenylphosphines (L-L = I - IV) and the chiral ones (L-L = V - VII), respectively.

5.1 FERROCENYLPHOSPHINE LIGANDS

5.1.1 Achiral Ligands

(A) Syntheses

Preparative routes to the achiral ferrocenylphosphines are shown in Fig. 5.1.

All routes involve the well documented procedure for the preparation of the 1,1'-dilithioferrocene-TMEDA adduct [97]. The orange precipitate separates from hexane solution as a pyrophoric powder when ferrocene is lithiated with two molar equivalents of n-BuLi in the presence of one equi-

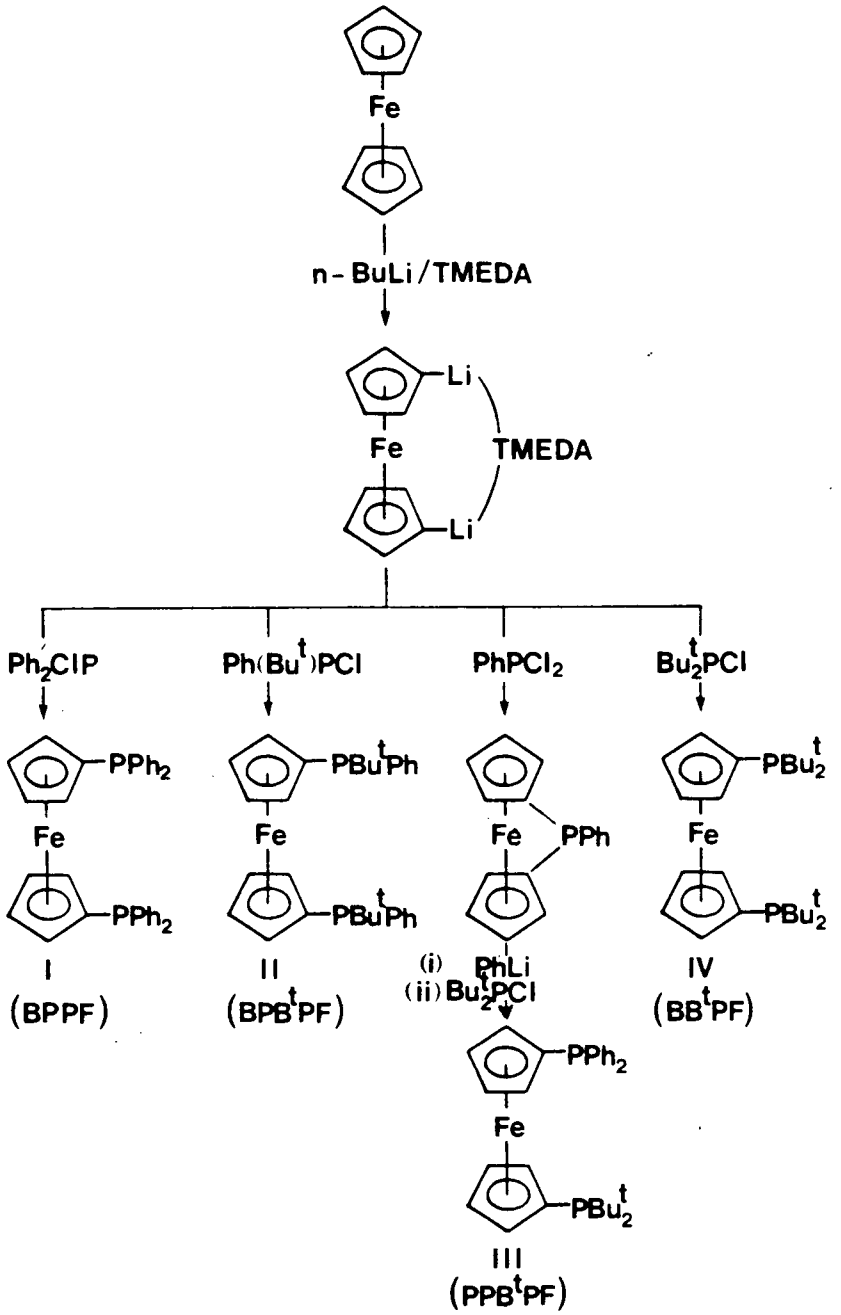

Fig. 5.1: Preparative routes to the achiral ligands I-IV.

valent of TMEDA. Although the crystal structure of this compound has not been determined, Davison [97] suggested that it be formulated as $(C_5H_4Li)_2Fe\cdot TMEDA$ on the basis of the analytical result. This stoichiometry has been found in the related compound $[(\eta^5\text{-}C_5H_4)_2Fe(N_3C_9H_{23})Li_2]_2$ [119]. There are distinct advantages in using the solid dilithioferrocene in these preparations, namely high yields and no monosubstituted phosphines are obtained.

The previously known compound I [97] was prepared by reacting a hexane slurry of dilithioferrocene with chlorodiphenylphosphine. This di(tertiary phosphine) is an orange, crystalline solid which is air stable in both the solid and solution. A simple extension replacing Ph_2PCl by $Bu^t(Ph)PCl$ and $Bu^t{}_2PCl$ allows the isolation of the new ferrocenylphosphine ligands II and IV, respectively. Both ligands were obtained as dark oils which slowly solidified on cooling at 0°C. In connection with the preparation of II, it should be pointed out that this compound can exist as both meso- and rac- isomers. In the present studies they were separated chromatographically as described in the experimental section, but only the rac-isomer has been used for further syntheses, spectroscopic (NMR), and hydrogenation studies.

The unsymmetrically 1,1'-disubstituted ligand III was prepared via the ring cleavage reaction (equation 5.1) of the [1]-ferrocenophane which was prepared from the reaction of $(C_5H_4Li)_2Fe\cdot TMEDA$ with $PhPCl_2$ [114].

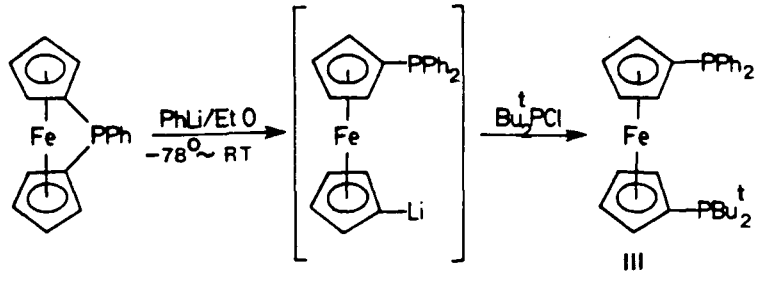

III

(5.1)

The subsequent synthetic route involved the reaction of the intermediate, 1-diphenylphosphino-1'-lithioferrocene with Bu^t_2PCl. The compound III was obtained as a yellow crystalline solid. Although this is an extremely useful method of activating the second ring for further substitution, care must be taken to minimize the formation of byproducts. For example, the initial product monolithioferrocene derivative may compete with PhLi for the substrate [1]-ferrocenophane, thus giving a monolithioferrocenyl derivative as shown in equation (5.2) [114c].

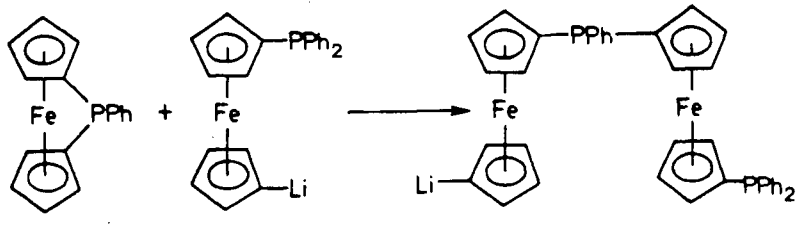

(5.2)

In order to avoid this potential complication, the preferred procedure involved the slow addition of 1.5 molar excess of PhLi to the [1]-ferrocenophane in diethyl ether maintained at -78°C. An alternative route involves the slow addition of the [1]-ferrocenophane to an equimolar quantity of PhLi in hexane [114c].

(B) Characterization

The analytical and NMR data listed in Tables 5.1 and 5.2 respectively, confirm the formulation of I and the new ligands II-IV.

The ^{1}H NMR spectra of the symmetric ligands I, II and IV show a pair of broad triplets for the symmetrically disubstituted ferrocene rings, $(C_5H_4-)_2Fe$, in the region $\delta = 4.0 \sim 4.6$ ppm. The ligand III, however, shows two pairs of broad triplets for the ring protons. This may be due to the presence of a pair of diastereotopic C_p rings, each ring containing two pairs of enantiotopic protons. The characteristic feature of the new ligands II - IV is the presence of a doublet in the range 1.1 to 1.3 ppm due to coupling between phosphorus (^{31}P, 100% abundance, spin = 1/2) and equivalent (or enantiotopic) protons of the tert-butyl groups.

The $^{31}P\{^{1}H\}$ spectra of the ligands I, II, and IV (Fig. 5.2) show a sharp singlet at -17.61, 7.77, and 26.48 ppm, respectively for the pair of equivalent phosphorus atoms. It can be noted that the resonance peak for the phosphorus atoms moves to the lower shielding region as the substitution of the phenyl groups by the tert-butyl groups proceeds. Although the ^{31}P NMR of the ligand III has yet to be obtained, two peaks are expected for the diastereotopic pair of P atoms.

5.1.2 Chiral Ligands

(A) Syntheses

Preparative routes to the chiral ferrocenylphosphines are shown in Fig. 5.3.

Table 5.1: Analytical and physical data for the achiral ligands I-IV.

Compound	mp,°C (decomp.)	Found(%) C	Found(%) H	Calcd(%) C	Calcd(%) H
I	183-185	73.46	4.96	73.67	5.06
II	56-58	68.91	6.95	70.06	7.00
III	-	69.95	6.95	70.06	7.00
IV	oil	-	-	65.84	9.29

Table 5.2: ^{1}H and $^{31}P\{^{1}H\}$ NMR data for the achiral ligands I-IV[a,b].

Compound	$-C_6H_5$	$(C_5H_4-)Fe$	$-CMe_3$	^{31}P
I	7.30(m,20)	4.28(bt,4)	-	($CDCl_3$)
		4.01(bt,4)		-17.61(s)
rac-II	7.80(m,4)	4.32(bt,4)	1.20(d,18)	(C_6D_6)
	7.50(m,6)	4.10(bt,4)	(J_{PH}=12)	7.77(s)
III	7.33(m,10)	4.62(bt,2)	1.12(d,18)	-
		4.48(bt,2)	(J_{PH}=11.5)	
		4.37(bt,2)		
		4.30(bt,2)		
IV	-	4.44(bt,4)	1.22(d,36)	(C_6D_6)
		4.28(bt,4)	(J_{PH}=11)	26.48(s)

a ^{1}H NMR spectra were obtained in $CDCl_3$.

b Coupling constants are in Hz: bt=broad triplet, d=doublet, m=multiplet, s=singlet.

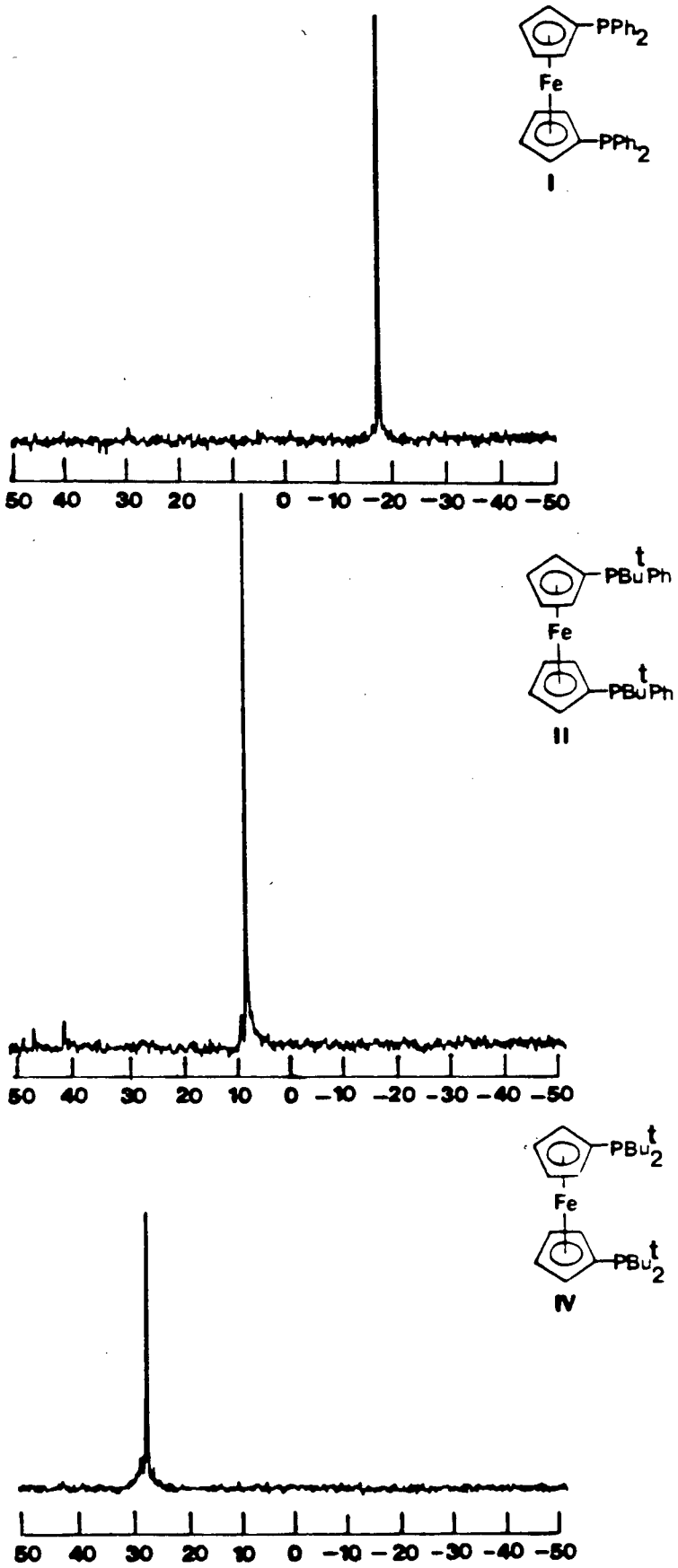

Fig. 5.2: 32.3 MHz $^{31}P\{^{1}H\}$ NMR spectra of the achiral ligands I, II and IV.

All routes require the preparation and the resolution of FA, a key intermediate in the syntheses of various chiral ligands of this sort. FA is readily prepared in high yields (> 75%) using the known procedure [115] as shown in the figure. Thus the nitrile derivative was obtained by reaction of the bisulfite adduct of ferrocene carboxaldehyde with dimethylamine and sodium cyanide. Subsequent reaction of the aminonitrile with MeMgI resulted in FA. There are several other methods to prepare FA [100, 120]. The resolution of FA with (R)-(+)-tartaric acid was achieved using Ugi's procedure [100] from which both antipodes were obtained. The (R)-tartrate of (S)-FA crystallized from methanol, and the (R,R)-diastereomer was obtained by evaporating the mother liquor and crystallizing from aqueous acetone.

The final synthetic routes to form the previously known compound V and the new chiral ligands VI and VII are based on the known procedure set out in Fig. 3.2. The figure shows that monolithiation of FA followed by treatment with halophosphines affords monophosphino-FA ligands, and that bisphosphino-FA ligands such as BPPFA can be prepared via the TMEDA adduct of dilithio-FA generated by stepwise dilithiation of FA in the presence of TMEDA. The figure also shows that the major diastereomeric products obtained from (S)- or (R)-FA have the configuration of (S,R) or (R,S). The minor (4%) diastereomers, (S,S)- or (R,R)-phosphine derivatives can be eliminated by simple recrystallization of the initial products.

In this way the previously known monophosphino-FA V was prepared using the monolithiation of FA followed by treatment with Bu^t_2PCl (a 1.2 molar excess). This compound was obtained as a red crystalline, air-stable solid.

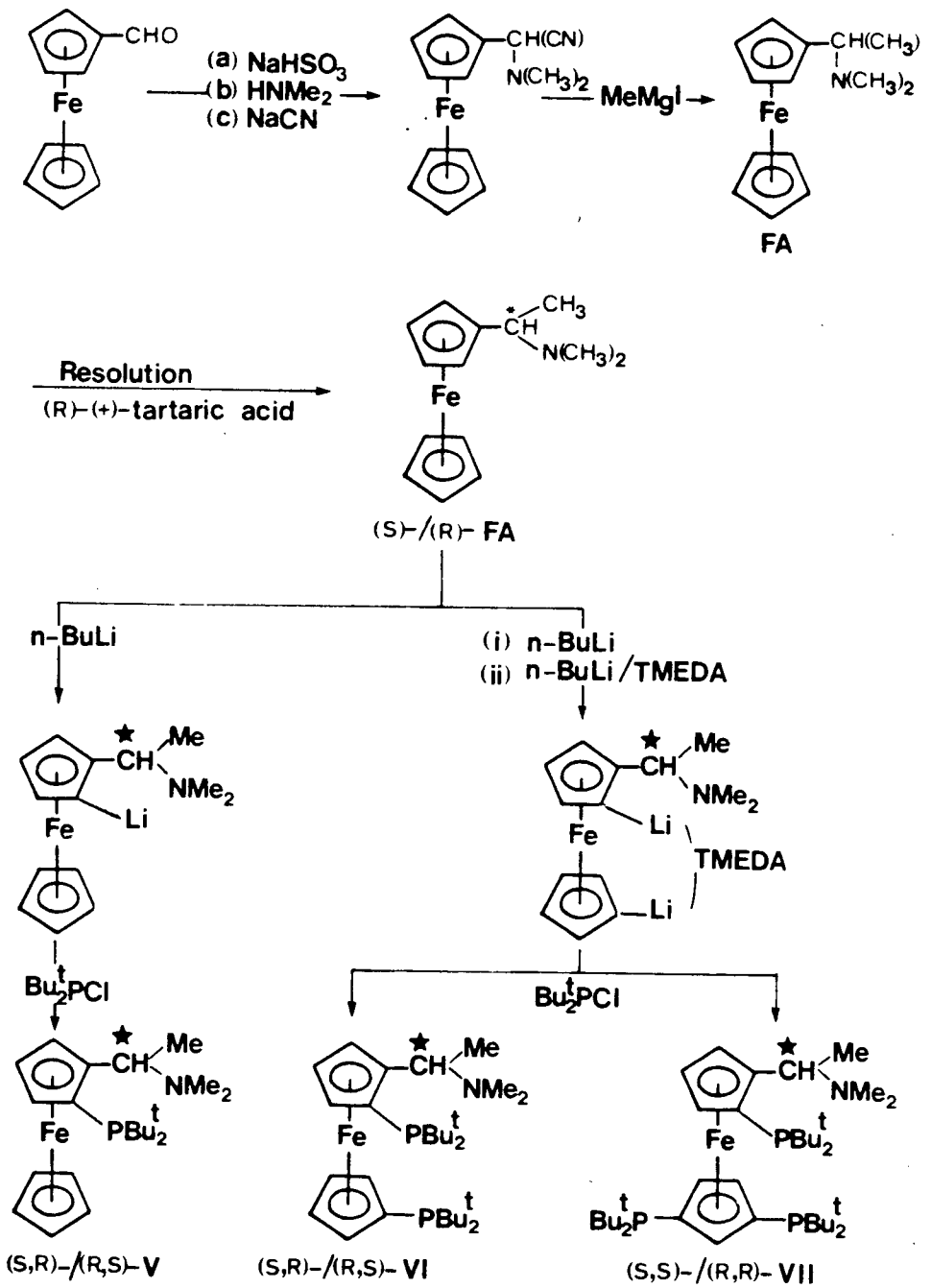

Fig. 5.3: Preparative routes to the chiral ligands V-VII.

As expected, the configuration of the major product (V) is (S,R) and (R,S), respectively when (S)- and (R)-FA is used. The CD spectrum of (R,S)-V is shown in Fig. 5.6.

The new chiral ligands VI and VII were prepared by reacting the *in situ* solution of $Li_2FA \cdot TMEDA$ with excess Bu^t_2PCl. In the present investigation the formation of the bisphosphino-FA ligand VI was found to be slow probably due to steric hindrance. Thus the preferred procedure was to add a 2.2 molar excess of Bu^t_2PCl to the *in situ* solution of $Li_2FA \cdot TMEDA$, and allow the mixture to stir for $1 \sim 2$ days at room temperature (Heating must be avoided). In this way the formation of the monophosphino-FA V as by-product was minimized (< 5%), thus allowing a chromatographic purification (The two phosphines V and VI are almost chromatographically inseparable). The use of the isolated solid $Li_2FA \cdot TMEDA$ [121] in this preparation has little advantage over the direct use of the *in situ* solution. The final product VI was obtained as a red oil (The attempted crystallization from acetone or ethanol was unsuccessful). This reaction also resulted in the formation of (R,S)- and (S,R)-VI as the major product when (R)- and (S)-FA was employed, respectively. This is confirmed by comparing the CD spectrum of the Rh(I) complex of VI with that of the rhodium complex of the monophosphino-FA V (cf. Fig. 5.14A).

During the preparation of the bisphosphino-FA ligand VI, it was accidentally found that further lithiation can take place. Thus in the presence of excess Bu^t_2PCl or under forcing reaction conditions an unexpected product, trisphosphino-FA VII, is obtained as described in the experimental section. This ligand (VII) was prepared either by reacting the *in situ* solution of

$Li_2FA \cdot TMEDA$ with a 3 ∿ 4 molar excess of Bu^t_2PCl at room temperature for 4 days or by adding the <u>in situ</u> solution of $Li_2FA \cdot TMEDA$ to a hexane solution of Bu^t_2PCl (∿ 2.5 molar excess) followed by refluxing the reaction mixture for about 20 h. The initial oily product was recrystallized from acetone or ethanol to give red air-stable crystals. These forcing conditions were initially used in the hope that the formation of the bisphosphino-FA VI would be effected more readily. Consequently, any preparation of the bisphosphino-FA should be carefully monitored to avoid the formation of both the monophosphino-FA V and the trisphosphino-FA VII.

Another striking feature concerning the preparation of the trisphosphino-FA VII is that the final product (crystalline solid) has the configuration of the anticipated minor diastereomer (S,S) or (R,R). Thus (R)-FA leads to (R,R)-VII, and (S)-FA to (S,S)-VII. The CD spectra of both (R,R)- and (S,S)-VII are shown in Fig. 5.8. The crystal structure is described below.

(B) Characterization

The formulation of the previously known V and the new chiral ligands VI and VII is confirmed by the analytical and the NMR data given in Tables 5.3 and 5.4, respectively. In Figs. 5.4 and 5.5 are also given their ^1H and $^{31}P\{^1H\}$ spectra.

The ^1H NMR spectra of both VI and VII show complex multiplets for the C_p ring protons in the range 4.0 to 4.8 ppm, whereas the monophosphine ligand V exhibits a sharp singlet F_2 at 4.07 ppm for the unsubstituted "second" ring as well as a multiplet F_1 for the disubstituted "first" ring in the

Table 5.3: Analytical and physical data for the chiral ligands V-VII.

Compound	mp,°C	(cl,C_6H_6)	Found(%)			Calcd(%)		
			C	H	N	C	H	N
(S,R)-V	55-58	+178.24	41.02	5.57	2.23	41.29	5.63	2.19
(R,S)-V		-178.97						
(S,R)-VI	oil	-22.20	-	-	-	66.07	9.73	2.57
(R,S)-VI		+21.93						
(S,S)-VII	135-137	-37.52	65.68	10.00	2.10	66.10	10.29	2.03
(R,R)-VII		+36.60						

Table 5.4: ^1H and $^{31}P\{^1H\}$NMR data for the chiral ligands V-VII[a,b].

Compound	$-P(CMe_3)_2$	Others	^{31}P
V	1.42(d,9,J_{PH}=12)	1.38(d,-CMe,J_{HH}=8)	13.32(s)
	0.86(d,9,J_{PH}=12)	3.57(dq,-C<u>H</u>Me,J_{HH}=8,J_{PH}=4)	
		2.11(s,$-NMe_2$)	
		4.07(s,(C_5H_5-)Fe)	
		4.16-4.46(m,(C_5H_3-)Fe	
VI	1.6(d,9,J_{PH}=12)	1.35(d,-CMe,J_{HH}=8)	14.53(s)
	1.3(d,9,J_{PH}=12)	4.00(dq,-C<u>H</u>Me,J_{HH}=8,J_{PH}=4)	26.74(s)
	1.2(d,9,J_{PH}=12)	2.20(s,$-NMe_2$)	
	1.1(d,9,J_{PH}=12)	4.1-4.5(m,($C_5\underline{H}_3$-)Fe($C_5\underline{H}_4$))	
VII	1.7(d,9,J_{PH}=12)	1.80(d,-CMe,J_{HH}=8)	17.67(s)
	1.5(d,9,J_{PH}=10)	3.80(dq,-C<u>H</u>Me,J_{HH}=8,J_{PH}=4)	23.49(s)
	1.2(d,9,J_{PH}=12)	2.40(s,$-NMe_2$)	26.63(s)
	1.1(d,9,J_{PH}=12)	4.4-4.8(m,($C_5\underline{H}_3$-)$_2$Fe)	

[a] All spectra were obtained in C_6D_6 using the racemic mixture of each ligand. Coupling constants are in Hz:dq=doublet of quart,s=singlet.

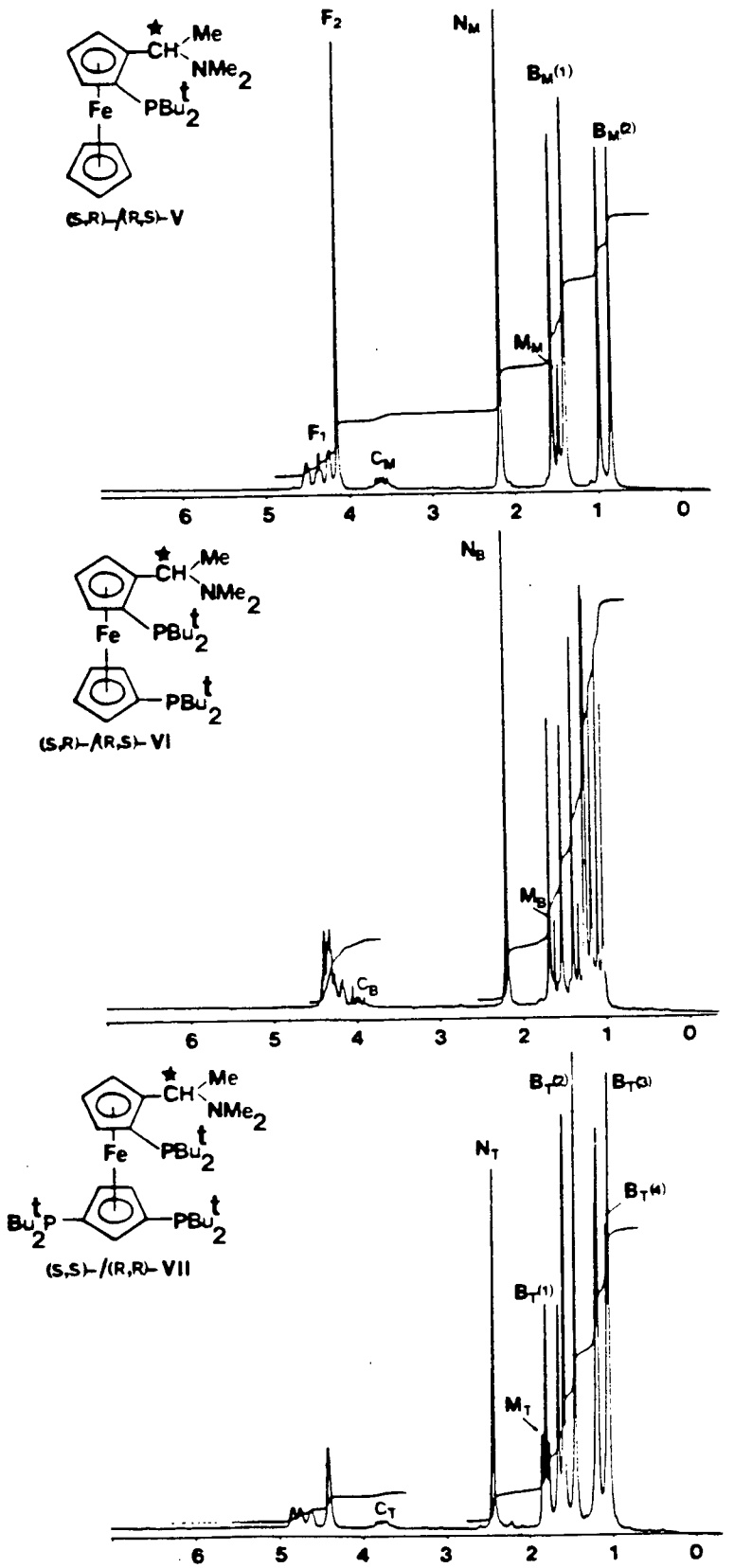

Fig. 5.4: 80 MHz ^{1}H NMR spectra of the chiral ligands V-VII in C_6D_6.

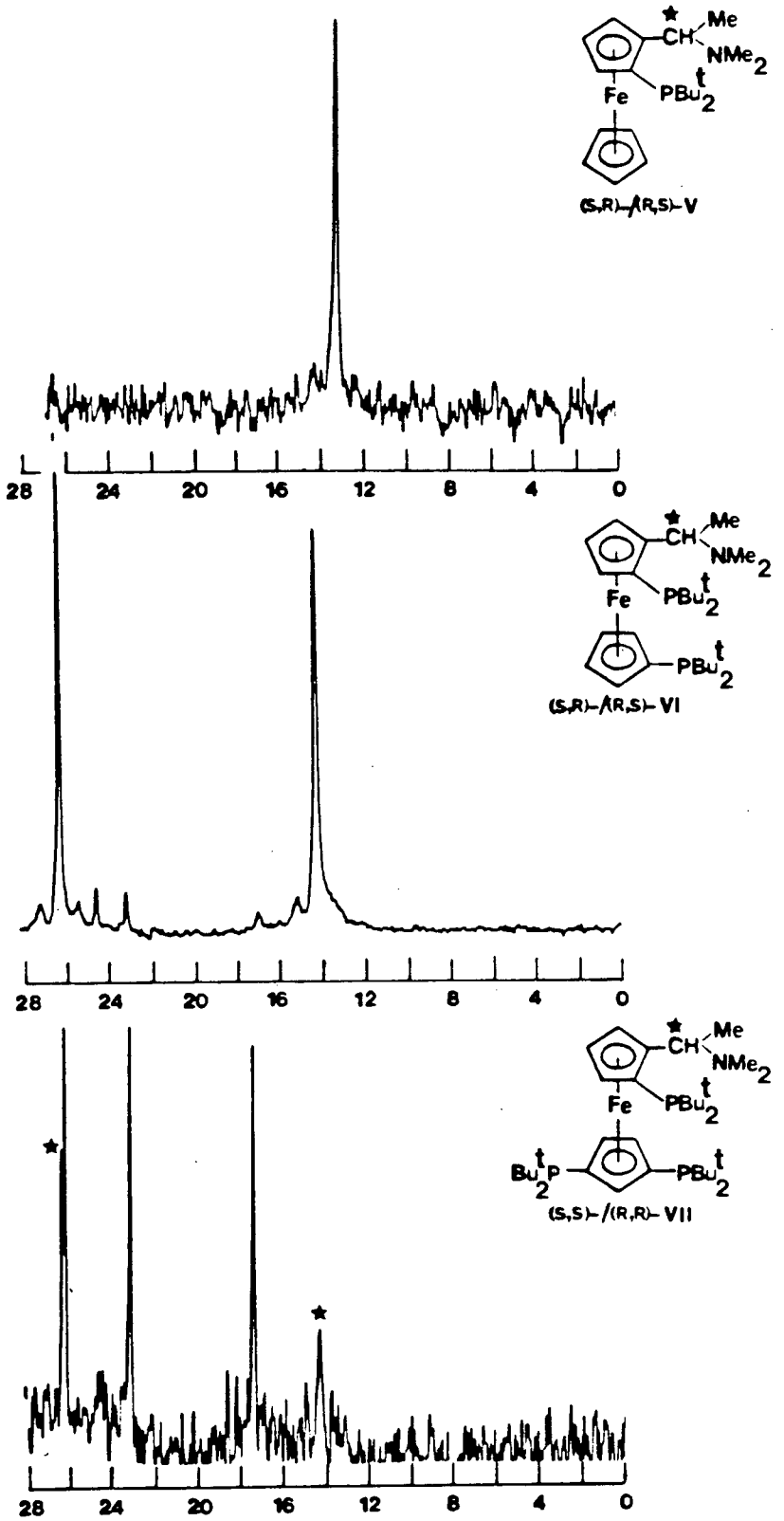

Fig. 5.5: 32.3 MHz $^{31}P\{^{1}H\}$ NMR spectra of the chiral ligands V-VII in C_6D_6. Resonances with the asterisk are due to VI as an impurity.

range 4.16 to 4.46 ppm. Here the terms "first" and "second" rings refer to the C_p ring containing the -CH(Me)NMe_2 group and the other C_p ring, respectively, and will be used in the subsequent discussion.

The methine proton (-C<u>H</u>Me) of the mono-, bis-, and trisphosphine ligands appears as a doublet of quartets centered at 3.57 (peak C_M), 4.0 (peak C_B), and 3.8 (peak C_T) ppm, respectively. This pattern arises due to the coupling with the neighboring phosphorus atoms ($^4J_{PH}$) as well as the methyl group (-CH<u>Me</u>) on the asymmetric center, as checked by homonuclear (H-H) coupling in these ligands. The coupling constants $^4J_{PH}$ and $^3J_{HH}$ in these ligands are listed in Table 5.4. The -NMe_2 group in the mono-, bis-, and trisphosphine ligands gives a sharp singlet at 2.11 (peak N_M), 2.20 (peak N_B), and 2.40 (peak N_T) ppm, respectively. This singlet arises because of rapid inversion at the N atom. The methyl group (-CH<u>Me</u>) on the asymmetric center in the mono-, bis-, and trisphosphine ligands gives a doublet at 1.38 (peak M_M), 1.35 (peak M_B), and 1.8 (peak M_T) ppm, respectively. The striking difference between V and VI or VII is that the former shows two doublets $B_M(1)$ and $B_M(2)$ at 1.42 and 0.86 ppm for the -$P(CMe_3)_2$ group, whereas the latter two ligands show four doublets in the range 1.1 to 1.7 ppm with coupling constants of 10 to 12 Hz (Table 5.4). Here it is interesting to note that the trisphosphine ligand VII gives only four doublets $B_T(1)$, $B_T(2)$, $B_T(3)$, and $B_T(4)$ instead of six for the three-$P(CMe_3)_2$ groups. Thus the doublets $B_T(2)$ and $B_T(3)$ of higher intensities can be reasonably assigned to the two -$P(CMe_3)_2$ groups in the second ring, and the other two $B_T(1)$ and $B_T(2)$ to the -$P(CMe_3)_2$ group in the first ring. The four doublets in the bisphosphine ligand VI can not be easily assigned.

The $^{31}P\{^{1}H\}$ NMR spectra of these ligands (V-VII) (Fig. 5.5) show, as expected, one, two, and three resonance peaks, respectively for the P atom(s) with the chemical shifts given in Table 5.4. Fig. 5.5 shows that the ^{31}P peak to higher shielding can be assigned to the P atom in the first ring, and the peak moves to lower shielding as substitution in the second ring proceeds. Thus the peak(s) with the higher chemical shifts can be assigned to the P atom(s) in the second ring.

(C) Determination of Configuration

As mentioned previously, the preparation of both V and VI led to the expected configuration (R,S) or (S,R) when (R)- or (S)-FA was used as the starting material. The CD spectrum of (R,S)-V is seen in Fig. 5.6 which shows the positive $\Delta\varepsilon(=\varepsilon_{\ell}-\varepsilon_{\gamma})$ values around 545 $\sim$ 570 and 340 $\sim$ 385 nm, and the negative maximum $\Delta\varepsilon$ value at about 465 nm. This pattern is in accordance with that of other known FA-based phosphine ligands [104b], allowing the identification of the configuration of this compound. Thus, for example, the ligands (S,R)-PPFA, (S,R)-BPPFA, and (R)-PPEF have the positive maximum and the negative maximum $\Delta\varepsilon$ values around 450 $\sim$ 470 nm and 340 $\sim$ 350 nm, respectively, whereas (R,S)-MPFA gives the spectrum which is virtually in the mirror image of those of the above three ligands. Here it can be noted that the ligands (R)-PPEF and (R,S)-MPFA have the opposite planar chirality. Although the CD spectrum of the bisphosphine ligand VI has yet to be obtained, the configuration of this compound can be easily determined by examining the CD spectrum of its Rh(I) complex. This will be discussed later in section 5.2.2(C).

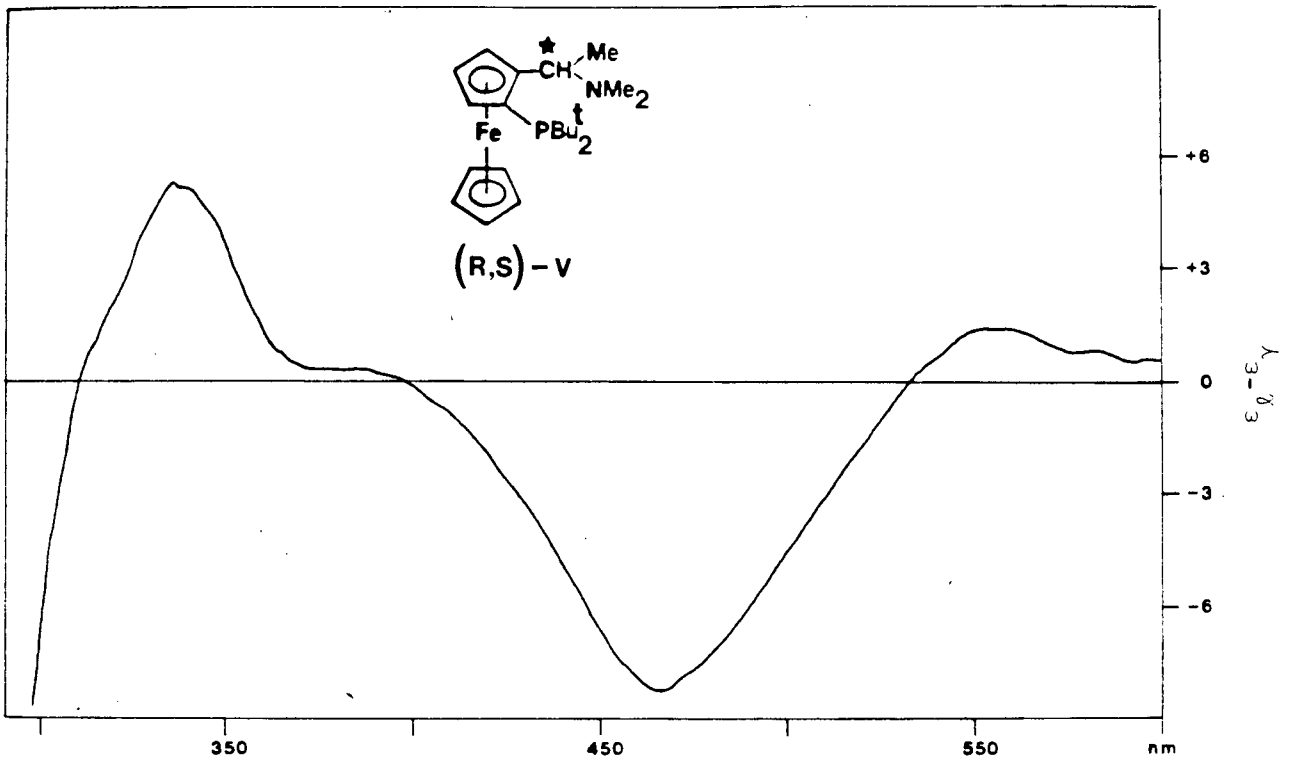

Fig. 5.6: CD spectrum of the chiral ligand (R,S)-V in $CHCl_3$;
[Ligand] = 4.0×10^{-4}M, $\Delta\varepsilon = \varepsilon_{\ell} - \varepsilon_{\gamma}$ = molar circular dichroism.

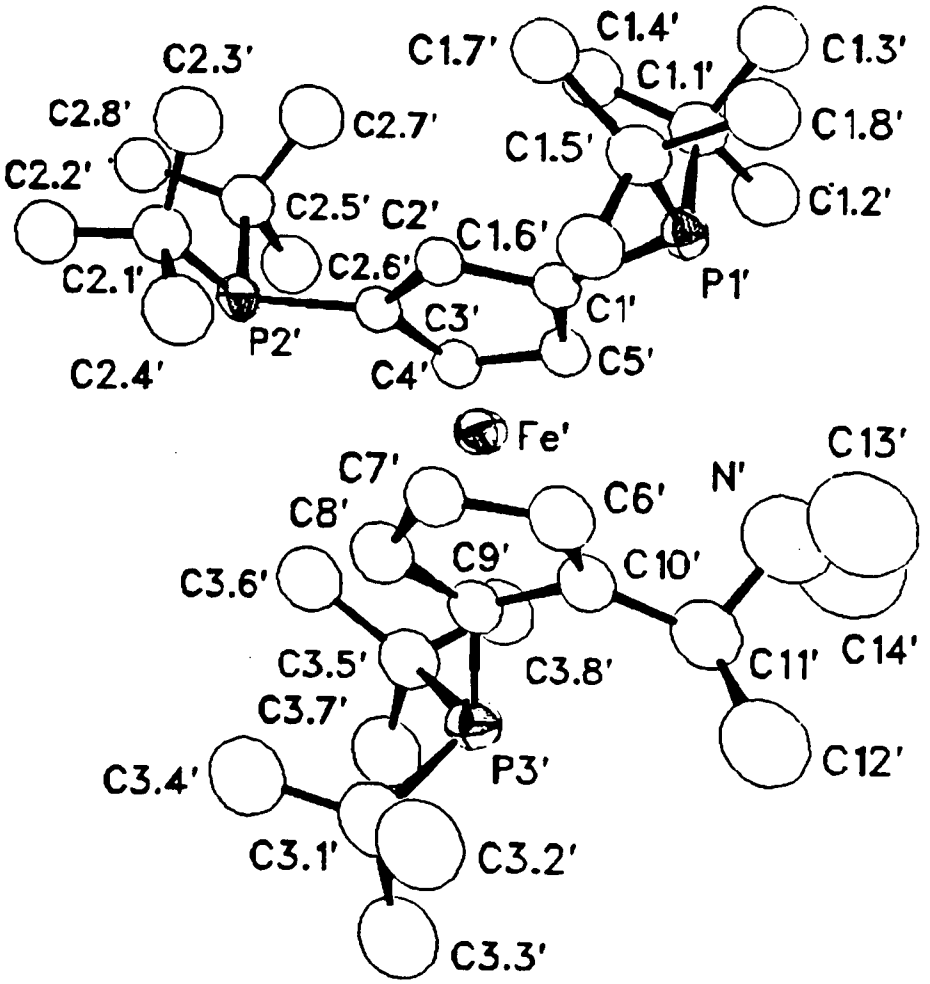

Fig. 5.7: The crystal structure of the chiral ligand (S,S)-VII [122].

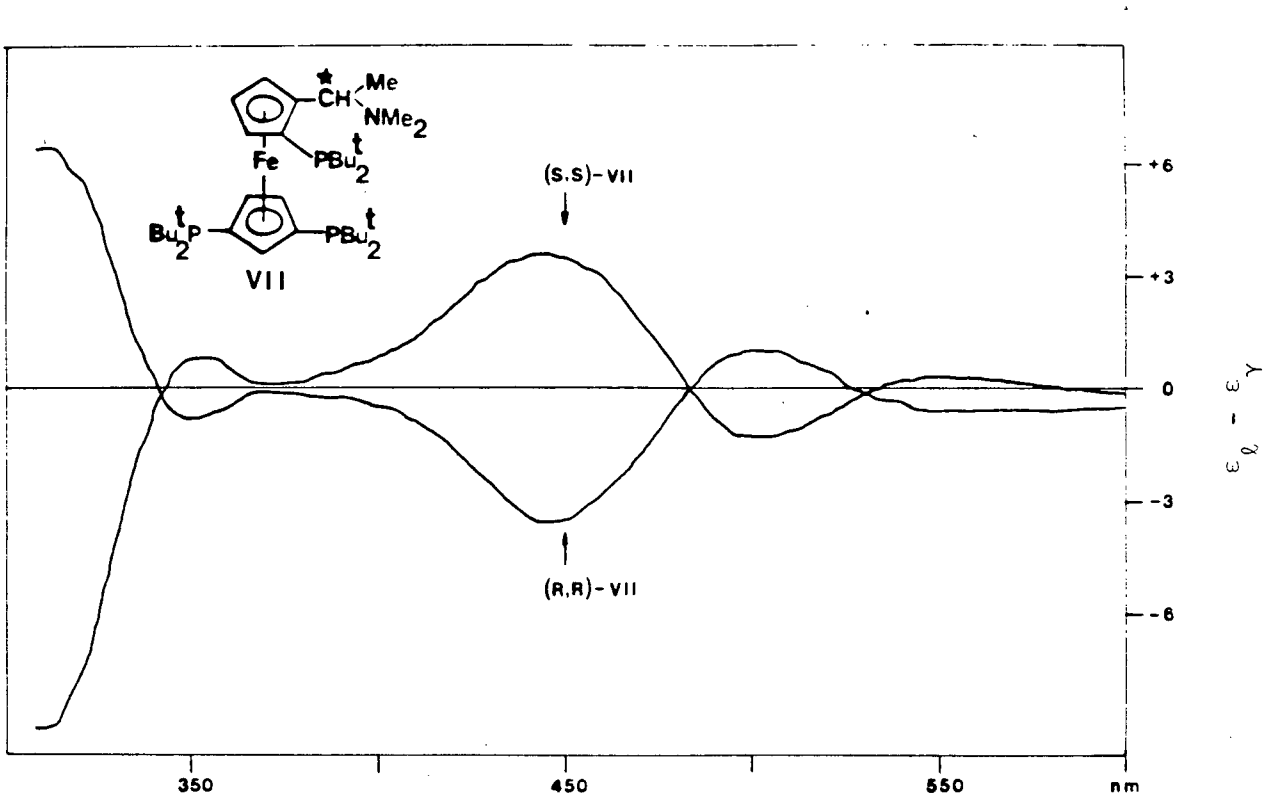

Fig. 5.8: CD spectra of the chiral ligand (S,S)- and (R,R)-VII in $CHCl_3$; [Ligand] = 4.5×10^{-4}M, $\varepsilon_\ell - \varepsilon_\gamma$ = molar circular diochroism.

Quite surprisingly, however, the configuration of the trisphosphine ligand VII is that of the supposed minor diastereomer, that is, (R,R)- or (S,S)-VII when (R)- or (S)-FA is employed as the starting material. This is confirmed by a crystal structure and the CD spectrum of a sample. Fig. 5.7 shows that the compound derived from (S)-FA has the (S,S)-configuration. The CD spectrum of this crystal, as shown in Fig. 5.8, is in the mirror image of that of (R,R)-VII which is prepared from (R)-FA. It may be noted by comparing Fig. 5.6 with Fig. 5.8 that the CD pattern of (R,S)-V is similar to that of (S,S)-VII rather than (R,R)-VII. It seems that planar chirality plays an important role in determining the signs of $\Delta\varepsilon$ values. Although the results are reproducible, it is not certain at this stage whether this unexpected diastereomer (R,R) or (S,S) is truely a thermodynamic product or the one preferentially isolated during the work up which involved chromatographic separation and recrystallization of the diastereomeric mixture.

5.2 CATIONIC RHODIUM(I) COMPLEXES OF FERROCENYLPHOSPHINES

5.2.1 Achiral Complexes

(A) Syntheses

The hydrogenation catalyst precursors VIII-XI of the type $[Rh(P\text{-}P)(NBD)]ClO_4$ (P-P = I-IV) were prepared using well-established procedures [32e] as described in equation (5.3).

$$[Rh(NBD)Cl]_2 + P\text{-}P \xrightarrow[THF]{NaClO_4} [Rh(P\text{-}P)(NBD)]ClO_4 \qquad (5.3)$$

VIII ; P-P = I
IX ; = II
X ; = III
XI ; = IV

The typical procedure was to dissolve $[Rh(NBD)Cl]_2$ and a 2 ∿ 2.5 molar excess of ligand in benzene, and add to this solution a 2 ∿ 2.5 molar excess of $NaClO_4$ dissolved in THF. As a precaution both solvents were degassed before the reactants were mixed. These complexes, except for XI, separated as orange precipitates from the reaction mixture after a short period of stirring (5 min - 1h) at room temperature. For the preparation of XI, the reaction mixture was stirred for 1 - 2 days to give a reddish brown solid after the solvents had been removed. All these catalyst precursors were obtained in high yields (70 - 80%) as deep red crystals on crystallization from CH_2Cl_2/cyclohexane solution. Although they are generally stable in both the solid and solution, the complex XI was found to undergo slight decomposition in $CHCl_3$.

(B) Characterization

The formulation of these products is confirmed by the analytical results (Table 5.5) and their NMR spectra (Table 5.6 and Fig. 5.9). More direct confirmation comes from the crystal structures shown in Figs. 5.10 - 5.13.

Table 5.5: Analytical and physical data for the achiral Rh(I) complexes $[Rh(P\text{-}P)(NBD)]ClO_4$.

Compound	P-P	mp°,C (decomp.)	Found C	Found H	Calcd(%) C	Calcd(%) H
VIII	I	192-194	57.16	4.22	58.00	4.24
IX	II	182-183	54.24	5.28	54.93	5.44
X	III	179-180	53.70	5.25	54.93	5.44
XI	IV	153-155	51.46	6.70	51.55	6.77

Table 5.6: ^1H and $^{31}P\{^1H\}$ NMR data for the achiral complexes VIII-XI[a,b].

Compound	$-C_6H_5$	$(C_5H_4-)Fe$	$-CMe_3$	NBD	^{31}P	Δ
VIII	7.5-8.0 (m,20)	4.4(bm,8)	-	4.4(bm,4) 4.1(bm,2) 1.5(bm,2)	(MeOH) 14.84(d) (J_{Rh}=161)	32.45
IX	7.78(m,6) 8.78(m,4)	4.3(bm,6) 4.05(bm,2)	1.1(d,18) (J_{PH}=14)	5.7(bm,2) 5.2(bm,2) 4.0(bm,2) 1.8(bm,2)	(MeOH) 32.51(d) (J_{Rh}=155)	24.74
X	7.65(m,5) 7.85(m,5)	4.62(bm,2) 4.48(bm,2) 4.35(bm,2) 4.20(bm,2)	1.5(d,18) (J_{PH}=12)	5.7(bm,4) 3.9(bm,2) 1.7(bm,2)	-	-
XI	-	4.6(bm,4) 4.55(bm,4)	1.6(d,36) (J_{PH}=12)	5.3(bm,4) 3.1(bm,2) 2.8(bm,2)	(CH_2Cl_2) 45.81(d) (J_{Rh}=148)	18.73

a ^1H NMR spectra were obtained in $CDCl_3$ except X(acetone-d^6).

b Coupling constants are in Hz, and coordination chemical shift (Δ) in ppm: d=doublet, m=multiplet, bm=broad multiplet.

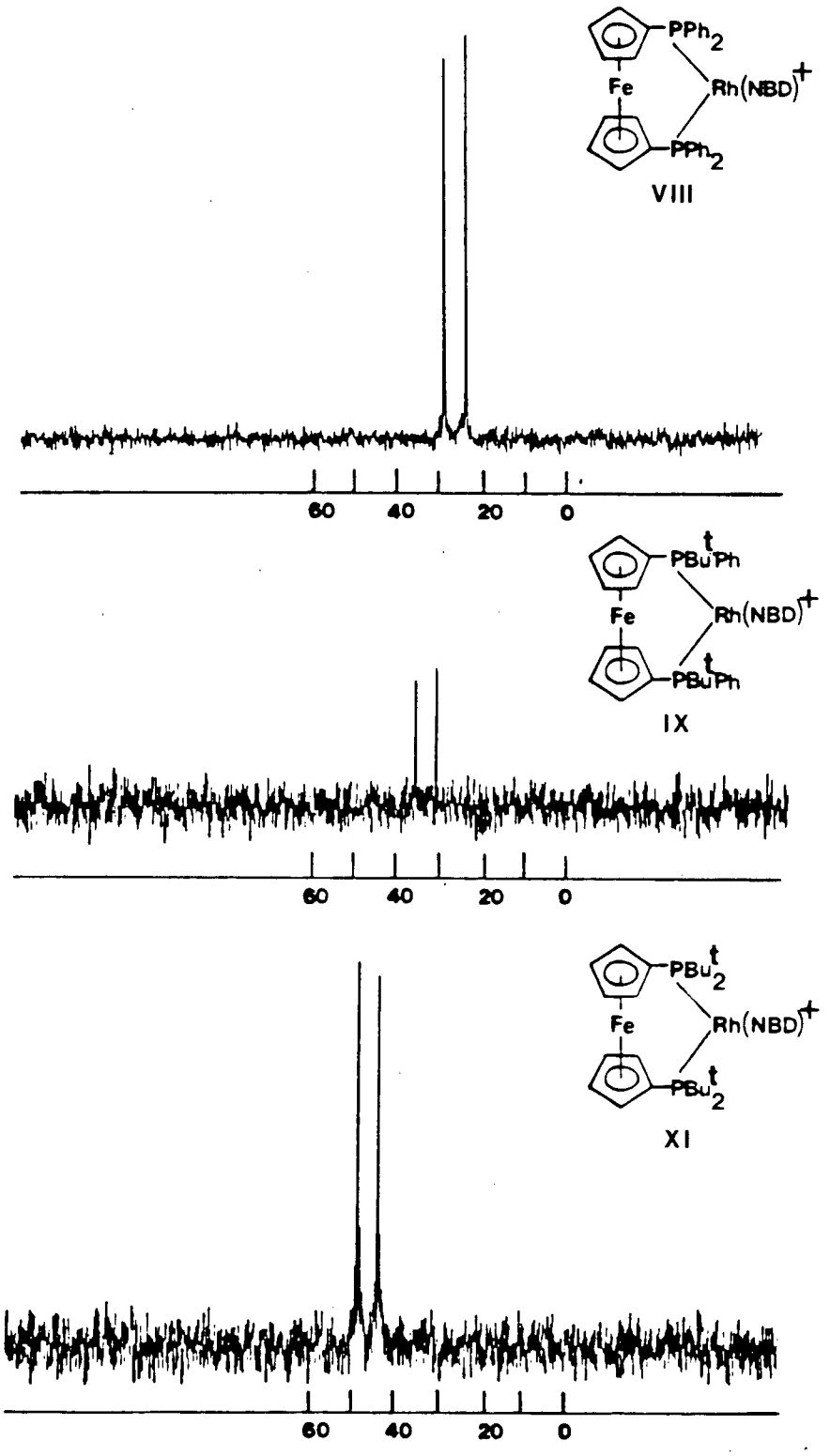

Fig. 5.9: 32.3 MHz $^{31}P\{^{1}H\}$ NMR spectra of the achiral complexes VIII, IX and XI.

The ^1H NMR spectrum of each of these complexes consists of resonance peaks from the coordinated phosphine ligand and from the NBD ligand. The ^1H NMR pattern of each ligand is virtually identical with that of the corresponding free ligand except for some line broadening accompanied by changes in chemical shifts. Thus, for example, resonances in the phenyl region and the ferrocenyl region are more spread out in the complex, indicating that their relative orientations and positions are more fixed upon complexation. However, little change in the chemical shift and coupling constant is observed in the $-P(CMe_3)$ region. The NBD ligand in the complexes VIII, X, and XI shows three broad multiplets, one for the bridging carbon protons ($-CH_2-$) in the region δ = 1.5 - 2.8 ppm, the other for the pair of protons (-CH) in the region δ = 3.1 - 4.1 ppm, and another for the four olefinic protons in the region δ = 4.4 - 5.7 ppm. As expected, the complex IX exhibits two broad multiplets of equal intensities at 5.2 and 5.7 ppm due to the two diastereotopic pair of equivalent protons (Note the ligand is a rac-isomer as shown in Fig. 5.11). Yet it is not clear why the complex X containing the unsymmetrically substituted C_p rings shows only one broad multiplet for the olefinic protons rather than two.

The $^{31}P\{^1H\}$ NMR spectra of VII, IX and XI show the expected doublets at 14.84, 32.51 and 45.81 ppm, respectively, due to the coupling of the chelating phosphines with the Rh atom (^{103}Rh, spin = 1/2). Coupling constants range from 148 to 161 Hz. It can be noted that the magnitude of coordination chemical shift (Δ) decreases as the phenyl group is substituted by the tert-butyl group (Table 5.6). Thus it is interesting to note that the Δ value for the complex IX

is approximately the arithmetic mean of those for the complexes VIII and XI.

The crystal structures of these complexes are shown in Figs. 5.10 - 5.13. The Rh atom in each complex may be described, very crudely, as lying in a square planar environment, assuming that two double bonds of the NBD ligand occupy single coordination sites. The complexes IX and XI have an approximate C_2 axis along the Rh-Fe direction, whereas VIII and X have a symmetry plane. The parent ferrocene moiety adopts the staggered conformation in all cases. A number of other interesting features can also be made. The most prominent of these features include, as summarized in Table 5.7, a very wide P-Rh-P angle, exceptionally long Rh-P(Bu^t,Bu^t) distances, and a large twist angle due to the steric crowding caused by the bulky tert-butyl groups. In general, as phenyl groups are replaced with the more sterically demanding tert-butyl groups, longer Rh-P bond, higher P-Rh-P angles, and higher twist angles are obtained. The bite angle (<MP(1)-Rh-MP(2)) in all compounds are essentially constant due to the rigidity of the NBD ligand.

5.2.2 Chiral Complexes

(A) Syntheses

The following chiral rhodium(I) complexes were prepared using the same procedure described for the preparation of the achiral complexes (equation 5.3).

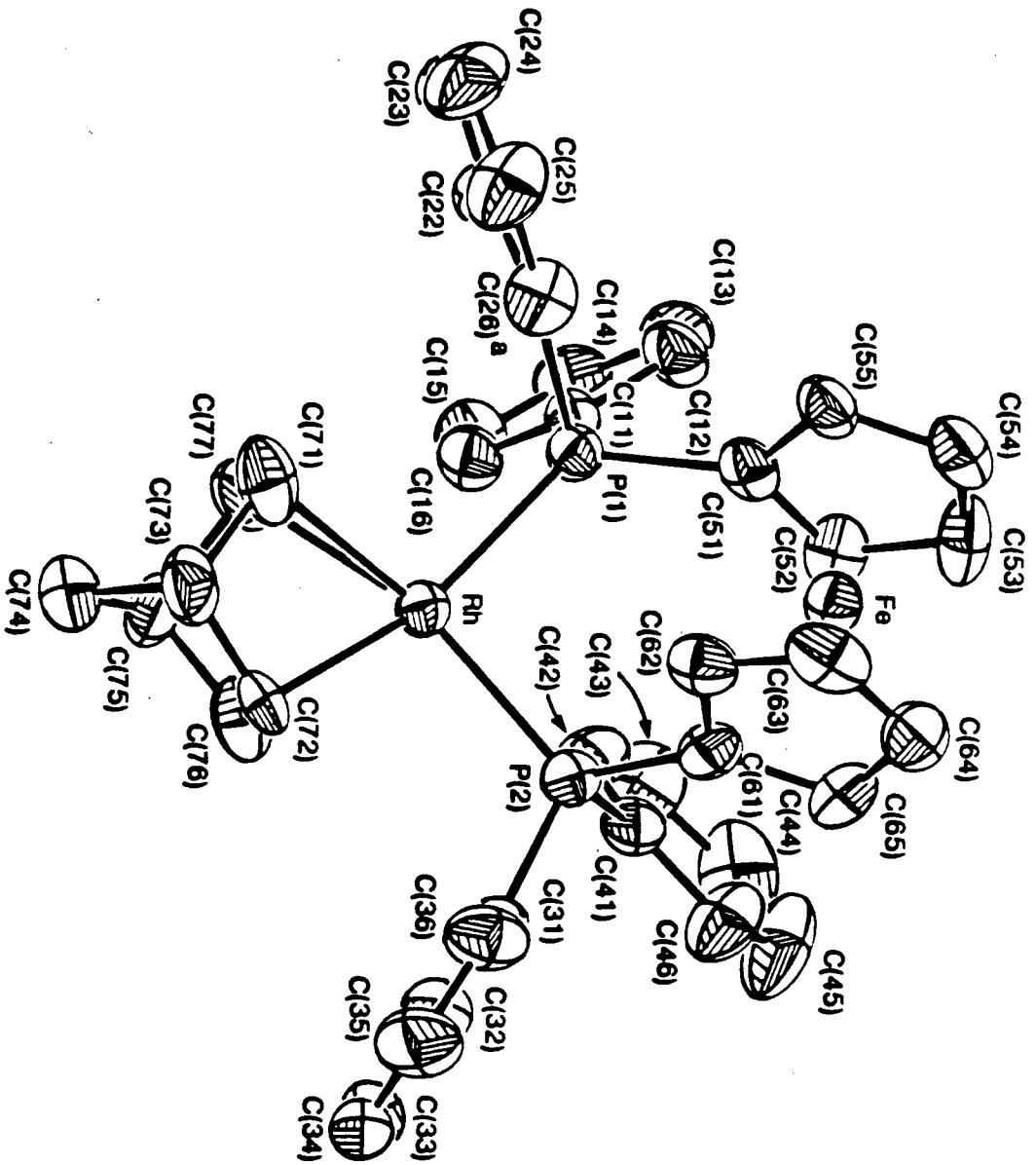

Fig. 5.10: The crystal structure of the Rh(I) complex VIII [123].

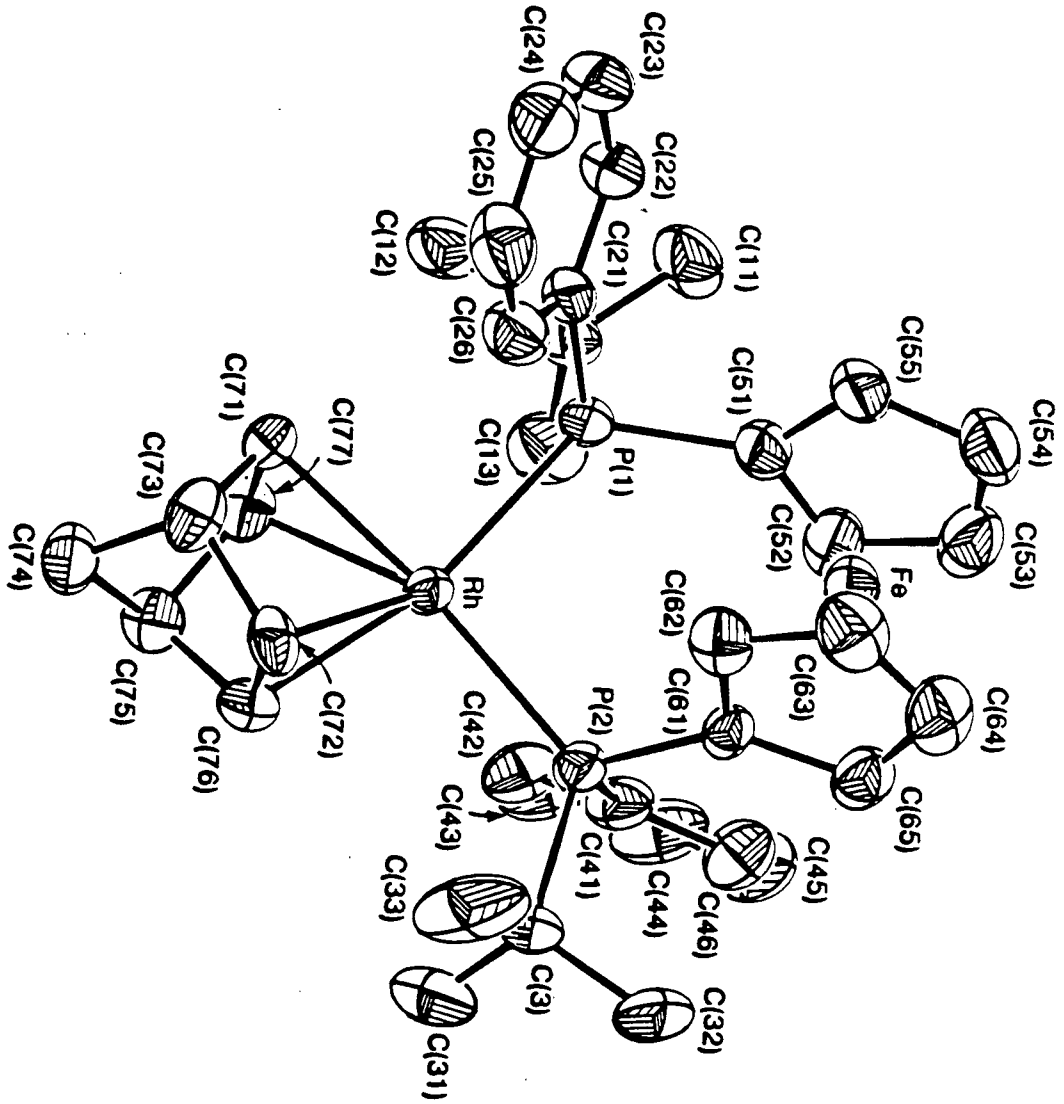

Fig. 5.11: The crystal structure of the Rh(I) complex IX [123].

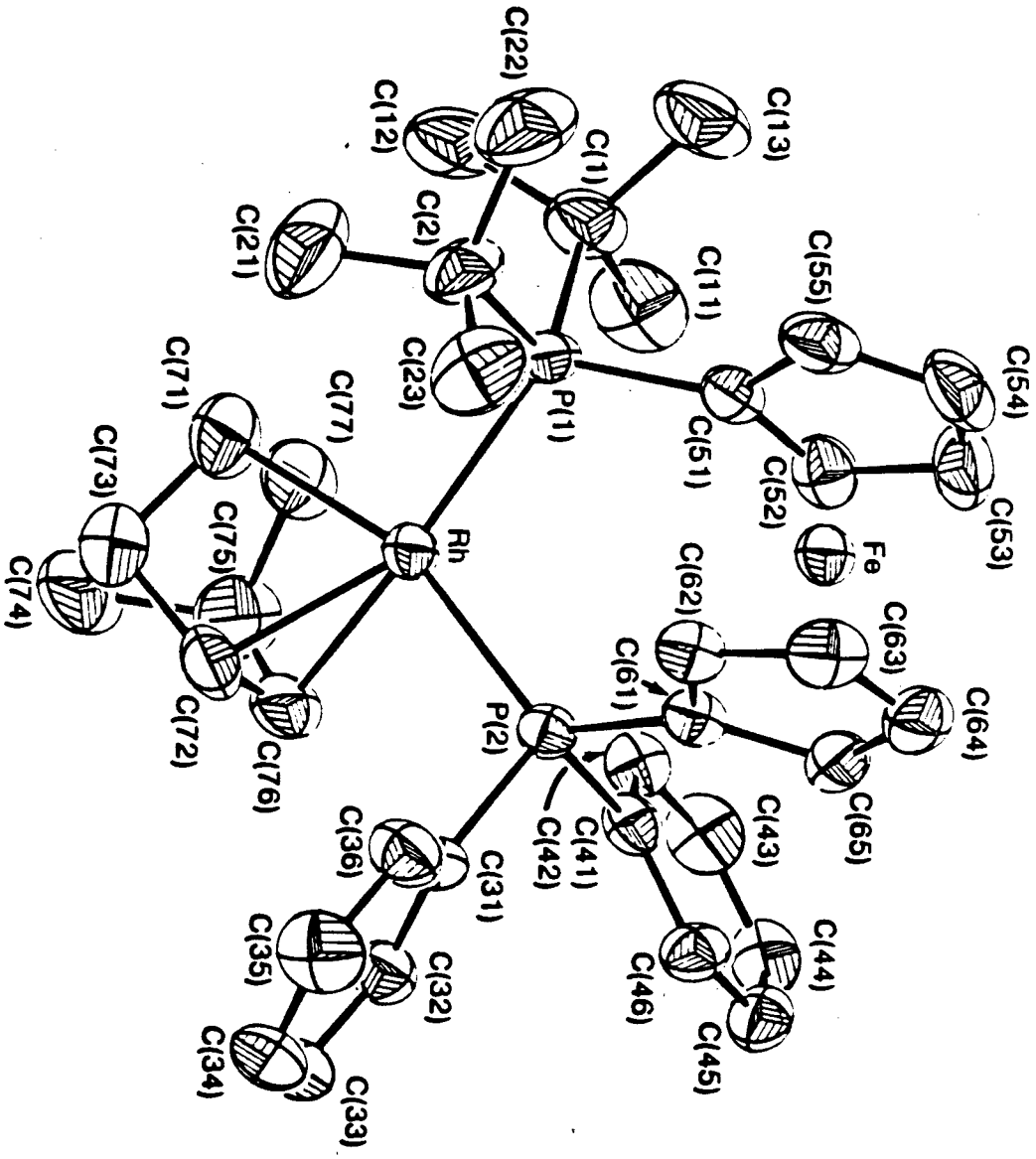

Fig. 5.12: The crystal structure of the Rh(I) complex of X [123].

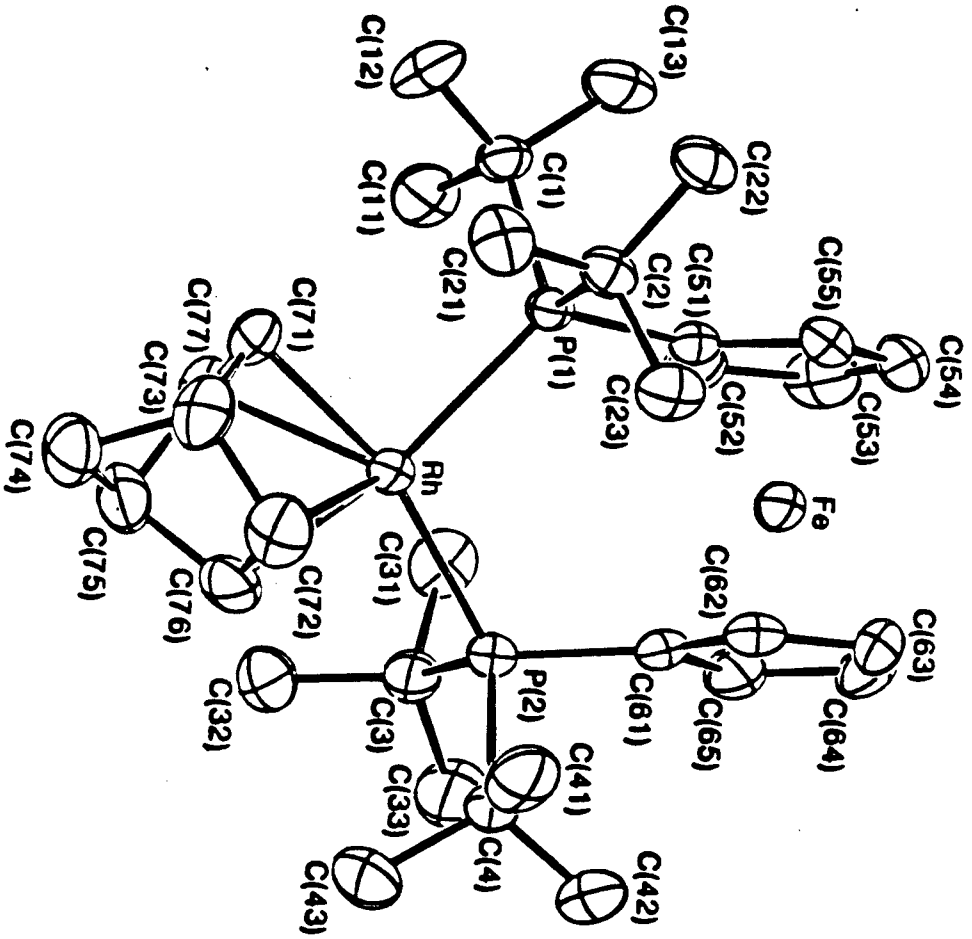

Fig. 5.13: The crystal structure of the Rh(I) complex XI [102d].

Table 5.7: Summary of important bond parameters for the achiral Rh(I) complexes VIII-XI [123].

	VIII	IX	X	XI
Rh-P(Bu^t,Bu^t) [a]	-	-	2.391	2.466 2.458
Rh-P(Bu^t,Ph)	-	2.416 2.388	-	-
Rh-P(Ph,Ph)	2.335 2.317	-	2.356	-
P-Rh-P	96.82	98.60	100.25	103.71
MP(1)-Rh-MP(2) [b]	68.2	69.1	68.0	68.4
Twist angle [c]	5.9	20.0	14.4	36.8

[a] The notations P(Bu^t,Bu^t) or P(Bu^t,Ph) etc., define the substituents, other than cyclopentadienyl, which are joined to phosphorus.

[b] MP(1) and MP(2) are the middle points of the two olefinic C atoms.

[c] Twist angle is defined as the angle between the Rh, P(1), P(2) plane and the Rh, MP(1), MP(2) plane.

$[Rh(P^{\sim}N)(NBD)]ClO_4$

XII ; $P^{\sim}N$ = V
XIII ; = VI
XIV ; = VII

Following the usual work-up procedures, all products were isolated as orange solids which were recrystallized from ethanol to give deep red crystals in moderate yields (50 - 55%). Although they are generally stable in both the solid and solution, slight decomposition was observed in $CHCl_3$.

(B) Characterization

The analytical results (Table 5.8) and $^{31}P\{^1H\}$ NMR data (Table 5.9) confirm the formulation of the previously known rhodium(I) complex XII and the new chiral complexes XIII and XIV. Here the configurations are those of the chiral ligands V - VII.

The CD spectra of (R,S)-XII and (S,S)-/(R,R)-XIV are shown in Figs. 5.14(A) and 5.14(B), respectively. It is interesting to note that the signs of specific rotation and $\Delta\varepsilon$ of the free ligands are reversed upon complexation (cf. Tables 5.3 and 5.8; Figs. 5.6, 5.8 and 5.14). In Fig. 5.14(A) is also shown the CD spectrum of the bisphosphine complex XIII prepared from (S)-FA. By examining the two spectra in Fig. 5.14(A) it can be concluded that the configuration of the free bisphosphine ligand VI in the complex XIII is (S,R)

Table 5.8: Analytical and physical data for the chiral complexes $[Rh(P\text{-}N)(NBD)]ClO_4$ [a].

Compound	mp,°C	$[\alpha]_D$ (c0.5,$CHCl_3$)	Found(%) C	Found(%) H	Found(%) N	Calcd(%) C	Calcd(%) H	Calcd(%) N
(S,R)-XII	-	-72.3	50.17	6.24	1.97	50.12.	6.19	2.02
(R,S)-XII		+71.9						
(S,R)-XIII	121-123	-295,52	52.17	7.45	1.63	52.90	7.27	1.67
(R,S)-XIII		+297.21						
(S,S)-XIV	147-149	+169.39	54.12	7.86	1.19	54.91	7.93	1.42
(R,R)-XIV		-170.82						

Table 5.9: $^{31}P\{^1H\}$ NMR data for the chiral Rh(I) complexes [a,b].

Compound	^{31}P
(S,R)-XII	($CDCl_3$) 34.0(bd,J_{Rh}=154)
(S,R)-XIII	($CDCl_3$) 36.46(bd,J_{Rh}=154) 25.87(bs)
(S,S)-XIV	(CD_2Cl_2) 38.02(d,J_{Rh}=152.6) 27.88(s) 25.38(s)

[a] The configurations (R,S) or (S,R) etc., are those of the chiral ligands V-VII.

[b] Coupling constants are in Hz:bd=broad doublet, bs=broad singlet, s=singlet.

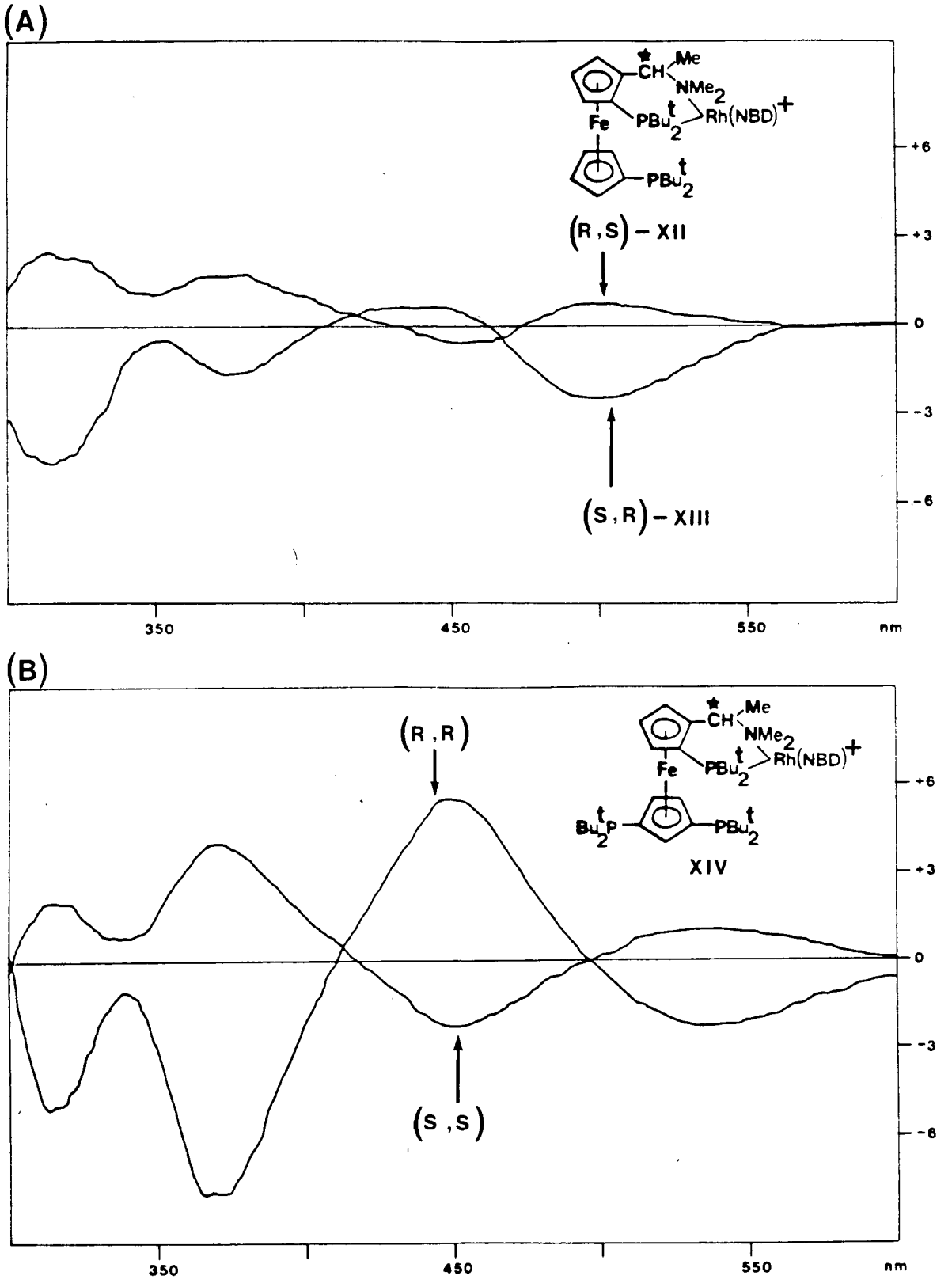

Fig. 5.14: (A) CD spectra of (R,S)-XII and (S,R)-XIII.

(B) CD spectra of (R,R)- and (S,S)-XIV.

as expected. This configuration is that of the expected major product when (S)-FA is used (the configuration of the ligands V and VII is well established).

The $^{31}P\{^{1}H\}$ NMR spectra (Fig. 5.15) indicate that all these complexes use N and P atoms to form the rhodium complex. The coordinated phosphine in these complexes XII - XIV is the one neighboring the $-CH(Me)NMe_2$ groups as is known for $[Rh(PPFA)(NBD)]^+$ (Fig. 5.16). This can be established by comparing the ^{31}P spectra of these complexes with those of the free ligands V - VII. Namely, the most shielded peak (Fig. 5.5) due to the phosphorus in the first ring disappears and is replaced by a doublet with greater chemical shift upon complexation (Fig. 5.15). Therefore the doublet can be assigned to the phosphine in the first C_p ring. Other phosphine signals are only slightly affected by complexation. The coordinated phosphine, in all cases, appearsas a doublet (D_M, D_B and D_T). The $-P(CMe_3)_2$ group in the second C_p ring appears as singlet with lower chemical shift: S_B and S_T/S_T' for XIII and XIV, respectively.

The most striking difference in the ^{31}P NMR pattern between the trisphosphine complex XIV and the mono- or bisphosphine complex (XII or XIII) is that the resonance signals for the latter two are quite broad, whereas the former gives sharp signals (Fig. 5.15). The broadening indicates the existence of conformers interconverting slowly on the NMR time scale. The sharp signals for the former (XIV) indicate that this complex adopts only one conformation on the NMR time scale. It is likely that the six-membered chelate ring conformation of this complex (XIV) is fixed because of steric crowding. Before presenting further evidence for these conformational effects, it is

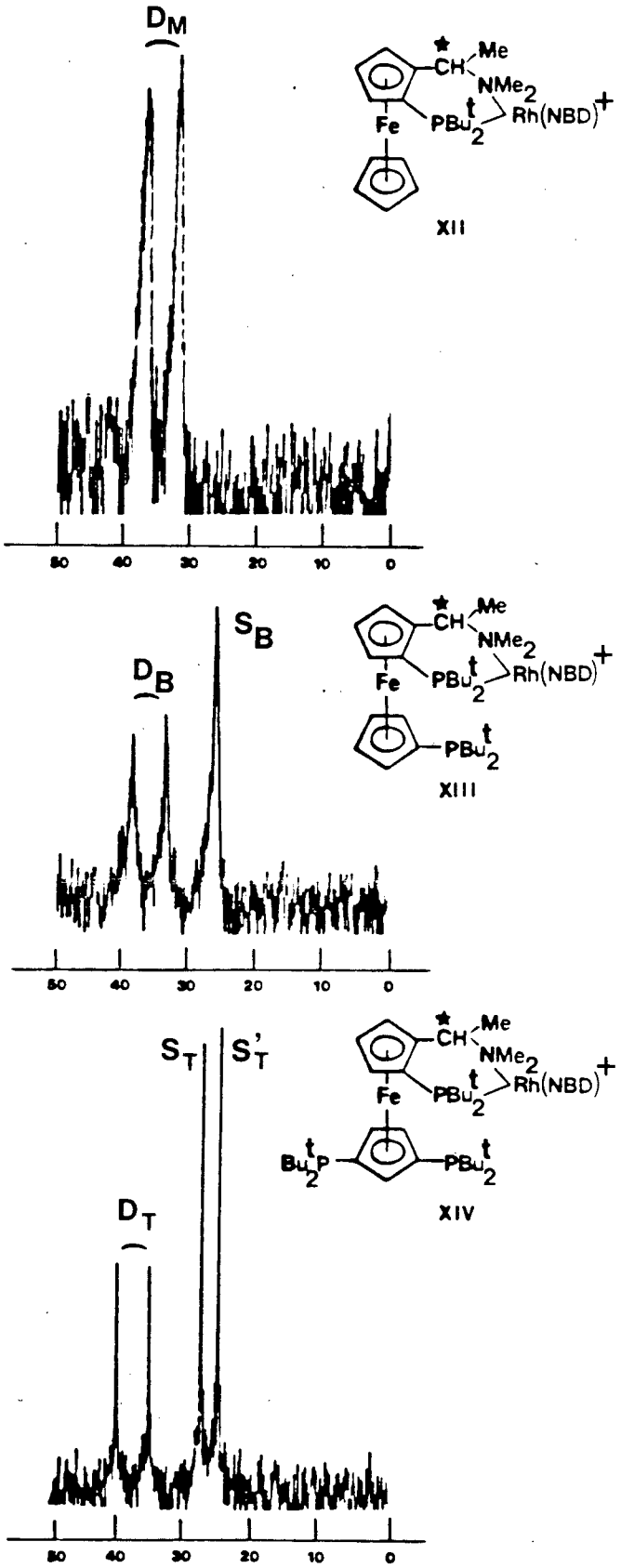

Fig. 5.15: 32.3 MHz $^{31}P\{^{1}H\}$ NMR spectra of the chiral Rh(I) complexes (S,R)-XII, (S,R)-XIII, and (S,S)-XIV.

useful to discuss possible conformational exchange processes.

The complexes XII-XIV contain a six-membered chelate ring whose conformation should be analogous to that of cyclohexene: that is, a half-chair (The C_p ring acts as the equivalent of a C=C bond). In Fig. 5.16 is shown the crystal structure of the known rhodium(I) complex, [Rh(S,R-PPFA)-(NBD)]PF_6 [102b].

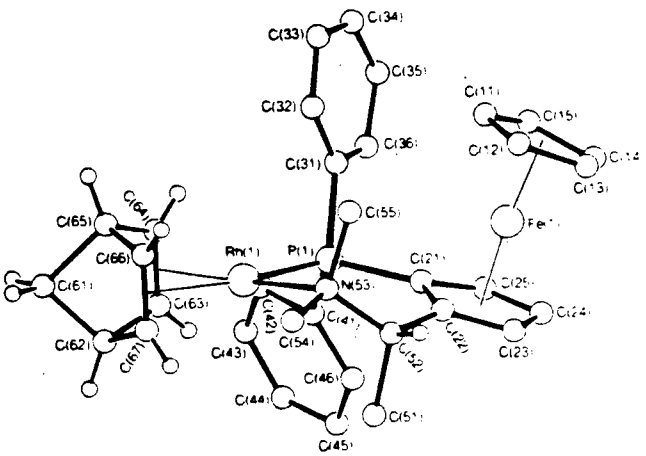

Fig. 5.16: The crystal structure of [Rh(S,R-PPFA)(NBD)]PF_6 [102b]; PPFA = $(Ph_2P)FA$.

The six-membered ring, as anticipated, has a half-chair conformation. It should be noted that, in the half-chair form, cyclohexene is a chiral molecule with planar chirality (or chiral conformation), but chair inversion readily converts one enantiomer to the other (vide infra) [124].

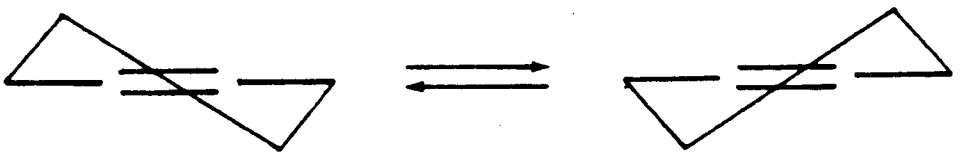

Apparently the analogous situation is found in the mono- and bisphosphine complexes XII and XIII, although the energy barriers to inversion appear to be higher than that required in cyclohexene (ca. 6 Kcal/mol) [124]. The trisphosphine complex XIV seems to have much higher energy barrier than XII and XIII, as suggested by the ^{31}P NMR results. On the basis of the crystal structure in Fig. 5.15, a model can be built to examine the possible inversion process in complexes (S,R)-XII and -XIII. This is shown in Fig. 5.17(A) together with the preferred chelate ring conformation of the trisphosphine complex (S,S)-XIV (Fig. 5.17B). Some of the observations that can be made on examining the model are: (i) the two conformers A and B (Fig. 5.17A) are diastereotopic by external comparison, thus the solution containing the mono- or bisphosphine complex should, in principle, give two sets of proton NMR signals, each set representing a diastereomeric conformer A or B; (ii) the relative stabilities of the two conformers A and B should be greatly affected by the presence or absence of phosphine(s) in the second C_P ring; (iii) the preferred conformation C of the trisphosphine complex (S,S)-XIV (Fig. 5.17B) is virtually enantiomeric with the conformation B of the bisphosphine complex (S,R)-XIII except for some slight changes in the relative orientations of the six-membered ring substituents, particularly the

(A)

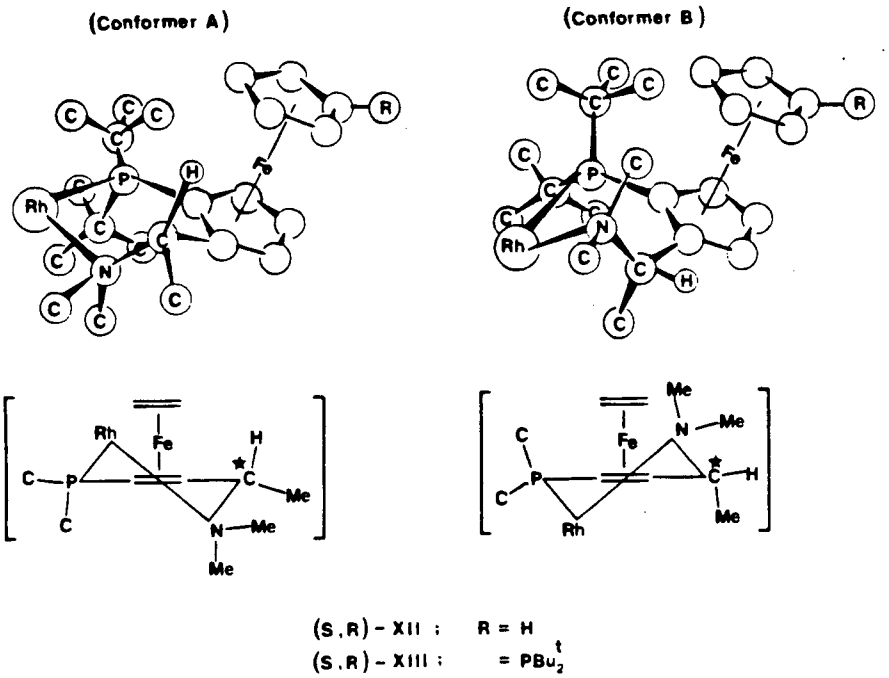

(B)

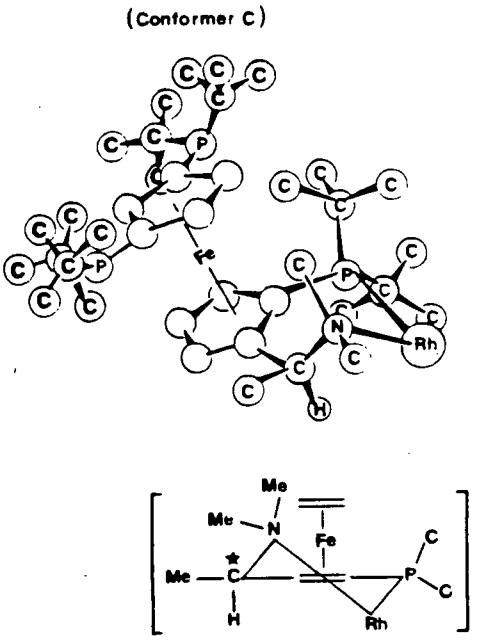

Fig. 5.17: (A) The proposed six-membered ring conformations A and B involved in the ring interconversion process of both (S,R)-XII and -XIII. (B) The preferred ring conformation of (S,S)-XIV.

methyl on the asymmetric center.

The ^1H NMR spectra of these three complexes are shown in Figs. 5.18 - 5.20. These provide the data relevant to the ring inversion process (Table 5.10) and provide some supporting evidences for the aforementioned conformational effects. The results relating to the individual complexes are as follows.

(a) Monophosphine Complex (S,R)-XII.

Both conformers A and B are equally populated (Ke = [B]/[A] $\approx$ 1), and the ratio does not change much over the whole temperature range studied (35° - -60°C). In Figs. 5.18(A) and (B) is shown the variable temperature ^1H NMR spectrum of the monophosphine complex (S,R)-XII. At 35°C, all peaks are quite broad as suggested by the ^{31}P NMR results. The lines begin to sharpen on cooling (0°C), showing clearly two sets of signals of equal intensities. Thus if a set of signals with subscript A is temporarily assigned to the conformer A, this conformer shows, as summarized in Table 5.10, a singlet F_A due to the unsubstituted C_P ring protons ($-C_5H_5$), a pair of singlets $N_A(1)$ and $N_A(2)$ for the $-NMe_2$ group, a broad quartet C_A for the methine proton (-C<u>H</u>Me) coupled with the vicinal methyl group, a doublet M_A for the methyl (-CH<u>Me</u>) group coupled with the methine proton, and a pair of doublets $P_A(1)$ and $P_A(2)$ for the $-P(CMe_3)_2$ group. The conformer B also shows a set of corresponding signals designated with subscript B. The doublet M_A can be seen more clearly on further cooling (-40°C) (Fig. 5.18B). The NMR pattern of other protons such as those of the disubstituted C_P ring ($-C_5H_3$) and of the NBD ligand is not so easily discussed, yet a similar situation appears to exist.

Table 5.10: Some ^1H NMR data relevant to the conformational effects observed in the chiral Rh(I) complexes XII-XIV[a,b].

Complex	Conformer	-CHMe	-CMe	$-NMe_2$	$-P(CMe_3)_2$
(S,R)-XII	A	3.20(bq)	1.63(d)	3.40(s)	1.76(d,J_{PH}=12)
		(J_{HH}=8)	(J_{HH}=8)	2.28(s)	1.00(d,J_{PH}=12)
	B	4.60 [c]	1.53(d)	2.24(s)	1.52(d,J_{PH}=12)
			(J_{HH}=8)	1.78(s)	1.35(d,J_{PH}=16)
(S,R)-XIII	A	3.22(bq)	1.67(d)	3.42(s)	1.00(d,J_{PH}=16)
		(J_{HH}=7)	(J_{HH}=7)	2.32(s)	1.09(d,J_{PH}=12)
					1.24(d,J_{PH}=12)
					1.80(d,J_{PH}=16)
	B	4.61 [c]	1.55 [c]	2.26(s)	1.07(d,J_{PH}=12)
				1.80(s)	1.22(d,J_{PH}=12)
					1.37(d,J_{PH}=12)
					1.58(d,J_{PH}=12)
(S,S)-XIV	C	2.97(q)	2.75(d)	1.90(s)	1.59(d,J_{PH}=16)
		(J_{HH}=8)	(J_{HH}=8)	2.42(s)	1.41(d,J_{PH}=12)
					1.40(d,J_{PH}=12)
					1.09(d,J_{PH}=16)
					0.91(d,J_{PH}=12)

a ^1H NMR spectra were obtained in CD_2Cl_2.

b Coupling constants are in Hz: bq=broad quart, d=doublet, s=singlet, q=quart.

c Chemical shifts are based on the homonuclear (H-H) decoupling experiments.

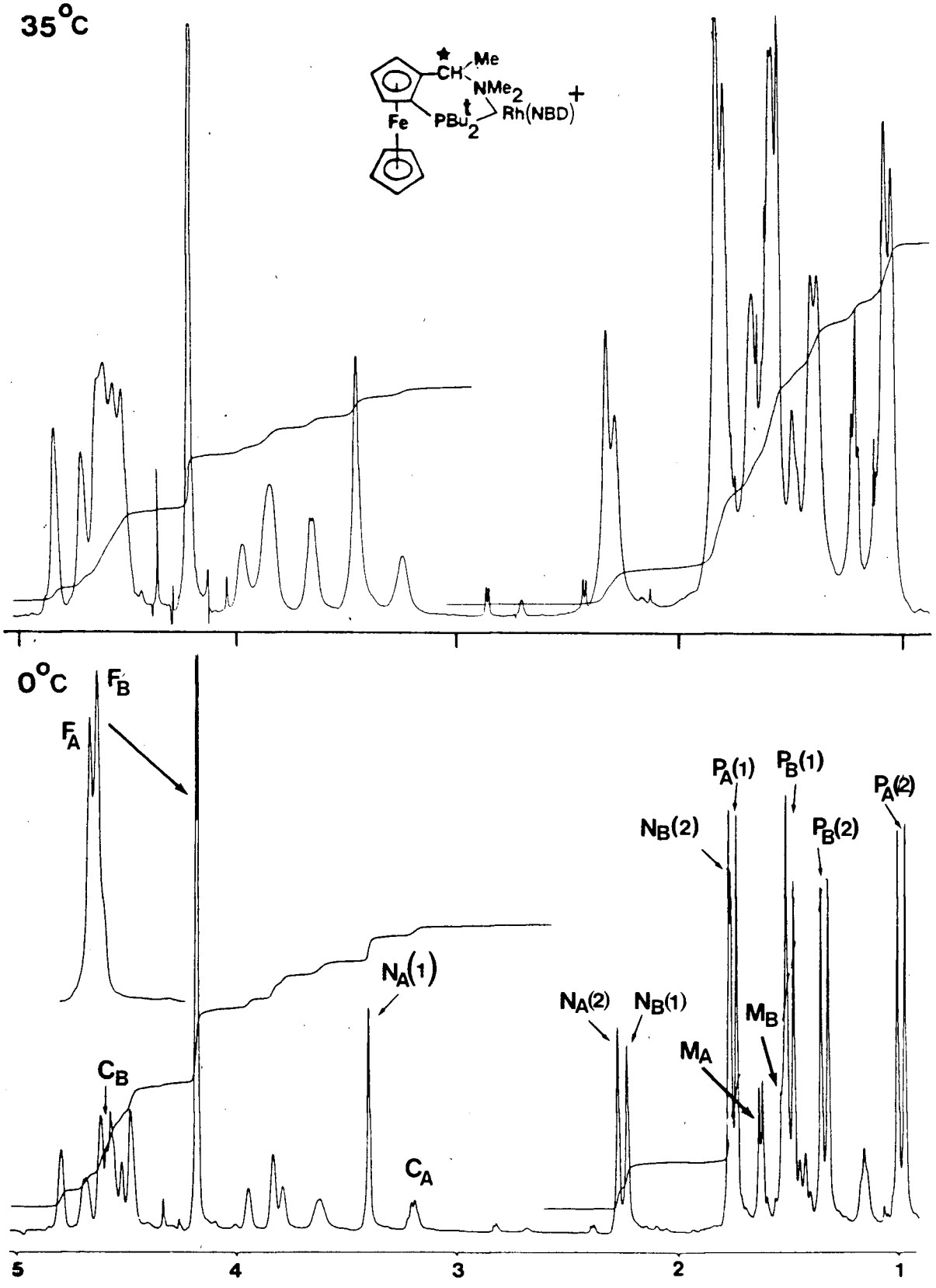

Fig. 5.18(A): Variable temperature ^{1}H NMR (400MHz) spectrum of (S,R)-XII in CD_2Cl_2.

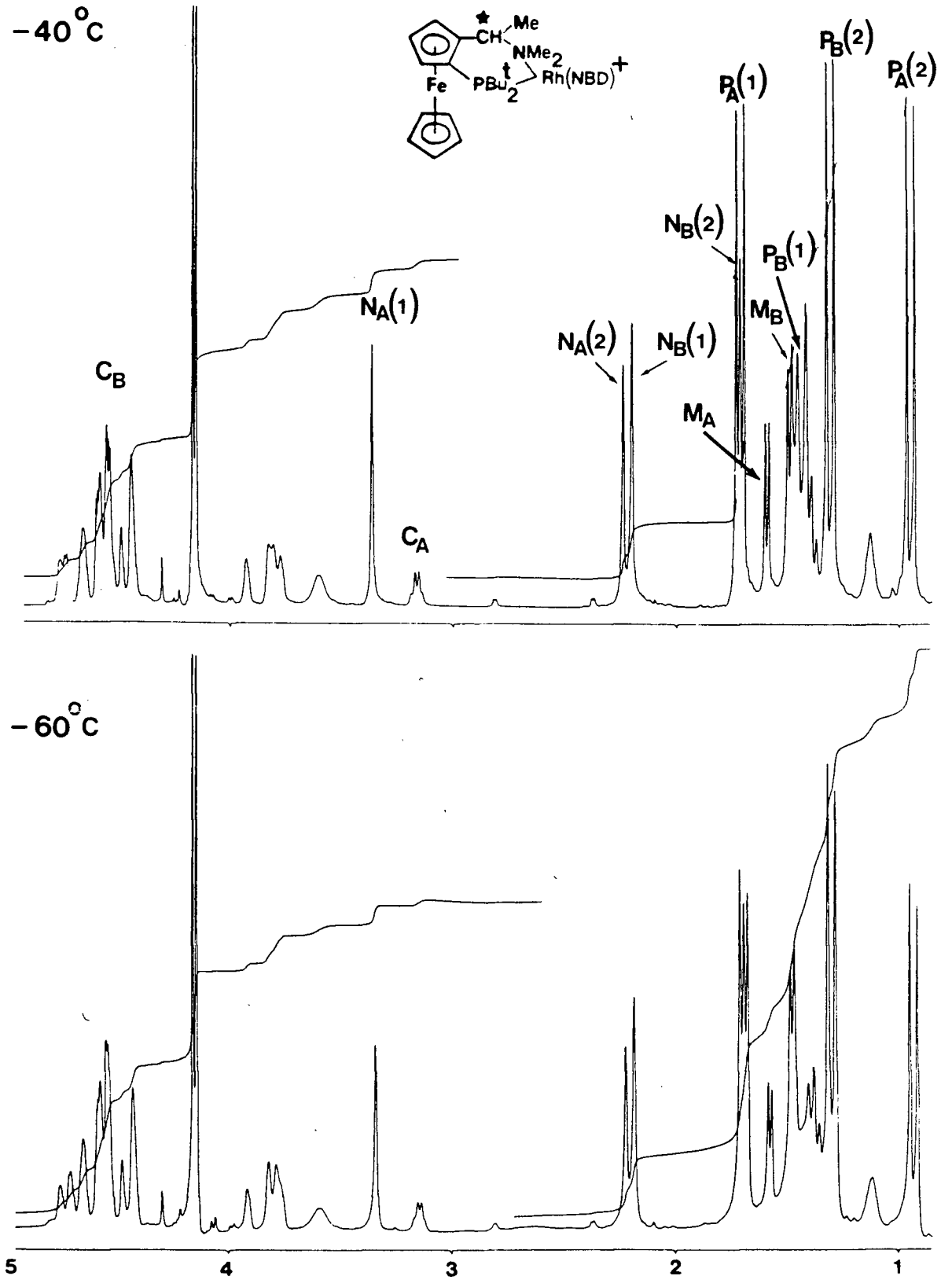

Fig. 5.18(B):: Variable temperature ^1H NMR (400MHz) spectrum of (S,R)-XII in CD_2Cl_2.

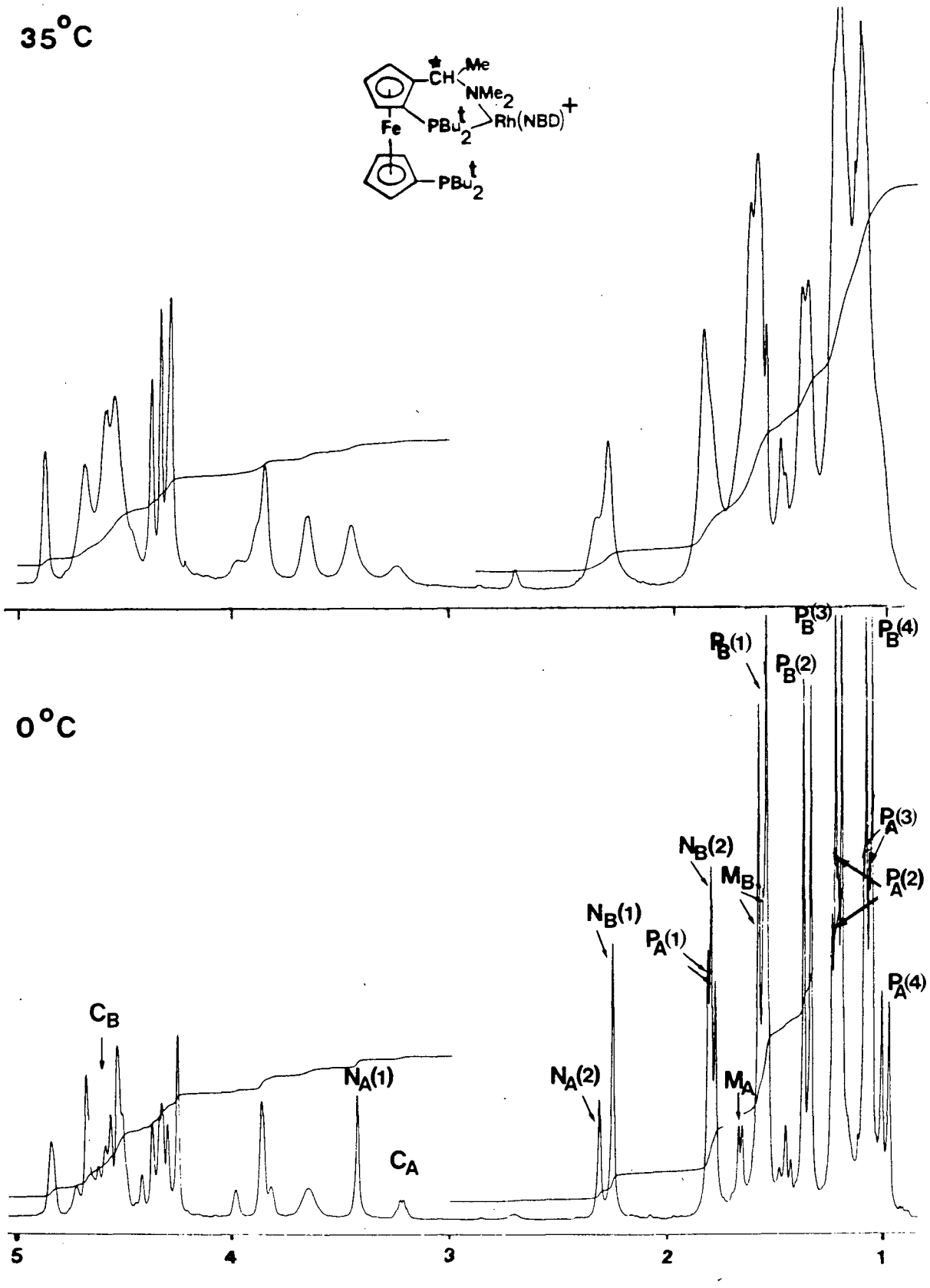

Fig. 5.19(A): Variable temperature ^{1}H NMR (400MHz) spectrum of (S,R)-XIII in CD_2Cl_2.

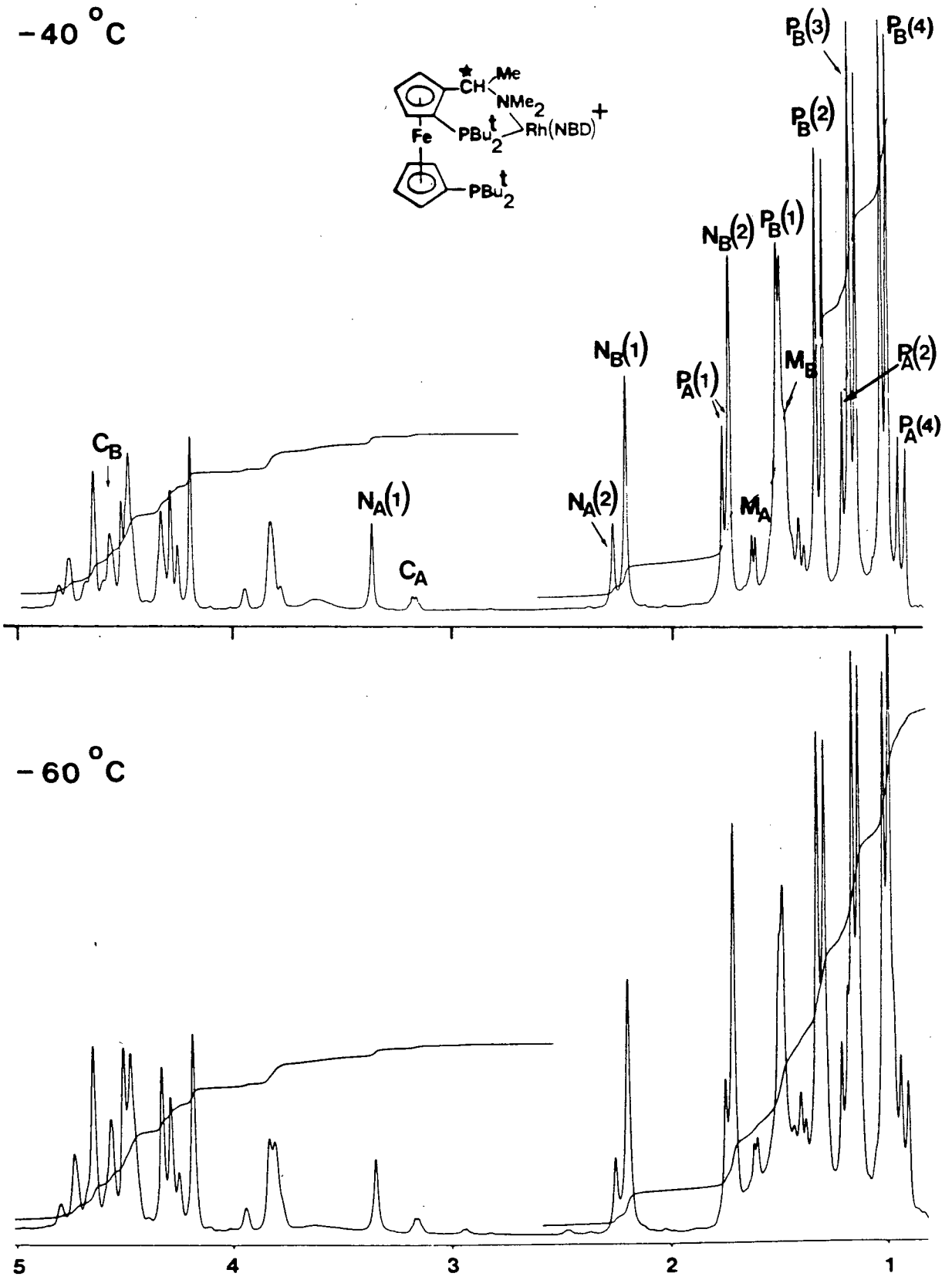

Fig. 5.19(B): Variable temperature ^{1}H NMR (400MHz) spectrum of (S,R)-XIII in CD_2Cl_2.

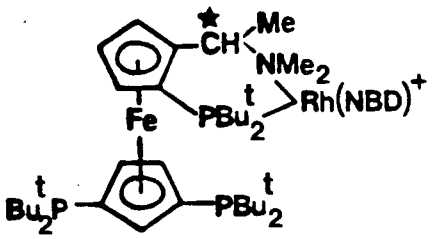

(S,S)-XIV

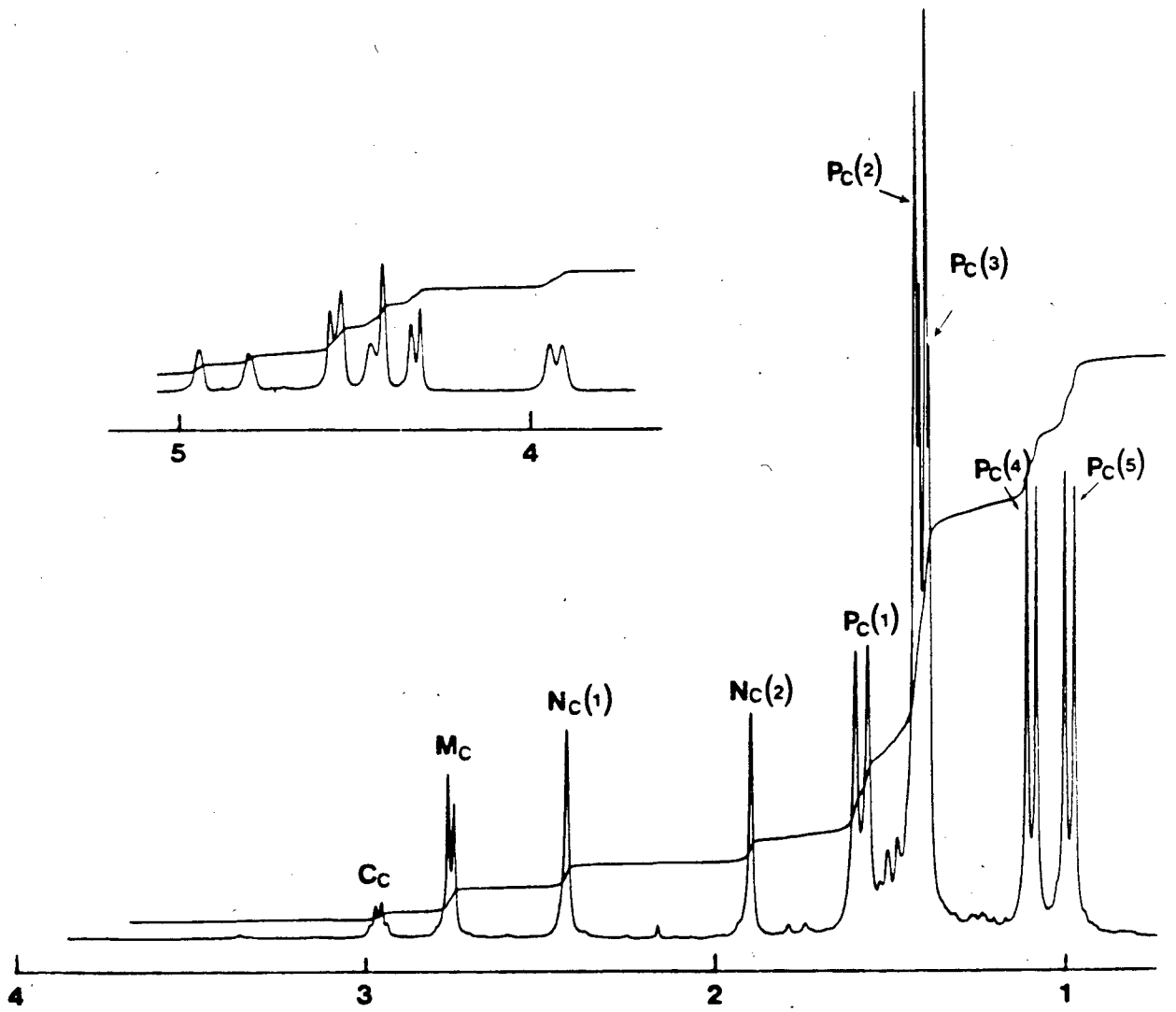

Fig. 5.20: 400MHz ^{1}H NMR spectrum of (S,S)-XIV in CD_2Cl_2 at 35°C.

Although the assignment of the peaks F and P to the corresponding conformer is purely arbitrary, the other peaks C, M, and N can be specifically assigned without much difficulty. Firstly, homonuclear (H-H) decoupling experiments reveal that the pair of peaks C_A and M_A belong to one set of signals, and the other pair of peaks C_B and M_B to the other set. Secondly, assignment of the peak C_B to the conformer B can be made based on the "ring current" effect. This resonance appears in an unusually lower shielding region than would be expected from a methine proton in conformer B which is almost coplanar with the C_P ring (Fig. 5.17A). Thus this proton can be treated as an aromatic ring proton rather than an acetylenic proton. It then follows that the pair of peaks C_A and M_A are associated with conformer A. The assignment of a pair of singlets N(1) and N(2) for the $-NMe_2$ group is based on the intensity ratio ($I(N_A)/I(N_B) \approx 1$) and the ^1H NMR pattern of the corresponding conformers of the bisphosphine complex (S,R)-XIII. Here, as described next, the pair of peaks N(1) and N(2) for the $-NMe_2$ group in the conformer A appear in a lower shielding region than those in conformer B (See Table 5.10 and Fig. 5.19).

(b) Bisphosphine Complex (S,R)-XIII.

The conformer B seems to be preferred over conformer A. The ratio of B to A is approximately 2:1 ($Ke \approx 2$) at 35°C, and changes to 3:1 ($Ke \approx 3$) on cooling (< -40°C) as seen in Figs. 5.19(A) and (B).

The ^1H NMR pattern of each conformer of this complex, (S,R)-XIII, is quite similar to that of the corresponding conformer of the monophosphine complex (S,R)-XII. Assignment of each set of signals (Table 5.10) is based

on similar results. Thus, at 0°C, the major conformer B shows a pair of singlets $N_B(1)$ and $N_B(2)$ for the $-NMe_2$ group, four doublets $P_B(1)$, $P_B(2)$, $P_B(3)$, and $P_B(4)$ for the two $-P(Me_3)_2$ groups, a doublet M_B for the methyl (-CHMe) on the asymmetric center, and a quartet C_B for the methine proton (-CHMe) as checked by homonuclear (H-H) decoupling at 4.60 and 1.55 ppm. The minor conformer A also exhibits a weaker set of signals labeled with subscript A. Here again the NMR pattern of the protons of the ferrocene moiety and of the NBD ligand is less easy to interpret.

Increased steric bulk in the second ring may cause the conformer B to be more stable than the conformer A. One possible explanation would be that the conformer B can reduce the ring strain by disposing the two methyl of the $-NMe_2$ group away from the methyl (-CHMe) of the asymmetric center. In the conformer A, those two methyl groups are both in an equatorial position and one tert-butyl group in an axial position (Fig. 5.17A).

(c) Trisphosphine Complex (S,S)-XIV

Only one conformation C is seen in the case of the trisphosphine complex (S,S)-XIV. Thus the NMR pattern (Fig. 5.20) of this complex consists of only one pair of singlets $N_C(1)$ and $N_C(2)$ for the $-NMe_2$ group, a broad quartet C_C for the methine proton, and five doublets $P_C(1)$, $P_C(2)$, $P_C(3)$, $P_C(4)$, and $P_C(5)$ for the three $-P(CMe_3)_2$ groups (although six doublets are expected). The unique feature of this conformation is that the singlet M_C for the -CMe group has a greater chemical shift than is found for the conformer B. This shift (deshielding) can also be explained in terms of the "ring current" effect since the methyl group in the conformer C (Fig. 5.17B) is now coplanar with the C_p ring. The methine proton is axially

disposed in this conformation. The C_p ring protons show a complex pattern in the range 4.3 to 4.6 ppm. Although again the NMR signals for the NBD ligand cannot fully be assigned, two broad singlets are seen at 3.92 and 3.95 ppm for the $-CH_2$ group and two broad singlets at 4.95 and 4.81 ppm for two olefinic protons. The other two olefinic protons are probably obscured by the C_p ring resonances. The remaining two protons for the -CH groups seem to appear in the range 1.48 to 1.51 ppm. All-in-all the spectrum is much as would be anticipated for a rigid system as described above.

The remaining aspects of these conformational effects will be discussed further in connection with asymmetric hydrogenation catalyzed by these complexes (cf. section 6.2.2).

5.3 OTHER METAL COMPLEXES OF FERROCENYLPHOSPHINES

5.3.1 Palladium Complexes

Palladium complexes of the type $[Pd(P\text{-}P)Cl_2]$ (P-P = I - IV) were readily prepared in high yields (> 70%) by the direct reaction of K_2PdCl_4 or $Pd(NBD)Cl_2$ with a slight molar excess of the appropriate ligand as shown in equation (5.4).

$$Pd(NBD)Cl_2 \text{ (or } K_2PdCl_4) + P\text{-}P \longrightarrow Pd(P\text{-}P)Cl_2 \qquad (5.4)$$

XV ; P-P = I
XVI ; = II
XVII ; = III
XVIII ; = IV

Table 5.11: Analytical results and melting points of $Pd(P\text{-}P)Cl_2$.

Compound	P - P	mp,°C (decomp.)	Found(%) C	Found(%) H	Calcd(%) C	Calcd(%) H
XV	I	163-165	55.41	3.92	55.79	3.83
XVI	II	210-212	51.98	4.96	52.08	5.21
XVII [a]	III	192-195	45.80	4.60	45.88	4.59
XVIII	IV	208-210	47.31	6.88	47.91	7.00

[a] Calculated value is based on $Pd(P\text{-}P)\cdot CHCl_3$.

Table 5.12: ^1H NMR data for $Pd(P\text{-}P)Cl_2$ [a,b].

Compound	$-C_6H_5$	$(C_5H_4-)_2Fe$	$-CMe_3$
XV	7.43(bm,6) 8.00(m,4)	4.18(bs,4) 4.40(bs,4)	-
XVI	7.68(m,6) 8.45(m,4)	4.0-4.4(m,8)	1.53(d,18) (J_{PH}=16)
XVII	7.32-7.52(m,6) 7.88-8.23(m,4)	3.85(bm,2) 4.32(bm,2) 4.61(bm,2) 4.90(bm,2)	1.63(d,18) (J_{PH}=15)
XVIII	-	4.65(bs,4) 4.50(bs,4)	1.65(d,36) (J_{PH}=14)

[a] All spectra were obtained in $CDCl_3$.

[b] Coupling constants are in Hz: bm=broad multiplet, bs=broad singlet, d=doublet, m=multiplet.

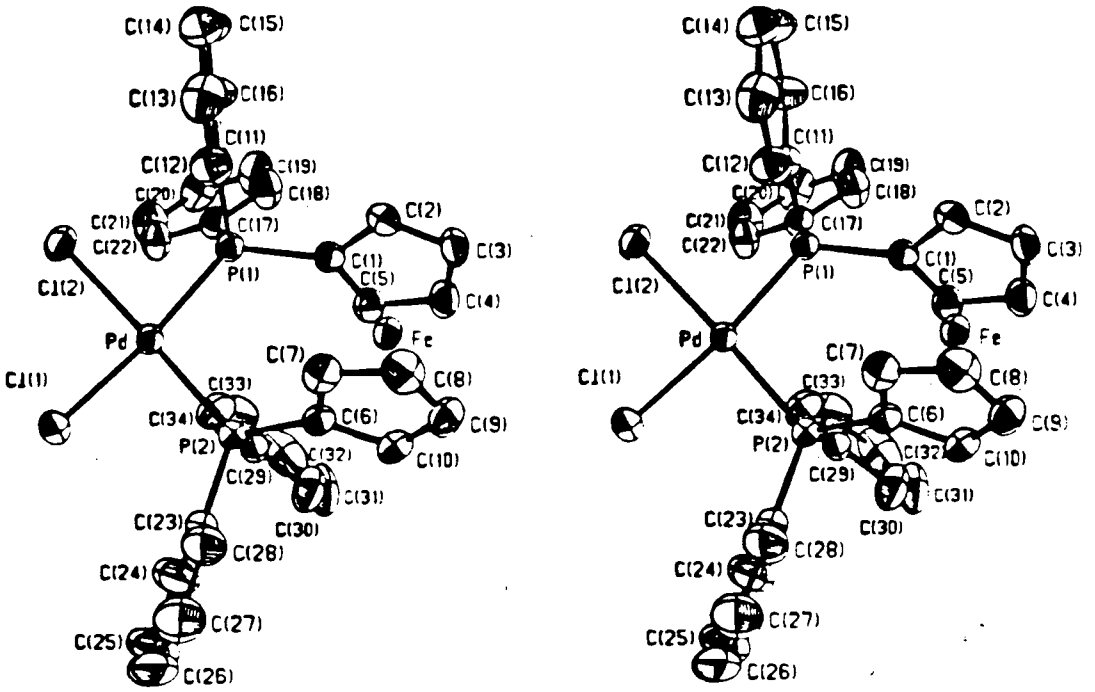

Fig. 5.21: The stereoview of the crystal structure of $Pd(P\text{-}P)Cl_2$: P-P = the ligand I [125, 126].

The typical procedure was to dissolve the palladium starting material in a minimum amount of CH_2Cl_2 or $CHCl_3$ and slowly add the corresponding ligand dissolved in diethyl ether. All complexes separated as air-stable, orange precipitates after stirring 2 ∿ 3h at room temperature. The isolated solid was then recrystallized from an appropriate solvent or solvent mixture as described in the experimental section.

The analytical results and ^1H NMR data are summarized in Tables 5.11 and 5.12. The ^1H NMR spectrum of each of these complexes is virtually identical with that of the corresponding free ligand (cf. Table 5.2) except for slight line broadening accompanied by a chemical shift change. Fig. 5.21 shows the crystal structure of XV [126] which has a staggered ring conformation and a square planar geometry around the Pd metal.

5.3.2. Nickel Complexes

Nickel complexes of the type $Ni(P\text{-}P)X_2$ (P-P = I,IV; X = Cl,Br) were prepared by simple reflux of an ethanolic solution of the ligand and $NiCl_2 \cdot 6H_2O$ (or anhydrous $NiBr_2$) as shown in equation (5.5).

$$NiCl_2 \cdot 6H_2O \text{ (or } NiBr_2) \xrightarrow[\text{reflux}]{P\text{-}P/EtOH} Ni(P\text{-}P)X_2 \qquad (5.5)$$

XIX : P-P = I ; X = Cl
XX : = I ; = Br
XXI : = IV; = Cl
XXII : = IV; = Br

Table 5.13: Melting points and analytical data for the Ni(II) complexes $Ni(P\text{-}P)X_2$.

Compound	P-P	X	mp,°C (decomp.)	Found(%)		Calcd(%)	
				C	H	C	H
XIX	I	Cl	283-285	59.81	4.05	59.70	4.09
XX	I	Br	296-298	52.76	3.72	52.82	3.62
XXI	IV	Cl	185-187	51.24	6.95	51.69	7.29
XXII	IV	Br	202-204	45.53	6.53	45.06	6.35

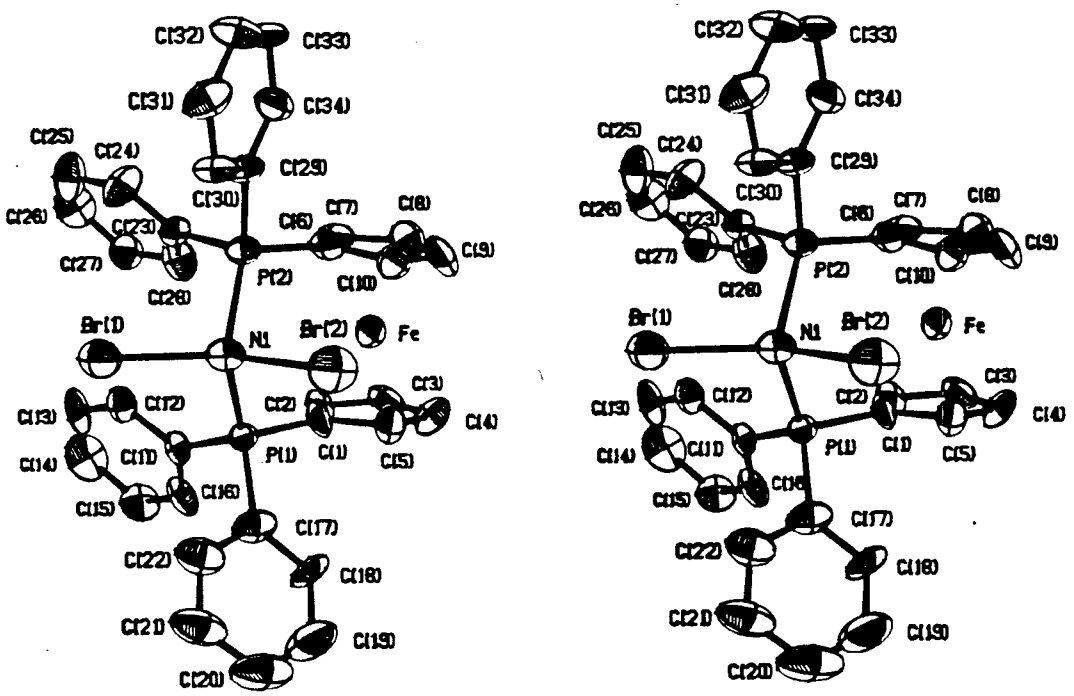

Fig. 5.22: The stereoview of the crystal structure of $Ni(P\text{-}P)Br_2$: P-P = the ligand I [126].

All products were isolated as dark green, air-stable, paramagnetic crystals.

The analytical results and melting points are listed in Table 5.13. The crystal structure of the previously known compound XX was determined during present studies [126], and shown in Fig. 5.22. It shows that this paramagnetic complex (and probably others XXI and XXII) resembled the high-spin, pseudotetrahedral bis(triphenylphosphine)nickel(II) halides [127] rather than the diamagnetic (DIPHOS)NiX_2 compounds [128]. The greater steric requirement and larger bite size of the ligands I and IV are probably responsible for this preferred geometry.

5.3.3 Iron Complexes

Iron complexes, $Fe(BPPF)(CO)_3$ (XXIII) and $Fe_2(BPPF)(CO)_8$ (XXIV), were prepared by the reaction of the ligand I (BPPF) with excess $Fe(CO)_5$ or $Fe_2(CO)_9$ as shown in equation (5.6).

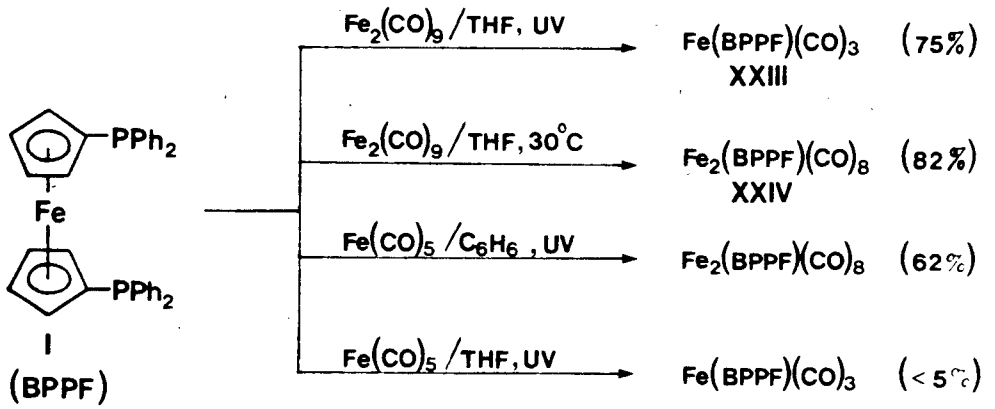

(5.6)

Both compounds were obtained as orange crystalline solids after the usual work-up procedures. The tricarbonyl complex XXIII was obtained in a high yield (75%) by UV irradiation of a THF solution of the ligand and a two molar excess of $Fe_2(CO)_9$. As shown in equation (5.6), the same reaction mixture under different reaction conditions, i.e. stirring at room temperature for 2h, yields predominantly the complex XXIV in which each $-PPh_2$ group functions as a monodentate ligand to the $-Fe(CO)_4$ moiety. This compound was also prepared in a high yield (62%) by UV irradiation of a benzene solution of the ligand and a 10 molar excess of $Fe(CO)_5$. It is worth noting that the disubstituted iron carbonyl, $(COD)Fe(CO)_3$ failed to give the expected product XXIII from the reaction with the ligand I in benzene (or THF) at room temperature. The starting material $(COD)Fe(CO)_3$ was quantitatively recovered after stirring overnight. The reaction of the ligand I with $Fe_3(CO)_{12}$ yielded a purple oil as a single product which readily decomposes in solution.

The analytical results and spectroscopic data for the complexes XXIII and XXIV are listed in Table 5.14. Mass spectra of XXIII and XXIV show the parent peaks at m/e 694 and 890, respectively in addition to other peaks associated with the loss of up to three and eight carbonyl groups, respectively. The structure of the $Fe(CO)_3$ derivative is expected to be a trigonal bipyramid which may be fluxional in solution [129]. In the solid state the ligand should be bound at axial and equatorial sites. In accord with this the tricarbonyl complex XXIII shows three strong $\nu(CO)$ bands at 1990, 1920 and 1892 cm^{-1}. The pattern of the bands is similar to that found for other

Table 5.14: Analytical and spectroscopic data for the iron complexes XXIII and XXIV .

Compound	Found(%) C	Found(%) H	Calcd(%) C	Calcd(%) H	ν(CO)(cm^{-1})	Mass spectra(m/e)
XXIII	63.35	4.14	64.01	4.03	1990(vs)	694(M^+)
					1920(s)	666(M^+-CO)
					1892(vs)	638(M^+-2CO)
						610(M^+-3CO)
						554(BPPF)
XXIV	56.00	4.35	56.66	3.85	2040(vs)	890(M^+)
					1978(vs)	862(M^+-CO)
					1948(s)	834(M^+-2CO)
					1930(s)	806(M^+-3CO)
						778(M^+-4CO)
						750(M^+-5CO)
						722(M^+-6CO)
						694(M^+-7CO)
						666(M^+-8CO)
						554(BPPF)[a]

[a] BPPF = the ligand I, vs=very strong, s=strong.

(L-L)$Fe(CO)_3$ derivatives (L-L = DIPHOS, DIARS). For example, $Fe(DIPHOS)(CO)_3$ [129] shows the $\nu(CO)$ bands at 1997, 1933 and 1913 cm^{-1}. In the case of $Fe(DIARS)(CO)_3$ (DIARS = 1,2-bis(dimethylarsino)benzene) [129], the $\nu(CO)$ bands appear at 1991, 1923, and 1909 cm^{-1}. However it can be noted that the $\nu(CO)$ bands for the complex XXIII appear in the lower frequency region than those for the DIPHOS and DIARS derivatives. Similar observation relating to a drop in CO stretching frequency can also be made for the monosubstituted iron carbonyl; complexes. Thus, for example. the complex XXIV shows the $\nu(CO)$ bands at 2040, 1978, 1948 and 1930 cm^{-1}, while $Fe_2(CO)_8(DIPHOS)$ [129] gives the $\nu(CO)$ bands at 2058, 1984, 1948 and 1941 cm^{-1}, and $Fe_2(CO)_8(DIARS)$ at 2053, 1981 and 1944 cm^{-1}. These differences may be explained in terms of the enhanced π-donating ability of the ligand I, as compared with that of DIPHOS and DIARS.

The unknown compound obtained from the reaction of I with $Fe_3(CO)_{12}$ appears to have at least 7 $\nu(CO)$ bands, one of which appears at 1770 cm^{-1}, indicating the presence of at least one bridging CO group in the molecule. However, the unstability and insolubility of this product prevented further characterization.

5.3.4 Group VI Metal Complexes

The reaction of I with $M(CO)_6$ (M=Cr,Mo) followed by chromatographic separation allowed the isolation of the previously known compounds $M(BPFF)(CO)_4$ (XXV, M=Cr; XXVI, M=Mo) [118] as yellow, air-stable crystals. The analytical results and spectroscopic data for XXV and XXVI are listed in Table 5.15.

Table 5.15: Analytical and spectroscopic data for the Gp VI metal complexes $M(P\text{-}P)(CO)_4$ [a,b].

Compound	M	Found(%) C	Found(%) H	Calcd(%) C	Calcd(%) H	^1H NMR ($CDCl_3$)	$\nu(CO)(cm^{-1})$
XXC	Cr	63.37	4.08	63.50	3.90	7.52(bm,4)	1995(vs)
						7.29(bm,6)	1925(sh)
						4.23(bt,4)	1890(s)
						4.21(bt,4)	1870(s)
XXVI	Mo	59.63	3.66	59.86	3.67	7.64(bm,4)	-
						7.42(bm,6)	
						4.37(bt,4)	
						4.30(bt,4)	

[a] Coupling constants are in Hz: bm=broad multiplet, bt=broad doublet.

[b] IR intensity: vs=very strong, sh=shoulder, s=strong.

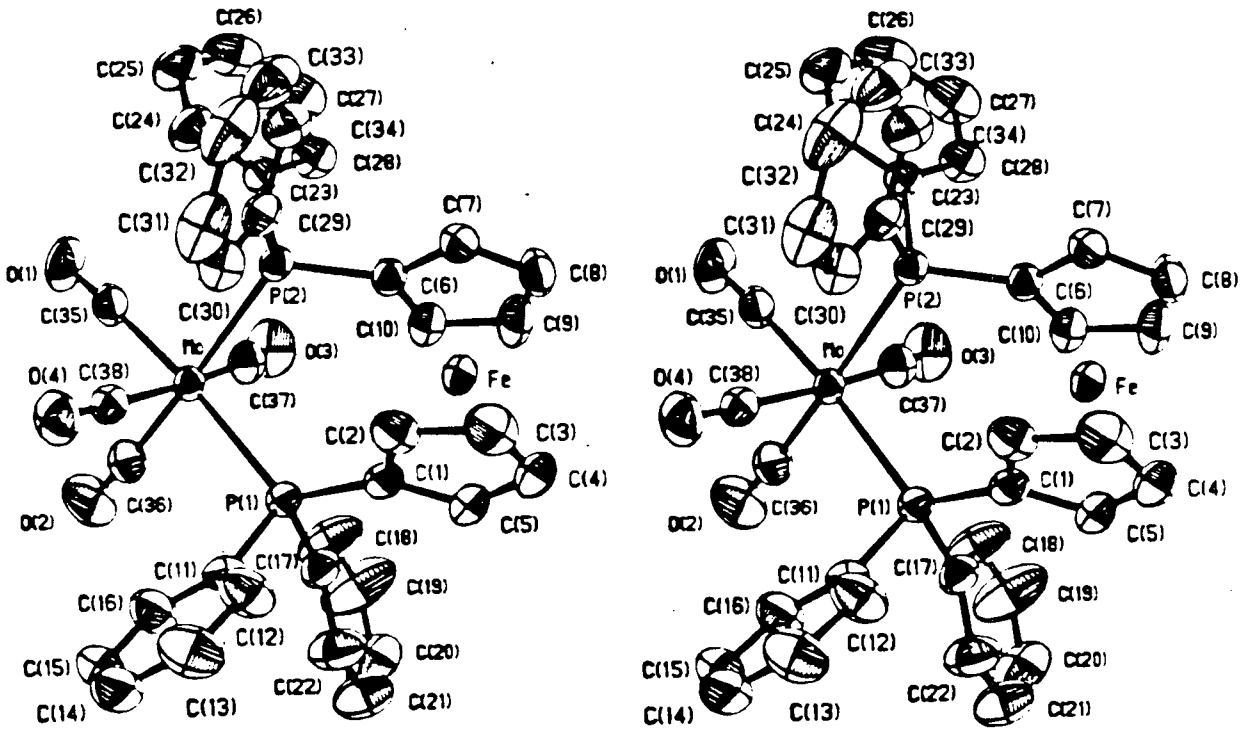

Fig. 5.23: The stereoview of the crystal structure of $Mo(P\text{-}P)(CO)_4$: P-P = the ligand I [126].

These complexes, like others (VIII - XXIV), can be viewed as [3]-ferrocenophanes. In principle, there are two limiting structures imposed upon these compounds by the steric requirement of the atoms in the bridge.

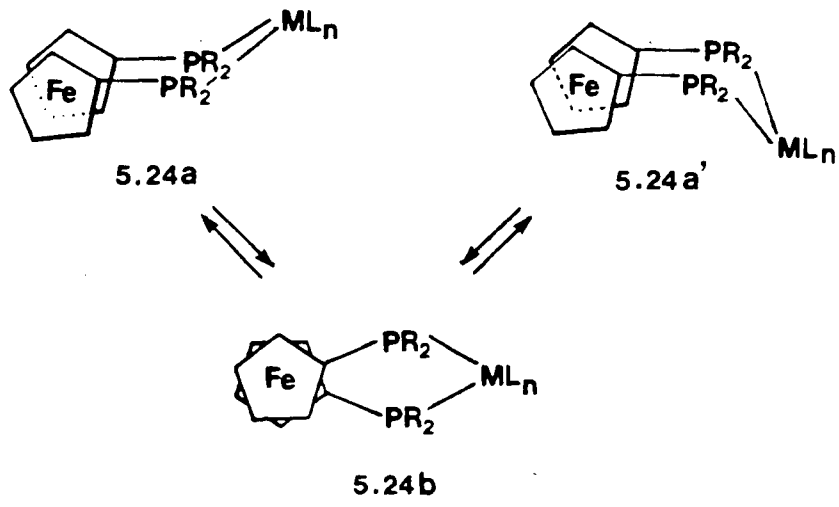

Fig. 5.24: Mechanism for [3]-ferrocenophane bridge reversal.

They are 5.24a (= 5.24a´) and 5.24b, in both of which an ABCD NMR pattern would be expected for the C_p ring protons. However, variable temperature NMR studies [130] indicate that this type of molecules is fluxional and undergoes ring inversion (Fig. 5.24) with the eclipsed conformation (5.24a) being preferred for most [3]-ferrocenophanes (M = Group IV and VI atoms). One exception is $[(C_5H_4)_2S_2C(C_6H_5)_2]$ where the C_p rings are believed to be staggered as in 5.24b. The barrier to chair to chair reversal can be high as in the S_3 bridge ($\Delta G^{\ddagger}$ = 80.4 Kj/mol) [130] in a limiting ABCD pattern for

the C_5H_4 group at ambient temperature. In other cases e.g. with $(-CH_2)_2S$ ($\Delta G^{\ddagger}$ = 34.6 kJ/mol) [130] or $(-S)GeMe_2$ bridges the limiting NMR spectra are obtained only on strong cooling (ca. -100°C) [130].

The ^1H NMR (400 MHz) spectra of XXV and XXVI exhibit the characteristic pair of triplets of a fluxional [3]-ferrocenophane for the C_p ring protons [126]. On cooling the solutions to -85°C only a slight broadening was observed in the spectrum. Since the Mo complex XXVI adopts the staggered ring conformation as shown in Fig. 5.23 the barriers to ring reversal must be low.

CHAPTER 6

RHODIUM COMPLEXES OF FERROCENYLPHOSPHINES AS HYDROGENATION CATALYSTS

6.1 CATALYST PRECURSORS

In the previous chapter, the preparation and some properties of the cationic Rh(I) complexes VIII - XIV have been described. Formally they belong to the group of di(tertiary phosphine)Rh(I) type catalysts (cf. section 1.4.2c), since in these complexes either both P atoms (VIII - XI) or N and P atoms (XII - XIV) are bound to the rhodium atoms.

The general catalytic properties and several of the notable advantages of this group of catalysts have been described in Chapters 1 and 2. In particular (i) they can be readily prepared, handled, and a wide variety of phosphine ligands can be introduced; (ii) they react readily with H_2 (1 atm, 25°C) in solution to generate active catalysts, the diene ligand being quantitatively reduced; (iii) they do not catalyze the isomerization of terminal olefins; (iv) they give more consistent and higher optical yields (L-L = chiral ligands) than their monodentate phosphine counterparts.

As will be discussed later, the present systems VIII - XIV exhibit several other possibly unique properties, one of the notable being the formation of metal hydrides by reaction with H_2 in the absence of the substrate.

6.2 CATALYTIC HYDROGENATION OF OLEFINS

6.2.1 Nonasymmetric Hydrogenation

The results of a number of hydrogenation reactions using the achiral catalyst precursors VIII - XI are listed in Table 6.1. Under the standard condition (30°C, 1 atm H_2), all reactions except one are stoichiometric as checked by NMR and gas chromatography. They all proceed very quickly, and most go to completion within 15 min. All the gas up-take plots have a short induction period (T_{in}) followed by an almost linear region corresponding with the maximum rate. Rates of the order of 7×10^{-6} mol/sec are about the maximum that can be measured using the manual gas-uptake system. However, there can be no doubt about the trends. Thus, with the exception of the reduction of acylamino-cinnamic and -acrylic acids, the rates obtained with the alkylphosphine complexes (IX - XI) are greater than those obtained with the tetraphenyl derivative VIII. These trends are reversed in the reduction of somewhat sterically demanding substrates such as acylamino-cinnamic and -acrylic acids (the first two substrates in Table 6.1). When the comparison is made among the three alkylphosphine complexes IX - XI, the rates are generally the slowest with the sterically most crowded complex XI. There is little to choose between IX and X so the electronic and steric effects seem to be balanced.

It is possible to account for some of the gross differences described above on the basis of the electronic and steric effects of the ligands employed. If catalysis by these systems, like other di(tertiary phosphine)-

Table 6.1: Hydrogenation of olefins catalyzed by the achiral Rh(I) complexes $[Rh(P\text{-}P)(NBD)]ClO_4$ (P-P = I-IV) [a].

Olefin	Catalyst precursor	Solvent	T_{in},S	T_{∞},s	Max. Rate, mol/s
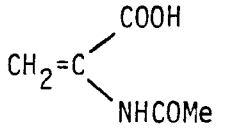	VIII	EtOH	8	60	5.9×10^{-6}
	IX	"	8	95	3.6×10^{-6}
	X	"	23	780	2.1×10^{-7}
	XI	"	27	700	3.2×10^{-7}
	XI	MeOH	17	375	7.1×10^{-7}
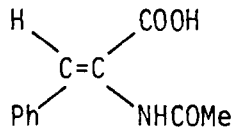	VIII	EtOH	8	150	3.4×10^{-6}
	IX	"	15	150	2.2×10^{-6}
	X	"	20	280	1.0×10^{-6}
	XI	"	30	1780	1.4×10^{-7}
	XI	MeOH	18	680	2.9×10^{-7}
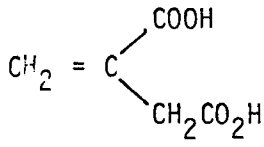	VIII	EtOH	8	180	1.8×10^{-6}
	VIII	MeOH	8	125	2.8×10^{-6}
	IX	"	8	75	5.9×10^{-6}
	X	"	7	62	6.9×10^{-6}
	XI	EtOH	9	90	4.1×10^{-6}
	XI	MeOH	8	200	5.5×10^{-6}
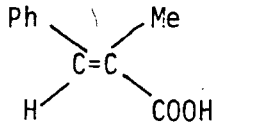	VIII	EtOH	-	-	0
	IX	"	25	780	5.0×10^{-7}
	X	"	30	950	4.5×10^{-7}
	XI	"	20	600	5.5×10^{-7}

Table cont'd...

Olefin	Catalyst precursor	Solvent	T_{in},s	T_{∞},s	Max. Rate, mol/s
1-Octene	VIII	MeOH	45	32,000	4.4×10^{-8}
	IX	"	5	60	6.8×10^{-6}
	X	"	7	200	6.2×10^{-6}
	XI	"	15	325	3.5×10^{-6}
Cyclohexene	VIII	MeOH	60	35,000	3.7×10^{-8}
	IX	"	10	200	2.2×10^{-6}
	X	"	20	520	3.7×10^{-6}
	XI	"	15	740	1.1×10^{-6}

[a] [Substrate] = 2.00×10^{-2}M in 10 mL of solvent; [Catalyst precursor] = 2.00×10^{-4}M; $p(H_2)$ = 1 atm; t = 30°C; t_{∞} = time to complete 100% uptake of H_2; T_{in} = induction period before measurable H_2 uptake; Max. Rate = maximum slope of gas uptake plot per 2.00×10^{-4}M of the catalyst precursor.

Rh(I) systems, proceeds via the "unsaturate" route (cf. section 1.4.2C) with the rate-determining step being the oxidative addition of H_2 to the catalyst-substrate intermediate (cf. Fig. 2.13), then the oxidative addition should be facilitated by the increased electron density on the Rh metal. Thus with sterically undemanding substrates, including those which occupy only one coordination site, rates of reaction should be enhanced by the presence of electron donating tert-butyl groups, as is dramatically shown in the reduction of 1-octene and cyclohexene (Table 6.1). These two substrates are hydrogenated approximately one hundred times faster using the alkylphosphine complexes (IX - XI) than using the tetraphenyl drivative (VIII). As is usual [131], the terminal olefin 1-octene is reduced faster than the internal olefin cyclohexene regardless of the catalysts employed. The hydrogenation of other non-chelating olefins such as styrene and 1-hexene was also studied in order to examine the generality of these trends in reaction rates. Within the experimental error, the reaction rates measured with the alkylphosphine complexes (IX - XI) were in the same order (10^{-6} mol/sec) as that for the reduction of 1-octene, once again the alkylphosphine complexes (IX - XI) being more efficient than the tetraphenylphosphine complex (VIII) which affords rates of the order of 10^{-8} mol/sec.

On the other hand, when olefins have the ability to chelate to the metal center such as acylamino-cinnamic and -acrylic acids, the electronic effects seem to be outweighed by the steric effects, and the overall rates are faster with the tetraphenyl derivative (VIII) than with the alkylphosphine complexes (IX -XI). However, it is difficult to explain the lack of reaction of

(E)-α-methylcinnamic acid.

In connection with these rate differences, it should be mentioned that all the rates are very much faster using these catalysts $[Rh(P\text{-}P)(NBD)]ClO_4$ (VIII - XI) than using the related catalysts $[Rh(P\text{-}N)(NBD)]ClO_4$ (XII - XIV) (cf. Tables 6.2 and 6.4). Here again the presence of phenyl groups (P-N = PPFA) results in slower reactions (Table 6.4). For example, itaconic acid is only 21% reduced in 72h when P-N = PPFA, yet is 100% reduced in 16h when P-N = V - VII. The rates are even faster as the numbers of tert-butyl groups are increased (Table 6.4). The effect of the $-NMe_2$ group in these chiral ligands (P-N) seems to be to lower the electron density on the metal without exerting much steric influence. This leads to slower rates with PPFA-based catalyst being less active than those containing the $-PBu^t_2$ group(s).

Finally, Table 6.1 shows that reaction rates in methanol are greater than in ethanol. This is probably due to the easier solubility of the catalyst precursors in methanol than in ethanol.

6.2.2 Asymmetric Hydrogenation

The results of asymmetric hydrogenation reactions using the new chiral catalyst precursors, (S,R)-XIII (from VI) and (S,S)-XIV (from VII) are listed in Table 6.2. Here the configuration is that of the free chiral ligands VI and VII. A number of interesting conclusions can be drawn from the table as follows.

Table 6.2: Asymmetric hydrogenation of some olefinic acids with $[Rh(P\text{-}N)(NBD)]ClO_4$ (P-N = VI and VII) [a,b].

Substrate	Catalyst Precursor[c]	Time(h) MeOH	Time(h) EtOH	%e.e MeOH	%e.e EtOH	Configuration
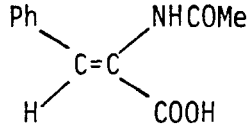	(S,R)-XIII	3.1	4.3	2	4	R
	(S,S)-XIV	4.2	4.8	86	91	S
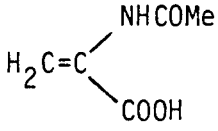	(S,R)-XIII	2.5	3.2	14	31	R
	(S,S)-XIV	3.2	3.6	82	95	S
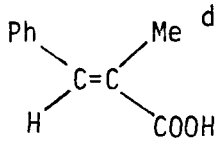 [d]	(S,R)-XIII	2.3	2.7	51	51	S
	(S,S)-XIV	3.0	3.5	59	61	R
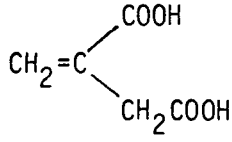	(S,R)-XIII	-	2.3	-	28	S
	(S,S)-XIV	4.5	4.7	19	38	R

[a] All reactions are stoichiometric. [Substrate] = 4.0×10^{-2}M in 10 mL of solvent; [Catalyst Precursor] = 4.0×10^{-4}M; $p(H_2)$ = 1 atm; t = 30°C; Time = approximate total reaction time.

[b] Optical yields are based on the rotation of the isolated products (cf. section 4.3).

[c] The configurations (S,R) and (S,S) are those of the chiral ligands VI and VII, respectively.

[d] This is reduced by H_2/(S,S)-XIV to give the (S)-isomer (28% e.e.) in benzene(reaction time >10 h).

Table 6.3: Asymmetric hydrogenation of amino acid precursors with Rh(I) complexes of (S,S)-VII and other representative di(tertiary phosphine) ligands [a].

Substrate	Chiral Ligand	%e.e. (Configuration)	Reference
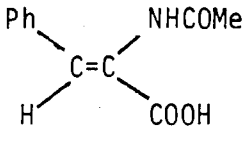	(R,R)-DIPAMP	94(S)	85
	(S,S)-CHIRAPHOS	89(R)	76a
	(R)-PROPHOS	91(S)	76b
	(S,S)-SKEWPHOS	93(R)	76c
	(S,R)-BPPFA	93(S)	94
	BPPM	91(R)	90a
	(R,R)-DIOP	72(R)	88b
	(S,S)-VII	91(S)	Table 6.2
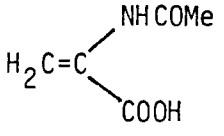	(R,R)-DIPAMP	90(S)	77b
	(S,S)-CHIRAPHOS	92(R)	76a
	(R)-PROPHOS	90(S)	76b
	(S,S)-SKEWPHOS	98(R)	76c
	(R,R)-DIOP	73(R)	88b
	(S,S)-VII	95(S)	Table 6.2

[a] The structures of the above chiral ligands are found in Chapter 2.

Table 6.4: Asymmetric hydrogenation of some olefins with $[Rh(P\text{-}N)(NBD)]ClO_4$ (P-N = V-VII and PPFA).

Substrate	Catalyst Precursor[a]	Time(h)	%e.e.	Configuration	Reference
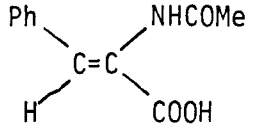	(S,R)-PPFA	24	76	S	102C
	(S,R)-XII	16	84	R	102C
	(S,R)-XIII	4.3	4	R	Table 6.2
	(S,S)-XIV	4.8	91	S	Table 6.2
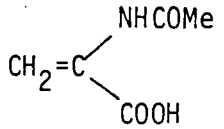	(S,R)-PPFA	18	49	S	102C
	(S,R)-XII	12	24	R	102C
	(S,R)-XIII	3.2	31	R	Table 6.2
	(S,S)-XIV	3.6	95	S	Table 6.2
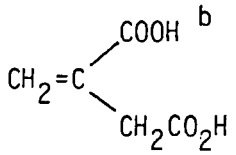 [b]	(S,R)-PPFA	72	33	R	102C
	(S,R)-XII	16	43	S	102C
	(S,R)-XIII	2.3	28	S	Table 6.2
	(S,S)-XIV	4.7	38	R	Table 6.2

[a] The configurations (S,R) and (S,S) are those of the chiral ligands, and (S,R)-PPFA represents the chiral catalyst precursor $[Rh(S,R\text{-}PPFA)(NBD)]ClO_4$.

[b] This is reduced 21% in 72h in the presence of (S,R)-PPFA.

(A) Optical Yields

The most significant finding is that the trisphosphine complex XIV is a very efficient catalyst precursor for the asymmetric hydrogenation of acylamino-cinnamic and -acrylic acids. The optical yields are 91% e.e. and 95% e.e., respectively when the hydrogenation is carried out in EtOH. Optical yields are slightly lower in MeOH. These high optical yields are comparable with those obtained with other representative chelating di(tertiary arylphosphine) derivatives, as shown in Table 6.3. These results are remarkable considering the fact that there is only one report [102c] of olefin reductions catalyzed by Rh complexes of alkylphosphines which lack the supposedly necessary $-PAr_2$ donors (cf. Table 6.4). A few reports have been published describing the reduction of other substrates. Thus Kumada et al [109] showed that a closely related P-N ligand, $(PMe_2)FA$ can be used to prepare an <u>in situ</u> Rh(I) catalyst precursor for the hydrosilation of ketones. The optical yields are moderate ($\sim$ 50%). Rhodium(I) complexes of alkylphosphines of the type $[Rh\{(iPr)_2P(CH_2)nP(iPr)_2\}]ClO_4$ (n = 3,4) are reported to be efficient for hydrogenation of a number of carbonyl compounds, including aldehydes [132a]. Ruthenium complexes of the DIOP derivatives [133] are also reported to catalyze the hydrogenation of carbonyl compounds and olefinic acids. These results are intriguing because the di(tertiary arylphosphine)-based catalysts are known to be inefficient for hydrogenation of the carbonyl group.

Using the same complex, (S,S)-XIV, as catalyst, only moderate to low optical yields are obtained in the hydrogenation of substrates lacking the

-NCOMe group such as (E)-α-methylcinnamic acid and itaconic acid (Table 6.2). These results seem to endorse the generally accepted fact that chelation of the substrate through both the olefinic double bond and the carbonyl of the -NCOMe group, for instance, is important in obtaining high optical yields. However, it is noteworthy that methylcinnamic acid is usually only slowly reduced using H_2 and Rh(I) type catalysts [56, 63, and Table 6.1], and optical yields greater than 60% have rarely been observed; the best to date being 61.4% using the ligand MMPP [92].

In general higher optical yields seem to be obtained when the reduction is carried out in EtOH, although reaction rates are slightly greater in MeOH than EtOH. In connection with these solvent effects it should be mentioned that they can be very significant and even reversal of the product configuration can be observed on changing the solvent [62, 76c]. The same phenomenon was observed in the present investigation. Thus the hydrogenation of (E)-α-methylcinnamic acid catalyzed by the trisphosphine complex (S,S)-XIV resulted in the product of opposite configuration (S) on changing the solvent EtOH (or MeOH) for benzene (Table 6.2). This was accompanied by a much slower reaction rate (>10h) and lower optical yield (28% e.e.). Other substrates have not been investigated to date.

(B) Comparative Studies: XIV vs XII and XIII

A further striking feature of the results in Table 6.2 is that the trisphosphine complex (S,S)-XIV is a more effective chiral catalyst than the bisphosphine complex (S,R)-XII and other monophosphine derivatives containing

(PR_2)FA (R = Ph, Bu^t) (cf. Table 6.4). Thus, for example, hydrogenation of acylamino-cinnamic, -acrylic acids, and itaconic acids results in a wide spread of optical yields using the catalyst precursors containing the P-N ligands, (PR_2)n FA (n = 1,2; R = Ph, Bu^t) (cf. Tables 6.2 and 6.4).

Another striking difference between the trisphosphine complex (S,S)-XIV and the other two complexes (S,R)-XII and -XIII is that the former gives hydrogenated products of the opposite absolute configuration to those obtained by the latters. For example, the hydrogenation of acylaminocinnamic acid using the (S,R)-mono, (S,R)-bis, and (S,S)-trisphosphine complexes (XII, XIII, and XIV) resulted in (R)-, (R)-, and (S)- phenylalanine respectively as the product. These results indicate that in the same solvent planar chirality plays an important role in determining the configuration of the hydrogenated products. The following considerations based on conformational effects provide a basis for understanding these differences in optical yields and product configurations.

(C) Conformational Effects

It has been shown in section 5.2.2(B) that the trisphosphine complex (S,S)-XIV adopts only one conformation C, whereas the other two complexes (S,R)-XII and -XIII show two conformers A and B in solution. The Ke($\equiv$[B]/[A]) value for (S,R)-XII and -XIII is approximately 1 and 2, respectively. The mechanism of hydrogenation for these systems may also be described by that outlined in Fig. 2.13 but because the two ends of the P-N ligands are different twice as many 4-coordinate intermediates need to be

considered. Namely, four diastereomers for the catalyst-substrate adduct $[Rh(P\text{-}N)(substrate)]^+$ are produced from each conformer (A, B, or C), as shown in Fig. 6.1(A). If catalysis proceeds via a hydride mechanism five diastereomers of $[Rh(P\text{-}N)(H)_2]^+$ can be formed from each conformer of the type $[Rh(P\text{-}N)(S)_2]^+$, as shown in Fig. 6.1(B).

Thus, in order to achieve high optical yields, catalysis by these systems (XII-XIV), like other catalysts, requires maximization of the $\Delta\Delta G^{\ddagger}$ value among various possible diastereomers in the rate-determining step (cf. equation 2.5). Then the high optical yields by the trisphosphine complex (S,S)-XIV may be associated with the strong conformational preference of the chiral chelate ring as argued by Bosnich et al (cf. Section 2.3.3A). The favored conformation C (Fig. 5. 7B) is the same as shown in Fig. 2.14 for (S,S)-CHIRAPHOS and (S,S)-SKEWPHOS. However the product configurations are reversed as seen in Table 6.3. Therefore the conformational arguments based entirely on chiral arrays of R groups in $-PR_2$ moieties do not hold in this system (XIV). Undoubtedly the bulky ferrocenyl group exerts some influence (let alone the kinetic factors).

In the case of catalysis by the mono- or bisphosphine complex ((S,R)-XII or -XIII), the number of the diastereomers for $[Rh(P\text{-}N)(substrate)]^+$ (or $[Rh(P\text{-}N)(H)_2]^+$) (Fig. 6.1) will be doubled due to the presence of the two diastereomeric conformers A and B. Under this circumstance either conformer A or B of the NBD precursor (XII or XIII) can, in principle, lead to a pair of the enantiomeric hydrido alkyl intermediates, (P-N)Rh(H)(R), which in turn yield a pair of enantiomeric products via reductive elimination

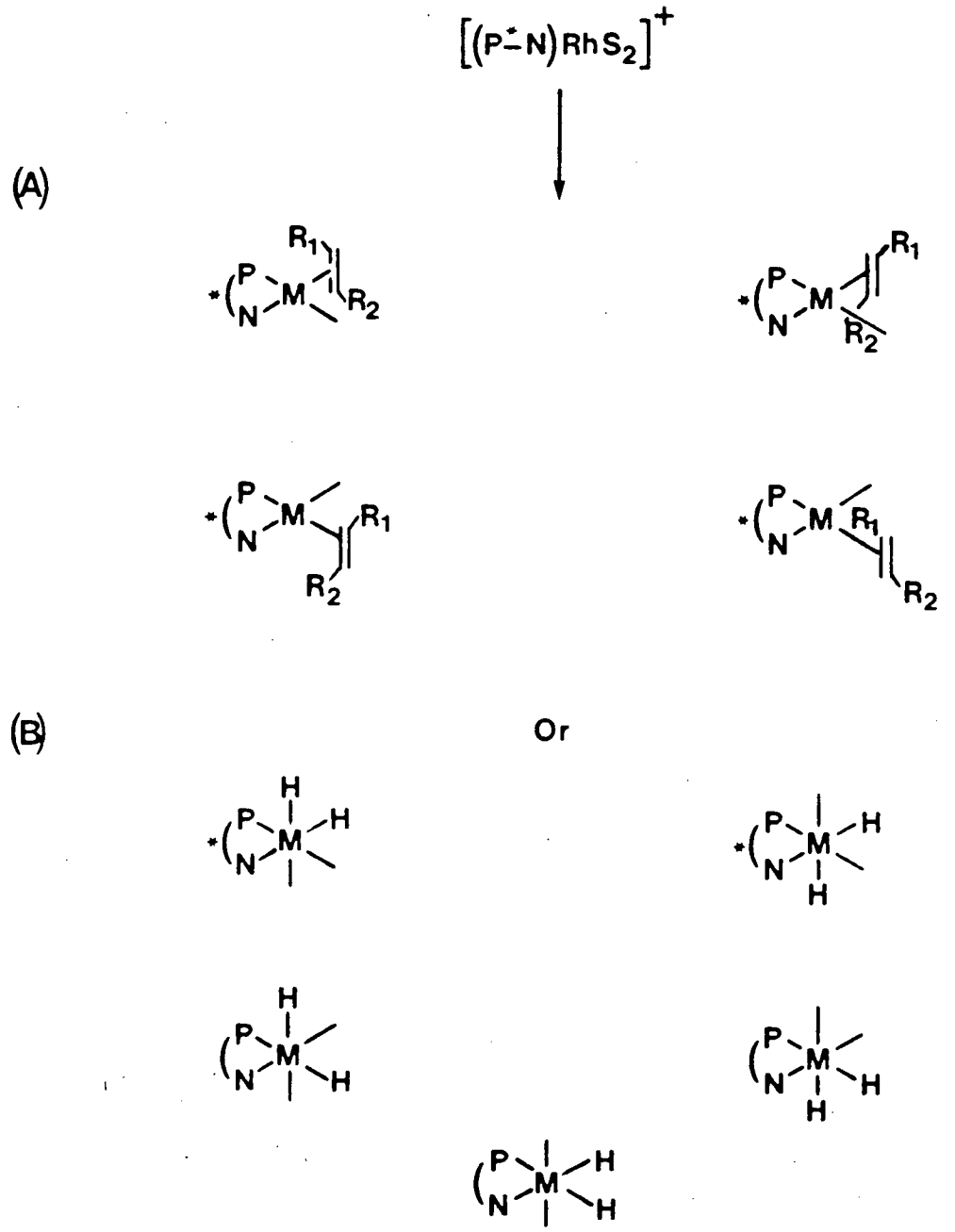

Fig. 6.1: (A) Four possible diastereomers of $[(P^{*}\text{-}N)Rh(substrate]^{+}$ generated from the conformer A, B, or C of $[(P^{*}\text{-}N)Rh(S)_2]^{+}$.

(B) Five possible diastereomers of $[(P^{*}\text{-}N)Rh(H)_2]^{+}$ generated from the conformer A, B, or C of $[(P^{*}\text{-}N)Rh(S)_2]^{+}$.
$P^{*}\text{-}N$ = the ligands V-VII, S = solvent, M = Rh.

of RH. Thus low optical yields obtained by (S,R)-XII or -XIII may be anticipated unless a route leading to any particular enantiomeric intermediate (P-N)Rh(H)(R) is preferred for any reason. The hydrogenation results in Table 6.4 indicate that no such preference is made in the case of (S,R)-XII and -XIII.

The conformational effects presented here may also account for the differences in the product configurations caused by these catalytic systems (XII-XIV). Fig. 5.17 shows that the preferred conformation (C) of (S,S)-XIV is enantiomeric with the major conformation (B) of (S,R)-XIII. Thus if these two conformers function in the opposite direction in inducing the enantioface-discrimination the results summarized in Table 6.4 are as anticipated; (S,S)-XIV and (S,R)-XIII give the enantiomeric products. However, apart from the consideration of planar chirality, it is difficult to explain why (S,R)-XII and -XIII give the same configuration of products. It is also difficult to account for the variation in optical yields (Table 6.4) caused by XII and XIII unless kinetic factors are considered.

Furthermore, electronic effects undoubtedly play some part. As seen in Tables 6.2 and 6.4, the bisphosphine complex XIII gives much higher reaction rates (4∿8 times) than the monophosphine complex XII in spite of increased steric bulk in the second Cp ring. This rate increase is probably due to electronic effects which are slightly outweighed by the steric effects in the case of the trisphosphine complex XIV, since reaction rates are slightly lower with XIV than those observed with the bisphosphine complex XIII (Table 6.2).

6.3 HYDROGENATION OF CATALYST PRECURSORS

6.3.1 Introduction

(A) Recent Development

As pointed out in section 1.4.2, an important distinction between the Rh-monophosphine catalyst $[Rh(L)_2(Diene)]A$ and the Rh-di(tertiary phosphine) catalyst $[Rh(L\text{-}L)(Diene)]A$ is that the former reacts with H_2 to form hydrides and the latter does not. Thus a solvate $[Rh(L\text{-}L)S)_2]^+$ (S = solvent) which is the catalyst in the hydrogenation reaction is formed in the initial hydrogenation of the catalyst precursor $[Rh(L\text{-}L)(Diene)]A$. On the other hand, catalytic hydrides ($[Rh(L)_2(H)_2]^+ \rightleftharpoons [Rh(L)_2H]^o + H^+$) are formed in the case of $[Rh(L)_2(Diene)]A$ (here the coordinated solvents are omitted). More recently, however, three important observations have been made which indicate that these generalities may not be correct. Those observations can be summarized as follows.

(a) Unsaturate Route with $[Rh(L)_2(Diene)]A$

Halpern et al [135] demonstrated that even some monophosphine derivatives can react via an unsaturate route when the following equilibrium is established under suitable reaction conditions (equation 6.1).

$$[Rh(L)_2(S)_2(H)_2]^+ \overset{K_e}{\rightleftharpoons} \underline{cis}\text{-}[Rh(L)_2(S)_2]^+ + H_2 \qquad (6.1)$$

The cis-structure for the solvate $[Rh(L)_2(S)_2]^+$ (L = PPh_3) was deduced from the large ^{31}P-Rh coupling constant ($^1J_{RhP}$ = 205 Hz). For example, the analogous cis-structure $[Rh(DIPHOS)(S)_2]^+$ has the value of 203 Hz for $^1J_{RhP}$ [135]. Additional evidence for the reversibility of reaction (6.1) has recently been reported [47d].

(b) Hydride Formation from [Rh(L-L)(Diene)]A

Brown et al [136] have recently published evidence for the formation of hydrides from di(tertiary phosphine)Rh(I) catalysts in the absence of substrate (equation 6.2).

$$[Rh(L\text{-}L)(NBD)]^+ \xrightarrow{2H_2} [Rh(L\text{-}L)(S)_2]^+ \underset{Ke}{\overset{H_2}{\rightleftharpoons}} [Rh(L\text{-}L)(H)x(S)_2]^+ \qquad (6.2)$$

The equilibrium constant Ke is very low when the ligands (L-L) are typical chelating diphosphines, and the hydrides are undetected by usual techniques. In the absence of substrate, hydride formation seems to be blocked by substrate coordination. Nevertheless, equation (6.2) suggests that the Ke value and thus the mechanism of hydrogenation could be greatly affected by the nature of the chelating di(tertiary phosphines). For instance a more basic phosphine could stabilize the hydride(s) and allow hydrogenation to proceed via either the hydride route or the unsaturate route. In this connection, Otsuka et al [132b] have recently reported the isolation of a solid rhodium hydride from the reaction of equation (6.3).

$$[Rh(L\text{-}L)(NBD)]ClO_4 + H_2/MeOH \longrightarrow [Rh(L\text{-}L)(H)_2]ClO_4 \qquad (6.3)$$

L-L =

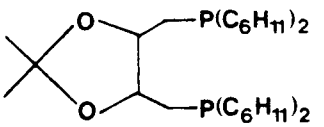

The suggested structure for the product is based on the analytical and spectroscopic data: IR ν(Rh-H) 2100, 2075 cm^{-1}; ^1H NMR(CD_2Cl_2) δ-8.2(br), -19.8(br) ppm. A crystal structure has not yet been reported, and the NMR data do not support two terminal hydrides although Brown et al [136] recently proposed the structure to be that shown below.

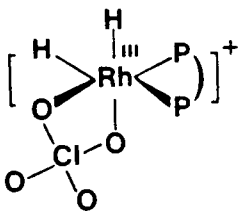

(B) Possible Hydrogenation Pathways for [Rh(L-L)(Diene)]A

The results described above indicate that various intermediates (or products) could be produced reversibly in a given reaction, even though they may not be isolable. Some possible hydrogenation pathways for the catalysts of the type [Rh(L-L)(Diene)]A are set out in Fig. 6.2. As will be discussed later, this general scheme seems to be applicable to the present catalyst systems VIII-XIV.

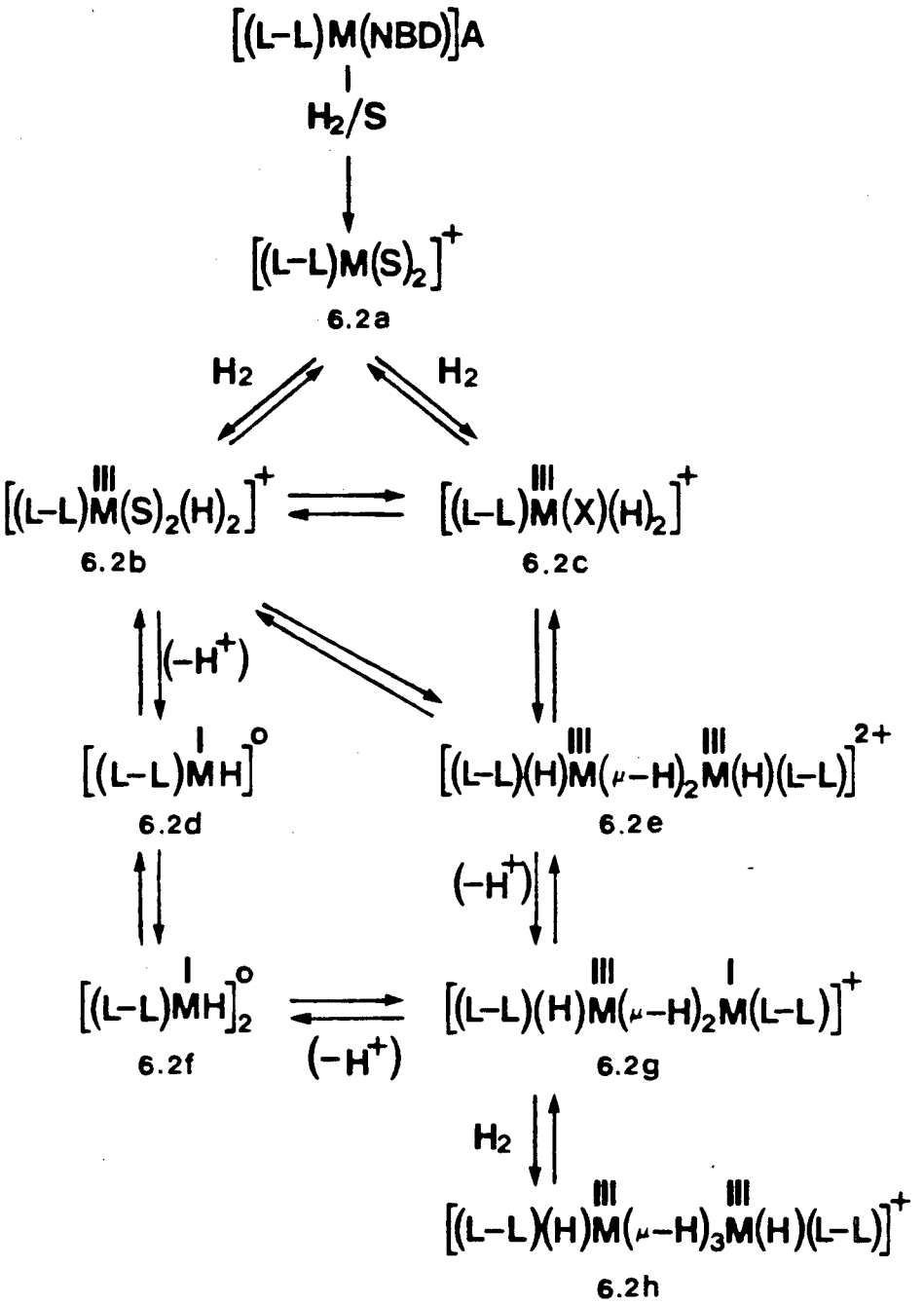

Fig. 6.2: Some possible hydrogenation pathways for [(L-L)Rh(Diene)]A. Vacant sites of metal may be filled with S. L-L = chelating bidentate ligands; M = Rh, A = ClO_4; X = A or S; S = solvent.

The first step, the formation of the disolvate 6.2a, is based on the commonly found result for typical di(tertiary phosphine)Rh(I) catalysts. The second step involves oxidative addition of H_2 to the disolvate to form the dihydrido Rh(III) species 6.2b or 6.2c. From these two species a number of other hydrides such as 6.2d-h could be formed reversibly by plausible dimerization, and deprotonation reactions.

(C) Relevant Metal Hydrides

Although there are no precedents for the monohydride Rh(I) species 6.2d, monophosphine analogues are quite common. In particular the 14 electron compounds $Rh(L)_2H$ can be synthesized and isolated as crystalline solids when the ligand L carries bulky electron donating alkyl groups such as tert-butyl or cyclohexyl (equation 6.4) [137].

$$\frac{1}{X}[RhH(L)_2]_X(N_2) \xrightarrow{-N_2} RhH(L)_2 \qquad (6.4)$$

$$X = 1,\ L = P(CMe_3)_3$$
$$= 2,\ \ = P(C_6H_{11})_3$$

It is interesting to note that cationic analogues such as $[(DIPHOS)Rh(H)(S)_3]^{2+}$ (S = MeCN) are known (equation 6.5) [46a].

$$[(DIPHOS)Rh(S)_2]^+ + HX \longrightarrow [(DIPHOS)Rh(H)(S)_3]^{2+} \qquad (6.5)$$

$$X = ClO_4^-,\ BF_4^-,\ PF_6^-$$

The hydrides of the type $[(L\text{-}L)RhH]_2^0$ (= 6.2f in Fig. 6.2) have been recently described by Fryzuk [138], as shown in equation (6.6).

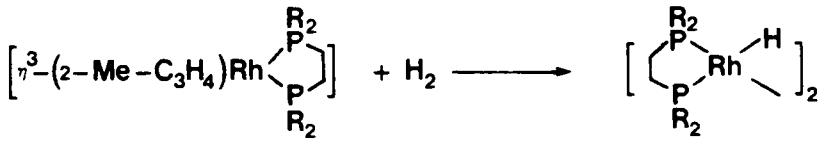

$$R = CHMe_2, OCHMe_2 \qquad (6.6)$$

The products are reported to be efficient catalysts for the hydrogenation and isomerization of simple olefins. The product, where R = $OCHMe_2$, reacts with H_2 to form a dimeric tetrahydride, $[(L\text{-}L)_2Rh_2H_4]$. The suggested structure for this compound is shown below [138a].

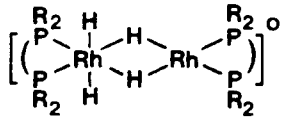

R = $OCHMe_2$

Muetterties et al [139] have recently reported the closely related neutral Rh(III)-Rh(I) dimers, $[(PR_3)_4Rh_2H_4]$ (R = OCHMe, NMe_2) which are the hydrogenation products of the catalyst precursors $[RhH(PR_3)_2]_2$.

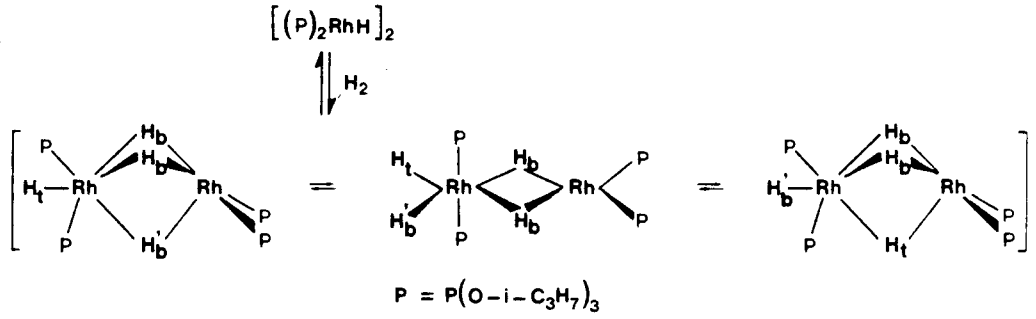

(6.7)

It has been shown that the product (R = ^{O}-$C_3H_7^{i}$) can be formed reversibly from the precursor dimer, and is fluxional in solution (equation 6.7). Based on the variable temperature NMR (^1H, ^{31}P) studies [139b], the triply bridged dimer was proposed as a ground state structure for the product and the doubly bridged dimer as an excited state. The proposed stereochemistry of the transition state (or intermediate) is based on the crystal structure of the related doubly bridged hydride (R = NMe_2) [139c]. Because it is of importance for future discussion, it is useful to briefly review the fluxional behavior of product of equation (6.7).

As summarized in the Appendix, the low temperature (-80°C) ^1H NMR is consistent with the triply bridged dimer (equation 6.7). Namely, it shows (i) a doublet of multiplets for the identical bridging hydrides H_b (δ - 7.8 ppm, trans $^2J_{PH}$ = 180 Hz, I = 2), (ii) a doublet of multiplets for the unique hydride H_b' (δ - 11.1 ppm, trans $^2J_{PH}$ = 89 Hz, I = 1), and (iii) a broad peak for the terminal hydride H_t (δ - 14.5 ppm, I = 1). The VT ^1H NMR study shows that on warming from -80° to 3°C the two resonances

ascribed to the terminal hydride (H_t) and the unique bridging hydride (H_b') merge and coalesce. The resonance for the two bridging hydrides (H_b) is unaltered in this temperature range. On warming to 26°C, all peaks collapse and on further warming to 46°C a new broad signal appears, indicating that all hydrido ligands are engaged in the exchange process of this temperature. The products in equation (6.7) were proposed as active intermediates in the olefin reductions catalyzed by the precursors $[RhH(PR_3)_2]_2$ [139].

In the Appendix are summarized the NMR (^1H, ^{31}P) data for some metal hydrides and other related compounds. This information is relevant to the future discussion.

6.3.2 Hydrogenation of the Catalyst Precursors VIII-XIV

(A) General Observations

The experimental procedures are described in section 4.2.4.

(a) Reaction in Alcohol

When solutions of the achiral catalyst precursors VIII-XI in MeOH or EtOH are exposed to H_2 (1 atm, 30°C) the initial reddish orange color deepens to red, and in most cases dark red crystals are obtained at 20°C or on cooling (0°C). The chiral complexes XII-XIV show a color change from reddish orange to wine red. The ^1H NMR spectra of these crystals or the solid residue after solvent removal are temperature dependent and show the presence of bridging and/or terminal hydrides. The solutions of the reactants

(CD_3OD) gave very complex NMR spectra (^1H, ^{31}P) which are not fully interpreted at this stage. Some representative spectra are presented in the next subsections.

(b) Reactions in Other Solvents

The reaction with H_2 was carried out in various other solvents such as acetone, CH_3CN, CH_2Cl_2, and $CHCl_3$. The general observations are similar to those described above. Thus, in most cases, the ^1H NMR spectra of the solid or crystalline products are strongly temperature dependent, and show the presence of bridging and/or terminal hydrides. NMR (^1H, ^{31}P) monitoring of the reactions in solution also reveals considerable complexities. Only a few particular examples will be discussed.

(c) Catalytic Properties

The hydrogenation products obtained as solids from MeOH are catalytically active in olefin reductions. The hydrogenation procedure generally used was the same as that described in section 4.2.2 except that the catalyst precursor was replaced by the isolated solid. In some cases the substrate was added to the in situ solution containing the hydride(s). All reductions are stoichiometric but no attempt was made to measure kinetic data or isolate any reaction intermediate. The catalytic properties of the hydrogenation products obtained from solvents other than MeOH have not been investigated.

(B) Hydrogenation of [Rh(BPPF)(NBD)]ClO_4 (VIII)

The reaction was carried out in three different solvents, MeOH, CH_3CN,

and $CHCl_3$.

(a) Reaction in MeOH

This reaction resulted in the uptake of 4.7 moles of H_2 per rhodium atom. A dark brown solid remained after solvent removal. The ^1H NMR spectrum (CD_2Cl_2) of either this solid or the *in situ* solution (CD_3OD) did not show any hydride resonance (35° - -90°C). Brown et al [47d] briefly reported that the same reaction gives a disolvate $[Rh(BPPF)(MeOH)_2]^+$ in solution. The assignment was made on the basis of the ^{31}P NMR data (δp 55.3 ppm, $^1J_{RhP}$ = 215 Hz), the large coupling constant being consistent with the phosphine *trans* to a relatively weak donor such as MeOH (see also Appendix for comparison with other related species). In the present investigation, however, hydrogenation for 25 min resulted in a more complex ^{31}P NMR spectrum.

(b) Reaction in $CHCl_3$

The ^{31}P NMR spectrum of the solution after hydrogenation for a short period ($\sim$ 5 min) shows a new pair of broad doublets ($\delta p(1)$ 44.60 ppm, J_{RhP} = 210 Hz; $\delta p(2)$ 44.48 ppm, J_{RhP} = 217 Hz) in addition to the doublet from the NBD precursor (VIII). No hydride coupling was observed for these signals. These peaks can be interpreted as arising from two nonequivalent phosphine groups in the η^6-arene complex 6.3b (Fig. 6.3). The structure of the DIPHOS analogue $[Rh_2(DIPHOS)_2](BF_4)_2$ is shown in Fig. 1.8. This $[Rh(DIPHOS)]_2^{2+}$ complex is known to dissociate into monomeric $[Rh(DIPHOS)]^+$ (or $[Rh(DIPHOS)(MeOH)_2]^+$) ions when dissolved in MeOH [46a]. The methanolic solution gives a single ^{31}P signal (δ80, d, J_{RhP} = 203 Hz). No NMR data have

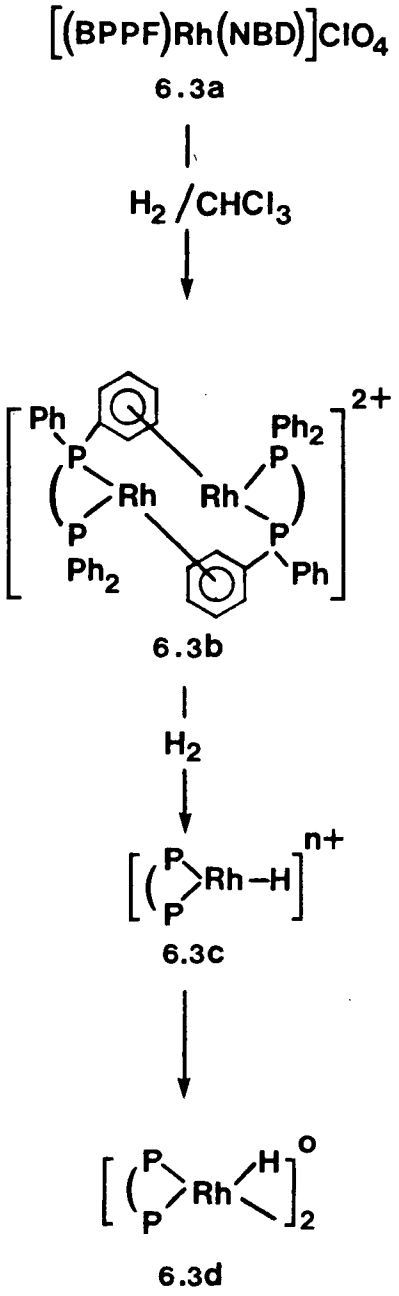

Fig. 6.3: Possible hydrogenation pathways for VIII in $CHCl_3$.
BPPF = the ligand I; n = 0 or 2.

been recorded for this species in a non-coordinating solvent. The analogous reaction has been carried out in benzene where the solvent again preferentially binds to the metal upon loss of the NBD ligand (equation 6.8) [140].

$$[Rh(L\text{-}L)(NBD)]ClO_4 + H_2/C_6H_6\text{-}THF \longrightarrow [Rh(L\text{-}L)(\eta^6\text{-}C_6H_6)]ClO_4 \quad (6.8)$$

L-L =

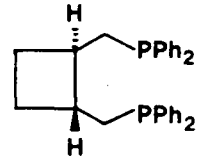

The ^{31}P NMR data (CD_2Cl_2) of this product of known structure are: δp 31.4(d), J_{RhP} = 201.4 Hz.

Further hydrogenation of VIII results in reaction of all the starting material (VIII), a reduction of the intensity of the doublets of the proposed η^6-arene complex 6.3b, and the appearance of a doublet at δp 54.41 ppm (J_{RhP} = 146.5 Hz). This species is a hydride (J_{PH} = 19.5 Hz). Addition of Et_3N removes this doublet. This species could be a simple monohydride $[(BPPF)RhH]^{n+}$ (6.3c) where the charge is either 0 or 2. When the same solution (without amine) is allowed to stand for longer period (>2h) after initial hydrogenation, a number of additional peaks arise including a doublet of 1:1:1 triplets at 53.79 ppm ($J_{RhP} \sim 144$ Hz). Triplet separation averages 12 Hz. This peak is not affected by base addition. The identity of this species is uncertain. Removal of solvent leaves a solid residue whose ^1H NMR spectrum is shown in Fig. 6.4.

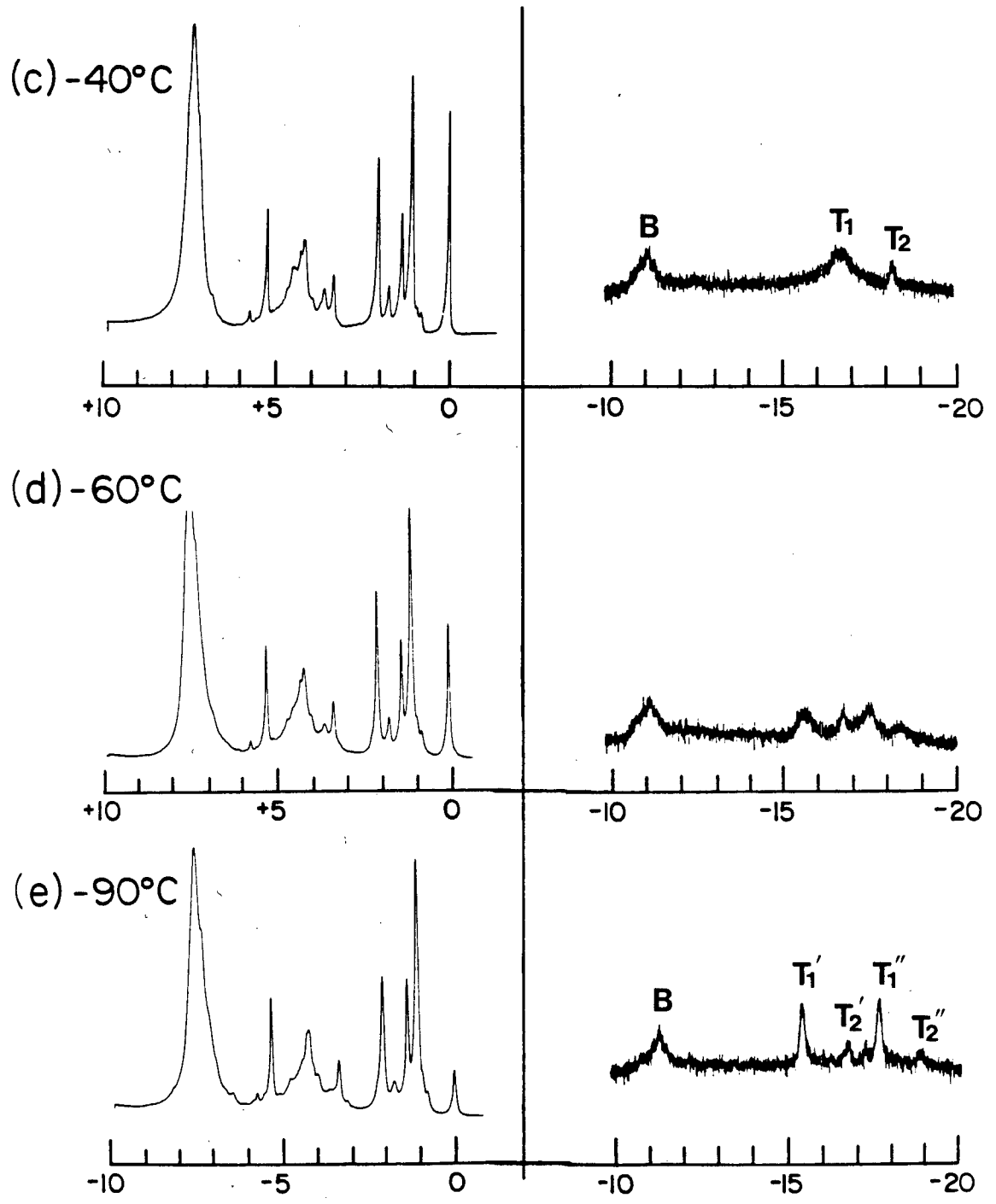

Fig. 6.4(A): Variable temperature 400 MHz ^{1}H NMR spectrum (CD_2Cl_2) of the hydrogenation product (S) of VIII from $CHCL_3$.

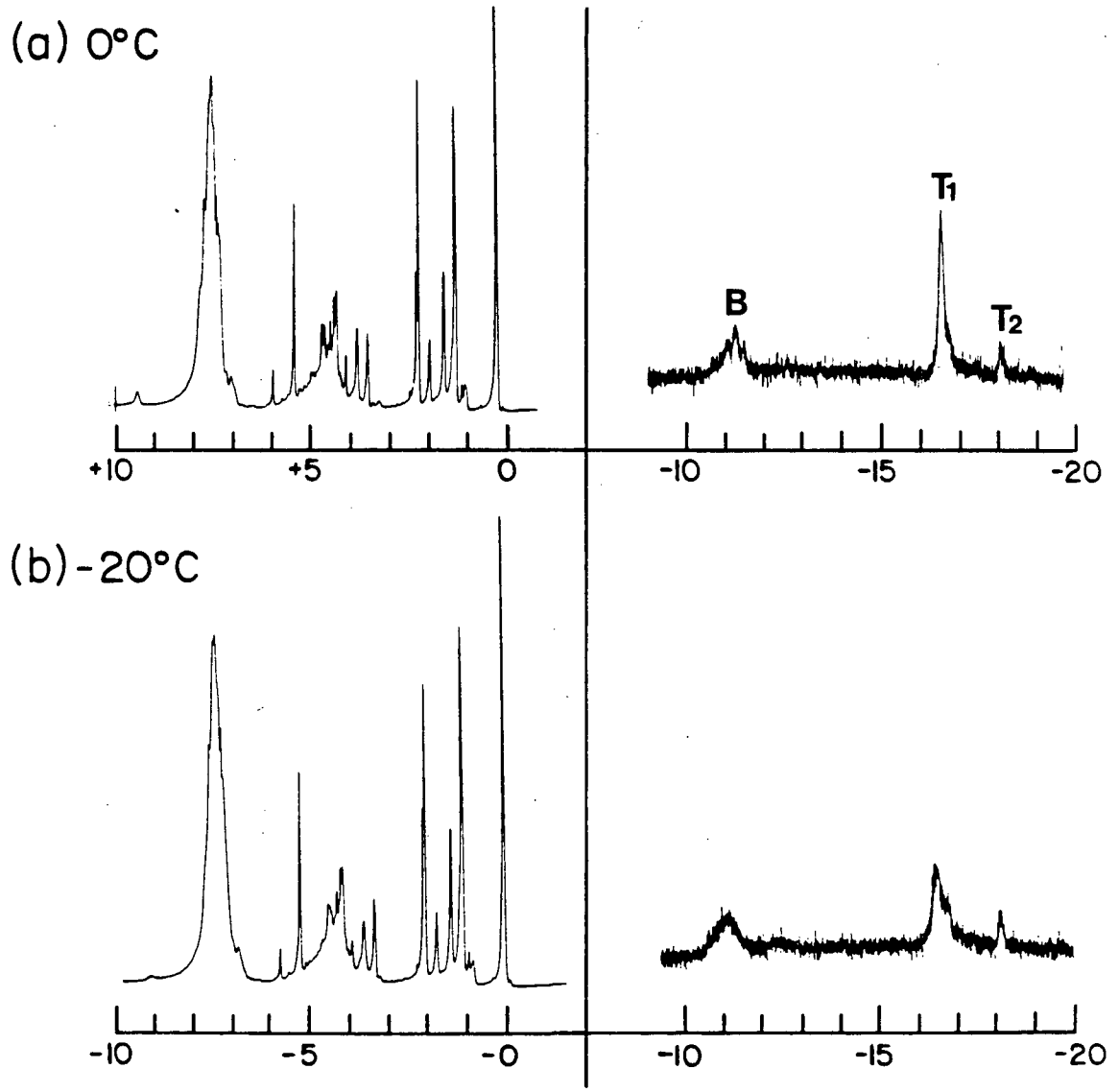

Fig. 6.4(B): Variable temperature 400 mHz ^1H NMR spectrum (CD_2Cl_2) of the hydrogenation product(s) of VIII from $CHCl_3$.

The hydride NMR pattern at -90°C consists of a temperature independent signal B ($\sim$ -11 ppm) and two pairs of temperature dependent multiplets T_1'/T_1'' and T_2'/T_2'' in the range -15 to -19 ppm, but the broadness of the peaks precludes any satisfactory interpretation. It is possible that the signal B is due to a neutral monomer or dimer such as 6.3d (Fig. 6.3), however, the data do not compare very satisfactorily with known compounds described in equations (6.6) and (6.7) (see also Appendix). Nevertheless there is no doubt about the formation of hydride species which will be established.

(c) Reaction in CH_3CN

This reaction resulted in the formation of large yellow crystals on allowing the hydrogenated solution to stand at room temperature. The $^{31}P\{^1H\}$ NMR spectrum (CH_2Cl_2) of the sample showed a doublet at 45.05 ppm ($^1J_{RhP}$ = 181.9 Hz) due to the disolvate $[(BPPF)Rh(MeCN)_2]ClO_4$. This formulation has been recently confirmed by a crystal structure determination [141], although the analytical data are not in agreement: C, 54.01; H, 3.32; N, 3.32. This type of complexes where the ligands are typical di(tertiary phosphines) have been well characterized in solution by NMR, and are known to be active hydrogenation catalysts formed from the diene precursors (cf. section 1.4.2B).

(C) Hydrogenation of $[Rh(BPB^tPF)(NBD)]ClO_4$ (IX)

(a) Reaction in MeOH

After passage of H_2 for 30 minutes the resultant solution deposited orange crystals on standing at 20°C. The crystal structure of this product

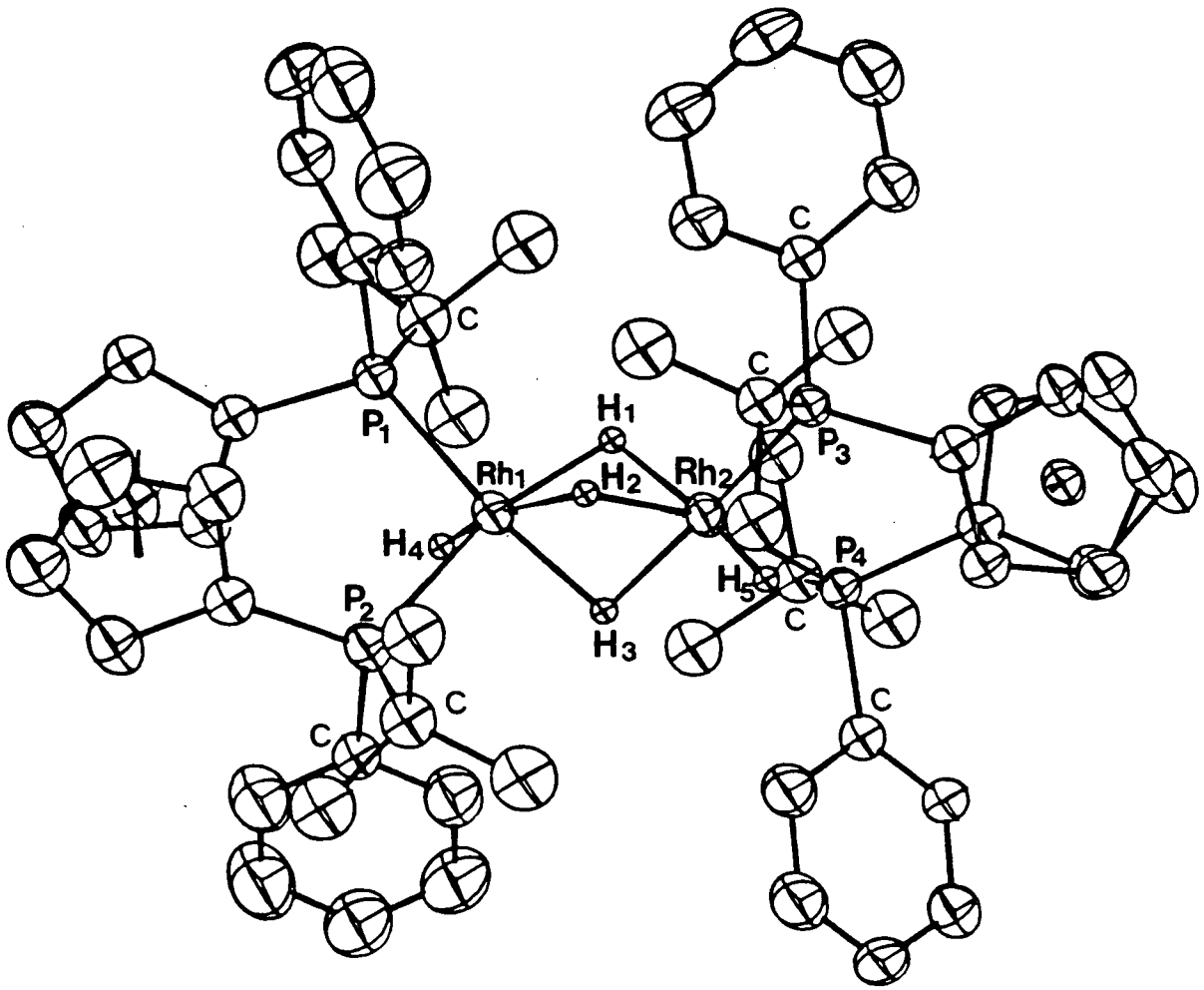

Fig. 6.5: The crystal structure of the hydrogenation product of IX from MeOH, $[(P\text{-}P)(H)Rh(\mu\text{-}H)_3Rh(H)(P\text{-}P)]^+$(P-P = the ligand II) [142].

is shown in Fig. 6.5. The molecule is a unipositive Rh(III) dimer with three bridging hydrides and one terminal hydride on each Rh metal. This molecule can be roughly described as possessing a C_2 axis along the line connecting H_3 and the middle point of two Rh atoms (vide infra). Each Rh atom adopts approximately an octahedral geometry (cf. 6.2h, Fig. 6.2).

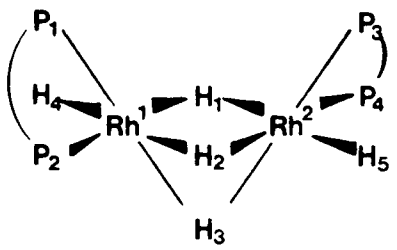

Therefore the ion has: (i) a pair of equivalent terminal hydrides H_4 and H_5 which are not <u>trans</u> to a phosphorus atom; (ii) a pair of equivalent bridging hydrides H_1 and H_2, each being <u>trans</u> to a single phosphorus atom (H_1 <u>trans</u> to P_2, H_2 <u>trans</u> to P_4); (iii) a unique bridging hydride H_3 <u>trans</u> to both P_1 and P_3. Thus, if this compound were nonfluxional in solution three hydride resonance signals would be seen. However, this product shows fluxional behavior in solution as seen in Fig. 6.6.

No hydride signal was observed at 35°C. Cooling to 0°C resulted in the appearance of (i) a broad terminal resonance at -23.3 ppm (I = 2) and (ii) a pair of broad signals of equal intensity at -8.0 and -9.4 ppm (I = 3). Both signals are slightly sharpened on further cooling (-40° ∿ -90°C). The fluxional processes in the two regions seem to be independent in the range -90° to 0°C as seen in Fig. 6.6. Thus a possible exchange process may

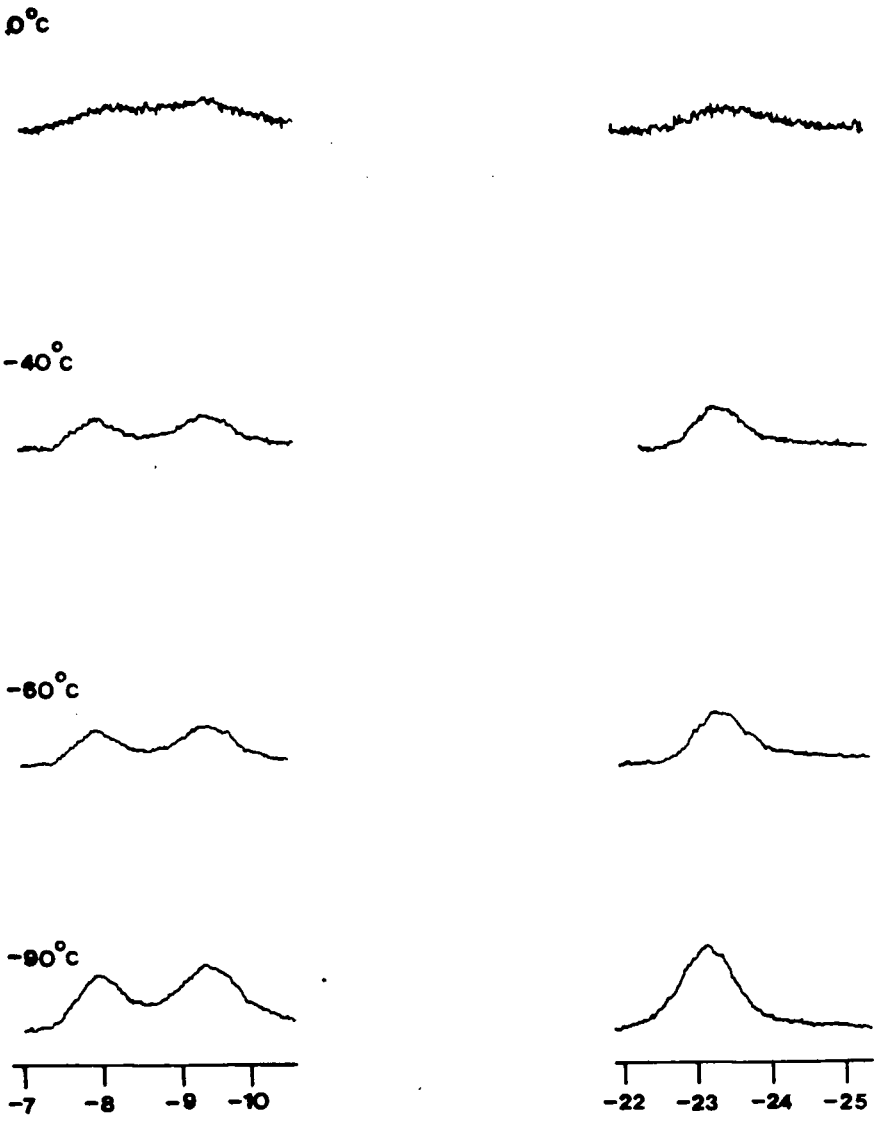

Fig. 6.6: Variable temperature 80 MHz ^{1}H NMR spectrum (CD_2Cl_2) of the hydrogenation product, $[(P\text{-}P)(H)Rh(\mu\text{-}H)_3Rh(H)(P\text{-}P)]^+$, of IX from MeOH. P-P = the ligand II.

involve the structure where all three bridging hydrides are equivalent and trans to a single phosphorus atom to give a broad doublet whose separation of 112 Hz is assignable to a trans P-H coupling ($^2J_{PH}$) (see also Appendix for comparison). Similar but better resolved and assignable spectra have been reported for the iridium analogues $[Ir_n(H)_{2n+1}(DPPP)_n](BF_4)_{n-1}$ (n = 2,3; DPPP = $Ph_2P(CH_2)_3PPh_2$) [143] and $[Ir_2(\mu\text{-}H)_3H_2(PPh_3)_4]PF_6$ [144].

The same reaction was carried out in CD_3OD, and the solution monitored by ^1H NMR ($\sim$ 30 min). The VT ^1H NMR spectra are shown in Fig. 6.7, and relevant hydride resonances are listed in Table 6.5. As summarized in Table 6.5, the low temperature (-90°C) hydride NMR pattern consists of (i) a set of temperature-independent signals T_1, T_2 and T_3 and (ii) a set of temperature-dependent signals B_1, B_2, T_4, T_5, T_6, and T_7. As the temperature is raised to -60°C, both pairs of bridging signals B_1/B_2 and terminal signals T_4/T_5 merge to give broad multiplets B and T', respectively. By 0°C all the signals except T_1, T_6 and T_7 have disappeared. Further warming (35°C) causes the pair of multiplets T_6 and T_7 to coalesce to a broad multiplet T, and thus only two signals T_1 and T are seen at this temperature. None of the signals associated with the isolated product are present in these spectra (cf. Figs. 6.5 and 6.6). The following attempted interpretation of all these spectra is based on Figs. 6.2 and 6.8.

(I) The Temperature-Independent Signals T_1 - T_3

The temperature invariant signal T_1 appears to be a doublet of doublets with small coupling constants (24 and 28 Hz). The weaker signals T_2 and T_3 also give the same pattern which is difficult to account for in terms of

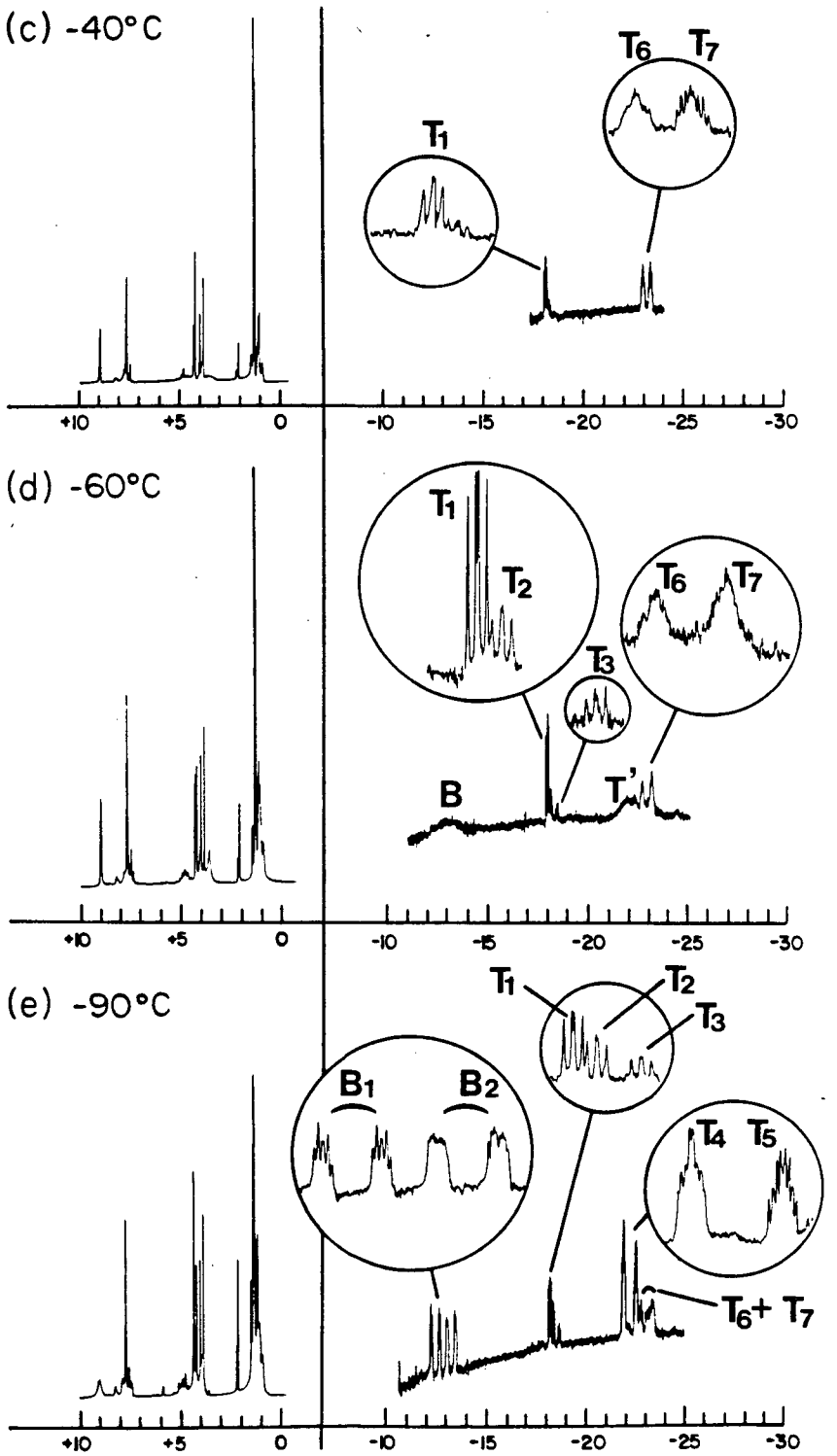

Fig. 6.7(A): Variable temperature 400 MHz ^{1}H NMR spectrum of the hydrogenated solution (CD_3OD) of IX.

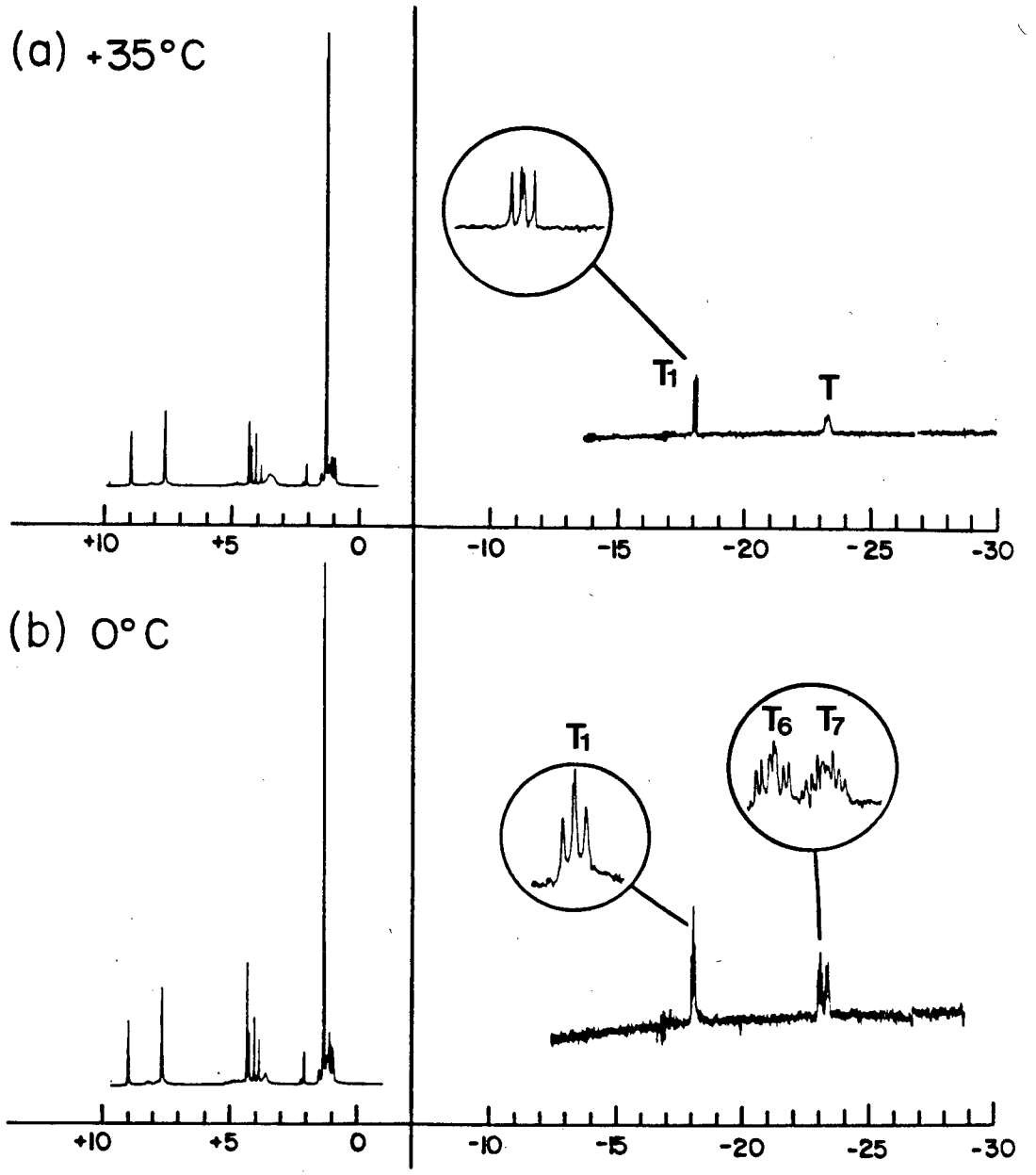

Fig. 6.7(B): Variable temperature 400 MHz ^{1}H NMR spectrum of the hydrogenated solution (CD_3OD) of IX.

Table 6.5: ^{1}H NMR data (hydride portion) for the hydrogenated solution (CD_3OD) of the catalyst precursor IX [a,b].

Temp °C	Temperature-dependent signals	Temperature-independent signals
-90	B_1(dm, -12.35, J(d)=172, I=2) B_2(dm, -13.23, J(d)=180, I=2) T_4(tm, -21.82, J(t)= 24, I=2) T_5(tm, -22.45, J(t)= 28, I=2) T_6(tbd, -22.88, J(t)= 28, J(bd)=12, I=1) T_7(m, -23.36, I=1)	T_1(dbd, -18.13, J(d)=24, J(bd)=28, I=1) T_2(dbd, -18.29) T_3(dbd, -18.53)
-60	B(m, -13.2) T´(m, -22.3) T_6 T_7	T_1 T_2 T_3
0	T_6 and T_7	T_1
+35	T(m, -23.3)	T_1

[a] See also Fig. 6.7.

[b] Coupling constants in Hz: dm = doublet of multiplets, dbd = doublet of broad doublets, tbd = triplet of broad doublets, m = multiplet; J(d), J(t), J(bd), J(dbd) = coupling constant in each pattern; I = relative intensity.

chelating ligands. One possibility involving a dangling phosphine is seen below.

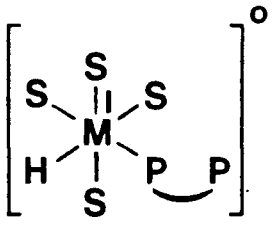

6.8e

As indicated in Fig. 6.2, this species is analogous to the monomeric Rh(I) species 6.2d which is a dissociation product of the Rh(III) dimer 6.2e. In Fig. 6.8 is proposed a possible dissociative process through which the above species can be formed.

The spectra in Fig. 6.7 shows that the intensity of T_2 and T_3 decreases as that of T_1 increases on warming (-90° →-60°C), and then T_2/T_3 disappear at -40°C. This fluxional behavior is hard to explain although the intramolecular exchange processes in Fig. 6.8 suggest that dissociation of the dimers 6.8a-d become irreversible at higher temperatures ($\geq$ -40°C) to result in the predominant formation of monomers such as shown above (6.8e). The remaining aspect of Fig. 6.8 is discussed below.

(II) Other Temperature-Dependent Signals

If the isolated product (Fig. 6.5) were formed reversibly through the route 6.2a$\rightleftharpoons$ 6.2c$\rightleftharpoons$ 6.2e$\rightleftharpoons$ 6.2g$\rightleftharpoons$6.2h (Fig. 6.2), then the solution could contain a doubly bridged Rh(III) dimer analogous to 6.2e. Since the ligand

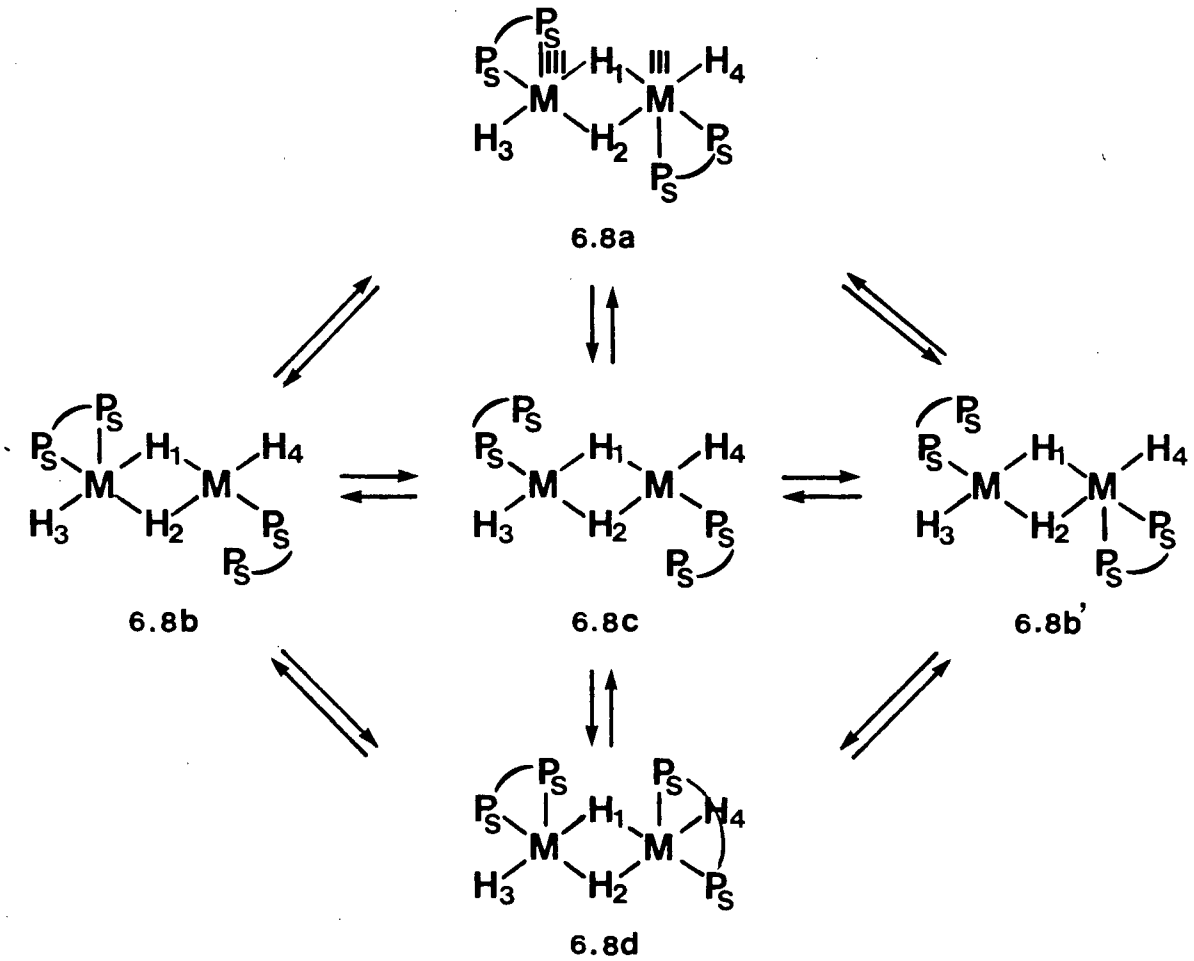

Fig. 6.8: The proposed intramolecular exchange processes in the hydrogenated solution (CD_3OD) of the complex IX. The vacant sites of metal may be filled with $S(CD_3OD)$. M = Rh, P-P = the ligand II.

in this case is rac-II ((S,S)-/(R,R)-II), there are two possible combinations to form this dimer: namely, an enantiomeric pair of dimers (S,S,S,S)-/-(R,R,R,R)- and an equivalent pair of dimers (S,S,R,R,)-/(R,R,S,S)-. Here S and R refer to the configuration at P atoms of the ligand II. Each enantiomer such as (S,S,S,S) possesses two pairs of diastereotopic hydrides H_1/H_2 and H_3/H_4 by internal comparison (6.8a) (vide infra).

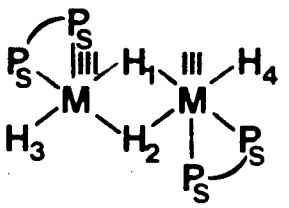

(S,S,S,S)-6.8a

On the other hand the (S,S,R,R)-/(R,R,S,S)-diastereomers possess an equivalent pair of bridging and of terminal hydrides by internal comparison.

Thus the signals B_1, B_2, T_4 and T_5 can be assigned to the structure (S,S,S,S)-6.8a shown above. Either the doublet of multiplets B_1 or B_2 is associated with H_1 or H_2 with $^2J_{PH}(B_1)$ = 172 Hz and $^2J_{PH}(B_2)$ = 180 Hz. The terminal hydrides H_3 and H_4 would appear as a triplet of multiplets with $^2J_{PH}$ value of 24 and 28 Hz as seen in T_4 and T_5. Additional small couplings to Rh and H_1/H_2 are responsible for the multiplicities. Although it is conceivable that the solution contains the equivalent pair of diastereomers (S,S,R,R)-/(R,R,S,S)-, the low temperature (-90°C) NMR pattern seems to exclude this possibility, since there should be additional

signals due to the pair of equivalent bridging and terminal hydrides.

Another possible intermediate on the same reaction route (6.2a⇌6.2c 6.2e⇌6.2g⇌6.2h) could be the five-coordinate dihydride Rh(III) species 6.8f analogous to 6.2c.

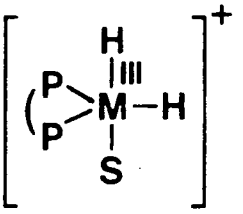

6.8f

The multiplets T_6 and T_7 can be assigned to this species. Thus the axial hydrogen is seen as a triplet of broad doublets T_6 ($^2J_{PH}$ = 28 Hz, $^1J_{RhH}$ = 12 Hz). The equatorial hydrogen has essentially the same but more spread-out pattern (signal T_7) probably because of a greater $^2J_{PH}$.

The principal feature of the temperature-dependent spectra is the collapse of the bridging resonances B_1 and B_2 at the same rate as the terminal resonances T_4 and T_5 without the appearance of any new "average" resonance. This indicates that the fluxional dimeric species 6.8a is stable only in the solid state or in solution at low temperatures. Any fluxional process must be such as the exchange terminal and bridging hydrogen atoms independently. Such a process is set out in Fig. 6.8. The most important feature of the equilibria shown is the requirement for phosphine dissociation (as suggested above for the structure of 6.8e). The exchange process could proceed in a stepwise manner (6.8a⇌6.8b⇌6.8c (or 6.8d)⇌6.8b⇌6.8a) or in

a simultaneous manner (6.8a⇌6.8c⇌6.8d). If the exchange is fast on the NMR time scale the diastereotopic pair of bridging hydrides H_1/H_2 and terminal ones H_3/H_4 become equivalent resulting in the broad signal B and T′ (at -60°C). As mentioned previously, at higher temperatures (> -60°C), the fluxional dimers 6.8a-d presumably dissociate to the monomers 6.8e and 6.8f shown above.

The remaining two temperature-dependent signals T_6 and T_7 are not altered in the temperature range -90° to 0°C, but the averaged signal T at 35°C suggests that the two distinct hydrides in 6.8f become equivalent.

(b) Reaction in Other Solvents

The reaction in CH_3CN resulted in a yellow oil after solvent removal (reaction time ∿ 30 min). The ^1H NMR spectrum (CD_2Cl_2) of this product or the in situ solution (CD_3CN) showed both bridging and terminal hydrides in the range -11 to -27 ppm at -40°C. Changing the solvent to acetone resulted in a different NMR pattern which also showed the presence of hydrides on cooling (≥ -20°C). All the peaks were poorly resolved.

(C) Hydrogenation of $[Rh(BB^tPF)(NBD)]ClO_4$ (XI)

The reaction was carried out in three different solvents, MeOH, CH_3CN, and C_6H_6. Data for the hydrogenation products obtained from each solvent are listed in Table 6.6.

(a) Reaction in MeOH

Deep red crystals deposited on cooling (0°C) the reaction mixture. Fig. 6.9 shows the partial crystal structure of this product which is a

Table 6.6: Hydrogenation products of $[Rh(BB^tPF)(NBD)]ClO_4$(XI); Analyses, NMR, and Others [a].

Reaction medium	Physical property	H_2(mol)	Analysis	^1H NMR(CD_2Cl_2)
MeOH	deep red crystal	3.3	C:49.23 H: 7.36 O: 6.30 Cl: 3.64	(hydride portion at -85°C)[b] B_1(bd, -9.96,J(d)=120,I=2) B_2(bd,-10.77,J(d)=120,I=3) T_1(dtd,-22.38,J(t)=17.2, J(d)=27,J(d)=4) T_2(dt,-25.46,J(d)=32, J(t)=32) T_3(dtd,-27.66,J(t)=16,J(d)= 39.6,J(d)=4) T_4(bm,-26.99,I=2) T_5(bm,-27.08,I=1)
C_6H_6	deep brown crystal	5.1	C:45.71 H: 6.55 O:16.00 Cl: 5.94	5.01(bs) 4.72(bs) 2.08(d,J_{PH}=12)
CH_3CN	yellow oil	-	-	-

[a] H_2(mol) represents the amount of H_2 consumed per mole of the catalyst precursor. Analysis and ^1H NMR data were obtained from the isolated crystalline product. Coupling constants in Hz; bd = broad doublet, m = multiplet, bm = broad multiplet, bs = broad singlet, d = doublet, dt = doublet of triplets, dtd = doublet of triplets of doublets. J(d), J(t) = coupling constant in each pattern. I = relative intensity.

[b] See also Fig. 6.10.

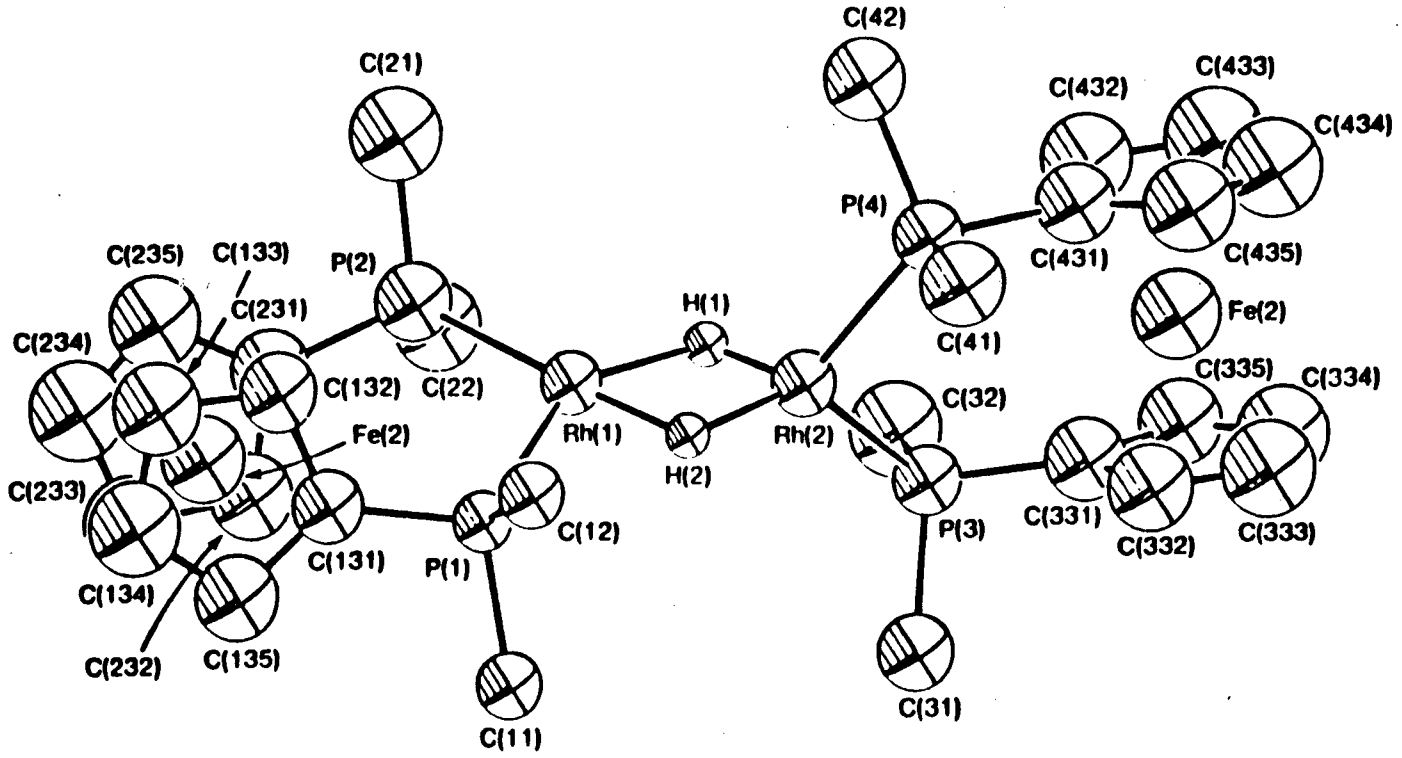

Fig. 6.9: The partial crystal structure of the hydrogenated product of the catalyst precursor XI [142].

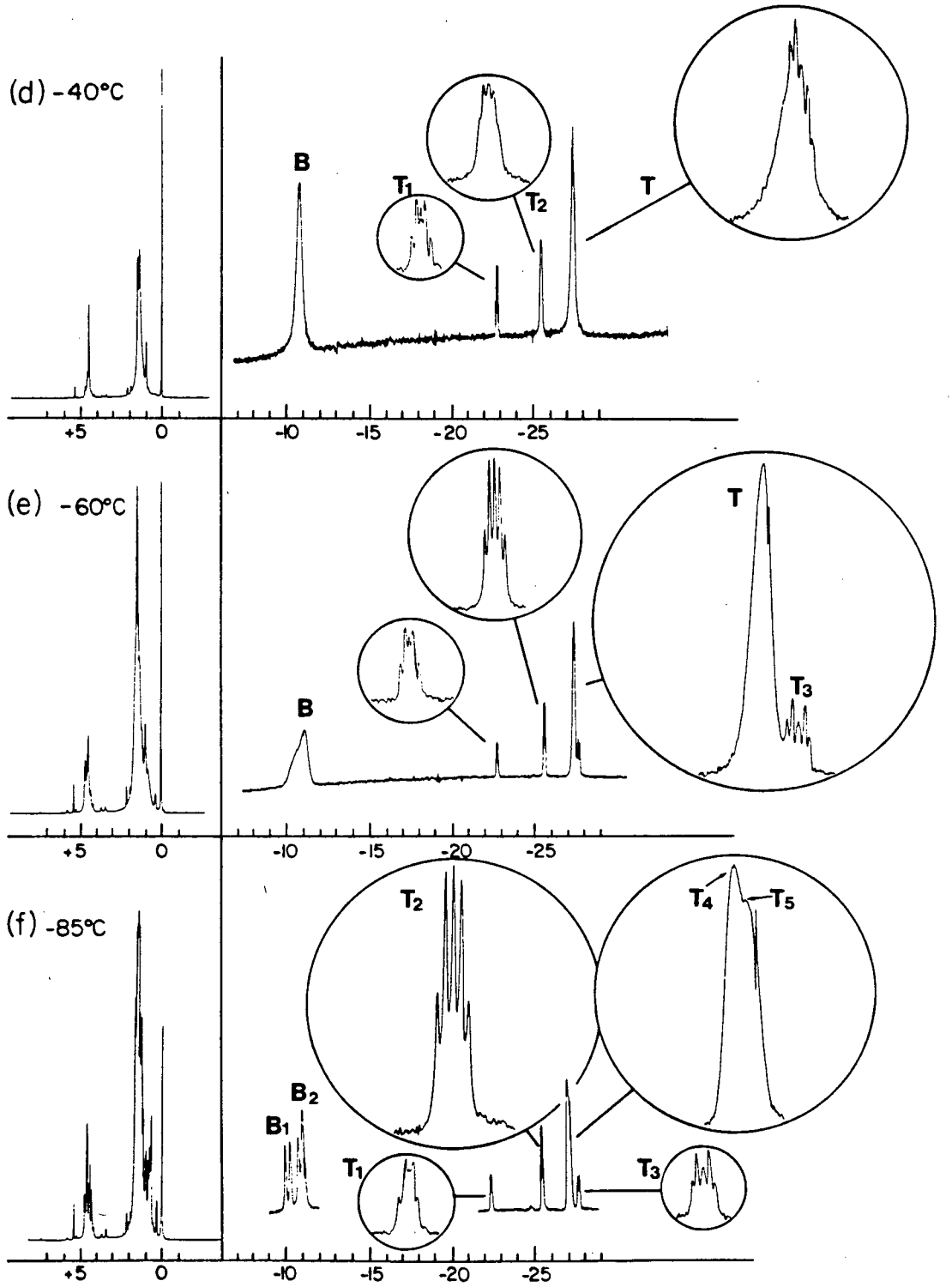

Fig. 6.10(A): Variable temperature 400 Mhz ^{1}H NMR spectrum (CD_2Cl_2) of the hydrogenation product of XI from MeOH.

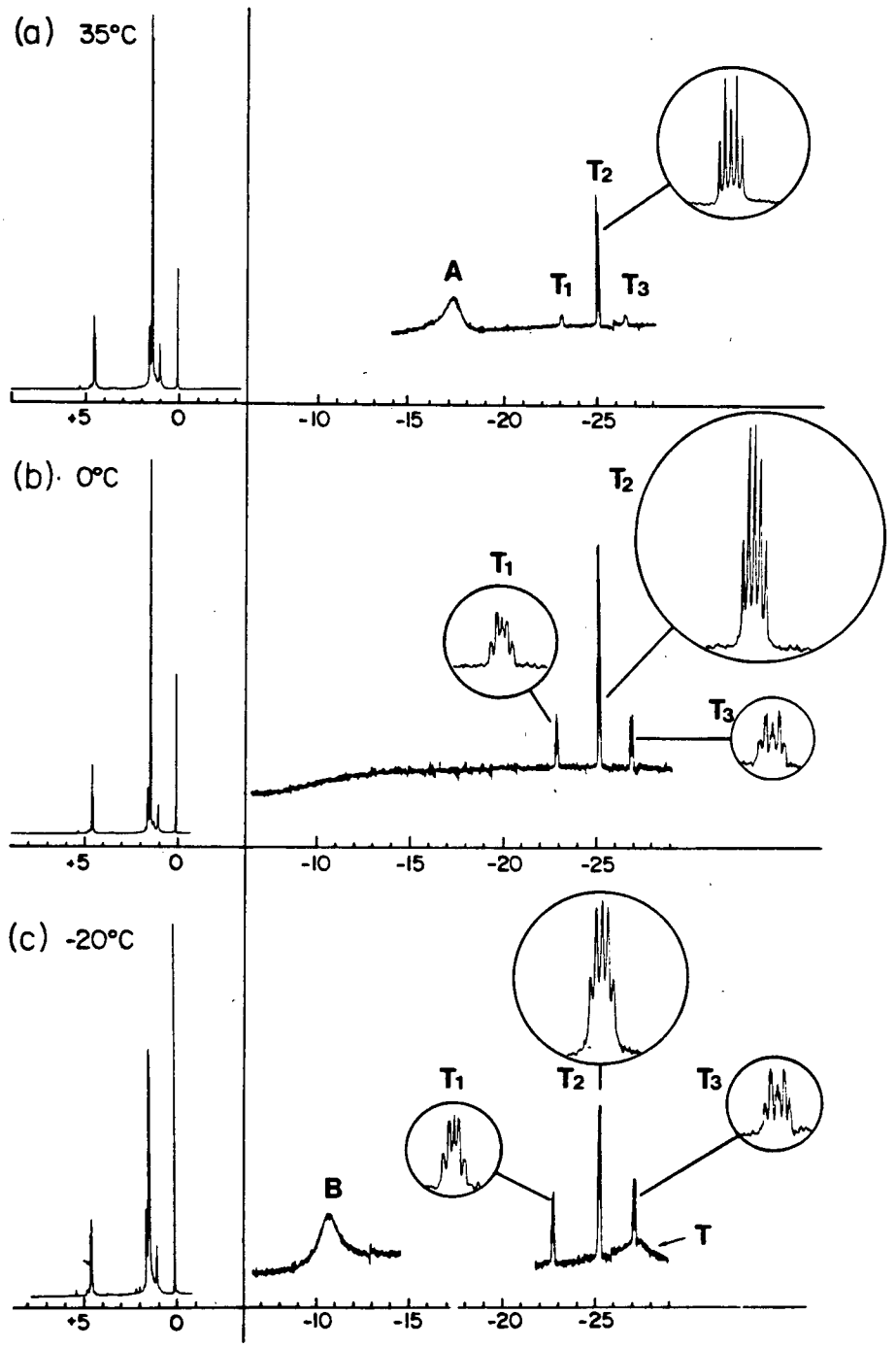

Fig. 6.10(B): Variable temperature 400 MHz ^{1}H NMR spectrum (CD_2Cl_2) of the hydrogenation product of XI from MeOH.

cationic Rh dimer. The +1 charge of the cation was established by the location of one perchlorate anion [142]. The bridging hydride ligands could not be located with any certainty, and the terminal ones were not seen. The structure must be of the type $[(P\text{-}P)_2Rh_2(H)_x]^+ClO_4$ (x = 3 or 5) based on the charge, and the best interpretation based on ligand disposition is a $(\mu\text{-}H)_3$ dimer (x = 5) analogous to that shown in Fig. 6.5. Once again Fig. 6.2 can be used to predict a possible route to this product: 6.2a $\rightleftharpoons$ 6.2b (or 6.2c) $\rightleftharpoons$ 6.2e $\rightleftharpoons$ 6.2g (x=3) $\rightleftharpoons$ 6.2h (x=5).

Further evidence for the presence of hydrido ligands is provided by the ^1H NMR spectrum (CD_2Cl_2) of the crystal, as shown in Fig. 6.10. As summarized in Table 6.6, the hydride NMR pattern at -85°C consists of (i) a set of temperature-independent signals T_1, T_2, and T_3 and (ii) a set of temperature-dependent signals B_1, B_2, T_4, and T_5. On warming the solution to -60°C, both bridging and terminal resonances B_1/B_2 and T_4/T_5 merge to give broad multiplets B($\sim$ -10.6 ppm) and T ($\sim$ -27.5 ppm), respectively. By 0°C both signals B and T have collapsed, and a new averaged signal A appears at -17.23 ppm on further warming to 35°C. The attempted interpretation of all these spectra is as follows.

(I) The Temperature-Independent Signals T_1 - T_3

As indicated in Fig. 6.2, any dimeric Rh(III) species 6.2e could dissociate reversibly to form $[(L\text{-}L)Rh(X)(H)_2]^+$ (6.2c) which in turn could produce $[(L\text{-}L)RhH]^0$ (6.2d). Here the perchlorate (X = ClO_4) is likely to be coordinating because the solvent in this case is CD_2Cl_2. The structures of these two species, where L-L = IV, are shown below.

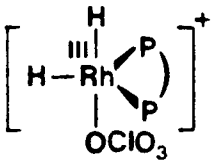

6.11d

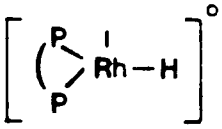

6.11e

The pair of signals T_1 and T_3 can be assigned to the two nonequivalent hydrides in 6.11d. They appear to be a doublet of triplets of doublets with coupling constants as follows: T_1 ($^1J_{RhH}$ = 27 Hz, $^2J_{PH}$ = 17.2 Hz, $^2J_{HH}$ = 4 Hz); T_3 ($^1J_{RhH}$ = 39.6 Hz, $^2J_{PH}$ = 16 Hz, $^2J_{HH}$ = 4 Hz). These coupling constants are not unreasonable as compared with those listed in Appendix. The signal T_2 with five lines can be treated as a doublet of triplets with separation of 32 Hz in both patterns. This signal can be assigned to the Rh(I) monohydride 6.11e.

In connection with the structure 6.11d, it should be mentioned that monitoring the same reacton by ^{31}P NMR in MeOH ($\sim$ 30 min) resulted in a broad doublet (δp 83.3 ppm, $^1J_{RhP}$ = 113.5 Hz). Each signal in the doublet was split into four lines ($^2J_{PH}$ = 10 Hz) when hydride coupling was left in. These observations are consistent with the formation of 6.11d although X could be MeOH or ClO_4 in this case. The anticipated disolvate $[(L\text{-}L)Rh(MeOH)_2]^+$ and the proposed monohydride 6.11e were not observed in this experiment. A number of species were formed on leaving the solution overnight.

(II) Temperature-Dependent NMR Pattern

The temperature-dependent signals (B_1, B_2, T_4, and T_5) can be explained in terms of the Rh(III) dimer 6.11a and its fluxional behavior as proposed in Fig. 6.11 (cf. equation 6.7).

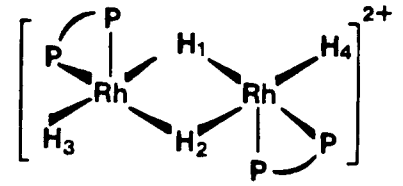

6.11a

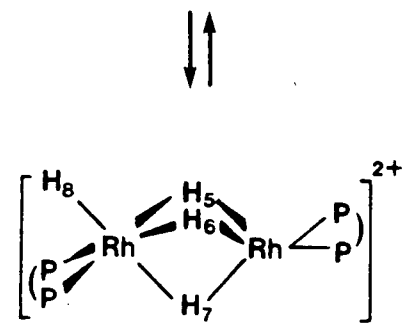

6.11b

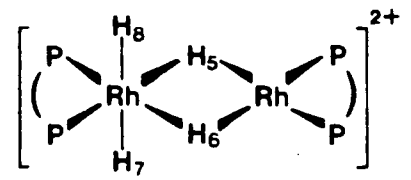

6.11c

Fig. 6.11: The proposed intramolecular exchange processes in the CD_2Cl_2 solution of the hydrogenation product (Fig. 6.9) of XI.

If, at -85°C, only one exchange process (6.11a⇌6.11b) were occurring slowly on the NMR time scale, the hydride NMR spectrum would consist of five distinct signals due to H_1/H_2, H_5/H_6, H_7, H_3/H_4, and H_8. On these bases the broad doublets B_1 and B_2 can be assigned to the pair of equivalent bridging hydrides H_1/H_2 and H_5/H_6, respectively. The resonance for the unique bridging hydride H_7 could be superposed on the higher shielding peak of the doublet B_2 since the signal B_2 is asymmetric (Note $I(B_2)/I(B_1)$ = 3/2 in Table 6.6). All the bridging hydrides except H_7 have a single <u>trans</u> P atom, accounting for the large separation (120 Hz) in both doublets B_1 and B_2. Their chemical shifts and coupling constants are consistent with those previously noted for related bridging hydrides (cf. Appendix). Other couplings, H-H, Rh-H, and <u>cis</u> P-H are too small to be observed. The broad signal T_4 and T_5 can then be assigned to the terminal hydrides H_3/H_4 and H_8, respectively.

On warming the solution (-85° → -60°C), the exchange 6.11a⇌6.11b should become fast to give the averaged signal B and T for the five bridging hydrides and the three terminal ones, respectively. The exchange is still slow enough for the bridging and terminal hydrides to be distinguished in the range -85° to -20°C (cf. Fig. 6.10). At higher temperatures (> -20°C) an exchange process such as 6.11b⇌6.11c (Fig. 6.11) seems operative and all the hydrido ligands become equivalent to give only one signal: signal A.

(b) Reaction in CH_3CN and C_6H_6

Hydrogenation in CH_3CN resulted in a yellow oil after solvent removal. At -95°C, the ^1H NMR spectrum (CD_2Cl_2) of this product exhibited at least

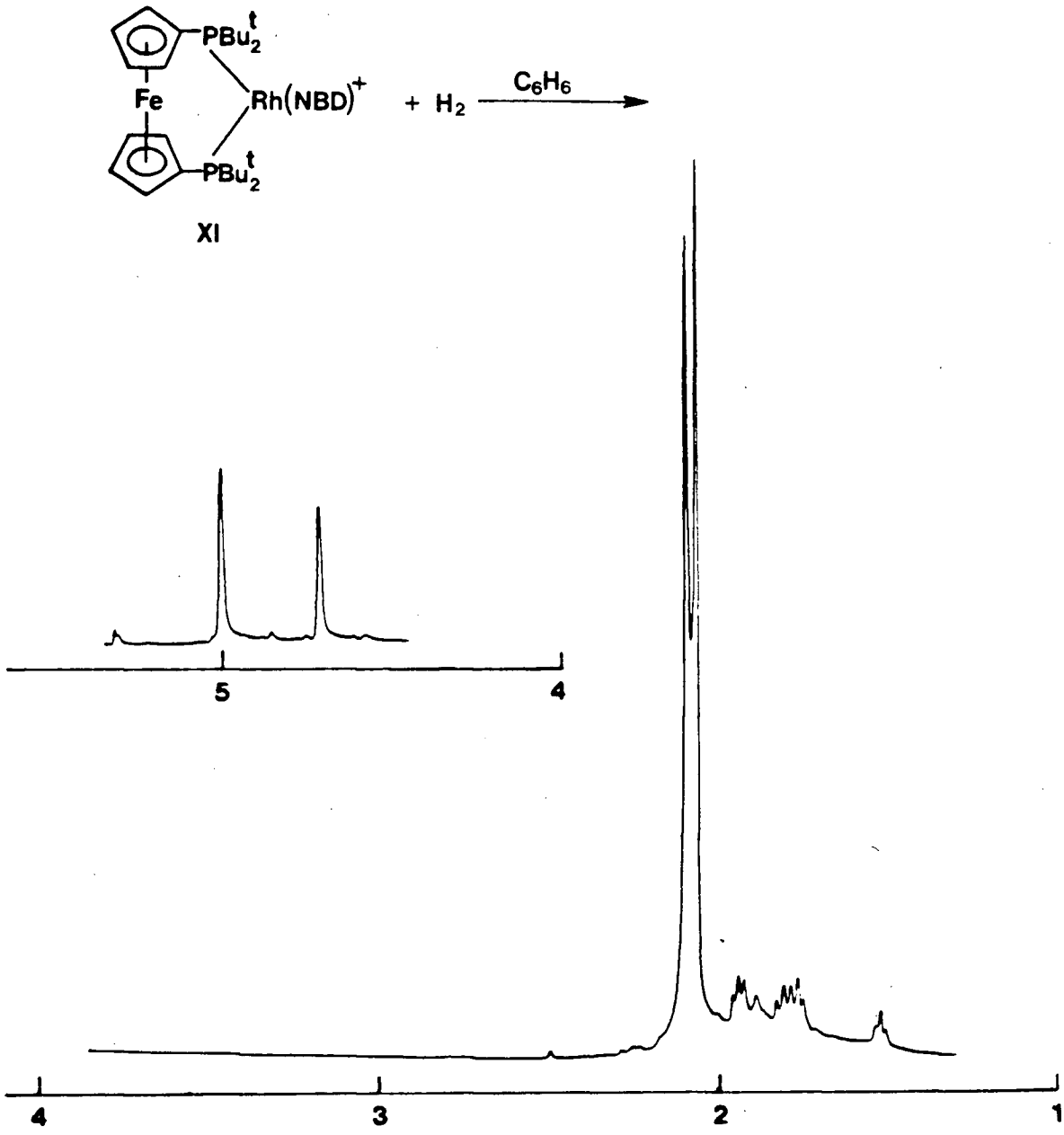

Fig. 6.12: Room temperature 400 MHz ^{1}H NMR spectrum (CD_2Cl_2) of the hydrogenation product of XI from benzene.

13 signals in the range -10 to -22 ppm, some of which are strongly temperature-dependent. All the peaks were poorly resolved.

When a benzene slurry of the catalyst precursor XI was exposed to H_2, the orange solution deposited a dark brown precipitate immediately. The solid was separated by filtration and recrystallized from a CH_2Cl_2/hexane solution to give deep brown crystals. In Fig. 6.12 is shown the room temperature ^1H NMR spectrum of this product. The spectrum is highly symmetric and very simple. No hydride resonance was observed on cooling to -90°C. On the basis of the reaction described in equation (6.8) the product could be a η^6-arene complex. However the ^1H NMR and analytical results (Table 6.6) are not consistent with this. A crystal structure determination is in progress [145].

(D) Hydrogenation of (R,R)-XIV

Reaction in MeOH resulted in the uptake of 2.5 equivalents of H_2 and a reddish brown solid after solvent removal. In Fig. 6.13 is shown the room temperature ^1H NMR spectrum of this product. The hydride NMR pattern consists of a pair of triplets of triplets centered at -8.98 and -8.50 ppm of intensity ratio 6 to 1. Couplings in signals are 60.4 and 17.6 Hz. These observations suggest that the product could be of the type $[(L\text{-}L)RhH]_2^o$. A possible route to this product can be deduced from Fig. 6.2: 6.2a$\rightleftharpoons$6.2b (or 6.2c)$\rightleftharpoons$6.2d$\rightleftharpoons$6.2f. The NMR spectrum further suggests that the following two geometrical isomers are slowly exchanging, each isomer undergoing a rapid intramolecular site-exchange (equation 6.9).

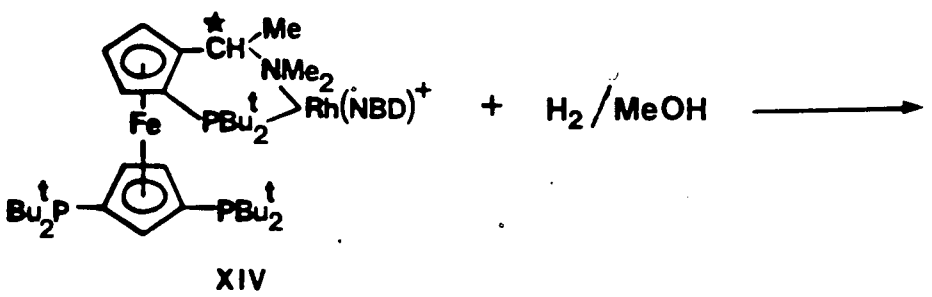

XIV

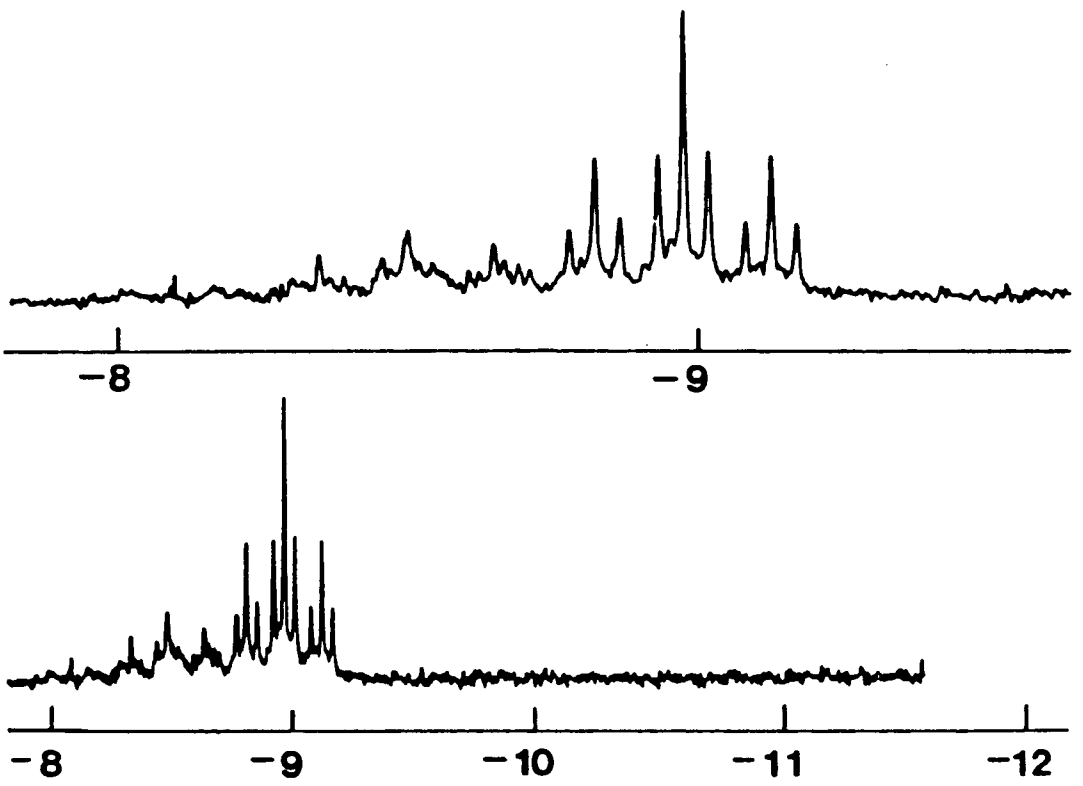

Fig. 6.13: Room temperature ^1H NMR (400 MHz) spectrum (CD_2Cl_2) of the hydrogenation product of (R,R)-XIV from MeOH. Only hydride portion is shown.

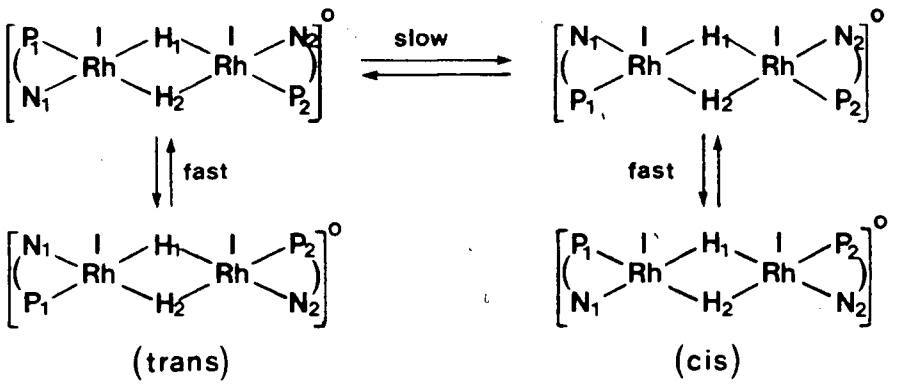

(6.9)

The pair of equivalent hydrides in the trans isomer would show a triplet of triplets from the result of the fast intramolecular process. The pair of diastereotopic hydrides in the cis isomer become equivalent through this process and result in the same NMR pattern. The trans isomer is expected to be more stable than the cis isomer because the cis isomer has one bridging hydride trans to both P atoms. Thus the sharp set is reasonably assigned to the trans isomer, and the weaker set to the cis isomer. The larger coupling (60.4 Hz) is probably due to $^{2}J_{PH}$, and the smaller one (17.6 Hz) to $^{1}J_{RhH}$, or vice versa.

6.3.3 Summary

It has been shown in this section that hydrogenation of VIII - XIV results in the formation of metal hydrides in various solvents such as MeOH,

CH_3CN, and $CHCl_3$. In many cases they can be isolated as crystalline solids, and their identity as $[(L\text{-}L)HRh(H)_3Rh(H)(L\text{-}L)]^+ClO_4$ has been established in two cases. The solid products not only show fluxional behaviors but also seem to produce reversibly other hydride species in solution. In other cases, NMR (^1H, ^{31}P) monitoring of reaction solution also reveals that more than one hydride species is produced in a given reaction.

CHAPTER 7

GENERAL CONCLUSION AND SUGGESTIONS FOR FUTURE STUDIES

7.1 FERROCENYLPHOSPHINE LIGANDS

The preparation and the properties of a wide range of ferrocenylphosphines have been described. Special emphasis has been placed on the synthesis of ligands containing bulky tert-butyl groups on the phosphorus atoms. One of the most intriguing findings relating to the synthesis of these ligands is that the chiral ligand precursor FA can undergo trilithiation leading to the isolation of the unexpected chiral trisphosphine ligand VII. This reaction is unprecedented, and it would be desirable to investigate its generality by attempting to prepare other alkyl- and arylphosphine derivatives. Furthermore, since the absolute configuration of the product (VII) was not that anticipated, this aspect needs to be further studied.

7.2 RHODIUM COMPLEXES OF FERROCENYLPHOSPHINES AS HYDROGENATION CATALYSTS

Cationic Rh(I) complexes of the ferrocenylphosphines are very effective catalyst precursors for hydrogenation of a wide range of olefinic substrates. In particular, greater reaction rates are obtained with tert-butylphosphine complexes than with phenylphosphine derivatives. Most significantly, the chiral trisphosphine complex XIV gives very high optical yields in hydrogenation of amino acid precursors. The results are comparable with those obtained with the best of other catalysts containing chelating di(tertiary arylphosphines). It is also a very effective catalyst for the reduction of (E)-α-

methylcinnamic acid, giving one of the highest optical yields ever reported. These results demonstrate that high optical yields can be achieved in the absence of the supposedly necessary aryl groups.

In striking contrast, the bisphosphine complex XIII is a poor catalyst precursor for asymmetric hydrogenation of the substrates so far investigated. Their different behaviors seem to be related to conformational effects since the complex XIII exists in solution as a mixture of two diastereomeric conformers, while the complex XIV exists as a single conformer. In this regard, it would be desirable to carry out comparative hydrogenation studies under various reaction conditions in order to investigate further the conformational effects. For example it has been shown that change of solvent results in reversal of the absolute configuration of products. Temperature should also be an important factor since the conformational interconversion has shown to be temperature-dependent. The chiral complexes XII - XIV could also be investigated for the hydrogenation of other functional groups such as C=O, C=N, etc., since some Rh(I) complexes derived from alkylphosphines have been reported to be more effective for the reduction of carbonyl group than their arylphosphine analogues.

7.3 KINETIC AND MECHANISTIC STUDIES OF HYDROGENATION

The most significant finding of this work is that the hydrogenation of the catalyst precursors VIII - XIV leads to the formation of metal hydrides in various solvents such as alcohol, CH_3CN, $CHCl_3$, etc. NMR (^1H, ^{31}P) monitoring suggests that various hydride species are formed reversibly in any

one reaction. Interestingly, the anticipated disolvate $[(L\text{-}L)Rh(S)_2]^+$ was not observed when S is MeOH or EtOH. In many cases hydrides can be isolated as crystalline solids which show fluxional behaviors in solution.

This unique behavior of the present catalyst systems (VIII - XIV) may be due to the presence of the bulky tert-butyl derivatives. However, this aspect needs further studies. It also seems inappropriate to make any dogmatic statement concerning the mechanism(s) of catalytic hydrogenation of olefins because hydrides are formed and could be involved in the initial steps. In this regard it is highly recommended that their catalytic properties be further investigated by carrying out careful kinetic and mechanistic studies of hydrogenation. These studies should include asymmetric hydrogenation in order to further investigate the electronic and steric effects of the chiral catalyst precursors on enantioface-discrimination. Other alkylphosphines containing $-PMe_2$ and $-P(iPr)_2$ could also be employed in these studies.

7.4 OTHER METAL COMPLEXES OF FERROCENYLPHOSPHINES

Palladium and nickel complexes of the type $M(L\text{-}L)X_2$ are known to be effective catalyst precursors for cross coupling and hydrosilation as well as hydrogenation. These reactions should be further investigated using the complexes described in chapter 5.

REFERENCES

1. M. Calvin, Trans. Faradays Soc., 34, 1181(1938)
2. M. Iguchi, J. Chem. Soc. Jpn., 63, 634, 1752(1942)
3. J. Kwiatek and J.K. Seyler, Advances in Chemistry, 70, American Chemical Society, Washington, D.C. 1968, p. 207.
4. I. Wender and H. Sternberg, Adv. Catalysis, 9, 594(1957)
5. M. Orchin, ibid, 5, 385(1953)
6. G.H. Flynn and H.M. Hulbert, J. Am. Chem. Soc., 76, 3393(1954)
7. J. Halpern, J.F. Harrod, and B.R. James, J. Am. Chem. Soc., 83, 753(1961)
8. J. Halpern, Abstracts, 141st Meeting of the American Chemical Society, Washington, D.C., 1962, p. 10Q.
9. J. Halpern and B.R. James, Abstracts, 142nd Meeting of the American Chemical Society, Atlantic City, 1962, p. 23N.
10. R.D. Cramer, E.L. Jenner, R.V. Lindsey Jr., and U.G. Stolberg, J. Am. Chem. Soc., 85, 1691(1963)
11. L. Vaska and J.W. Diluzio, J. Am. Chem. Soc., 84, 679(1962)

12a. F.H. Jardin, J.A. Osborn, G. Wilkinson, and J.F. Young, Chem. Ind., 1965, 560

b. Idem, Chem. Comm., 1965, 131

13. D. Evans, J.A. Osborn, F.H. Jardin, and G. Wilkinson, Nature, 208, 1203(1965)
14. J. Kwiatek, "Hydrogenation and Dehydrogenation", in G.N. Schrauzer, ed., Transition Metals in Homogeneous Catalysis, Marcel Dekker, Inc., New York, 1971, p. 13.

15. W. Strohmeier, Fortsch. Chem. Forsch., 25, 71(1972)

16. B.R. James, "Homogeneous Hydrogenation", Wiley, New York, 1973.

17. R.E. Harmon, S.K. Gupta, and D.J. Brown, Chem. Rev., 73, 1(1973)

18. G. Dolcetti and N.W. Hoffman, Inorg. Chim. Acta , 9, 269(1974)

19. S.S. Jewur, J. Rajaram, and J.C. Kuriacose, J. Sci. Ind. Res., 33, 651(1974)

20. A.J. Birch and D.H. Williamson, Organic Reactions, 24, 1(1976)

21. F.K. McQuillin, "Homogeneous Hydrogenation in Organic Chemistry", Reidel Publ., Dordrecht, Netherlands, 1976.

22. A.P.G. Kieboom and F. van Rantwijk, "Hydrogenation and Hydrogenolysis in Synthetic Organic Chemistry", Delft. Univ. Press, Delft, 1977.

23. G. Webb, Catalysis, 2, 145(1978)

24. B.R. James, Adv. Organometal. Chem., 17, 319(1979)

25. J.P. Collman and L.S. Hegedus, "Principles and Application of Organotransition Metal Chemistry", University Science Books, Mill Valley, CA. 1980.

26. G.W. Parshall, "Homogeneous Catalysis", Wiley, New York, 1980.

27. C. Master, "Homogeneous Transition-Metal Catalysis", Chapman and Hall Ltd., London, 1981.

28. F. Moranini and S. Bresadola, Inorg. Chem., 15, 650(1976)

29. J.P. Jesson, in Transition Metal Hydrides, ed., E.L. Muetterties, Marcel Dekker, 1971, p. 84.

30. J.F. Harrod, G. Hamer, and W. Yorke, J. Am. Chem. Soc., 101, 3987(1979)

31. P.S. Hallman, B.R. McGarvey, and G. Wilkinson, J. Chem. Soc., A, 3143(1968)

32a. J.R. Shapley, R.R. Schrock, and J.A. Osborn, J. Am. Chem. Soc., 91, 2816(1969)

b. R.R. Schrock and J.A. Osborn, Chem. Comm., 567(1970)

c. Idem, Inorg. Chem., 9, 2339(1970)

d. Idem, J. Am. Chem. Soc., 93, 2397(1971)

e. Idem, ibid, 98, 2135, 2143, 4450(1976).

33. H. Wender and R. Feser, Angew. Chem. Int. Ed. Engl., 18, 157(1979)

34. J. Halpern, J. Harrod, and B.R. James, J. Am. Chem. Soc., 88, 5150(1966)

35. J. Halpern and B.R. James, Can. J. Chem., 44, 495(1966)

36. G. Longato and S. Bresadola, Inorg. Chem., 21, 168(1982)

37. J. Halpern, Acc. Chem. Res., 15, 332(1982)

38. G. Wilkinson, Bull. Soc. Chim. Fr., 35, 3055(1968)

39. C. O'Conner and G. Wilkinson, J. Chem. Soc(A), 2665(1968)

40. M. Yagupsky and G. Wilkinson, ibid, 941(1970)

41. J. Trocha-Grimshaw and H.B. Henbest, Chem. Comm., 757(1968)

42. J.A. Osborn, F.H. Jardine, J.F. Young, and G. Wilkinson, J. Chem. Soc. (A), 1711(1966)

43a. J. Halpern, Trans. Am. Crystallogr. Assoc., 14, 59(1978)

b. J. Halpern, T. Okamoto, and A. Zakhariev, J. Mol. Cat., 2, 65(1976)

44. P. Meakin, J.P. Jesson, and C.A. Tolman, J. Am. Chem. Soc., 94, 3240 (1972)

45. C.A. Tolman, P. Meakin, D.L. Lindner, and J.P. Jesson, J. Am. Chem. Soc., 96, 2762(1974)

46a. J. Halpern, D.P. Riley, A.S.C. Chan, and J.J. Pluth, J. Am. Chem. Soc., 99, 8055(1977)

b. A.S.C. Chan, J.J. Pluth, and J. Halpern, Inorg. Chim. Acta, L477(1979)

c. A.S.C. Chan, J. Jalpern, J. Am. Chem. Soc., 102, 838(1980)

47a. J.M. Brown and P.A. Chaloner, J. Chem. Soc., Chem. Commun., 321(1978)

b. Idem, 646(1978)

c. Idem, Tetrahedron Lett., 21, 1877(1978)

d. J.M. Brown, P.A. Chaloner, A.G. Kent, B.A. Murrer, P.M. Nicholson, D.P. Parker, and P.J. Sidebottom, J. Organometal. Chem., 216, 263(1981)

e. J.M. Brown and D.P. Parker, J. Chem. Soc., Chem. Commun., 342(1980)

f. J.M. Brown, P.A. Chaloner, R. Glasser, and S. Geresh, Tetrahedron, 36, 815(1980)

g. J.M. Brown and P.A. Chaloner, J. Am. Chem. Soc., 102, 3040(1980)

h. J.M. Brown and D. Parker, Organometallics, 1, 950(1982)

48. O.A. Slack, I. Greveling, and M.C. Baird, Inorg. Chem., 18, 3125(1979)

49. J. Mathieu and J. Weil-Raynal, Bull. Soc. Chim. Fr., 1211(1968)

50. D.R. Boyd and M.A. Mckervey, Q. Rev., 22, 95(1968)

51. T.D. Inch, Synthesis, 466(1970)

52. H.J. Schneider and R. Haller, Pharmazie, 28, 417(1973)

53. J.W. Scott and D. Valentine, Jr., Science, 184, 943(1974)

54. J.D. Morrison and H.S. Mosher, "Asymmetric Organic Reaction", Prentice-Hall, Englewoods Cliff, N.J., 1971; Paperbook reprint, American Chemical Society, Washington, D.C. 1976.

55. Y. Izumi and A. Tai, "Stereo-Differentiating Reactions", Kodansha Scientific Books, Tokyo, Japan, 1977.

56. J.D. Morrison, W.F. Masler, and M.K. Neuberg, Adv. Catalysis, 25, 81(1976)

57. P. Pino and G. Consiglio, "Asymmetric Homogeneous Catalysis by Chiral Transition Metal Complexes", in M. Tsutsui and R. Ugo, ed., Fundamental Research in Homogeneous Catalysis, Plenum, New York, 1977, p. 147.

58. D. Valentine and J.W. Scott, Synthesis, 329(1978)

59. H.B. Kagan and J.C. Fiaud, Top. Stereochem., 10, 175(1978)

60. H.B. Kagan, Ann. N.Y. Acad. Sci., 333, 1(1980)

61. B. Bosnich and M.D. Fryzuk, Top. Stereochem., 12, 119(1981)

62. V. Caplar, G. Commisso, V. Sunjic, Synthesis, 85(1981)

63. W.S. Knowles, Acc. Chem. Res., 16, 106(1983)

64. J. Halpern, Science, 217, 401(1982)

65a. R.S. Cahn and C.K. Ingold, J. Chem. Soc., 612(1951)

b. R.S. Cahn, C.K. Ingold, and V. Prelog, Experientia, 12, 81(1956)

c. Idem, Angew. Chem. Int. Ed. Engl., 5, 385(1966)

d. R.S. Cahn, J. Chem. Educ., 41, 116(1964)

66. K.R. Hanson, J. Am. Chem. Soc., 88, 2731(1966)

67a. K. Mislow, "Introduction to Stereochemistry", Benjamin, New York, 1965.

b. K. Mislow and M. Raban, Top. Stereochem., 1, 1(1967)

c. K. Mislow and P. Bickart, Isr. J. Chem., 15, 1(1976/77)

68. E. Ruch and I. Ugi, Top. Stereochem., 4, 99(1969)

69. M.D. Fryzuk, Ph.D. thesis, University of Toronto, 1978.

70. E. Fisher, Ber., 23, 2611(1890)

71. W. Marckwald, Ber., 37, 1368(1904)

72. A.S.C. Chan, J.J. Pluth, J. Halpern, J. Am. Chem. Soc., 18, 5952(1980)

73. P.S. Chua, N.K. Robert, B. Bosnich, S.J. Okrasinski, and J. Halpern, J. Chem. Soc. Chem. Commun., 1278(1981)

74. J.M. Brown, P.A. Chaloner, and D. Parker, Advances in Chemistry, 196, 355(1982)

75. E.L. Eliel, "Stereochemistry of Carbon Compounds", McGraw-Hill, New York, 1962, chapter 8.

76a. M.D. Fryzuk and B. Bosnich, J. Am. Chem. Soc., 99, 6262(1977)

b. Idem, ibid, 100, 5491(1978)

c. P.A. MacNiel, N.K. Roberts, B. Bosnich, J. Am. Chem. Soc., 103, 2273 (1981)

d. B. Bosnich and N.K. Roberts, Advances in Chemistry, 196, 337(1982)

77a. W.S. Knowles, B.D. Vineyard, M.J. Sabacky, and B.R. Stults, "Use of x-ray crystal structure in the study of asymmetric catalysis", in M. Tsutsui ed., Fundamental Research in Homogeneous Catalysis, Plenum Press, New York, 1979, p. 537.

b. K.E. Koenig, M.J. Sabacky, G.L. Bachman, W.C. Christopfel, H.D. Barnstorff, R.B. Friedman, W.S. Knowles, B.R. Stults, B.D. Vineyard, and D.J. Weinkauff, Ann. N.Y. Acad. Sci., 333, 16(1980)

78. B.D. Vineyard, W.S. Knowles, M.J. Sabcky, G.L. Bachman, and D.J. Weinkauff, J. Am. Chem. Soc., 99, 5946(1977)

79a. I. Ojima, T. Kogure, and N. Yoda, Chem. Lett., 1979, 495(1975)

b. Idem, J. Org. Chem., 45, 4728(1980)

c. D. Sinou, Tetrahedron Lett., 22, 2987(1981)

80a. O. Korpium, R.A. Lewis, J. Chickos, and K. Mislow, J. Am. Chem. Soc., 90, 4842(1968)

b. K. Naumann, G. Zon, and K. Mislow, J. Am. Chem. Soc., 91, 8012(1969)

c. W.B. Farnham, R.K. Murray, and K. Mislow, J. Am. Chem. Soc., 92, 5809 (1970)

81. L. Horner, H. Buthe, and H. Siegel, Tetrahedron Lett., 4023(1968)

82. W.S. Knowles and M.J. Sabacky, J. Chem. Soc. Chem. Commun., 1445(1968)

83. L. Horner, H. Siegel, and H. Buthe, Angew. Chem. Int. Ed. Engl., 7, 942(1968)

84a. W.S. Knowles, M.J. Sabacky, and B.D. Vineyard, J. Chem. Soc. Chem. Commun., 10(1972)

b. Idem, Chem. Eng. News, 50(6), 4(1972)

c. Idem, Ann. N.Y. Acad. Sci., 214, 119(1973)

d. Idem, Chem. Tech., 591(1972)

e. Idem, J. Am. Chem. Soc., 97, 2567(1975)

85a. B.D. Vineyard, W.S. Knowles, M.J. Sabacky, G.K. Bachman, and D.J. Weinkauff, J. Am. Chem. Soc., 99, 5946(1977)

b. W.S. Knowles, M.J. Sabacky, B.D. Vineyard, and D.K. Weinkauff, ibid, 97, 2567(1975)

86. U.S. Patent 4008281(1975), Monsanto; C.A. 83, 164367(1975)

87. J.D. Morrison, R.E. Burnett, A.M. Aguiar, C.J. Morrow, and C.J. Phillips, J. Am. Chem. Soc., 93, 1301(1971)

88a. T.-P. Dang and H.B. Kagan, J. Chem. Soc. Chem. Commun., 481(1971)

b. Idem, J. Am. Chem. Soc., 94, 6429(1972)

89. T.-P. Dang, J.-C. Poulin, and H.B. Kagan, J. Organometal. Chem., 91, 105(1975)

90a. K. Achiwa, J. Am. Chem. Soc., 98, 8266(1976)

b. Idem, Tetrahedron. Lett., 3735(1977)

c. Idem, Chem. Lett., 777(1977)

d. K. Achiwa, T. Kogure, and I. Ojima, Tetrahedron Lett., 4431(1977)

91. W.R. Cullen and Y. Sugi, Tetrahedron Lett., 1635(1978)

92. C. Fisher and H.S. Mosher, Tetrahedron Lett., 2487(1977)

93a. K. Tamao, H. Yamamoto, H. Matsumoto, N. Miyake, H. Hayaski, and M. Kumada, Tetrahedron Lett., 1389(1977)

b. R.H. Grubbs and R.A. de Vries, Tetrahedron Lett., 1879(1977)

94. T. Hayashi, T. Mise, S. Mitachim, K. Yamamoto, and M. Kumada, Tetrahedron Lett., 1133(1976)

95. T.J. Kealy and P.L. Pauson, Nature, 168, 1039(1951)

96a. M. Rosenblum, "Chemistry of Iron Group Matallocenes", John Wiley, New York, 1965.

b. K. Schlögl and H. Falk, Method. Chim., 8, 469(1976)

c. W.R. Cullen and J.D. Woollins, Coord. Chem. Rev., 39, 1(1981)

97. J.J. Bishop, A. Davison, M.L. Katcher, D.W. Lichtenberg, R.E. Merrill, and J.C. Smart, J. Organometal. Chem., 27, 241(1971)

98a. K. Schlögl and M. Fries, Monatsh. Chem., 95, 558(1964)

b. H. Falk, Ch. Krasa, and K. Schlögl, ibid, 100, 254(1969)

c. D. Marquarding, P. Hoffman, H. Heitzer, and I. Ugi, J. Am. Chem. Soc., 92, 1969(1970)

99. K. Schlögl, Top. Stereochem., 1, 39(1967)

100a. D. Marquarding, H. Klusacek, G. Gokel, P. Hoffman, and I. Ugi, J. Am. Chem. Soc., 92, 5389(1970)

b. G. Gokel and I. Ugi, J. Chem. Educ., 49. 294(1972)

101a. T. Hayashi and M. Kumada, Acc. Chem. Res., 15, 395(1982)

b. M, Kumada, T. Hayashi, and K. Tamao, "Fundamental Research in Homogeneous Catalysis", M. Tsutsui ed., Plenum Press, New York, 1982, P.175.

102a. W.R. Cullen and E.-S. Yeh, J. Organometal. Chem., 139, C13(1977)

b. W.R. Cullen, F.W.B. Einstein, C.-H. Huang, A.C. Willis, and E.-S. Yeh, J. Am. Chem. Soc., 102, 988(1980)

c. W.R. Cullen and D.J. Woollins, Can. J. Chem., 60, 1793(1982)

d. W.R. Cullen, T.-J. Kim, F.W.B. Einstein, and T. Jones, Organometallics, 2, 714(1983)

103. W.R. Cullen and T.-J. Kim, unpublished results

104a. K. Yamamoto, J. Wakatsuki, and R. Sugimoto, Bull. Chem. Soc. Jpn., 53, 1132(1980)

b. T. Hayashi, T. Mise, M. Hukushima, M. Kagotani, N. Nagashima, Y. Hamada, A. Matsumoto, S. Kawakami, M. Konishi, K. Yamamoto, and M. Kumada, Bull. Chem. Soc. Jpn., 53, 1138(1980)

105a. T. Hayashi, T. Mise, and M. Kumada, Tetrahedron Lett., 4351(1976)

b. T. Hayashi, A. Katsumura, and M. Kumada, ibid, 425(1979)

c. T. Hayashi, K. Kanchira, and M. Kumada, ibid, 22, 4417(1981)

106. C. Pradat, J.G. Riess, D. Bonoux, B.F. Mentzen, I. Tkatchenke, and D. Houalla, J. Am. Chem. Soc., 103, 2234(1979)

107a. M.D. Fryzuk and P.A. MacNeil, J. Am. Chem. Soc., 103, 3592(1981)

b. G.E. Rodgers, W.R. Cullen, and B.R. James, Can. J. Chem., 61, 1314 (1983)

108. T. Hayashi, K. Tamao, Y. Katsuro, and M. Kumada, Tetrahedron Lett., 21, 1871(1980)

109. T. Hayashi, K. Yamamoto, and M. Kumada, Tetrahedron Lett., 4405 (1974)

110. M. Kumada, Pure & Appl. Chem., 52, 669(1980)

111a. F. Knoop and J.G. Planco, Z. Phys. Chem., 146, 272(1925)

b. S.M. Birbaum, L. Levintow, R.B. Kingsley, and J.P. Greenstein, J. Biol. Chem., 194, 455(1952)

c. J.P. Bakhshi and E. Turner, J. Chem. Soc., 171(1961)

d. R. Rossi and P. Diversi, Gazz. Chim. Ital., 98, 1391(1968)

112, M. Fild, O. Stelzer, and R. Schmutzler, Inorganic Syntheses, XIV, 4(1973)

113. J.R. Corfield, N.J. Death, and S. Trippett, J. Chem. Soc. (C), 1930(1971)

114a. A.G. Osborn, R.H. Whiteley, and R.E. Meads, J. Organometal. Chem., 193, 345(1980)

b. D. Seyferth and H.P. Withers, Organometallics, 1, 1275(1982)

c. H.P. Withers, D. Seyferth, J.D. Fellmann, P.E. Garrou, and S. Martin, Organometallics, 1, 1283(1982)

115. C.R. Hauser and J.K. Lindsay, J. Org. Chem., 22, 906(1957)

116. E.W. Abel, M.A. Bennett, and G. Wilkinson, J. Chem. Soc., 3178(1959)

117. F.R. Hartley, Organometal. Chem. Rev. A., 6, 119(1970)

118. A.W. Rudie, D.W. Lichtenberg, M.L. Katcher, and A. Davison, Inorg. Chem., 17, 2859(1978)

119. M. Walczak, K. Walczak, R. Mink, M.D. Rausch, and G. Stucky, J. Am. Chem. Soc., 100, 6382(1978)

120. I.R. Butler and W.R. Cullen, Can. J. Chem., 61, 2354(1983)

121. I.R. Butler, W.R. Cullen, F.W.B. Einstein, S.J. Rettig, and A.C. Willis, Organometallics, 2, 128(1983)

122. W.R. Cullen, T.-J. Kim, J. Trotter, S. Evans, and T.G. Appleton, J. Organometal. Chem., submitted for publication

123. W.R. Cullen, T.-J. Kim, F.W.B. Einstein, and T. Jones, Organometallics, submitted for publication

124. E.L. Eliel, "Elements of Stereochemistry", Wiley, New York, 1969, chapter IV.

125. T. Hayashi, M. Konishi, Y. Kobori, M. Kumada, T. Higuchi, and K. Hirotsu, J. Am. Chem. Soc., 106, 158(1984)

126. I.R. Butler, W.R. Cullen, T.-J. Kim, and S.J. Rettig, Organometallics. submitted for publication

127. L.M. Venanzi, J. Chem. Soc., 719(1958)

128a. G.R. van Hecke and W.D. Horrocks, Inorg. Chem., 5, 1968(1966)

b. G. Booth and J. Chatt, J. Chem. Soc., 3238(1965)

129. W.R. Cullen, D.A. Harbourne, B.V. Liengme, and J.R. Sams, Inorg. Chem., 8, 1464(1969)

130a. A. Davison and J.C. Smart, J. Organometal. Chem., 174, 321(1979)

b. E.W. Abel, M. Booth, and K.G. Orrell, J. Organometal. Chem., 208, 213(1981)

c. E.W. Abel, M. Booth, C.A. Brown, K.G. Orrell, and R.L. Woodford, ibid, 214, 93(1981)

131. Reference 25, chapter 6.

132a. K. Tani, K. Suwa, E. Tanigawa, T. Yoshida, T. Okano, and S. Otsuka, Chem. Lett., 261(1982)

b. K. Tani, K. Suwa, T. Yamagata, and S. Otsuka, ibid, 265(1982)

133. B.R. James and R.S. McMillan, Can. J. Chem., 55, 3927(1977)

134. K.C. Dewhirst, W. Keim, and C.A. Reiley, Inorg. Chem., 7, 546(1968)

135. C.R. Landis and J. Halpern, J. Organometal. Chem., 250, 485(1983)

136. J.M. Brown, L.R. Canning, A.J. Downs, and A.M. Forster, J. Organometal. Chem., 255, 103(1983)

137a. T. Yoshida, T. Okano, and S. Otsuka, J. Chem. Soc. Chem. Commun., 855(1978)

b. T. Yoshida, T. Okano, D.L. Thorn, T.H. Tulip, S. Otsuka, and J.A. Ibers, J. Organometal. Chem., 181, 183(1979)

138a. M.D. Fryzuk, Can. J. Chem., 61, 1347(1983)

b. Idem, Organometallics, 1, 408(1982)

139a. V.W. Day, M.F. Fredrich, G.S. Reddy, A.J. Sivak, W.R. Pretzer, and E.L. Muetterties, J. Am. Chem. Soc., 99, 8091(1977)

b. A.J. Sivak and E.L. Muetterties, ibid, 101, 4878(1979)

c. E.B. Meier, R.R. Burch, E.L. Muetterties, and V.W. Day, ibid, 104, 2661(1982)

139d. R.R. Burch, A.J. Shusterman, E.L. Muetterties, R.G. Teller, and J.M. Williams, ibid, 105, 3546(1983)

140. J.M. Townsend and J.F. Blount, Inorg. Chem., 20, 269(1981)

141. L. Hichuk, personal communication

142. I.R. Butler, W.R. Cullen, T.-J. Kim, F.W.B. Einstein, and T. Jones, J. Chem. Soc. Chem. Commun., submitted for publication

143. H.H. Wang and L.H. Pignolet, Inorg. Chem., 19, 1470(1980)

144a. R.H. Crabtree, H. Felkin, G. Morris, T.J. King, and J.A. Richards, J. Organometal. Chem., 113, C7(1976)

b. R.H. Crabtree, Acc. Chem. Res., 12, 331(1979)

145. F.W.B. Einstein and T. Jones, personal communication

APPENDIX

TABLE OF SELECTED NMR (^{1}H, ^{31}P) DATA FOR SOME RHODIUM AND IRIDIUM COMPLEXES [a].

Complex Type	^{1}H(hydride portion)			$^{31}P\{^{1}H\}$			Ref.
	δH	J_{RhH}	J_{PH}	δP	J_{RhP}	J_{PP}	
(A) Nonhydrides							
(a) $[Rh(L\text{-}L)(Diene)]^{+}$/ $[Rh(L)_2(Diene)]^{+}$							
L-L=CHIRAPHOS				58.4	154		47d
DIOP				17.1	152		47d
DIPAMP				50.9	159		47d
DIPHOS				56.9	156		47d
PROPHOS				60.5	172		48
				41.8	139	34	
L=PPh_3				27.6	156		47d
PPh_2Me				3.5	140		47d
(b) $[Rh(L\text{-}L)(MeOH)_2]^{+}$/ $[Rh(L)_2(MeOH)_2]^{+}$							
L-L=CHIRAPHOS				83.9	200		47d
DIOP				43.0	199		47d
DIPAMP				80.8	209		47d
DIPHOS				81.2	203		47d
PROPHOS				86.7	204		48
				68.9	202	55	
L=PPh_3				57.2	207		47d

Table cont'd ...

Complex Type	^1H(hydride portion)			$^{31}P\{^1H\}$			Ref.
	δH	J_{RhH}	J_{PH}	δP	J_{RhP}	J_{PP}	
(B) Monomeric Hydrides							
(a) $[Rh(DIPHOS)H]^{2+}$/MeCN	-15.7	12.1	17.2				46a
(b) $[Rh(L)_nH]^{\circ}$							
L=PBu^t_3; n=2	-13.9 (dt)	11	19				137a
$P(C_6H_{11})_3$; n=2	-14.9 (dt)	19	23				137a
PPh_3; n=3	-8.9 (bd)	13					146
$P(O\text{-}iPR)_3$; n=3	-7.2 (m)		120 (trans)				139b
			16 (cis)				
PPh_3; n=4	-10.6 (bs)	0		31.7 (m)	113	27	134
				28.2 (dld)	162		
$P(OMe)_3$; n=4	-11.6 (qnd)	9.8	35				139b
(c) $[Rh(L\text{-}L)(L)_2H]^{\circ}$							
L-L= $R_2P(CH_2)_2PR_2$ (R= OMe)	-9.8 (tdlt)	10.6	88.5	228.7 (dt)	185	70.5	138a
L=PMe_3			22.6	-22.6 (odt)	141		
L-L= $R_2P(CH_2)_2PR_2$ (R= O-iPr)	-10.4 (tdlt)	10.7	85.4				138a
L= PMe_3			21.1				
(d) trans-(L,L)-$[Rh(L)_2(H)_2(S)_2]^+$							
L= PPh_3; S=MeOH				41.8	121		47d
PPh_2Me; S= MeOH				23.8	118		47d

Table cont'd ...

Complex Type	^1H(hydride portion)			$^{31}P\{^1H\}$			Ref.
	δH	J_{RhH}	J_{PH}	δP	J_{RhP}	J_{PP}	
(C) Dimeric Hydrides							
(a) $[Rh(L\text{-}L)H]_2^\circ$							
L-L= $R_2P(CH_2)_2PR_2$ (R= O-iPr)	-4.3 (bsep)	34.1	33-35	196.4	212.4 ($^1J+^3J$)		138a
(b) $[Rh(L)_2(H)_2]_2^\circ$							
L= P(O-iPr) (35°C)	-7.1 (otqnt)	34.2	36.6	3.2 (bd)	249		139b
$P(NMe_2)_3$ (28°C)	-9.2 (qrt)	33.3	30.7	132.2			139c
(c) $[Rh_2(L\text{-}L)_2(H)_4]^\circ$							
L-L=$R_2P(CH_2)_2PR_2$ (R= O-iPr)	-7.2 (bm)		148				138a
	-12.0 (bs)						
(d) $[Rh_2(L)_4(H)_4]^\circ$							
L= $P(O\text{-}iPr)_3$ (-85°C)	-7.8 (dm)		180 (trans)				139b
	-11.1 (dm)		89 (trans)				
	-14.5 (bs)						
(e) $[Ir_2(H)_2(\mu\text{-}H)_3(L\text{-}L)_2]^+$							
L-L= $R_2P(CH_2)_3PR_2$ (R= Ph) (-45°C)	-6.9 (d)		70				143
	-7.9 (t)		65				
	-20.6 (m)		19				

Table cont'd ...

Complex Type	^1H(hydride portion)			$^{31}P\{^1H\}$			Ref.
	δH	J_{RhH}	J_{PH}	δP	J_{RhP}	J_{PP}	
(f) $[Ir_2(H)_2(\mu\text{-}H)_3(L)_4]^+$	(-90°C)			(-80°C)			
L= PPh_3	-6.9 (d)		86	15.3		95	144a
				18.5			
	-8.4 (t)		65				
	-23.9 (s)						

[a] Coupling constants are in Hz: dt = doublet or triplets, bd = broad doublet, bs = broad singlet, m = multiplet, dld = double doublet, qnd = quintet of doublets, odt = overlapping doublet of triplets, tdlt = triplet of double triplets, bsep = broad septet, otqn = overlapping triplet of quintets, bm = broad multiplet, dm = doublet of multiplets, d = doublet, t = triplet, s = singlet, qrt = quartet of triplets.

PUBLICATIONS:

W.R.Cullen, T.J.Kim, F.W.B.Einstein, and T.Jones,

The structure of the hydrogenation catalyst $[(P\text{-}P)Rh(NBD)]ClO_4$, P-P= $(n^5\text{-}((CH_3)_3C)_2P(C_5H_5)_2)_2Fe$ and some comparative rate studies. Organometallics, 2, 714-719(1983)

W.R.Cullen, T.J.Kim, I.Butler, and S.Rettig,

1,1'-Bisphosphinoferrocenes: Synthesis, Metal Complex Formation and Crystal Structure of Three Metal Complexes.

Organometallics, in press

W.R.Cullen, I.Butler, and T.J.Kim,

Synthesis of some isopropylphosphinoferrocenes.

J. Organometal. Chem., in press

W.R.Cullen, T.J.Kim, I.Butler, F.W.B.Einstein, and T.Jones,

Metal hydrides from cationic rhodium(I) complexes of di(tertiary phosphines); implication for asymmetric catalysis.

J. Chem. Soc., in press

W.R.Cullen, T.J.Kim, F.W.B.Einstein, and T.Jones,

The structures of three hydrogenation catalysts $[(P\text{-}P)Rh(NBD)]ClO_4$ and some comparative rate studies, P-P=$(n^5\text{-}R^1R^2PC_5H_4)(n^5\text{-}R^3R^4PC_5H_4)Fe$: $R^1=R^2=R^3=R^4=Ph$; $R^1=R^2=Ph$; $R^3=R^4=CMe_3$; $R^1=R^3=Ph$; $R^2=R^4=Ph$.

Organometallics, in press

W.R.Cullen, T.J.Kim, S.Evans, and J.Trotter

Asymmetric hydrogenation catalyzed by $[(L^*\text{-}L)Rh(NBD)]ClO_4$: Comparative studies and the structure of a chiral ferrocenylphosphine: $L^*\text{-}L= (n^5\text{-}C_5H_{5-n}(PR_2)_nFe(n^5\text{-}C_5H_3(PR_2)(CHMeNMe_2)\text{-}1,2)$;n=0-2,R=$CMe_3$.

J. Organometal. Chem., submitted for publication

..... continued to the next page.

In addition to the above publications the following papers have been and will be presented at the chemical conference of Canada and of Australia.

W.R.Cullen, T.J.Kim*, S.Rettig, F.B.W.Einstein, T.Jones, and A.J.Willis,
Ferrocenylphosphine Rh(I) hydrogenation catalysts.
The 66th Canadian Chemical Conference and Exhibition, June, 1983,
Calgary, Ed., Canada

W.R.Cullen, T.J.Kim, T.G.Appleton, N.F.Han, and I.Butler,
NMR spectra of ferrocenylphosphines and their complexes with platinum metals,
The Royal Australian Chemical Conference, January, 1984, Hobart, Australia

W.R.Cullen, T.J.Kim, and N.F.Han,
Cationic Rhodium(I) and Palladium(II) Complexes as Catalyst Precursors for Olefin Hydrogenation.
The 67th Canadian Chemical Conference and Exhibition, June, 1984,
Montreal, Quc., Canada, presented as an invited paper